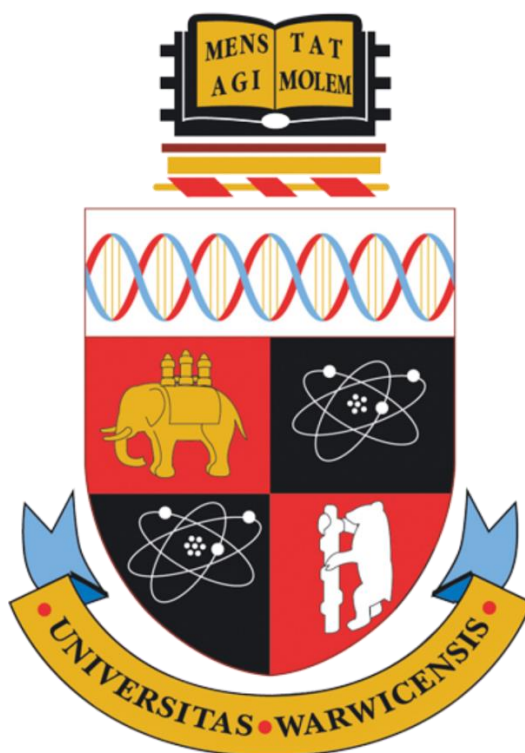


Glycosylated Materials to Probe the Role of Heterogeneity

Benjamin Thomas Martyn

A thesis submitted in partial fulfilment of the requirements for
the degree of Doctor of Philosophy in Chemistry



University of Warwick
Department of Chemistry

October 2017

Table of Contents

Acknowledgements	v
List of Figures	vii
List of Tables	xii
List of Schemes	xiv
List of Equations	xv
List of Abbreviations	xvi
Declaration	xx
1. Chapter One: Introduction	1
1.1. The antibiotics resistance crisis	1
1.2. Protein-carbohydrate interactions	2
1.2.1. Glycans	2
1.2.2. Lectins	7
1.2.3. Plant lectins	7
1.2.4. Plant toxins	8
1.2.5. Bacterial lectins	9
1.2.6. Anti-adhesion therapy	11
1.3. Multivalency	12
1.4. Heterogeneity	15
1.5. Polymerisation techniques	17
1.5.1. Living radical polymerisation	17
1.5.2. Reversible addition fragmentation chain transfer	18

polymerisation (RAFT)	
1.5.3. Post-polymerisation modification	20
1.5.4. Glyco-polymers	20
1.6. Glyco-nanoparticles	22
1.6.1. Gold nanoparticles	22
1.7. Imaging the glycocalyx	23
1.7.1. Metabolic labelling	24
1.8. Summary	25
1.9. Aims	26
1.10. References	27
2. Chapter Two: Heterogeneous Glycopolymers to Target Bacterial Toxins	39
2.1. Abstract	39
2.2. Introduction	40
2.3. Results and discussion	45
2.3.1. Synthesis of glycopolymers	45
2.3.2. Competitive binding assay to determine inhibition	52
2.3.2.1. Inhibition of RCA ₁₂₀ discussion	59
2.3.2.2. Inhibition of CTxB	66
2.3.3. Biolayer interferometry analysis of glycopolymer binding	67
2.3.3.1. Biolayer interferometry of RCA ₁₂₀	71
2.3.3.2. Biolayer interferometry of CTxB	78
2.4. Conclusions and further work	82

2.5. Experimental	84
2.5.1. Materials	84
2.5.2. Analytical Methods	85
2.5.3. Synthetic Procedures	88
2.6. References	95
3. Chapter Three: Semi Automated Assembly of Heterogeneous Glycosylated Gold Nanoparticles for High-Throughput Screening	99
3.1. Abstract	100
3.2. Introduction	101
3.3. Results and discussion	106
3.3.1. Polymerisation	106
3.3.2. Synthesis of gold nanoparticles <i>via</i> one-pot citrate reduction	110
3.3.3. Synthesis of azido-sugars and assembling a heterogeneous library	113
3.3.4. Assay of 35nm gold nanoparticle library	117
3.3.5. Determining the limit of detection	151
3.3.6. Synthesis of gold nanoparticles	154
3.3.7. Synthesis of 1-azido-1-deoxy-sugar coated 40nm gold nanoparticle library	156
3.3.8. Determining the effect of purification: can the multivalency effect out-compete monosaccharide binding?	158
3.3.9. Assay of heterogeneous 1-azido sugar coated 40nm	164

gold nanoparticle library	
3.3.10. The role of the octyl-linker in the binding of mannosylated nanoparticles	168
3.4. Conclusions and further work	171
3.5. Experimental	172
3.5.1. Materials	172
3.5.2. Analytical Methods	172
3.5.3. Synthetic Procedures	175
3.6. References	182
4. Chapter Four: Remodelling Cell Surfaces with Synthetic Polymers by Tandem Glycan Metabolic Labelling and Copper-Free Click Conjugation	186
4.1. Abstract	186
4.2. Introduction	187
4.3. Results and discussion	197
4.3.1. Synthesis of Ac4GalNAz metabolic label	197
4.3.2. Synthesis of fluorescent polymers	198
4.3.3. Testing the surface bound alkyne-azide coupling reaction with azide functionalised glass slides	201
4.3.4. Metabolic labelling of A549 carcinoma cells	204
4.3.5. Titration of sugar concentration	209
4.3.6 Investigating cell surface viability with fluorescently labelled WGA	213
4.4. Conclusions	216
4.5. Experimental	217

4.5.1. Materials	217
4.5.2. Analytical Methods	217
4.5.3. Synthetic Procedures	222
4.6. References	227
5. Chapter Five: Conclusions	234
6. Appendix One: Supplementary Information: Chapter Two	237
7. Appendix Two: Consortium of Functional Glycomics Nomenclature	254
8. Appendix Three: Collaborative Papers	255
9. Appendix Four: Intended Publications	256
10. Appendix Five: CV Copyright permissions for reused Figures	257

Acknowledgements

First and foremost I would like to thank my supervisor Professor. Matt Gibson for giving me both the opportunity to undertake this PhD but also for his support and enthusiasm throughout. His optimism, support and guidance have made this research possible, and he has always encouraged my participation in my teaching and outreach activities as well as my less academic endeavours. Secondly I would like to thank Dr. Gemma Davies, not only for the TEM images obtained for this research but also for always giving me time for advice, scientific discussion and a friendly chat. I have enjoyed my time in the Gibson group immensely, and it has been a privilege to be a part of the “2nd generation” of Gibson PhDs. Caroline, Sarah-Jane, Lucienne, Dan, Dan, Tom, and Rick made me feel welcome from the start and while some of you have moved on to bigger things you have all always been there for me to bounce ideas off , chat to and ask advice. Thanks also to the newer students to the group, Alice, Chris, Ben, Trisha, Marie, Sang-ho, Laura, Julia, and Henry for putting up with me in the office, listening to my complaints and always offering support and having time for discussing ideas. Thanks go to Ben G for synthetic advice and political discussions, Chris for our efforts to make the perfect old fashioned, Collette for her always good advice, Trisha for her endless patience with both my biology knowledge and my untidy desk, and Alice for quickly becoming one of my closest friends.

I would like to thank those that have given me training and guidance with equipment, including, Ben Douglas for teach me to use the Raman, Dan Leister for help with SEC, and Phil Aston for MALDI and mass spec training.

I would like to thank everyone in Warwick Chemistry for their support over the (many) years, including various members of the Haddleton and Clarke groups, as well as Lynne Bailey, Nick Barker and Selina Kermode, your advice, guidance and support and helped shape my time here.

I would like to thank all my friends, especially Cosmo, Laneo, Jess, and Danielle. To Cosmo and Laneo for always being the irreverent friends I knew I could count on. To Jess for somehow not just surviving 8 years of my friendship, but 2 years of living with me, I can't imagine what it would have been like without you and you're one of my best friends. Now stop following me. Finally, to Danielle for always having a laugh, inspiring me to work harder, and being supportive, I'm glad I 'bumped' into you during team building. To everyone else and all my friends made through climbing and photography, thank you for your interest, the adventure, and keeping me sane.

A huge thanks go to my family, in particular my mum, dad and brother. It is not an exaggeration to say I would not be who I am or where I am today without their constant love, support and encouragement, I cannot thank them enough.

Finally, I want to say thank you to my wife, Josie, for being the absolute best. Thank you for your unwavering support and belief in me, as well as your endless patience throughout the highs and lows of the last 4 years. Without you this would have been impossible; I love you.

List of Figures

Chapter 1

- Figure 1.1** Protein-Carbohydrate interactions play a central role in multiple biological processes. **3**
- Figure 1.2** Conformational complexity of glycan structures. **5**
- Figure 1.3** The 10 mammalian monosaccharides. **6**
- Figure 1.4** RCA₁₂₀ protein structure (Protein data bank structure 1RZO), showing location of β -D-Galactose binding domains.. **9**
- Figure 1.5** (A) Top down view and (B) Side view of the CtxB subunit and 5 binding sites (Protein data bank structure 1JR0). **10**
- Figure 1.6** The GM-1 ligand, D-galactose- β (1-3)-N-acetyl-D-galactosamine- β (1-4)-D-galactose- (α (2-3)-neuraminic acid)- β (1-4)-D-glucose- β (1-1)- ceramide. **11**
- Figure 1.7** The binding interactions of multivalent ligands. **13**
- Figure 1.8** The bind and slide mechanism. **16**
- Figure 1.9** Mechanism of RAFT polymerisation showing initiation, pre-equilibrium, propagation and termination. **18**

Chapter 2

- Figure 2.1** Receptor binding mechanisms that are unique to multivalent ligands. **42**
- Figure 2.2** (A) Diagram representing a BLI sensor, (B) Graph showing the shift in wavelength ($\Delta\lambda$). **44**
- Figure 2.3** SEC trace of master PPFMA polymer. **46**
- Figure 2.4** (A) IR of P(PFPMA) showing C-F halide bond 950 cm^{-1} (B) ^{19}F NMR. **47**
- Figure 2.5** (A) ^{19}F NMR showing two step reaction of PPPFMA (blue), DBCO functionalisation to 30 % (red) then following quenching with ethanolamine (green). (B) DOSY NMR, showing aromatic peaks (7.5ppm) at the same diffusional coefficient of $-9.25\text{ log}(\text{m}^2\text{s}^{-1})$, as polymer backbone peaks, marked by red line. (C) Raman spectra showing aromatic C-C **48**

	and alkyne peaks.	
Figure 2.6	¹⁹ F NMR of PG ₇₅ (red) PG ₅₀ (grey) PG ₂₅ (green) and HEMA (blue) post addition of DBCO (or ethanolamine for HEMA control).	50
Figure 2.7	Infrared spectrum of 1-azido-1-deoxy galactose (black), P(DBCO) ₁₅ (HEMA) ₃₅ (red) and PGal ₁₀₀ (blue) showing the disappearance of the azide stretch at 2100cm ⁻¹ .	52
Figure 2.8	(A) The CtxB pentamer from PDB file 1JR0 (B) RCA ₁₂₀ lectin from PDB file 1RZO.	53
Figure 2.9	The GM-1 ligand, D-galactose-β(1-3)-N-acetyl-D-galactosamine-β(1-4)-D-galactose- (α(2-3)-neuraminic acid)-β(1-4)-D-glucose-β(1-1)- ceramide.	55
Figure 2.10	Schematic of inhibitory assay demonstrating the inverse relationship between inhibitory activity and fluorescence readout.	56
Figure 2.11	Fluorescence linked inhibitory assay results. (A) Heterogeneous polymers vs RCA ₁₂₀ inhibition, n=18 (B) Heterogeneous polymers vs CTxB inhibition n=3 (C) Homogeneous polymers vs RCA ₁₂₀ , n= 6 (D) Homogenous polymers vs CTxB, n=6.	58
Figure 2.12	Maximum inhibition achieved by heterogeneous (black) and homogenous (red) polymer libraries.	59
Figure 2.13	Fitted curves of heterogenous (A-D) and homogeneous libraries (E-H) binding with RCA ₁₂₀ .	61
Figure 2.14	Relative IC ₅₀ values in (A) polymer concentration and (B) galactose concentration.	63
Figure 2.15	Results of the inhibitory assay against CTxB for (A) Heterogenous polymers (B) Homogenous polymers.	66
Figure 2.16	BLI response of PG ₁₀₀ showing the characteristic association phase, followed by the dissociation phase starting at t ≈4250s.	68
Figure 2.17	The heterogeneous binding model.	69
Figure 2.18	A more realistic depiction of the interactions taking place between bivalent RCA ₁₂₀ and the glycopolymers.	70
Figure 2.19	Where the ratio of (x1):(x2) varies as the heterogeneity of the polymers change. As the BLI method measures the size of the	70

bound layer onto the tip, we can gain a value for the K_d of the formation of all the protein-polymer complexes by plotting the end points of the dissociation curves *vs* polymer concentration.

Figure 2.20	Calculated values of (A) K_d , (B) k_{on} , and (C) k_{off} , as determined by the heterogeneous fitting model applied to BLI binding curves.	72
Figure 2.21	Homogeneous polymers: (A) K_d (B) k_{on} (C) k_{off} .	74
Figure 2.22	Heterogeneous polymers: (A) K_d (B) k_{on} (C) k_{off} .	75
Figure 2.23	For PG ₂₅ M ₇₅ : (A) Fitting of the dissociation phase to extract the end point (B) End point <i>vs</i> Concentration fit to extract an overall K_d .	76
Figure 2.24	Attempted fits of homogeneous polymers steady state K_d .	77
Figure 2.25	Steady State K_d for RCA ₁₂₀ .	78
Figure 2.26	For the binding of heterogenous polymers with CTxB (A) Dissociation constants (K_d) (B) Association rate constants (k_{on}) (C) Dissociation rate constants (k_{off}).	80
Figure 2.27	Comparison of K_d 's obtained from either the BLI method or end point analysis method.	81
 Chapter 3		
Figure 3.1	Overall schematic for the robotic assembly and label-free detection of lectins.	100
Figure 3.2	Assembly of functionalised gold nanoparticles using raft polymerisation, where X,Y and Z are potential chemical functionality that can be incorporated. This figure ignores co-polymer effects.	104
Figure 3.3	DBCO.	104
Figure 3.4	SEC trace of pHEAA-PFP at different degrees of polymerisation.	108
Figure 3.5	Solid phase Raman spectra of PHEAA ₂₅ -DBCO.	110
Figure 3.6	(A) Histogram of AuNP size, n= 567 (B) Example TEM showing nanoparticle morphology.	111

Figure 3.7	(A) DLS trace of Citrate and PHEAA ₂₅ -DBCO-stabilised polymers N.B. small intensity peak at very low size. (B) UV-Vis of Citrate and PHEAA ₂₅ -DBCO-HEAA stabilised polymers.	112
Figure 3.8	(A) Example of 384 well plate. Red indicates no binding has occurred while blue shows lectin binding induced aggregation of the gold nanoparticles. (B) Example binding curve showing the change in the absorption spectrum for galactosylated AuNP induced aggregation by SBA. The decrease in absorbance at the SPR peak at $\lambda=530$ nm and increase in absorbance at 700nm are clearly seen.	118
Figure 3.9	Raw UV-Vis spectra for each lectin concentration of the binding between Sample F6 (6-AzGal-pHEAA ₂₅ AuNP ₃₅) and DBA.	120
Figure 3.10	DBA binding to Nanoparticle group A containing sugars 2-Azido-2-deoxy Glucose and 2-Azido-2-deoxy Galactose	121
Figure 3.11	DBA binding to nanoparticle group B; containing sugars 2-Azido-2-deoxy Glucose and 6-Azido-6-deoxy Glucose.	122
Figure 3.12	DBA binding to nanoparticle group C; containing sugars 2-Azido-2-deoxy Glucose and 6-Azido-6-deoxy Galactose	123
Figure 3.13	DBA binding to nanoparticle group D; containing sugars 2-Azido-2-deoxy Galactose and 6-Azido-6-deoxy Glucose	124
Figure 3.14	DBA binding to nanoparticle group E; containing sugars 2-Azido-2-deoxy Galactose and 6-Azido-6-deoxy Galactose	125
Figure 3.15	DBA binding to nanoparticle group F; containing sugars 6-Azido-6-deoxy Glucose and 6-Azido-6-deoxy Galactose	126
Figure 3.16	PNA binding to nanoparticle group A containing sugars 2-Azido-2-deoxy Glucose and 2-Azido-2-deoxy Galactose	127
Figure 3.17	PNA binding to nanoparticle group B; containing sugars 2-Azido-2-deoxy Glucose and 6-Azido-6-deoxy Glucose	128
Figure 3.18	PNA binding to nanoparticle group C; containing sugars 2-Azido-2-deoxy Glucose and 6-Azido-6-deoxy Galactose	129
Figure 3.19	PNA binding to nanoparticle group D; containing sugars 2-Azido-2-deoxy Galactose and 6-Azido-6-deoxy Glucose	130
Figure 3.20	PNA binding to nanoparticle group E; containing sugars 2-	131

	Azido-2-deoxy Galactose and 6-Azido-6-deoxy Galactose	
Figure 3.21	PNA binding to nanoparticle group F; containing sugars 6-Azido-6-deoxy Glucose and 6-Azido-6-deoxy Galactose	132
Figure 3.22	RCA binding to nanoparticle group A containing sugars 2-Azido-2-deoxy Glucose and 2-Azido-2-deoxy Galactose	133
Figure 3.23	RCA binding to nanoparticle group B; containing sugars 2-Azido-2-deoxy Glucose and 6-Azido-6-deoxy Glucose	134
Figure 3.24	RCA binding to nanoparticle group C; containing sugars 2-Azido-2-deoxy Glucose and 6-Azido-6-deoxy Galactose	135
Figure 3.25	RCA binding to nanoparticle group D; containing sugars 2-Azido-2-deoxy Galactose and 6-Azido-6-deoxy Glucose	136
Figure 3.26	RCA binding to nanoparticle group E; containing sugars 2-Azido-2-deoxy Galactose and 6-Azido-6-deoxy Galactose	137
Figure 3.27	RCA binding to nanoparticle group F; containing sugars 6-Azido-6-deoxy Glucose and 6-Azido-6-deoxy Galactose	138
Figure 3.28	SBA binding to nanoparticle group A containing sugars 2-Azido-2-deoxy Glucose and 2-Azido-2-deoxy Galactose	139
Figure 3.29	SBA binding to nanoparticle group B; containing sugars 2-Azido-2-deoxy Glucose and 6-Azido-6-deoxy Glucose	140
Figure 3.30	SBA binding to nanoparticle group C; containing sugars 2-Azido-2-deoxy Glucose and 6-Azido-6-deoxy Galactose	141
Figure 3.31	SBA binding to nanoparticle group D; containing sugars 2-Azido-2-deoxy Galactose and 6-Azido-6-deoxy Glucose	142
Figure 3.32	SBA binding to nanoparticle group E; containing sugars 2-Azido-2-deoxy Galactose and 6-Azido-6-deoxy Galactose	143
Figure 3.33	SBA binding to nanoparticle group F; containing sugars 6-Azido-6-deoxy Glucose and 6-Azido-6-deoxy Galactose	144
Figure 3.34	WGA binding to nanoparticle group A containing sugars 2-Azido-2-deoxy Glucose and 2-Azido-2-deoxy Galactose	145
Figure 3.35	WGA binding to nanoparticle group B; containing sugars 2-Azido-2-deoxy Glucose and 6-Azido-6-deoxy Glucose	146
Figure 3.36	WGA binding to nanoparticle group C; containing sugars 2-Azido-2-deoxy Glucose and 6-Azido-6-deoxy Galactose	147

Figure 3.37	WGA binding to nanoparticle group D; containing sugars 2-Azido-2-deoxy Galactose and 6-Azido-6-deoxy Glucose	148
Figure 3.38	WGA binding to nanoparticle group E; containing sugars 2-Azido-2-deoxy Galactose and 6-Azido-6-deoxy Galactose	149
Figure 3.39	WGA binding to nanoparticle group F; containing sugars 6-Azido-6-deoxy Glucose and 6-Azido-6-deoxy Galactose	150
Figure 3.40	Incubation of GalNH ₂ -pHEAA ₂₅ @AuNP ₄₀ particles with SBA at at 6.25x10 ⁻³ mg.mL ⁻¹ in HEPES buffered saline, against varying gold concentrations to investigate the limit of detection.	152
Figure 3.41	Multivalency effects should allow us to outcompete monosaccharide binding and eliminate the need for purification methods.	153
Figure 3.42	UV-Vis spectra of the step growth of gold nanoparticles.	154
Figure 3.43	(A) Histogram of nanoparticle sizes obtained from TEM n=160 (B) TEM image showing gold nanoparticle morphology.	155
Figure 3.44	Effect of washed versus non-washed nanoparticles. Samples containing no lectin are represented at log -9.	159
Figure 3.45	SPR absorbance value at 530nm plotted against log DBA concentration for the heterogeneous coated nanoparticles. Particles are labelled galactose percentage (G), mannose percentage (M), gold nanoparticle size (AuNP _{40nm}).	164
Figure 3.46	SPR absorbance value at 530nm plotted against log PNA concentration for the heterogeneous coated nanoparticles. Particles are labelled galactose percentage (G), mannose percentage (M), gold nanoparticle size (AuNP _{40nm}).	165
Figure 3.47	SPR absorbance value at 530nm plotted against log SBA concentration for the heterogeneous coated nanoparticles. Particles are labelled galactose percentage (G), mannose percentage (M), gold nanoparticle size (AuNP _{40nm}).	165
Figure 3.48	SPR absorbance value at 530nm plotted against log WGA concentration for the heterogeneous coated nanoparticles. Particles are labelled galactose percentage (G), mannose percentage (M), gold nanoparticle size (AuNP _{40nm}).	166

Figure 3.49	SPR absorbance value at 530nm plotted against log RCA concentration for the heterogeneous coated nanoparticles. Particles are labelled galactose percentage (G), mannose percentage (M), gold nanoparticle size (AuNP _{40nm}).	166
Figure 3.50	Estimated Kd's for heterogeneous galactose-mannose particles against (A) DBA and (B) SBA. (Kd's with error greater than 1SD removed).	167
Figure 3.51	Binding curves for 100% mannosylated nanoparticles with and without octyl linker.	170
Chapter 4		
Figure 4.1	(A) A representation of the cell surface showing the lipid membrane in pink, important proteins in blue and the glycocalyx in orange. Heterogeneity in the lipid membrane has been ignored for simplicity (B) Relative size of the glycocalyx. (C) Pictorial representation of the over expression of HER2 protein in cancerous cells vs healthy cells. (D) Examples of the chemical modifications which the carbohydrates of the glycocalyx can undergo.	188
Figure 4.2	(A) Labelling the <i>N</i> -acetylgalactosamine salvage pathway with unnatural GalNAz (B) Introducing a probe to the labelled <i>O</i> -glycosylated proteins using the Staudinger ligation.	191
Figure 4.3	Bio-orthogonal reagents for metabolic labelling.	192
Figure 4.4	Dibenzocyclooctyne (DBCO).	193
Figure 4.5	¹⁹ F NMR of PFP-PHEAA ₇₅ -co-HMA _{1.5} on addition of DBCO at time = 0 (Red) and time = 16 hours (green).	201
Figure 4.6	Synthetic procedure for the production of azide coated glass slides.	202
Figure 4.7	(A) Graph to show observed water contact angle measurements (B) Drop shape analysis of uncoated SiO ₂ (C) Drop shape analysis of azide functionalised slide.	203
Figure 4.8	The localisation of PHEAA ₂₅ -co-HMA _{0.5} on the slide at 0.1 (Left two columns) and 0.01 (right three columns) mg.mL ⁻¹ .	204

Figure 4.9	(A) 20x magnification image, showing healthy cell morphology (B) Cell counts, concentrations are of final plate concentration of Ac ₄ GalNAz.	205
Figure 4.10	Microscope images of A549 cells metabolically labelled with PHEAA ₂₅ -co-HMA _{0.5} at a concentration of 0.31 mg.mL ⁻¹ .	207
Figure 4.11	Left: PHEAA ₂₅ -co-HMA _{0.5} . Right: PHEAA ₇₅ -co-HMA _{1.5} . Concentration expressed in Log Molar with blank set to -7.	208
Figure 4.12	(A) 10x objective brightfield image (B) 10x objective fluorescence image with blue filter. Both images at a polymer concentration of 10 mg.mL ⁻¹ .	208
Figure 4.13	Plate reader obtained fluorescence data for titration of Ac ₄ GalNAz against PHEAA ₂₅ -co-HMA _{0.5} . Concentration expressed in Log Molar with blank set to -1.	209
Figure 4.14	(A) Example of the reduced cell count observed in the higher concentration samples and (B) The output after processing with ImageJ to allow cell counts.	210
Figure 4.15	Results after incubation with pHEAA ₂₅ -co-HMA _{0.5} . (A) Average cell counts (n=3). (B) The calculated average fluorescence per cell (n=3) In both cases concentration expressed in Log Molar with blank set to -1.	211
Figure 4.16	40x fluorescence images of (A)(C) and (E) 5000μM positive azide and (B)(D) and (F) 5000μM negative azide after incubation with 0.6 mg.mL ⁻¹ PHEAA ₂₅ -co-HMA _{0.5} for 2 hours. Each image is from a separate repeat. Inset: Slice of fluorescent intensity averaged from entire image area shown in yellow.	212
Figure 4.17	Titration curve of FITC-WGA against unlabelled A549 cells. Circled data point represents the concentration chosen for further experiments.	214
Figure 4.18	Fluorescent response of cells after incubation with pHEAA ₂₅ -DBCO or pHEAA ₇₅ -DBCO and subsequent addition of FITC-WGA.	215

List of Tables

Chapter 2

Table 2.1	Polymers synthesised.	49
Table 2.2	Summary of the DBCO-substitution of P(PFPMA).	51
Table 2.3	Table showing average galactose spacing for each polymer.	54
Table 2.4	Summary of relative IC ₅₀ values obtained.	60
Table 2.5	Hill Cooperativity Coefficients.	64
Table 2.6	Summary of rate constants and R ² and χ^2 values associated with the fitting.	71
Table 2.7	Steady state K _d against RCA ₁₂₀ in polymer concentration (M).	77
Table 2.8	Summary of BLI derived rate constants against CTxB.	79
Table 2.9	Steady state K _d against CTxB in polymer concentration.	81

Chapter 3

Table 3.1	Lectin and stated specificity.	105
Table 3.2	Characterisation of p(hydroxyethyl acrylamide) pentafluorophenol ester.	108
Table 3.3	Summary of UV-Vis and DLS characterisation.	112
Table 3.4	Heterogenous AuNP library formed with 2-azido-2-deoxy glucose, 2-azido-2-deoxy galactose, 6-azido-6-deoxy glucose, and, 6-azido-6-deoxy galactose.	116
Table 3.5	Lectin binding specificities.	117
Table 3.6	Determination of the size of gold nanoparticles by UV-Vis.	154
Table 3.7	Dynamic light scattering and zeta potential.	156
Table 3.8	Heterofunctional library created using 1-azido-1-deoxy galactose, 1-azido-1-deoxy mannose and 1-(8-azidoethyl)-1-deoxy mannose.	156
Table 3.9	T test to determine if washed and unwashed give statistically difference results in the binding of DBA.	160
Table 3.10	T test to determine if washed and unwashed give statistically	161

	difference results in the binding of PNA.	
Table 3.11	T test to determine if washed and unwashed give statistically difference results in the binding of SBA.	161
Table 3.12	T test to determine if washed and unwashed give statistically difference results in the binding of WGA.	162
Table 3.13	T test to determine if washed and unwashed give statistically difference results in the binding of RCA.	162
Table 3.14	Estimated K_d values extracted from fitting a dose-response curve. Particles that did not show potential inhibition are not shown. Estimated K_d is defined as the concentration of lectin predict to be at the midpoint of the dose dependent response curve.	168
 Chapter 4		
Table 4.1	Summary of some of the unnatural sugars and probes used for metabolic glycan labelling.	194
Table 4.2	Table summarising characterisation of fluorescent polymers.	200
Table 4.3	Water contact angle measurements of coated and uncoated glass slides.	203

List of Schemes

Chapter 2

- Scheme 2.1** Synthesis of heterogeneous glycopolymers. (i) DBCO (0.3 eq, Dioxane, 16 hours 50°C) (ii) Ethanolamine (3 eq, dioxane, 16 hours 50°C); (iii) Sugar-N₃ (2.5 eq, DMF, 16 hours, room temperature). **45**
- Scheme 2.2** Synthesis of PFPMA. **46**
- Scheme 2.3** Synthesis and mechanism of 1-azido-1-deoxy hexoses. **49**

Chapter 3

- Scheme 3.1** Two step synthesis of 2-(dodecylthiocarbonothioylthio)-2-methylpropionic acid pentafluorophenyl ester. **106**
- Scheme 3.2** Polymerisation of PFP-HEAA synthetic scheme. **107**
- Scheme 3.3** Nucleophilic addition of DBCO-amine to the amine reactive PFP-endgroup. **109**
- Scheme 3.4** General synthesis for forming 1-azido-1-deoxy hexoses. **113**
- Scheme 3.5** The structure of 1-(8-azidooctyl)-1-deoxy mannose (mannose-C8-azide) **114**
- Scheme 3.6** The strain promoted azide alkyne coupling reaction **114**

Chapter 4

- Scheme 4.1** Synthesis of Ac₄GalNAz. **197**
- Scheme 4.2** Reaction scheme for the synthesis of (A) the statistical copolymer PFP terminated Poly(*N*-hydroxyethyl acrylamide-co-hostasol methacrylate) (B) Functionalisation of end group with DBCO. **199**

List of Equations

Chapter 1

Equation 1.1 Gibbs free energy **14**

Chapter 2

Equation 2.1 Percentage Inhibition of FLSA. **59**

Equation 2.2 Hill-Waud Equation. **63**

Equation 2.3 Relationship of BLI Observed Rate Constant to Association Rate Constant, Dissociation Rate Constant and Ligand Concentration. **68**

Chapter 3

Equation 3.1 The Beer Lambert Law **115**

Equation 3.2 The Beer Lambert Law **174**

Abbreviations

ACVA	4,4'-Azobis(4-cyanovaleric acid)
A549	Human carcinoma cells
AIBN	2,2'-Azobis(2-methylpropionitrile)
ATRP	Atom Transfer Radical Polymerisation
AuNP	Gold Nanoparticle
AVCA	4,4'-Azobis(4-cyanovaleric acid)
BLI	Biolayer interferometry
BSA	Bovine Serum Albumin
cAMP	Cyclic adenosine monophosphate
CCT	Catalytic Chain Transfer
CFG	Consortium for functional glycomics
Con A	Concanavalin Agglutinin
CRP	Controlled radical polymerisation
CT	X-ray computed tomography
CTA	Charge transfer agent
CTx	Cholera Toxin from <i>Vibrio Cholerae</i>
CuAAC	Copper catalysed Alkyne Azide Cyclisation
DBA	Dolichos biflorus agglutinin
DBCO	Dibenzocyclooctyne
DBU	1,8-Diazabicyclo(5.4.0)undec-7-ene
DCM	Dichloromethane
DC-SIGN	Dendritic Cell-Specific Intercellular adhesion molecule-3-Grabbing Non-integrin

DLS	Dynamic Light Scattering
DMC	2-Chloro-1,3-dimethylimidazolium chloride
DMF	Dimethylformaide
DMSO	Dimethyl sulfoxide
DNA	Deoxyribonucleic acid
DOSY	Diffusion Ordered Spectroscopy
DP	Degree of polymerisation
Đ	Dispersity
<i>E.coli</i>	<i>Escherichia coli</i>
EDC	N-(3-Dimethylaminopropyl)-N'-ethylcarbodiimide hydrochloride
ELISA	Enzyme-linked immunosorbent assay
ELLA	Enzyme-linked lectin assay
FITC	Fluorescein isothiocyanate
FLSA	Fluorescent linked sorbant assay
Fucosyl	
GM-1	Fucosyl-monosialotetrahexosylganglioside
GalN ₃	1-deoxy-1-azide galactose
glycoAuNP	Glycosylated gold nanoparticles
GM1	Monosialotetrahexosylganglioside
GM-2	Monosialotrihexosylganglioside
HEAA	Hydroxyethyl acrylamide
HEPES	(4-(2-hydroxyethyl)-1-piperazineethanesulfonic acid
HIV	hHuman immunodeficiency virus
HPLC	High performance liquid chromatography
IC50	Inhibition concentration 50

IR	Infrared Spectrometry
ITC	Isothermal titration calorimetry
Ka	Equilibrium association constant
Kd	Equilibrium disassociation constant
Koff	Rate of disassociation
Kon	Rate of association
LD50	Lethal Dose 50
LRP	Living radical polymerisation
LTB	E.Coli heat labile toxin
MADIX	Macromolecular design <i>via</i> interchange of xanthates
ManN3	1-azido-1-deoxy mannose
Mn	Number average molar mass
MRI	Magnetic Resonance Imaging
MS	Mass spectrometry
Mw	Weight average molar mass
MWCO	Molecular weight cut off
NHS	N-Hydroxysuccinimide
NMP	Nitroxide mediated polymerisation
NMR	Nuclear magnetic resonance
OD	Optical density
PBS	Phosphate buffered saline
PCR	Polymerase chain reaction
PDB	protein databank
PET	Positron emission tomography
PFP	Pentafluorophenol

pHEAA	Poly hydroxyethylacrylamide
pHEMA	poly hydroxyethylmethacrylamide
pHEMA	poly hydroxyethylmethacrylamide
PNA	Arachis hypogaea (peanut) agglutinin
POC	Point of care
pPFPMA	Poly pentafluorophenol
PS DCL's	Polymer scaffolded dynamic combinatorial libraries
RAFT	Reversible addition fragmentation transfer
RCA ₁₂₀	Ricinus Communis agglutinin
RCA60	Ricin
SBA	Glycine mas (soybean) agglutinin
SEC	Size exclusion chromatography
SET-LRP	Single electron transfer - living radical polymerisation
SPR	Surface plasmon resonance
TEM	Transmission electron microscopy
UEA	Ulex Europaeus agglutinin
UV-Vis	Ultraviolet visible spectroscopy
WGA	Triticum Vulgaris (wheat germ) agglutinin
XPS	X-ray photoelectron spectroscopy
ΔG	Change in Gibbs free energy
ΔH	Change in enthalpy
ΔS	Change in entropy
$\Delta\lambda$	Change in wavelength

Declaration

The work present in this thesis is entirely original and my own work, except where acknowledged at the start of each chapter. I confirm that this thesis has not been submitted for another degree at another university.

Abstract

Identifying and treating infectious diseases remains a challenge for modern healthcare professionals. Proper identification of infectious diseases and understanding of the means of infection will allow for optimal use of antibiotics and the development of alternative therapies such as anti-adhesion therapy. It is therefore important to develop tools that can probe the processes involved in infection, or that can be used as point of care diagnostics. *In vivo* glycosylated surfaces are inherently heterogeneous, increasing the complexity of the interactions that take place, and with a corresponding increase in analytical difficulty. Glycopolymers and glycosylated nanoparticles are ideal methods for incorporating synthetic functionalisation into a biological setting to probe interactions between glycosylated surfaces and carbohydrate recognising proteins (lectins).

This work utilises heterogeneously glycosylated polymers to probe the inhibitory and kinetic activity of the polymers towards various lectin targets. We see further evidence of the “heterocluster effect” whereby nominally non-binding sugar epitopes give rise to faster association rates and increase overall residence time of bound lectins to the polymers. Highly coloured heterogeneously glycosylated gold nanoparticles are used to develop a high throughput screening library for the identification of binding patterns with lectins that could lead to use as an identification system of unknown lectins. Finally, unnatural azide containing sugars are used to metabolically label the surface of A549 carcinoma cells and tagged using fluorescent polymers. This system provides a robust way of introducing polymeric functionality onto the surface of cells, opening the ability to probe in-depth the cell surface.

Chapter One

Introduction

1.1. The antibiotic resistance crisis

The antibiotic resistance crisis has been building for several decades. The discovery of penicillin by Alexander Fleming in 1928 has brought about nearly 100 years of improved healthcare.¹ Despite this infectious diseases are still one of the world's top killers. Respiratory tract infections (3rd), tuberculosis (8th) and diarrhoeal diseases (9th) are amongst the top 10 causes of death. Globally they alone accounted for 10.6% of deaths worldwide in 2015.² On top of this the rate of discovery of antibiotics has slowed considerably, from 33 in the period from 1985-2000 to just 13 from 2000-2014.³

There are a number of ways to combat this growing problem; changing industry dependence upon combinatorial libraries would allow access to larger synthetic spaces, as well as targeting a broader range of inhibition pathways,^{4,5} greater understanding of the development of resistance mechanisms, finding alternative methods for combating infectious disease (for example anti-adhesion therapy), and, more effective use of the antibiotics we currently have. To facilitate this we require better tools that will allow us to identify unknown samples from both biological sera and contaminated water supplies. We need the ability to differentiate quickly between bacterial and viral infections in order to effectively target our treatments.

On top of this, cancer is the 2nd leading cause of death globally. Having better tools to investigate the bio-markers associated with the development and metastasis of cancer related diseases will be vital to reduce the loss of life. The development of tools to investigate the interactions of infectious agents and biomarkers of cancerous cells have significant overlap,

and may lead to the development of point of care (POC) diagnostic and prognostic techniques for both.⁶⁻⁹ One of the most ubiquitous information containing biological macromolecules are carbohydrates (glycans, or ‘sugars’) which coat all cells and direct a vast range of infectious processes.

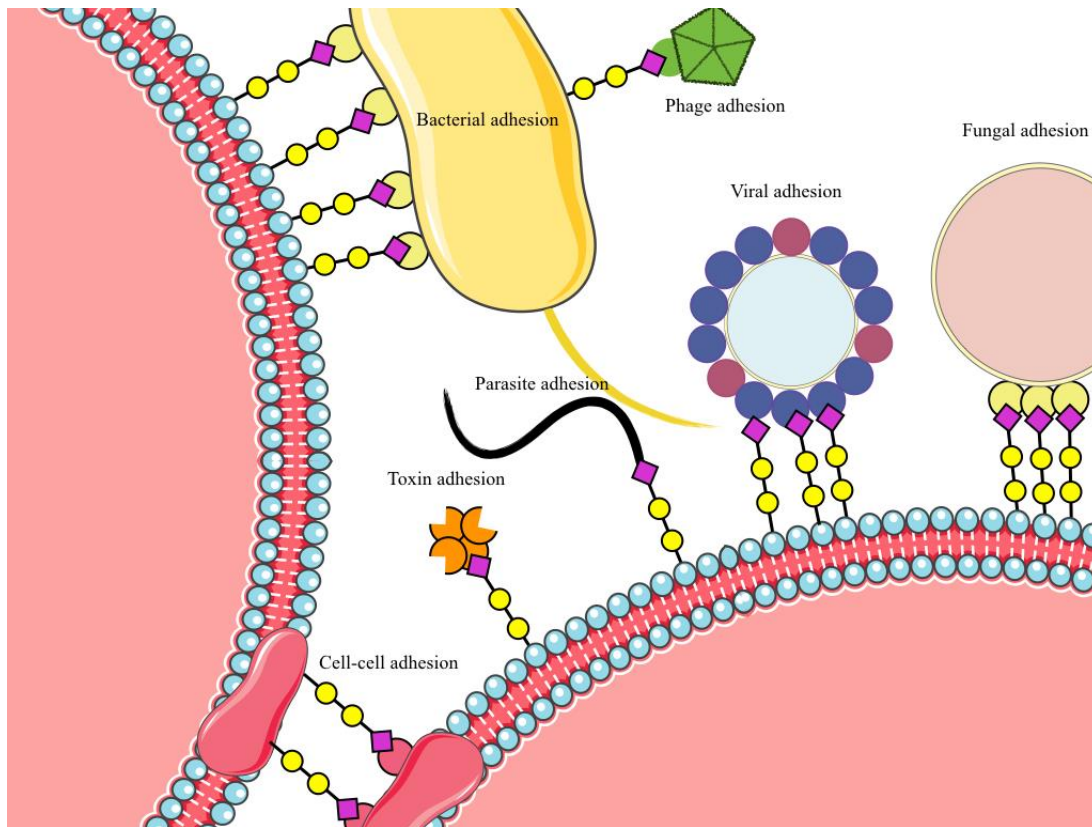
1.2. Protein-Carbohydrate interactions

1.2.1. Glycans

The four main classes of cellular macromolecules are nucleic acids, proteins, lipids and glycans. Glycans are poly- or oligo- saccharides and are found conjugated to proteins (glycoproteins and proteoglycans) and lipids (glycolipids) within the body. They can have linear, complex branched structures or they can be free-standing entities involved in both metabolism and signalling. Until recently, the main focus of biochemical research has been on DNA and proteins, due to the fact that they are pure and discrete macromolecules and the biochemical tools used to access and characterise these (PCR and mass spectrometry) are readily available. Conversely glycans are dynamic, changing over time and many sugars have the same mass, complicating analysis by mass spectrometry. Glycans are also not templated (e.g. DNA-RNA-protein) but are a post-translation modifications; successes in genomics and proteomics unfortunately cannot translate into knowledge of the genome.

Despite this, glycans form a major part of the extracellular matrix, as well as the external cell surface, and as such are vital in determining how cells interface with their environment. A cell’s glycosylation state affects its biological activity and can give an indication of the underlying cell physiology,¹⁰⁻¹⁶ and glycans play a vital role in inflammation processes.¹⁷⁻²⁰ For example, overexpression of sialic acid residues has been observed in the glycome of cancer cells derived from gastric, colon, pancreatic, liver, lung, prostate and breast tissue, as well as in several types of leukemia.²¹⁻²⁶

A greater understanding of glycan biology is also vital for treatment of infection. Many parasites, viruses, bacteria, and their toxins, initiate infection through glycan mediated adhesion to the cell surface, shown in Figure 1.1.



Reproduced with permission from L. Otten, Pathogen Detection Based on Carbohydrate Adhesion, Thesis, University of Warwick, 2015.

Figure 1.1: Protein-Carbohydrate interactions play a central role in multiple biological processes.

However, analysis of glycans is not easy; glycans are not directly encoded genetically, instead they are directed by metabolism, signal transduction and cellular status²⁷⁻³⁰ and offer a stunning level of complexity that is orders of magnitude greater than that offered by proteins and DNA.³¹⁻³³ Theoretically just four monosaccharides can create 35,560 unique tetra-saccharides,³⁴ although in practise not all of this space is utilised in nature. This complexity arises from the number of structural isomers that exist for each sugar, Figure 1.2:

Structural Isomerism, the different arrangement of bonds (i.e. Pyranose vs Furanose)

- Enantiomers, the non-superimposable mirror images of each other in which nature has favoured the d configuration (D/L)
- Diastereoisomers, special stereoisomers that are not mirror images (Glucose, Galactose, Mannose)
- Anomers, the stereochemistry position of the C1 substituent alcohol (Alpha vs Beta)
- Branching, the bond formation between the C1 position and any of the C2-6 positions (1-2/1-3)

This complexity greatly increases the difficulty of analysis, reducing the analytical power of mass Spectrometry but also complicating the interpretation of other analytical methods. No single method can be used to analyse the glycome. Fortunately, in mammalian biology the most common glycan structures are composed of only 10 monosaccharide base units, see Figure 1.3. This reduces the conformational space used in nature, but still presents a staggeringly complex array of structures.

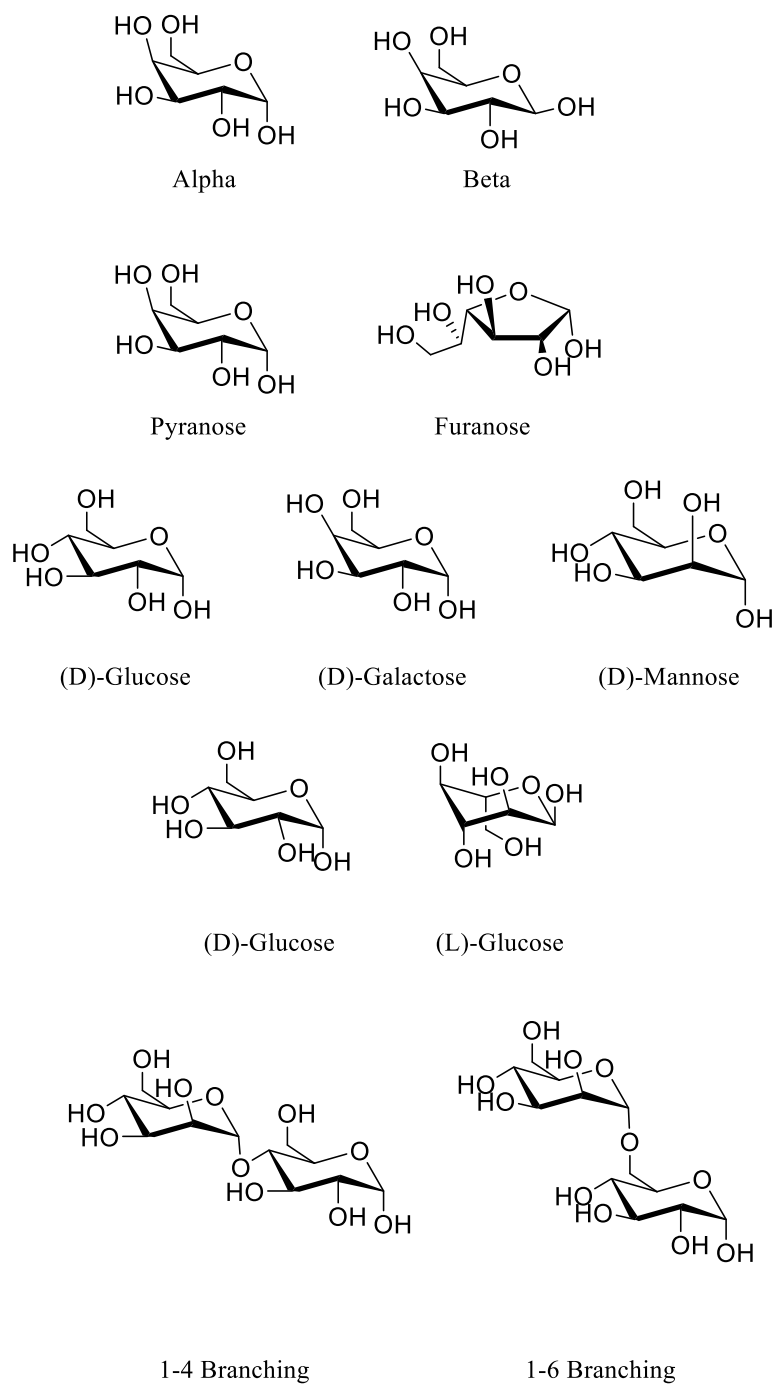


Figure 1.2: Conformational complexity of glycan structures.

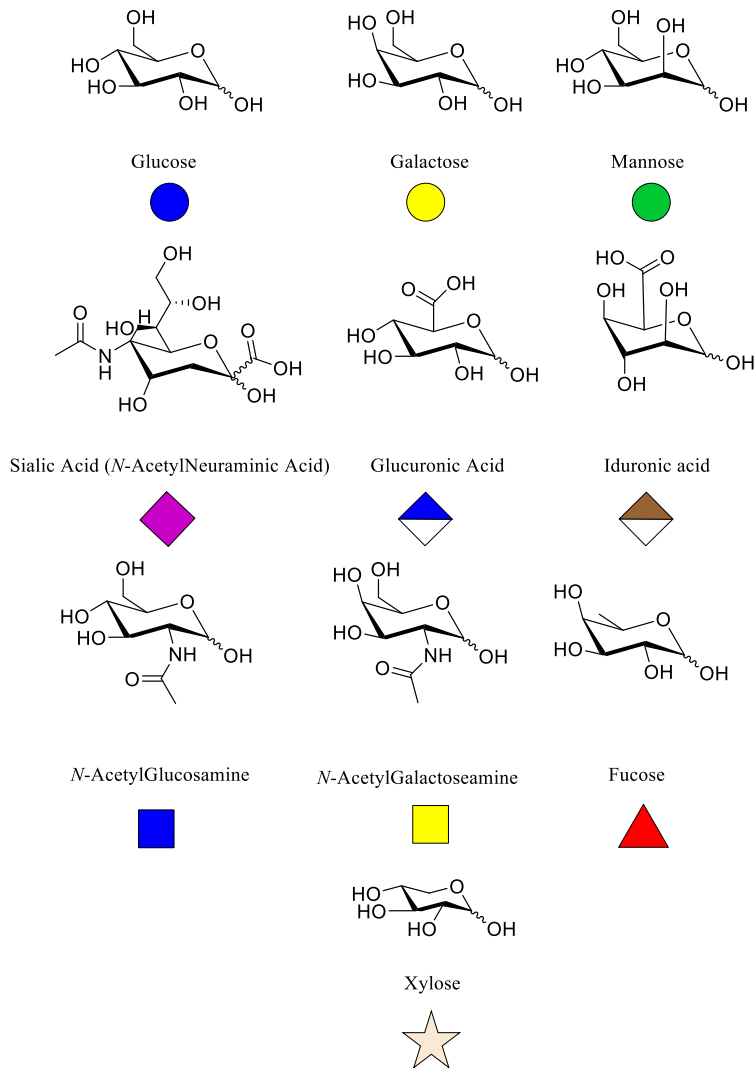


Figure 1.3: The 10 D-mammalian monosaccharides and their consortium of functional glycomics (CFG) representations

This complexity makes glycans very information dense and allows them to be used by nature in recognition events. This role is also how pathogenic species take advantage and attempt to hijack natural pathways to adhere to host cells and/or gain entry to do damage or replicate.

1.2.2. Lectins

Carbohydrate binding proteins that are neither enzymes or antibodies are known as lectins.³⁵ They are ubiquitous in nature, found in plants, animals, viruses and bacteria. Lectins are utilised in a wide range of biological processes, including inflammation, adhesion of infectious agents, tumour cell differentiation and metastasis, and immune system interactions.³² They interact with carbohydrates in a reversible and non-covalent manner.

1.2.3. Plant Lectins

Legume lectins are the most studied group of lectins. The first pure lectin to be isolated was *Concanavalin A* (Con A) from the seeds of jack beans in 1919 by Sumner.³⁶ Legume lectins typically consist of 2 or 4 identical subunits that associate/dissociate dependent upon pH. Each subunit typically contains one carbohydrate binding domain, a Ca^{2+} binding site, and a transition metal binding site, often Mn^{2+} . Without these metals present carbohydrate binding is severely diminished or negated completely. Approximately 20% of the amino acid residues are conserved across all legume lectins and a further 20% are similar. Of the conserved amino acids, several are found within the carbohydrate binding domains; aspartic acid, asparagine, a glycine (except in Con A) and an aromatic amino acid^{37,38} or leucine.³⁹ Almost all the metal binding domains are invariant. Despite this, lectins have a wide range of binding specificities and can be highly specific for di-,tri-,and tetra saccharides. The binding domain itself is often a shallow depression on the surface of the protein, with the Ca^{2+} and transition metal in close proximity. The cations do not necessarily participate in binding, but help place the amino acids into the correct configuration to facilitate binding. Water molecules also play a vital role in carbohydrate binding by being both hydrogen bond donors and acceptors; in the peanut agglutinin lectin (PNA), some of the high specificity for T-antigenic disaccharide ($\text{Gal}\beta(1-3)\text{GalNAc}$) is due to two water bridges.³⁹

Legume lectins are highly abundant and provide a diverse range of saccharide specificities with which to probe lectin-carbohydrate interactions. This makes them ideal for use as model systems and developing biomedical applications.

1.2.4. Plant Toxins

Plant lectins can also be toxic to humans; of particular note is the lectin ricin, RCA₆₀, derived from the seeds of the castor oil plant. Ricin is highly toxic with the potential to be used as a chemical weapon. It is a dimeric protein consisting of a lectin subunit, which allows entry to the cell, and a toxophoric subunit, which causes cell death by disrupting protein biosynthesis. It is more toxic than cyanide with an LD₅₀ of 20 µg/Kg, meaning 1.6mg can kill the average adult male.

RCA₁₂₀ is a less toxic analogue to RCA₆₀ that facilitates study of ricin within a laboratory setting without requiring extensive safety procedures, Figure 1.4. It shares the carbohydrate recognition subunit with RCA₆₀, while the other subunit is non-toxic.

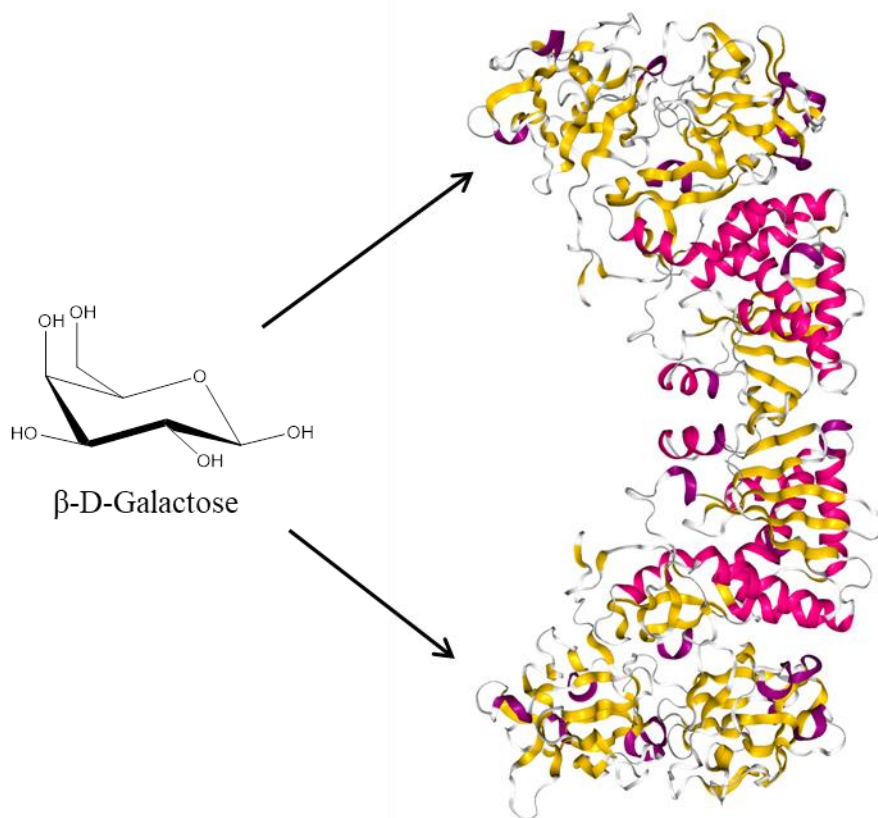


Figure 1.4: RCA₁₂₀ protein structure (Protein data bank structure 1RZO⁴⁰), showing location of β-D-Galactose binding domains.

1.2.5. Bacterial Lectins

Bacteria often secrete toxins to directly damage the host and its immune system. Cholera (*Vibrio cholerae*) causes between 21,000 and 143,000 deaths per year⁴¹ but it is the cholera toxin (CTx) that causes its pathogenicity. Cholera Toxin is an AB₅ protein consisting of a dimeric, toxic, A domain bound through a sulphide bridge and a pentameric B domain of five α-Helices. The B domain, shown in Figure 1.5, of the toxin binds with nanomolar affinity to the GM-1 carbohydrate present on the surface of the intestine, where it is internalised. The toxic A subunit then raises the concentration of cellular cyclic adenosine monophosphate (cAMP). This results in fluid expulsion from the infected cells and the symptoms of cholera.

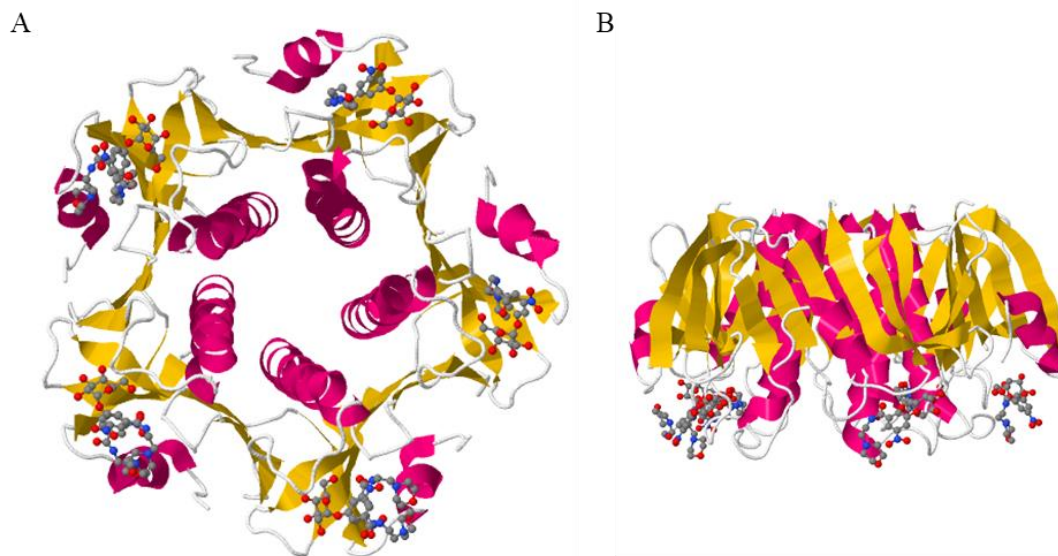


Figure 1.5: (A) Top down view and (B) Side view of the CtxB subunit and 5 binding sites (Protein data bank structure 1JR0⁴²).

The GM-1 binding domain of the B subunit contains a primary binding site that binds to the terminal galactose residue of GM-1, Figure 1.6 Blue. It binds to this domain with a K_d of ~50 mM, while the secondary binding domain binds to the neuraminic acid residue, Figure 1.6 Red, with a K_d of 210 mM. Finally the remainder of the GM-1 scaffold severely restricts the conformational space available to the galactose and neuraminic acid residues.^{43,44} This rigidity greatly reduces the entropic penalty paid when GM-1 binds to CTxB. These three interactions result in one of the highest avidity carbohydrate-protein interactions known.⁴⁴ The factors contributing to this high binding affinity will be discussed in further detail in section 1.3 below.

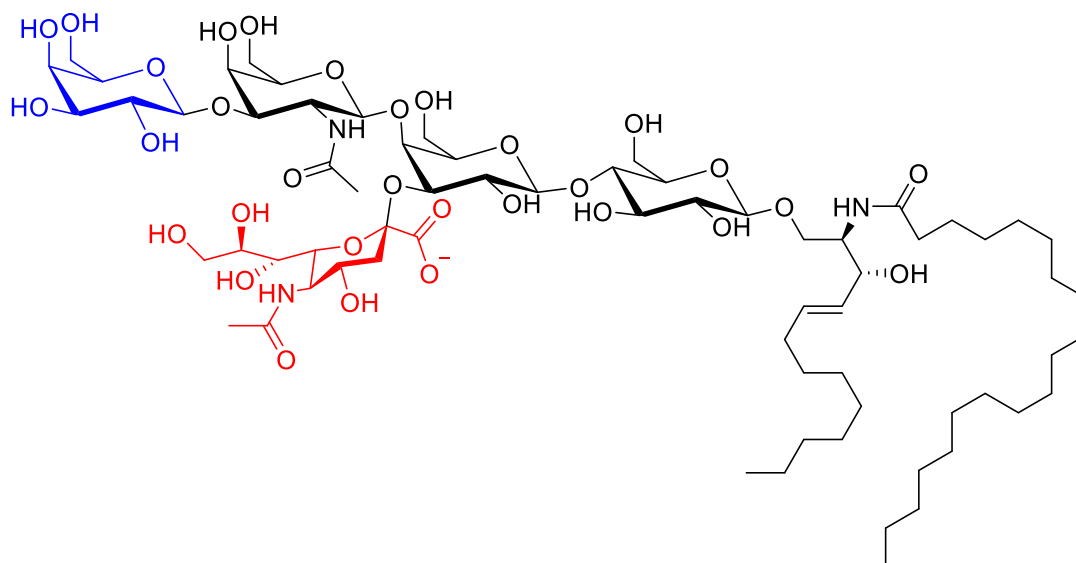


Figure 1.6: The GM-1 ligand, D-galactose- β (1-3)-N-acetyl-D-galactosamine- β (1-4)-D-galactose- (α (2-3)-neuraminic acid)- β (1-4)-D-glucose- β (1-1)- ceramide.

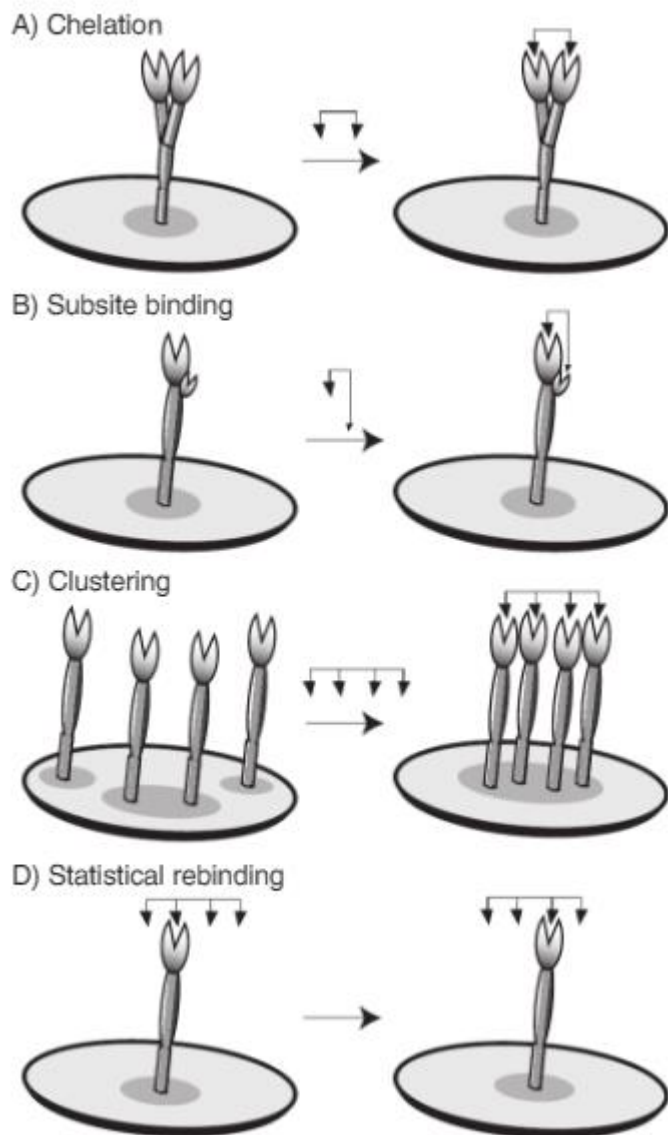
1.2.6. Anti Adhesion Therapy

Anti-adhesion therapy aims to prevent the effects of pathogen infection by using a glycan substrate (or decoy) with a higher binding affinity for the pathogen than the intended target, preventing the initial engagement and hence reducing infection.⁴⁵ Bacteria often gain significant resistance to antibiotics and the immune response after adherence to surfaces, due to the formation of intransient biofilms.⁴⁶⁻⁴⁸ Furthermore adherent bacteria acquire nutrients with more ease and thus are better able to survive and cause re-infection.⁴⁹

While anti-adhesion resistance may also be expected to arise, through mutation or the acquisition of new genetic material, it would be expected to arise at a much slower rate. This is due to the lack of a selection pressure being applied by not killing or slowing the growth of the bacterial population. This results in a lack of separation between resistant and susceptible strains, preventing predominately resistant strains from emerging. Considering this, glycan decoys are a potential target for new anti-adhesion therapies.

1.3. Multivalency

The interaction between a single carbohydrate and individual lectin binding site is typically very weak, with a dissociation constant (K_d) in the mM range. To overcome this, nature utilises multiple carbohydrate binding interactions simultaneously to allow the formation of reversible, non-covalent, yet strong bonds. These multivalent interactions result in a total avidity which is greater than the sum of the individual affinities, up to a system dependent limit.⁵⁰ This effect was first noted by Lee *et al.*⁵¹ and is referred to as the “cluster glycoside” or “multivalency” effect. This multivalent effect is a result of the multiple binding modes that multivalent receptors and ligands can under-go, each leading to a non-linear increase in affinity, Figure 1.7.



From L.L.Kiessling, J.E.Gestwicki, L.E. Strong, *Angew. Chem Int. Ed.*, **2006**, 4, 2348-68. Reprinted with permission from John Wiley and sons.

Figure 1.7: The binding interactions of multivalent ligands.

In all of these binding events the same basic thermodynamic principles apply. As in all interactions, the energy of binding is governed by the Gibbs free energy as given by Equation 1.1:

$$\Delta G = \Delta H - T\Delta S$$

1.1

In the binding of a multivalent ligand to a multivalent receptor, the enthalpy (ΔH) for the interaction of one ligand of a polyvalent ligand is equivalent to the enthalpy of the monovalent interaction. The enthalpy term associated with subsequent binding can be either enhanced or diminished depending on the relative physical dimensions of the receptor and polyvalent ligand. If the binding of one ligand causes a change that allows the next ligand to bind with greater enthalpy (more negative) then the system is said to have positive cooperativity. This is most famously exemplified by the binding of oxygen to haemoglobin, although this is admittedly not a multivalent system. Positive cooperativity has also been observed in the binding of cholera toxin to its native ligand GM-1.⁵² If the orientation of the polyvalent ligand is such that there is not a perfect conformational match between it and the receptors, any secondary binding will introduce conformational strain into the system by distorting either the receptor, the ligand, or both. This situation is described as negative cooperativity as the secondary binding has a smaller binding enthalpy. As such the more conformationally rigid a system, the more likely there will be a mismatch between receptor and polyvalent ligand, resulting in diminished enthalpy of binding.

In contrast, in multivalent binding the entropic (ΔS) contribution is largely paid upon the binding of the first ligand to the receptor and secondary binding is entropically neutral. In this case the intramolecular binding of the second ligand will have a greater change in free energy as $\Delta S \approx 0$ and therefore $\Delta G \approx \Delta H$. While this approximation is valid for many systems, it is unrealistic, as the linker between ligands of a multivalent ligand will have an associated flexibility. With an increase in flexibility comes a decrease in degrees of freedom after secondary binding. This will come with an associated entropic penalty for secondary binding

events. Therefore when designing multivalent ligands, consideration of rigidity of the system is important.

Since the enthalpy of binding is approximately equal for both a monovalent ligand and the first binding event of a multivalent ligand, the rate of association (k_{on}) will largely be the same for both the monovalent and multivalent ligand. Therefore any differences in the affinity between monovalent and multivalent ligands is due to the rate of dissociation (k_{off}). However this is only true for homogeneous multivalent ligands. Considering this, multivalent glycopolymers (see below) offer an exciting route to high-affinity glycan mimetics.

1.4. Heterogeneity

In 2010 Jiménez Blanco *et al.* used heterogenous glycoclusters with a β -cyclodextrin core to probe the role of heterogenous glycoenvironments that contain nominally non-binding sugars alongside native ligands.⁵³ From this work they reported evidence for a heterocluster effect:

*“The term heterocluster effect refers to the increase in the intrinsic binding affinity of a carbohydrate ligand towards a lectin in the presence of a second sugar that itself is not a ligand for this lectin (intrinsic affinity means in a per-ligand basis, keeping the same overall topology and preventing contributions to binding from aggregation phenomena.”*⁵⁴

Thermodynamically, the explanation for this effect is that while the enthalpic contribution is lower due to the inclusion of “non-binding” sugars, this is compensated for by an increased entropy of binding. These observations correlate with a “bind and slide effect”, as has already been proposed for the binding of lectins to multivalent glyco-arrays,⁵⁵ whereby the lectin moves between binding domains along the surface, resulting in an increased residence time and therefore a longer macroscopic off rate, Figure 1.8.

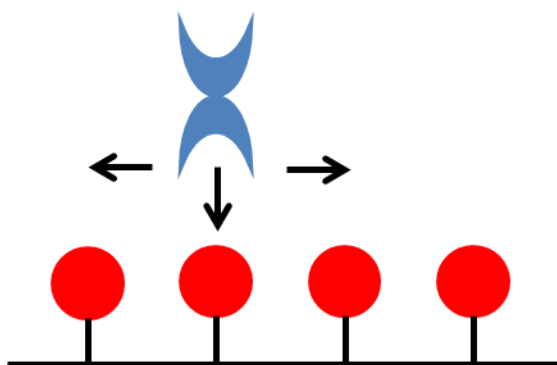


Figure 1.8: The bind and slide mechanism, where-by a lectin initially binds to a surface and then moves or “slides” along the surface, resulting in an increased time spent “bound” to the overall surface and a slower dissociation rate overall.

Therefore, it will be vital going forward to reflect the inherent heterogeneity of the cellular milieu when designing probes to investigate carbohydrate binding.

Greater understanding of the multivalency mechanism and the effect of linkers, non-binding partners, desolvation effects, and, secondary binding domains opens up the possibility for the rational design of ligands. Rationally designed ligands have the potential to allow the development of more sensitive assays and diagnostic tools, as well as acting as anti-adhesion prophylactics. To do this requires an underlying scaffold, chiefly either polymeric and particle based. Both of these options will be discussed in further detail later, in sections 1.5 and 1.6 In particular synthetic glycopolymers and glycoparticles, where the sugars are presented pendant to the polymer backbone, are an established class of multivalent probes which often present significant binding enhancements.

1.5. Polymerisation techniques

1.5.1. Living Radical Polymerisation

The development of living radical polymerisation (LRP) techniques has given chemists unprecedented control over polymer architecture. Living polymerisation techniques allow the synthesis of polymers with linear, branched or more complex architectures while maintaining strict molecular weight control with narrow dispersity. Added to this is the ability to introduce functionality to either chain ends or side-chains on the backbone, making polymer chemistry a versatile platform from which to develop new materials for medicinal applications. Living polymerisation techniques have already found medicinal uses in the cases of biodegradable implants^{56–59} and as drug conjugates to improve pharmacokinetics.⁶⁰

Living radical polymerisation techniques all use different modes of action to achieve ‘living’ status: but they aim to limit termination and transfer reactions and can continue to polymerise after the initial monomer stock has been depleted upon the addition of more monomer. LRP techniques are based around several different mechanisms of action: (1) Stable free-radical polymerisation, for example nitroxide mediated polymerisation (NMP); (2) Reversible chain transfer polymerisation such as reversible addition – fragmentation chain transfer (RAFT), also known as macromolecular design *via* the interchange of xanthates (MADIX) depending on the class of chain transfer agent (CTA) used; (3) Metal mediated polymerisation such as atom transfer radical polymerisation (ATRP) and single electron transfer living radical polymerisation (SET-LRP). Each of these categories contains many more examples of LRP systems but these examples are the most commonly used due to their applicability to a wide range of monomers and solvent systems.

1.5.2. Reversible Addition Fragmentation Chain Transfer Polymerisation

RAFT is a LRP technique that is particularly well suited to the synthesis of polymers for use in a biological setting. RAFT does not require the use of a toxic copper catalyst as in ATRP and SET, and the chain transfer agents used allow facile introduction of end group functionality at both the α and ω positions. The RAFT mechanism is shown in Figure 1.9:

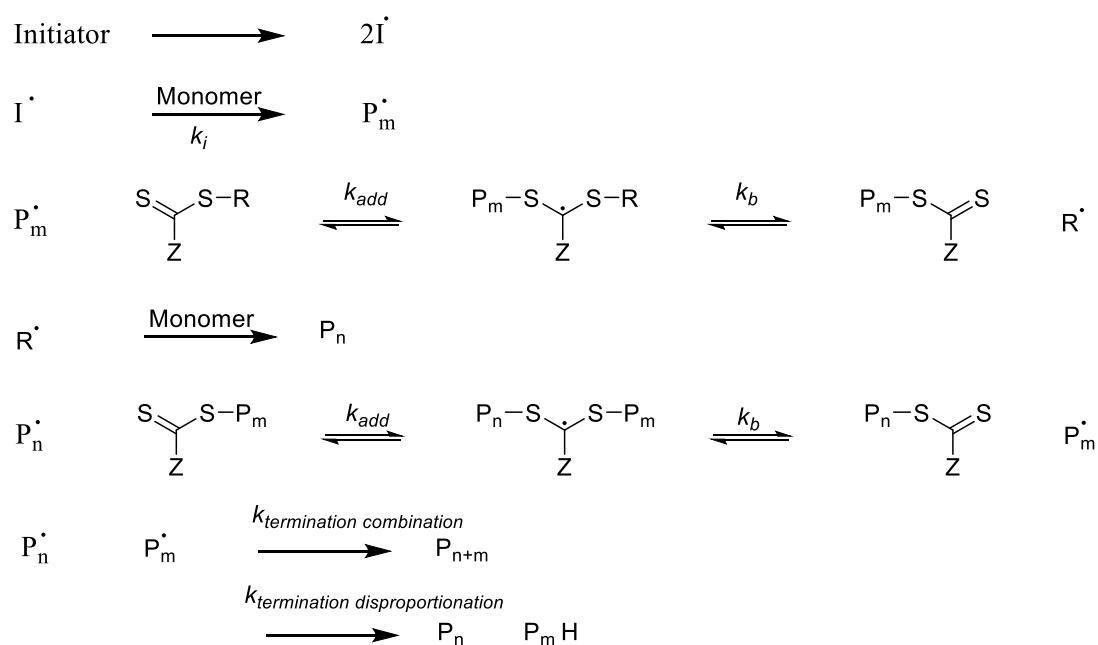


Figure 1.9: Mechanism of RAFT polymerisation showing initiation, pre-equilibrium, propagation and termination.

The first step is the initiation step where radicals are generated. Thermal decomposition or photolysis of the initiator is typically used. Following this, the oligomeric radicals add to the chain transfer agent (CTA). Evidence in the literature suggests that all RAFT agents are consumed in this step before any propagation of the polymer chain occurs.⁶¹ This is due to the reactive C=S bond being favoured over any vinyl monomer bonds. Following this the R

group can leave to initiate another growing polymer chain or P_m can fragment and propagate. The R group should be a good reinitiating group and must fragment at a similar rate to the initiator or growing polymer chain. The Z group must activate the C=S bond towards radical addition and stabilise the radical adduct as little as possible. By keeping the number of propagating chains as low as possible, compared to the number of stabilised radicals termination is reduced, imparting control over the polymerisation. However termination does still occur, either by combination between two propagating radicals, or by disproportionation. This mechanism allows us to easily introduce α -end group functionality simply by modifying the R group of the RAFT agent while ω -end group functionality can be introduced by changing the Z group or by post polymerisation modification of the thiocarbonyl end group. RAFT polymerisation is particularly useful if you wish to coat gold nanoparticles (AuNPs) with polymer, as the ω -end group is easily reduced to a thiol, which will spontaneously self-assemble onto the gold surface,⁶² and is exploited later in this thesis.

1.5.3. Post polymerisation modification

When designing a polymeric system for a diagnostic application, the inherent dispersity of polymer samples must be taken into account. While LRP gives us access to almost any polymer architecture we wish, even at low dispersity the polymer sample is inherently a mixture of many chain lengths. If two different monomers are polymerised then each resulting polymer will not be identical in terms of distribution. This is crucial in glycoscience, as valency (i.e number of sugars) plays a dramatic role in affinity, hence small differences in dispersity might translate to false positive/negative results in binding assays. This means using a single batch of master polymer with a reactive monomer unit that allows varying functionality to be added in a post polymerisation modification process, enables an extra level of control to be imposed, assuming the modification reactions are efficient, and go to quantitative conversion.

1.5.4 Glyco-polymers

Glycopolymers offer a route to well-defined multivalent glycoassemblies. The vast array of polymeric architectures available means that glyco-polymers can offer almost any array and orientation of carbohydrate, through either pendant or terminal carbohydrates. Glycopolymers have the advantage of being easy to synthesise and can they can be produced on a large scale. They can easily span large dimensions, which is vital for probing the multivalent interactions with lectins, which can have large distances between binding sites, such as RCA₁₂₀ which has two binding domains separated by 110 Å.⁶³

Initial work using glycopolymers was focussed on glyco-mimetics of natural carbohydrate ligands, as a method for probing carbohydrate-lectin interactions.^{51,64} Work by Cameron and co-workers used synthetic glycopolymers to probe the binding interaction of both RCA₁₂₀⁶⁵

and peanut agglutinin (PNA)⁶⁶. In the case of RCA₁₂₀ it was observed that the enhancement in binding of multivalent galactosides over the monovalent sugar was a result of contributions from both the chelation mechanism and the bind and slide mechanism. Meanwhile for PNA, the 50-fold increase in affinity observed for the galactosides were attributed to the cross-linking of proteins, such that the multivalent glycopolymers were inhibiting multiple PNA proteins simultaneously. Glycopolymers also offer opportunities for therapeutic and other biomedical applications. They have been used for drug release,^{67,68} scaffolds for tissue engineering,⁶⁹⁻⁷¹ and, as inhibitors to block immune response during surgery.⁷² Notably, they are ideal candidates for the development of anti-adhesion therapeutics. Haddleton and co-workers used mannosylated glycopolymers to inhibit dendritic cell specific ICAM-3 grabbing non-integrin (DC-SIGN), a lectin present on immune response cells that contributes to the infectivity of HIV-1.⁶⁶ By increasing the density of mannose on the glycopolymer from 20 to 90 sugar moieties,⁷³ a decrease in the concentration required for 50% inhibition (IC₅₀) from 1453 to 37 nM was observed. In order to side-step the difficulties in attempting to rationally design multivalent ligands, Fulton *et al.* have used polymer scaffolded dynamic combinatorial libraries (PS-DCL'S)^{74,75} to generate high affinity heterogeneous glycopolymers through templating with lectins. By templating heterogeneous galactose and mannose polymers against *Concanavalin A* (Con A) and *E.Coli* heat labile toxin (LTB), they saw an increase in the free energy of binding of 5.2-8.8 kJ mol⁻¹.⁷⁶ This method provides a way to 'screen' for anti-adhesion leads as well as probe the nature of carbohydrate binding in a high-throughput manner.

This highlights the potential of glycopolymers and multivalent glycosylated structures in general, for both fundamental studies of carbohydrate binding, as well as for medical applications. Another method of preparing multivalent glycoassemblies are nanoparticles, that offer their own advantages and disadvantages in probing carbohydrate binding.

1.6. Glyco-nanoparticles

Nanoparticles are easy to synthesise in a manner which is simple to scale up.⁷⁷⁻⁷⁹ They offer the possibility of multi-functionality such that the same particle might act in both a diagnostic and therapeutic manner (so called “theranostics”).⁸⁰ While tuning the carbohydrate coating of nanoparticles allows probing of biological interactions, changing the nanoparticle core used offers a wide variety of tools for use in both a research and medical setting. The use of optical tags, magnetic particles and/or radionuclei allows nanoparticles to be used as biosensors,⁸⁰ therapeutics,⁸¹⁻⁸³ in optical imaging,⁸⁴⁻⁸⁸ magnetic resonance imaging (MRI),⁸⁹⁻⁹¹ positron emission tomography imaging (PET),⁹²⁻⁹⁴ and, x-ray computed tomography (CT).⁹⁵⁻⁹⁷

1.6.1. Gold nanoparticles

Gold nanoparticles (AuNPs) in particular offer some unique properties that have seen them widely employed for the design of biosensors and elsewhere.^{77,78,98-101} They are easy to synthesise and receptive to surface functionalisation, they have highly tuneable optical properties and are biocompatible for both *ex* and *in vivo* applications. Monodisperse solutions of gold nanoparticles are highly coloured. The electromagnetic field of incident light induces an oscillation of the free electrons in the conduction band of the metal. This oscillation induces a dipole in the particles with respect to the ionic lattice of the gold atoms along the plane of the electric field of light. The maximum amplitude of this oscillation occurs at a particular frequency, known as the surface plasmon resonance (SPR).¹⁰²⁻¹⁰⁵ For gold the SPR wavelength occurs around 520nm.¹⁰⁶ The SPR wavelength and the intensity of the absorption depends on factors that affect the charge density at the surface of the particle, including the size of the particles. Importantly, as the particle separation distance is reduced to less than the diameter of a single particle, dipole-dipole coupling causes a red shift and broadening of the absorption spectrum which can be detected through UV-Vis spectroscopy.⁷⁷

The first use of gold nanoparticles in this manner was by Mirkin *et al.* for the colourimetric detection of bacterial DNA¹⁰⁷ (based on work by Leuvering *et al.* that proposed a gold nanoparticle based immunoassay, but did not utilise a colourimetric detection method¹⁰⁸). Since then this method has been used to probe proteins,^{109,110} peptides,¹¹¹ antibodies^{112–116} and DNA^{117,118} in a label free manner. More recently work by Richards *et al.* has used glycosylated gold nanoparticles to probe carbohydrate-lectin interactions.^{119–124}

Glycosylated nanoparticle surfaces effectively mimic the cell glycocalyx and so are ideal for studying or interrupting biological interactions, while allowing label free monitoring. By functionalising AuNPs with a mixture of galactose and mannose sugars Gibson and co-workers started to mimic the natural heterogeneity of the cell for identification and concentration of unknown lectins.¹²² This highlights the power of gold nanoparticles as a label free system that can be utilised in a high throughput manner cheaply and easily when compared to other techniques such as glyco-arrays, which often require more extensive synthesis.^{125,126}

1.7. Imaging the glycocalyx

While it is important to develop methods for investigating carbohydrate binding interactions in a separate and controlled environment, it is also vital to develop tools for probing the glycocalyx of a cell directly. Tools for probing *in vivo* protein interactions have been in use for a number of years, largely by utilising genetic modification to generate fluorescent mutants that are easily visualised.¹²⁷ However as glycans are dynamic biomolecules that are not directly encoded by DNA,¹²⁸ glycans are resistant to imaging in this manner. Work has been made to utilise lectin binding to visualise cell surface glycans,^{129,130} but lectins are unsuited for *in vivo* work due to their inability to cross cell membranes, as well as their potential toxicity.^{131,132}

1.7.1. Metabolic labelling

To circumvent this issue this issue Bertozzi and co-workers have developed a method of metabolic glycan labelling for direct imaging of the glycome (the complete glycan profile produced by a cell). This is achieved *via* the incorporation of unnatural sugars bearing a reactive tag functionality, typically an azide, however many others have been reported.^{16,133–}

¹⁴⁰ Various bio-synthetic pathways have been utilised for the labelling of glycans through this method: sialic acid biosynthesis,^{135,140} *O*-linked¹⁴¹ and *N*-linked glycosylation,¹⁴² fucosylation¹³⁷ and glycolipids¹⁴³ have all been accessed. Even more impressively this technique has been used to directly observe the development of glycosylation in developing zebrafish embryos.^{144–147}

To achieve the biocompatibility necessary perform these labelling experiments *in vivo* with no detrimental effects requires the use of “bio-orthogonal reagents” as proposed by Bertozzi.¹³³ These reagents are an extension of the principles of “click” chemistry and must fulfil the requirement of being small enough to be tolerated by the cells native enzymatic pathways, and chemically inert towards the chemical functionality of the cell.¹⁴⁸ In order to further extend this methodology to labelling of multiple biosynthetic pathways, new chemistries and strategies must be produced.

1.8. Summary

It is obvious that the development of tools to better investigate the glycome are vitally important. The staggering complexity presented by carbohydrate chemistry has allowed nature to develop glycosylation as an information dense mediator for a huge range of biological processes. Furthermore, the glycosylation of cells is not dependant on direct genetic encoding and is instead a function of a cell's genome, transcriptome, proteome, and its extra cellular environment and varies with access to nutrients. This dependency on such a wide array of cellular processes means that analysis of a cell's glycome is intrinsically linked to its physiological state, and will vary with the progression of disease. Changes in the glycome are linked to cancer,^{26,132,149–151} Alzheimer's disease,^{142,152,153} and malaria.^{154,155}

Meanwhile, cell surface glycans are the primary attack vectors for infectious diseases and some toxic plant proteins. Cellular adhesion of bacteria greatly increases the ability of bacteria to survive, while bacterial toxins weaken the host and reduce its ability to effectively combat the infection. A greater understanding of the dynamics of these multivalent interactions within a heterogeneous environment is vital to make progress towards effectively combating these diseases with alternative therapies such as by preventing adhesion.

Finally, the ability to easily and at scale, investigate carbohydrate binding events is vital for the discovery of lead compounds, as well as providing a platform from which to effectively screen environmental and biological samples for the identification of unknown pathogens.

1.9. Aims

Considering the above, this thesis aims to investigate three aspects of carbohydrate interactions. In **Chapter Two**, a panel of homo and heterogeneous glycopolymers are synthesised *via* a sequential three step procedure to generate a glycopolymer library. The binding properties of these polymers are then investigated against the biologically relevant toxins *26omofun communis agglutinin 120* (RCA₁₂₀) and toxin secreted by *Vibrio cholerae* (CtxB) using both a competitive binding assay to assess the inhibitory potential of the glycopolymers and a biolayer interferometer (BLI) to investigate the effect on the binding kinetics. In **Chapter Three**, we propose a method for the generation of a high throughput, heterogeneous, glycosylated gold nanoparticle library that is synthetically simple and widely applicable. The limit of detection for assays of this type is investigated, and the gold nanoparticle library is screened against five lectins. In **Chapter Four**, acetylated azidogalactose is used to metabolically label human carcinoma cells (A459), which are then labelled using fluorescent polymers. It is then demonstrated that the labelling of the cell surface with polymers doesn't inhibit the viability of the cell surface.

1.10. References

- 1 S. Y. Tan and Y. Tatsumura, *Singapore Med. J.*, 2015, **56**, 366–7.
- 2 World Health Organisation, January 2017. URL:
<http://www.who.int/mediacentre/factsheets/fs310/en/> accessed 20th January 2018
- 3 C. Dye, *Philos. Trans. R. Soc. Lond. B. Biol. Sci.*, 2014, **369**, 20130426.
- 4 C. Nathan, *Nature*, 2004, **431**, 899–902.
- 5 J.-L. Reymond and M. Awale, *ACS Chem. Neurosci.*, 2012, **3**, 649–57.
- 6 P. Yager, G. J. Domingo and J. Gerdes, *Annu. Rev. Biomed. Eng.*, 2008, **10**, 107–144.
- 7 C. D. Chin, V. Linder and S. K. Sia, *Lab Chip*, 2012, **12**, 2118–2134.
- 8 S. Sharma, J. Zapatero-Rodríguez, P. Estrela and R. O’Kennedy, *Biosensors*, 2015, **5**, 577–601.
- 9 S. A. Soper, K. Brown, A. Ellington, B. Frazier, G. Garcia-Manero, V. Gau, S. I. Gutman, D. F. Hayes, B. Korte, J. L. Landers, D. Larson, F. Ligler, A. Majumdar, M. Mascini, D. Nolte, Z. Rosenzweig, J. Wang and D. Wilson, in *Biosensors and Bioelectronics*, 2006, vol. 21, pp. 1932–1942.
- 10 M. M. Fuster and J. D. Esko, *Nat. Rev. Cancer*, 2005, **5**, 526–42.
- 11 J. D. Marth and P. K. Grewal, *Nat. Rev. Immunol.*, 2008, **8**, 874–87.
- 12 R. S. Haltiwanger and J. B. Lowe, *Annu. Rev. Biochem.*, 2004, **73**, 491–537.
- 13 S.-K. Cha, B. Ortega, H. Kurosu, K. P. Rosenblatt, M. Kuro-O and C.-L. Huang, *Proc. Natl. Acad. Sci. U. S. A.*, 2008, **105**, 9805–10.

- 14 K. Ohtsubo, S. Takamatsu, M. T. Minowa, A. Yoshida, M. Takeuchi and J. D. Marth, *Cell*, 2005, **123**, 1307–21.
- 15 E. A. Partridge, C. Le Roy, G. M. Di Guglielmo, J. Pawling, P. Cheung, M. Granovsky, I. R. Nabi, J. L. Wrana and J. W. Dennis, *Science*, 2004, **306**, 120–4.
- 16 Y.-C. Liu, H.-Y. Yen, C.-Y. Chen, C.-H. Chen, P.-F. Cheng, Y.-H. Juan, C.-H. Chen, K.-H. Khoo, C.-J. Yu, P.-C. Yang, T.-L. Hsu and C.-H. Wong, *Proc. Natl. Acad. Sci. U. S. A.*, 2011, **108**, 11332–7.
- 17 L. A. Lasky, *Annu. Rev. Biochem.*, 1995, **64**, 113–140.
- 18 Y. Kaneko, F. Nimmerjahn and J. V. Ravetch, *Science*, 2006, **313**, 670–673.
- 19 D. H. Dube and C. R. Bertozzi, *Nat. Rev. Drug Discov.*, 2005, **4**, 477–488.
- 20 G. A. Rabinovich and M. A. Toscano, *Nat. Rev. Immunol.*, 2009, **9**, 338–52.
- 21 G. Yogeeswaran, B. S. Stein and H. Sebastian, *Cancer Res.*, 1978, **38**, 1336–44.
- 22 J. Roth, C. Zuber, P. Wagner, D. J. Taatjes, C. Weisgerber, P. U. Heitz, C. Goridis and D. Bitter-Suermann, *Proc. Natl. Acad. Sci. U. S. A.*, 1988, **85**, 2999–3003.
- 23 S. Sell, *Hum. Pathol.*, 1990, **21**, 1003–19.
- 24 E. P. Scheidegger, P. M. Lackie, J. Papay and J. Roth, *Lab. Invest.*, 1994, **70**, 95–106.
- 25 R. Takano, E. Muchmore and J. W. Dennis, *Glycobiology*, 1994, **4**, 665–74.
- 26 J. Zhao, W. Qiu, D. M. Simeone and D. M. Lubman, *J. Proteome Res.*, 2007, **6**, 1126–38.
- 27 J. W. Dennis, I. R. Nabi and M. Demetriou, *Cell*, 2009, **139**, 1229–41.

- 28 K. Yarema and C. Bertozzi, *Genome Biol.*, 2001, **2**, 1-10.
- 29 R. B. Parker and J. J. Kohler, *ACS Chem. Biol.*, 2010, **5**, 35–46.
- 30 M. A. Breidenbach, J. E. G. Gallagher, D. S. King, B. P. Smart, P. Wu and C. R. Bertozzi, *Proc. Natl. Acad. Sci. U. S. A.*, 2010, **107**, 3988–93.
- 31 R. D. Cummings, *Mol. Biosyst.*, 2009, **5**, 1087–104.
- 32 H.-J. Gabius, H.-C. Siebert, S. André, J. Jiménez-Barbero and H. Rüdiger, *Chembiochem*, 2004, **5**, 740–64.
- 33 S. M. Muthana, C. T. Campbell and J. C. Gildersleeve, *ACS Chem. Biol.*, 2012, **7**, 31–43.
- 34 R. Mody, S. H. Antara. Joshi and W. Chaney, *J. Pharmacol. Toxicol. Methods*, 1995, **33**, 1–10.
- 35 S. H. Barondes, *Trends Biochem. Sci.*, 1988, **13**, 480–2.
- 36 J. B. Sumner, *J. Biol. Chem.*, 1919, **37**, 137–142.
- 37 R. Adar and N. Sharon, *Eur. J. Biochem.*, 1996, **239**, 668–674.
- 38 N. Sharon, *Trends Biochem. Sci.*, 1993, **18**, 221–6.
- 39 A. Imberty, F. Casset, C. V. Gegg, M. E. Etzler and S. Pérez, *Glycoconj. J.*, 1994, **11**, 400–413.
- 40 S. Sharma, S. Bharadwaj, A. Surolia and S. K. Podder, *Biochem. J.*, 1998, **333**, 539–42.
- 41 M. Ali, A. R. Nelson, A. L. Lopez and D. A. Sack, *PLoS Negl. Trop. Dis.*, 2015, **9**, 1-13.

- 42 J. C. Pickens, E. A. Merritt, M. Ahn, C. L. M. J. Verlinde, W. G. J. Hol and E. Fan, *Chem. Biol.*, 2002, **9**, 215–24.
- 43 H.-A. Tran, P. I. Kitov, E. Paszkiewicz, J. M. Sadowska and D. R. Bundle, *Org. Biomol. Chem.*, 2011, **9**, 3658.
- 44 W. Bruce Turnbull, and Bernie L. Precious and Steve W. Homans, 2004.
- 45 I. Ofek, D. L. Hasty and N. Sharon, *FEMS Immunol. Med. Microbiol.*, 2003, **38**, 181–191.
- 46 R. M. Donlan, *Clin. Infect. Dis.*, 2001, **33**, 1387–1392.
- 47 S. Wagner, D. Hauck, M. Hoffmann, R. Sommer, I. Joachim, R. Müller, A. Imberty, A. Varrot and A. Titz, *Angew. Chemie Int. Ed.*, 2017.
- 48 D. Tielker, S. Hacker, R. Loris, M. Strathmann, J. Wingender, S. Wilhelm, F. Rosenau and K.-E. Jaeger, *Microbiology*, 2005, **151**, 1313–1323.
- 49 I. Ofek and R. J. Doyle, in *Bacterial Adhesion to Cells and Tissues*, Springer US, Boston, MA, 1994, pp. 513–561.
- 50 J. J. Lundquist and E. J. Toone, *Chem. Rev.*, 2002, **102**, 555–578.
- 51 Y. C. Lee and R. T. Lee, *Acc. Chem. Res.*, 1995, **28**, 321–327.
- 52 N. C. Worstell, P. Krishnan, J. D. Weatherston and H. J. Wu, *PLoS One*, 2016, **11**, e0153265.
- 53 M. Gómez-García, J. M. Benito, R. Gutiérrez-Gallego, A. Maestre, C. O. Mellet, J. M. G. Fernández and J. L. J. Blanco, *Org. Biomol. Chem.*, 2010, **8**, 1849.
- 54 M. Gómez-García, J. M. Benito, A. P. Butera, C. Ortiz Mellet, J. M. García Fernández

- and J. L. Jiménez Blanco, *J. Org. Chem.*, 2012, **77**, 1273–88.
- 55 T. K. Dam, T. A. Gerken and C. F. Brewer, *Biochemistry*, 2009, **48**, 3822–3827.
- 56 I. Armentano, M. Dottori, E. Fortunati, S. Mattioli and J. M. Kenny, *Polym. Degrad. Stab.*, 2010, **95**, 2126–2146.
- 57 J. P. Santerre, K. Woodhouse, G. Laroche and R. S. Labow, *Biomaterials*, 2005, **26**, 7457–70.
- 58 J. C. Middleton and A. J. Tipton, *Biomaterials*, 2000, **21**, 2335–2346.
- 59 B. D. Ulery, L. S. Nair and C. T. Laurencin, *J. Polym. Sci. B. Polym. Phys.*, 2011, **49**, 832–864.
- 60 S. M. Ryan, G. Mantovani, X. Wang, D. M. Haddleton and D. J. Brayden, *Expert Opin. Drug Deliv.*, 2008, **5**, 371–83.
- 61 J. B. McLeary, F. M. Calitz, J. M. McKenzie, M. P. Tonge, R. D. Sanderson and B. Klumperman, *Macromolecules*, 2005, **38**, 3151–3161.
- 62 H. Willcock and R. K. O'Reilly, *Polym. Chem.*, 2010, **1**, 149-157.
- 63 S. G. Spain and N. R. Cameron, *Polym. Chem.*, 2011, **2**, 1552-1560.
- 64 Eric E. Simanek, Glenn J. McGarvey, and Jill A. Jablonowski and C.-H. Wong, *Chem. Rev.*, 1998, **98(2)**, 833-862
- 65 S. G. Spain and N. R. Cameron, *Polym. Chem.*, 2011, **2**, 1552.
- 66 M. Ambrosi, N. R. Cameron, B. G. Davis and S. Stolnik, *Org. Biomol. Chem.*, 2005, **3**, 1476.
- 67 J. I. Murata, Y. Ohya and T. Ouchi, *Carbohydr. Polym.*, 1996, **29**, 69–74.

- 68 W. Musiał and A. Kubis, *Polim. Med.*, 2005, **35**, 51–61.
- 69 Y. Miura, *Polym. J.*, 2012, **44**, 679–689.
- 70 S.-H. Kim, M. Goto, C.-S. Cho and T. Akaike, *Biotechnol. Lett.*, 2000, **22**, 1049–1057.
- 71 J. K. Suh and H. W. Matthew, *Biomaterials*, 2000, **21**, 2589–98.
- 72 Hitoshi Sashiwa, Jennifer M. Thompson, Sanjoy K. Das, Yoshihiro Shigemasa, and Sasmita Tripathy and René Roy, *Biomacromolecules*, 2000, **1(3)**, 303-305.
- 73 Vincent Ladmiral, Giuseppe Mantovani, Guy J. Clarkson, Solene Cauet, and Jacob L. Irwin and D. M. Haddleton, 2006, *JACS*, **128**, 4823-4830.
- 74 D. A. Fulton, *Org. Lett.*, 2008, **10**, 3291–3294.
- 75 C. S. Mahon and D. A. Fulton, *Nat. Chem.*, 2014, **6**, 665–672.
- 76 C. S. Mahon, M. A. Fascione, C. Sakonsinsiri, T. E. McAllister, W. Bruce Turnbull and D. A. Fulton, *Org. Biomol. Chem.*, 2015, **13**, 2756–2761.
- 77 L. Dykman and N. Khlebtsov, *Chem. Soc. Rev.*, 2012, **41**, 2256–2282.
- 78 A. L. Parry, N. A. Clemson, J. Ellis, S. S. R. Bernhard, B. G. Davis and N. R. Cameron, *J. Am. Chem. Soc.*, 2013, **135**, 9362–9365.
- 79 A. K. Adak, H.-J. Lin and C.-C. Lin, *Org. Biomol. Chem.*, 2014, **12**, 5563–5573.
- 80 S. M. Janib, A. S. Moses and J. A. MacKay, *Adv. Drug Deliv. Rev.*, 2010, **62**, 1052–1063.
- 81 M. E. Davis, Z. (Georgia) Chen and D. M. Shin, *Nat. Rev. Drug Discov.*, 2008, **7**, 771–782.

- 82 C. J. Cheng, G. T. Tietjen, J. K. Saucier-Sawyer and W. M. Saltzman, *Nat. Rev. Drug Discov.*, 2015, **14**, 239–247.
- 83 J. B. Hall, M. A. Dobrovolskaia, A. K. Patri and S. E. McNeil, *Nanomedicine*, 2007, **2**, 789–803.
- 84 A. M. Gobin, M. H. Lee, N. J. Halas, W. D. James, R. A. Drezek and J. L. West, *Nano Lett.*, 2007, **7**, 1929–1934.
- 85 K. Sokolov, M. Follen, J. Aaron, I. Pavlova, A. Malpica, R. Lotan and R. Richards-Kortum, *Cancer Res.*, 2003, **63**, 1999–2004.
- 86 C.-H. Lee, S.-H. Cheng, Y.-J. Wang, Y.-C. Chen, N.-T. Chen, J. Souris, C.-T. Chen, C.-Y. Mou, C.-S. Yang and L.-W. Lo, *Adv. Funct. Mater.*, 2009, **19**, 215–222 .
- 87 A. M. Coto-García, E. Sotelo-González, M. T. Fernández-Argüelles, R. Pereiro, J. M. Costa-Fernández and A. Sanz-Medel, *Anal. Bioanal. Chem.*, 2011, **399**, 29–42.
- 88 J.-L. Coll, *Nanomedicine (Lond.)*, 2011, **6**, 7–10.
- 89 E. Valero, S. Tambalo, P. Marzola, M. Ortega-Muñoz, F. J. López-Jaramillo, F. Santoyo-González, J. De Dios López, J. J. Delgado, J. J. Calvino, R. Cuesta, J. M. Domínguez-Vera and N. Gálvez, *J. Am. Chem. Soc.*, 2011, **133**, 4889–4895.
- 90 S. Heydarnezhadi, N. Riyahi-Alam, S. Haghoo, M. Khobi, B. Nikfar, E. Gorji and B. Rafiei, *IFMBE Proceedings*, Springer, Cham, 2015, 119–122.
- 91 B. Mehraei, M. Ahmadi, M. Amanlou, A. Mostaar, M. S. Ardestani and N. Ghalandarlaki, *Int. J. Nanomedicine*, 2013, **8**, 3209–3216.
- 92 R. Chakravarty, S. Goel, H. Hong, F. Chen, H. F. Valdovinos, R. Hernandez, T. E. Barnhart and W. Cai, *Nanomedicine*, 2015, **10**, 1233–1246.

- 93 M. K. Yu, J. Park and S. Jon, *Theranostics*, 2012, **2**, 3–44.
- 94 O. Keinänen, E. M. Mäkilä, R. Lindgren, H. Virtanen, H. Liljenbäck, V. Oikonen, M. Sarparanta, C. Molthoff, A. D. Windhorst, A. Roivainen, J. J. Salonen and A. J. Airaksinen, *ACS Omega*, 2017, **2**, 62–69.
- 95 O. Rabin, J. Manuel Perez, J. Grimm, G. Wojtkiewicz and R. Weissleder, *Nat. Mater.*, 2006, **5**, 118–122.
- 96 T. Reuveni, M. Motiei, Z. Romman, A. Popovtzer and R. Popovtzer, *Int. J. Nanomedicine*, 2011, **6**, 2859–2864.
- 97 I. Rosenberger, A. Strauss, S. Dobiasch, C. Weis, S. Szanyi, L. Gil-Iceta, E. Alonso, M. González Esparza, V. Gómez-Vallejo, B. Szczupak, S. Plaza-García, S. Mirzaei, L. L. Israel, S. Bianchessi, E. Scanziani, J. P. Lellouche, P. Knoll, J. Werner, K. Felix, L. Grenacher, T. Reese, J. Kreuter and M. Jiménez-González, *J. Control. Release*, 2015, **214**, 76–84.
- 98 X. Huang and M. A. El-Sayed, *J. Adv. Res.*, 2010, **1**, 13–28.
- 99 M. I. Gibson, M. Danial and H.-A. Klok, *ACS Comb. Sci.*, 2011, **13**, 286–97.
- 100 S.-J. Richards, L. Otten and M. I. Gibson, *J. Mater. Chem. B*, 2016, **4**, 3046–3053.
- 101 V. Berry and R. F. Saraf, *Angew. Chemie Int. Ed.*, 2005, **44**, 6668–6673.
- 102 M.-C. Daniel and D. Astruc, *Chem. Rev.*, 2004, **104**, 293–346.
- 103 P. K. Jain, K. S. Lee, I. H. El-Sayed and M. A. El-Sayed, *J. Phys. Chem. B*, 2006, **110**, 7238–48.
- 104 W. Haiss, N. T. K. Thanh, J. Aveyard and D. G. Fernig, *Anal. Chem.*, 2007, **79**, 4215–

- 21.
- 105 S. Link and M. A. El-Sayed, *J. Phys. Chem. B*, 1999, **103**, 4212–4217.
- 106 T. K. Dam and C. F. Brewer, *Glycobiology*, 2010, **20**, 270–279.
- 107 C. A. Mirkin, R. L. Letsinger, R. C. Mucic and J. J. Storhoff, *Nature*, 1996, **382**, 607–609.
- 108 J. H. W. Leuvering, P. J. H. M. Thal, M. van der Waart and A. H. W. M. Schuurs, *J. Immunoassay*, 1980, **1**, 77–91.
- 109 G. J. Nusz, S. M. Marinakos, A. C. Curry, A. Dahlin, F. Hook, A. Wax and A. Chilkoti, *Anal. Chem.*, 2008, **80**, 984–989.
- 110 J. E. Ghadiali and M. M. Stevens, *Adv. Mater.*, 2008, **20**, 4359–4363.
- 111 Anna Laromaine, Liling Koh, Muthu Murugesan, A. Rein V. Ulijn, and Molly M. Stevens, *J. Am. Chem. Soc.*, 2007, **129**, 4156–4157.
- 112 P. Englebienne, *Analyst*, 1998, **123**, 1599–1603.
- 113 A. J. Haes, L. Chang, W. L. Klein and R. P. Van Duyne, *J. Am. Chem. Soc.*, 2005, **127**, 2264–2271.
- 114 S. H. Huang, *Sensors Actuators, B Chem.*, 2007, **127**, 335–340.
- 115 K. M. Mayer, S. Lee, H. Liao, B. C. Rostro, A. Fuentes, P. T. Scully, C. L. Nehl and J. H. Hafner, *ACS Nano*, 2008, **2**, 687–692.
- 116 A. K. Singh, D. Senapati, S. Wang, J. Griffin, A. Neely, P. Candice, K. M. Naylor, B. Varisli, J. R. Kalluri and P. C. Ray, *ACS Nano*, 2009, **3**, 1906–1912.
- 117 P. V. Baptista, M. Koziol-Montewka, J. Paluch-Oles, G. Doria and R. Franco, *Clin.*

- Chem.*, 2006, 52, 1433–1434.
- 118 R. Elghanian, J. J. Storhoff, R. C. Mucic, R. L. Letsinger and C. A. Mirkin, *Science*, 1997, **277**, 1078–81.
- 119 S.-J. Richards, E. Fullam, G. S. Besra and M. I. Gibson, *J. Mater. Chem. B*, 2014, **2**, 1490–1498.
- 120 S.-J. Richards and M. I. Gibson, *ACS Macro Lett.*, 2014, **3**, 1004–1008.
- 121 S.-J. Richards, L. Otten and M. I. Gibson, *J. Mater. Chem. B*, 2016, **4**, 3046–3053.
- 122 L. Otten, D. Vlachou, S.-J. Richards and M. I. Gibson, *Analyst*, 2016, **141**, 4305–4312.
- 123 S. Won, S.-J. Richards, M. Walker and M. I. Gibson, *Nanoscale Horiz.*, 2017, **3**, 1593–1608.
- 124 C. Freese, L. Anspach, R. C. Deller, S.-J. Richards, M. I. Gibson, C. J. Kirkpatrick and R. E. Unger, *Biomater. Sci.*, 2017, **5**, 707–717.
- 125 J. E. Turnbull and R. A. Field, *Nat. Chem. Biol.*, 2007, **3**, 74–77.
- 126 N. Laurent, J. Voglmeir and S. L. Flitsch, *Chem. Commun.*, 2008, **0**, 4400–4412.
- 127 I. M. Dobbie, N. F. Lowndes and K. F. Sullivan, in *Methods in cell biology*, 2008, **85**, 1–22.
- 128 J. A. Prescher and C. R. Bertozzi, *Cell*, 2006, **126**, 851–854.
- 129 S. Carlsson, M. C. Carlsson and H. Leffler, *Glycobiology*, 2007, **17**, 906–912.
- 130 A. R. Lizzi, A. M. D’Alessandro, A. Bozzi, B. Cinque, A. Oratore and G. D’Andrea, *Mol. Cell. Biochem.*, 2007, **300**, 29–37.

- 131 H. Ohba and R. Bakalova, *Cancer Chemother. Pharmacol.*, **51**, 451–458.
- 132 R. E. Schwarz, D. C. Wojciechowicz, A. I. Picon, M. A. Schwarz and P. B. Paty, *Br. J. Cancer*, 1999, **80**, 1754–1762.
- 133 E. M. Sletten and C. R. Bertozzi, *Angew. Chem. Int. Ed. Engl.*, 2009, **48**, 6974–98.
- 134 L. Feng, S. Hong, J. Rong, Q. You, P. Dai, R. Huang, Y. Tan, W. Hong, C. Xie, J. Zhao and X. Chen, *J. Am. Chem. Soc.*, 2013, **135**, 9244–9247.
- 135 J. Thorner, S. D. Emr, J. N. Abelson, C. L. Jacobs, K. J. Yarema, L. K. Mahal, D. A. Nauman, N. W. Charters and C. R. Bertozzi, *Metabolic labeling of glycoproteins with chemical tags through unnatural sialic acid biosynthesis*, 2000, vol. 327.
- 136 S. T. Laughlin and C. R. Bertozzi, *Nat. Protoc.*, 2007, **2**, 2930–44.
- 137 T.-L. Hsu, S. R. Hanson, K. Kishikawa, S.-K. Wang, M. Sawa and C.-H. Wong, *Proc. Natl. Acad. Sci. U. S. A.*, 2007, **104**, 2614–9.
- 138 C. R. Bertozzi and M. D. Bednarski, *Tetrahedron Lett.*, 1992, **33**, 3109–3112.
- 139 M. A. Breidenbach, J. E. G. Gallagher, D. S. King, B. P. Smart, P. Wu and C. R. Bertozzi, *Proc. Natl. Acad. Sci. U. S. A.*, 2010, **107**, 3988–93.
- 140 J. Du, M. A. Meledeo, Z. Wang, H. S. Khanna, V. D. P. Paruchuri and K. J. Yarema, *Glycobiology*, 2009, **19**, 1382–401.
- 141 H. C. Hang, C. Yu, D. L. Kato and C. R. Bertozzi, *Proc. Natl. Acad. Sci. U. S. A.*, 2003, **100**, 14846–51.
- 142 N. E. Zachara, K. Vosseller and G. W. Hart, *Curr. Protoc. Mol. Biol.*, 2011, **Chapter 17**, Unit 17.6.

- 143 B. Belardi, G. P. O'Donoghue, A. W. Smith, J. T. Groves and C. R. Bertozzi, 2012.
- 144 J. M. Baskin, K. W. Dehnert, S. T. Laughlin, S. L. Amacher and C. R. Bertozzi, *Proc. Natl. Acad. Sci. U. S. A.*, 2010, **107**, 10360–5.
- 145 S. T. Laughlin, J. M. Baskin, S. L. Amacher and C. R. Bertozzi, *Science*, 2008, **320**, 664–7.
- 146 K. W. Dehnert, J. M. Baskin, S. T. Laughlin, B. J. Beahm, N. N. Naidu, S. L. Amacher and C. R. Bertozzi, *Chembiochem*, 2012, **13**, 353–7.
- 147 K. W. Dehnert, B. J. Beahm, T. T. Huynh, J. M. Baskin, S. T. Laughlin, W. Wang, P. Wu, S. L. Amacher and C. R. Bertozzi, *ACS Chem. Biol.*, 2011, **6**, 547–52.
- 148 S. T. Laughlin and C. R. Bertozzi, *Proc. Natl. Acad. Sci. U. S. A.*, 2009, **106**, 12–7.
- 149 S. S. Pinho and C. A. Reis, *Nat. Rev. Cancer*, 2015, **15**, 540–555.
- 150 K. Fukase and K. Tanaka, *Curr. Opin. Chem. Biol.*, 2012, **16**, 614–621.
- 151 M. V. Croce, M. T. Isla-Larrain, S. O. Demichelis, A. Segal-Eiras, J. R. Gori and M. R. Price, *Breast Cancer Res. Treat.*, 2003, **81**, 195–207.
- 152 S. Schedin-Weiss, B. Winblad and L. O. Tjernberg, *FEBS J.*, 2014, **281**, 46–62.
- 153 L. A. Robertson, K. L. Moya and K. C. Breen, *J. Alzheimers. Dis.*, 2004, **6**, 489–95.
- 154 G. Lauc, M. Pezer, I. Rudan and H. Campbell, *Biochim. Biophys. Acta - Gen. Subj.*, 2016, **1860**, 1574–1582.
- 155 M. Cova, J. A. Rodrigues, T. K. Smith and L. Izquierdo, *Malar. J.*, 2015, **14**, 427.

Chapter Two

Heterogeneous Glycopolymers to Target Bacterial Toxins

Declarations

The work submitted in this chapter was performed by myself, except for NMR DOSY experiments which were performed by Dr. Ivan Prokes

2.1. Abstract

The incorporation of ‘non-binding’ sugars into low density glycopolymers is found to enhance both avidity and inhibitory activity against toxins, despite seeming counter-intuitive. A library of homogenous and heterogeneous glycopolymers were synthesised by a three-step post-polymerisation modification process, with a final copper-free ‘click’ conjugation. Inhibitory assays showed it was possible to inhibit ricin over cholera toxin. Detailed analysis using biolayer interferometry assessed avidity and also rates of binding. This demonstrated binding towards cholera toxin did in fact occur and highlighted the need for multiple analytical techniques when investigating multivalent binding. The findings demonstrate that mimicking the natural display of heterogeneous, or branched, glycans is a powerful, yet simple, tool to improve the function of glycomimetics.

2.2. Introduction

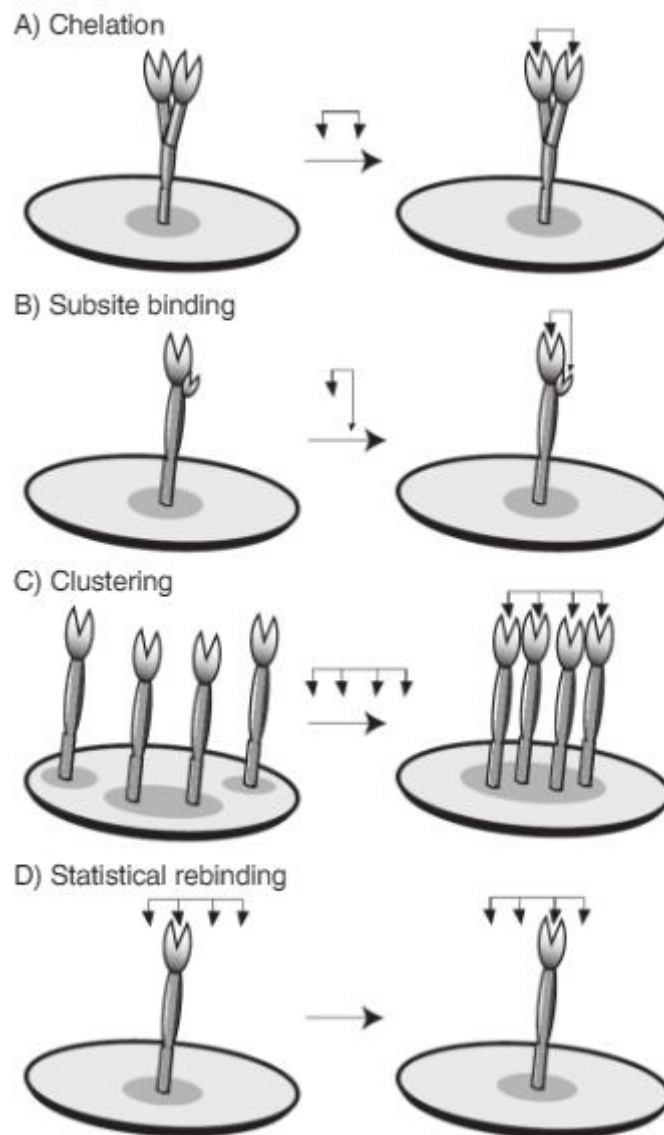
Many pathogenic bacteria secrete toxins as their primary mode of pathogenicity, including *E. coli* O-157 shiga toxins (the cause of food poisoning) and the toxin from *Vibrio cholerae* (cholera).¹⁻⁴ Plant toxins can also cause significant harm, such as Ricin (from *Ricinus communis*) which has a lethal dose of $\sim 20 \mu\text{g.Kg}^{-1}$ and is more toxic than cyanide.⁵ A common feature is that these proteins contain a carbohydrate binding domain to hijack host cell-surface glycans and gain entry. Carbohydrate-protein interactions mediate a huge range of recognition/signalling events including inflammation⁶, immune-responses⁷ and cell-cell signalling.⁸ The ‘reader’ proteins that mediate these interactions are known as lectins, which typically have very weak binding affinities (mM).⁹ Nature therefore presents multiple copies of each glycan, giving a non-linear increase in affinity, known as “the cluster glycoside effect”.^{10,11} This has inspired the use of glyco-materials, such as polymers or particles, which use polyvalent presentation of carbohydrates to enhance affinity.^{12,13} This enhanced affinity offers a route to prophylactic anti-adhesion therapies against pathogens/toxins as an alternative to traditional antibiotics or small molecule drugs.¹⁴ ‘Starfish’ glyco-dendrimers have 10^6 fold enhanced activity against shiga toxins compared to the free glycan,¹⁵ linear poly(mannose) is a nM inhibitor of DC-Sign/GP120 interactions,¹⁶ and inhibition of the Ebola virus by a 120-valent mannose glycofullerene cluster has been observed.¹⁷ High affinity sialic acid glycopolymer arrays have been used by Godula and coworkers to dissect how influenza engages with its host.¹⁸ Whilst these multivalent systems all show high avidity, they typically present monosaccharides and hence do not have high specificity.

Glycopolymers have been developed by Kiick *et al.*, and Gibson *et al.*, with high avidity for the cholera toxin by modulation of the linker length to match the binding pocket depth, increasing avidity without additional synthetic complexity.^{19,20} In addition to the chemical

complexity of oligosaccharides, cell surfaces are heterogeneous and dynamically display many different glycans.²¹ Evidence is emerging that these ‘*non-binding*’ glycans play a key role in the overall avidity, and that reproduction of this heterogeneity in glycomaterials can enhance avidity towards inhibitory targets.²² Percec *et al.* have introduced non-binding units into amphiphilic Janus-glycodendrimers resulting in a 12-fold increase in agglutination activity for the particles.²³ Wu *et al.* reported that cholera toxin has increased binding capacity towards heterogeneous mixtures of GM-2 and fucosyl-GM-1, despite homogenous GM-2 having far lower binding affinity compared to homogenous fucosyl GM-1.

This was reported to be due to an increased cooperativity of the system. The fucosyl GM-1 activates the CtxB protein towards binding GM-2, which alone effectively does not bind. Fucosyl-GM-1 caused less cooperativity compared to the native GM-1 ligand, however this counter intuitively lead to a higher binding capacity²⁴ Multivalency is also observed to result in changed binding affinities compared to monovalent systems. Richards *et al.* have reported that mannosylated gold nanoparticles have affinity towards communis agglutinin 120 (RCA₁₂₀), a non-toxic derivative of ricin, despite the monosaccharides having little or no affinity.²⁵

The extreme variation observed in glycan binding is a direct result of the variation in the modes of multivalent binding to varied receptors. Multivalent ligands bind to receptors in multiple ways that do not apply to monovalent binders. Figure 2.1 shows the different modes of binding that apply to multivalent binding.



From L. L. Kiessling, J. E. Gestwicki, L.E. Strong, *Angew. Chem. Int. Ed.*, **2006**, 4, 2348-68. Reprinted with permission from John Wiley and sons.

Figure 2.1: Receptor binding mechanisms that are unique to multivalent ligands. (A) The chelation of a multi-dentate ligand to two equal and independent receptor sites. (B) Subsite binding whereby either a secondary binding ligand or a part of the multivalent scaffold can reach a secondary binding domain that would be impossible for a monovalent ligand to reach. (C) The clustering of receptors by binding to multiple independent and equal receptors

simultaneously. (D) The statistical rebinding of a multivalent ligand with a single receptor due to increased proximity to the binding domain and a neutral entropic penalty.^{26,27}

The variety of interactions possible between multivalent ligands and their receptors therefore complicates the process of accurately describing and quantifying the strength of the interactions. It has become commonly accepted that the strength of the interaction between a single ligand and receptor is known as the affinity, while the overall strength of the interaction between a multivalent ligand and receptor is the avidity. Both affinity and avidity are described by the association constant K_a or, more commonly the dissociation constant K_d (equal to K_a^{-1}). While end-point assays are typically employed to determine the dissociation constant, a truer picture of the nature of binding can be obtained, by measuring both the rates of association and dissociation of the ligand-receptor complex. One method of directly measuring these quantities is biolayer interferometry (BLI).

Biolayer interferometry is a technique analogous to surface plasmon resonance (SPR) assays that allows for the direct observation of both the association and dissociation rate constants for binding events. It works by shining white light down a glass tip with a partially reflective surface at the end, Figure 2.2A, any change to the optical thickness of the bound layer at the tips surface will result in a shift in the interference pattern observed between the two reflected light sources, Figure 2.2B.

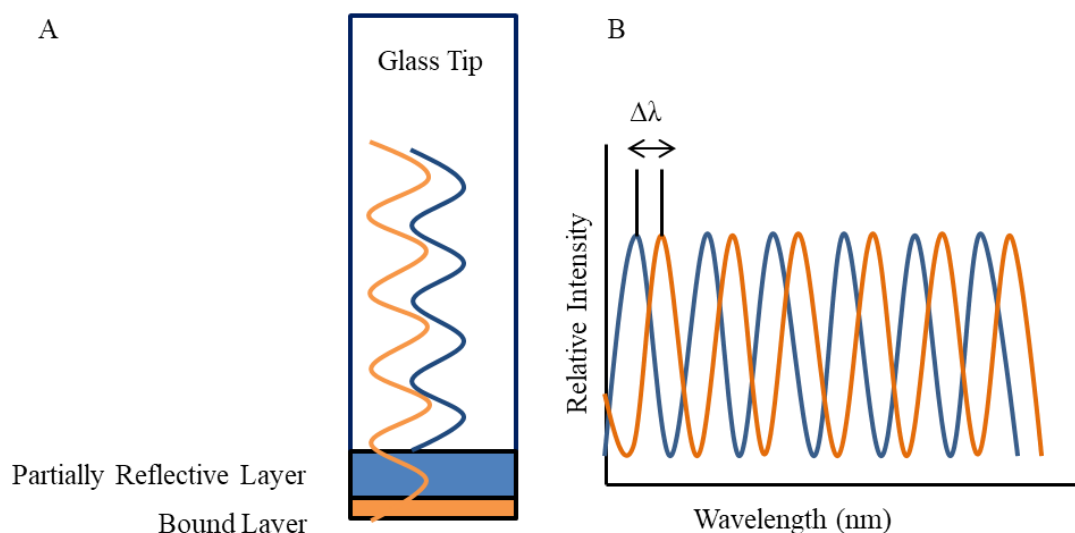


Figure 2.2: (A) Diagram representing a BLI sensor, showing the light source reflected from the partially reflective tip end (blue) and the bound layer (orange) (B) Graph showing the shift in wavelength ($\Delta\lambda$) between the two reflected sources.

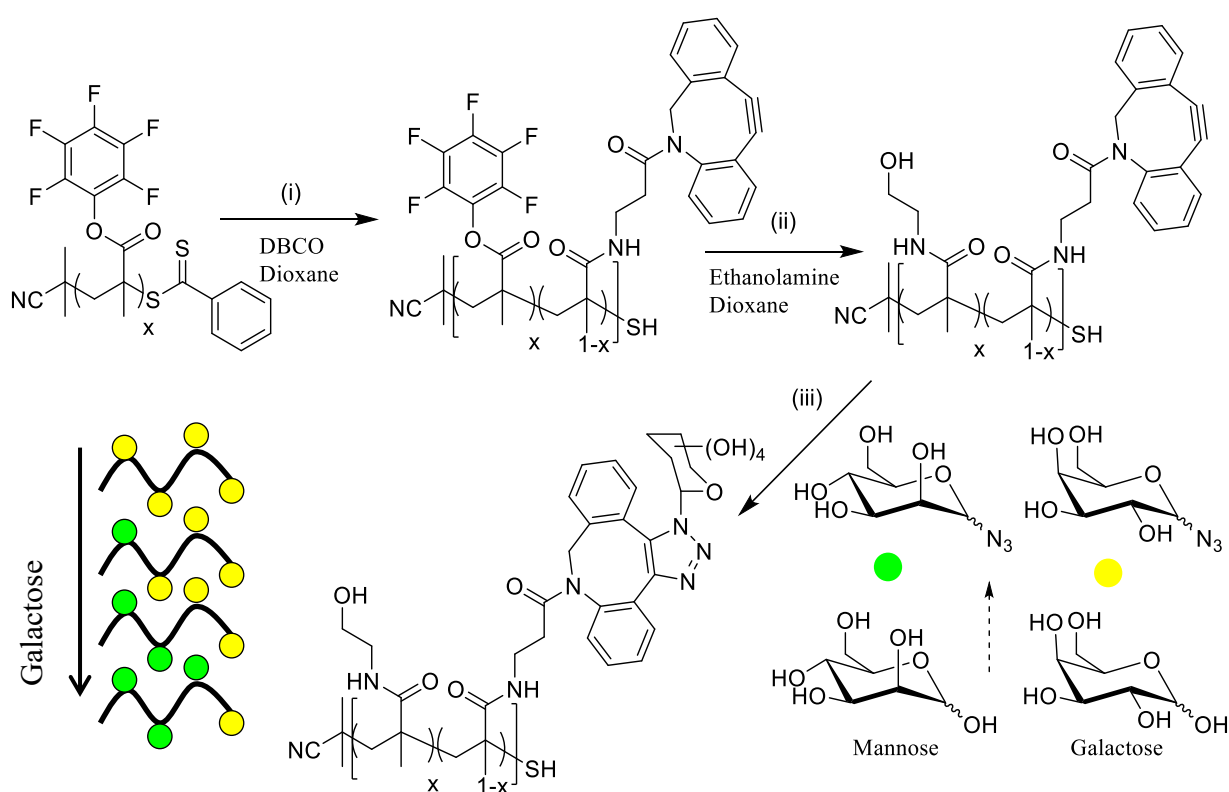
$\Delta\lambda$ can therefore be directly linked to amount of bound analyte to the tip surface. By utilising chemically reactive tips for the immobilisation of proteins onto the tip surface, protein binding interactions can be directly observed. By plotting the size of the bound layer with time, values for the rate constants can be extracted. This is discussed in more detail later. BLI has several advantages as a technique; it allows real-time, label-free detection in a high throughput manner and is relatively insensitive to pH, solvent, and any changes to the refractive index of the sample.

Considering the above, the aim of this work was to probe the effect of mixing ‘non-binding’ with ‘binding’ carbohydrates on a single multivalent scaffold using both an assay to screen for inhibition, and BLI to investigate the binding affinity, to screen for the next generation of glycomaterials.

2.3. Results and Discussion

2.3.1. Synthesis of Glycopolymers

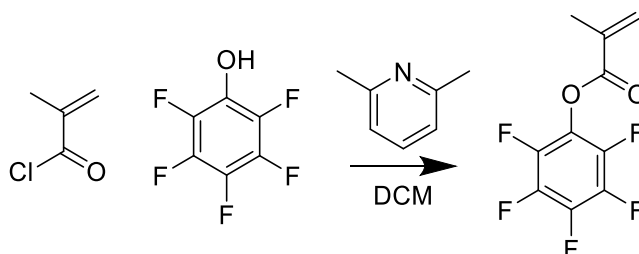
To access heterogeneous glycopolymers, a three step sequential post-polymerization modification strategy was developed, Scheme 2.1.



Scheme 2.1: Synthesis of heterogeneous glycopolymers. (i) DBCO (0.3 eq, Dioxane, 16 hours 50°C) (ii) Ethanolamine (3 eq, dioxane, 16 hours 50°C); (iii) Sugar-N₃ (2.5 eq, DMF, 16 hours, room temperature).

The method ensured that only a single reactive monomer (pentafluorophenyl methacrylate, PFMA)²⁰ needs to be polymerised, and avoids the issue of copolymer reactivity ratios. PFMA

was synthesised using a previously reported protocol²⁸, through the reaction of PFP with methacroyl chloride, Scheme 2.2.



Scheme 2.2: Synthesis of PFPMA.

PFPMA was characterised by ¹H and ¹³C NMR, IR spectroscopies and mass spectrometry, before being polymerised using 4,4'-azobis(4-cyanovaleric acid) (AVCA) as the initiator and 2-cyano-2-propyl benzodithioate as the RAFT agent. 2-Cyano-2-propyl benzodithioate gives reasonable control over methacrylates. A poly(pentafluorophenol methacrylate) master polymer with M_n=8900 was obtained. Figure 2.3.

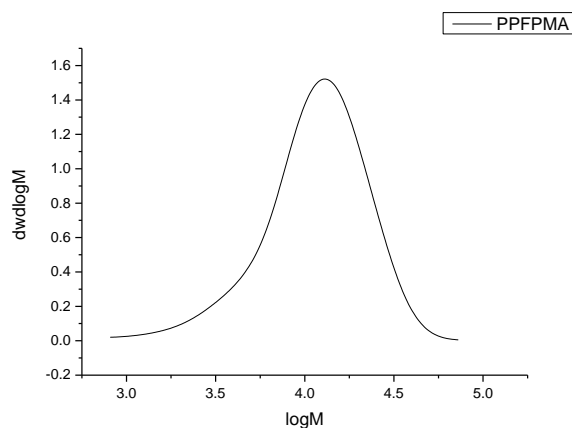


Figure 2.3: SEC trace of master PFPMA polymer.

The dispersity was higher than expected due to the elution behaviour of the PFPMA in SEC, but the use of a 'master batch' means the actual dispersity is not crucial here as all further

polymers synthesised will be equivalent.²⁹ ^{19}F NMR and IR spectroscopy confirmed that the PFP group was retained during polymerisation, Figure 2.4.

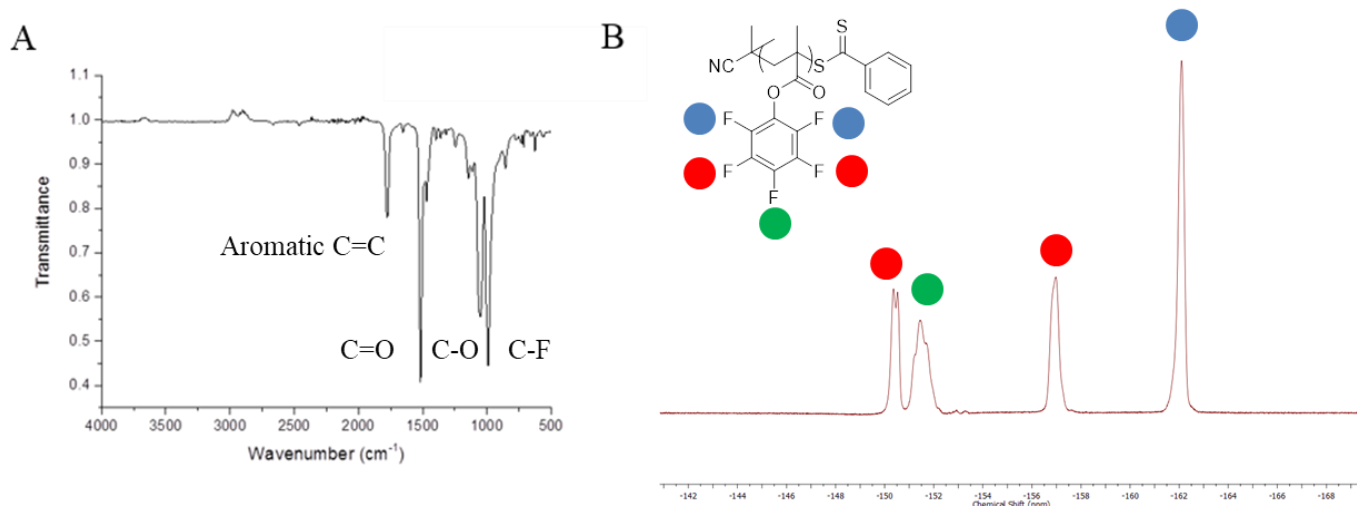


Figure 2.4: (A) IR of P(PFPMA) showing C-F halide bond 950 cm^{-1} (B) ^{19}F NMR spectrum.

The PFP group was displaced by addition of 30 mol % of dibenzocyclooctyne-amine (DBCO) followed by excess ethanolamine to generate a water soluble, copper-free ‘clickable’ template polymer.³⁰ DBCO incorporation was confirmed by observing the changes to the ^{19}F NMR spectrum, Figure 2.5A. The integral ratios of free PFP to polymer conjugated PFP in the crude reaction mixture (Red) showed 30% displacement, while after addition of ethanolamine 100% displacement was observed (Green). Inclusion of DBCO was also confirmed via diffusion ordered spectroscopy (DOSY) NMR spectroscopy, Figure 2.5B, and Raman spectroscopy 2.5C.

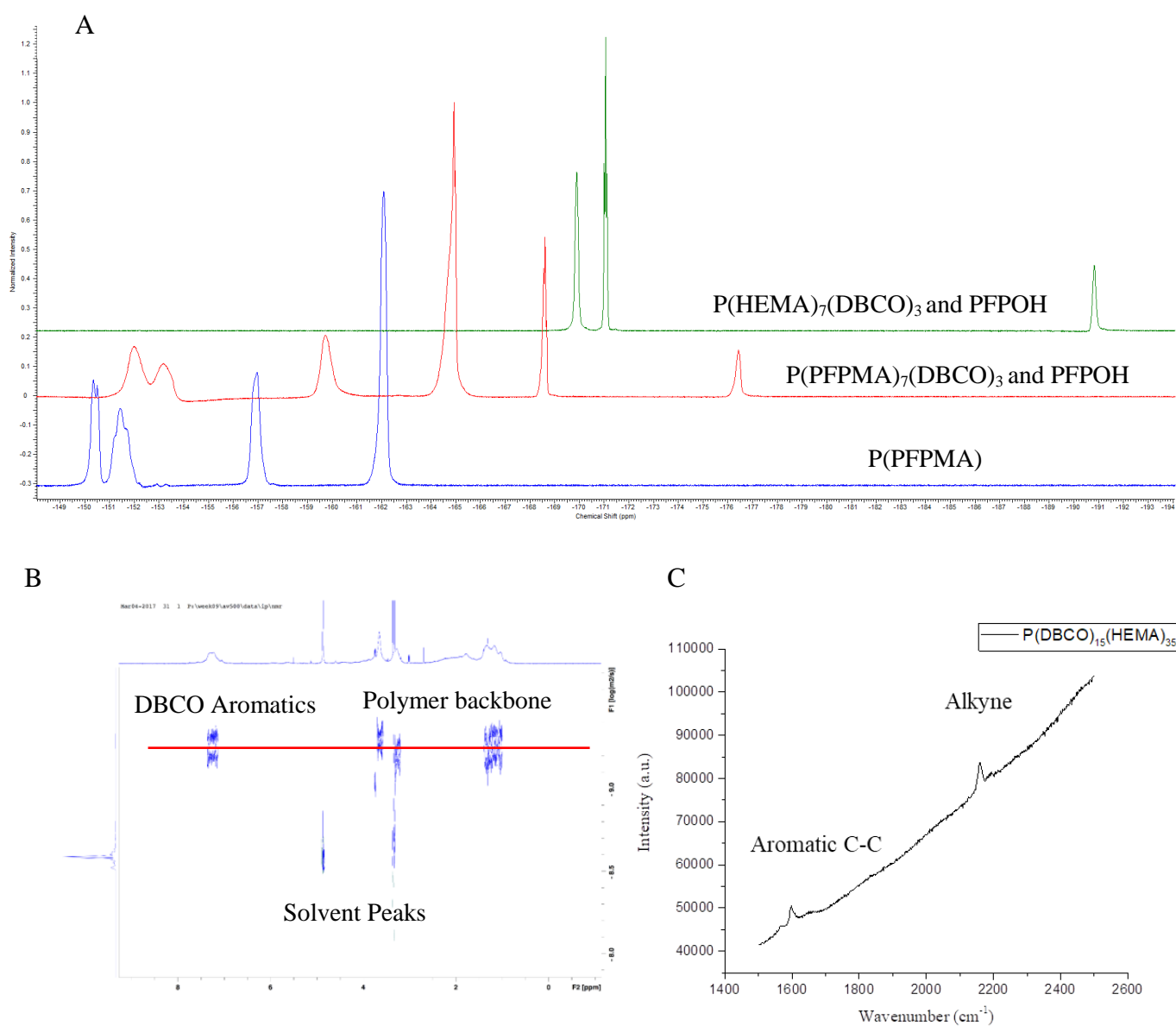
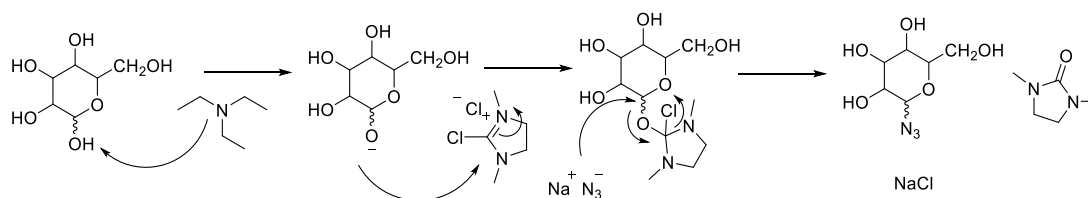


Figure 2.5: (A) ^{19}F NMR showing two step reaction of PPFMA (blue), DBCO functionalisation to 30 % (red) then following quenching with ethanolamine (green). (B) DOSY NMR, showing aromatic peaks (7.5ppm) at the same diffusional co-efficient of $-9.25 \log(\text{m}^2\text{s}^{-1})$, as polymer backbone peaks, marked by red line. (C) Raman spectra showing aromatic C-C and alkyne peaks.

With this reactive precursor to hand, 1-azido-1-deoxy- β -D-galactose (GalN₃) and 1-azido-1-deoxy- α -D-mannose (ManN₃) were synthesised using 2-chloro-1,3-dimethylimidazolium chloride to activate the anomeric position towards nucleophilic attack from the azide anion, as per a previously reported procedure, Scheme 2.3³¹



Scheme 2.3: Synthesis and mechanism of 1-azido-1-deoxy hexoses

The resulting 1-azido-1-deoxy hexoses were characterised by ¹H and ¹³C NMR spectroscopy, mass spectrometry, and the inclusion of the azide group was confirmed by infrared spectroscopy, Figure 2.7. To obtain heterogeneous, galactose-rich polymers, GalN₃ and ManN₃ were mixed in the indicated ratios and then applied to the ‘clickable’ polymer such that the overall ratio [alkyne]:[N₃] was 1:2.5, Table 2.1.

Table 2.1. Polymers synthesised.

Polymer	Conversion(%) ^(a)	M _{theoretical}	M _n (g.mol ⁻¹)	M _w /M _n ^(a)	Gal ^(c)	Gal ^(c)	Man ^(c)
					(%)		
PPFPMA	62	11600	8900 ^(a)	1.7	-	-	-
PG₂₅M₇₅	-	12900	12900 ^(b)	-	25	4	11
PG₅₀M₅₀	-	12900	12900 ^(b)	-	50	7.5	7.5
PG₇₅M₂₅	-	12900	12900 ^(b)	-	75	11	4
PG₁₀₀	-	12900	12900 ^(b)	-	100	15	0

(a) Determined by NMR relative to mesitylene reference (b) Determined by SEC (DMF);(c)

From feed ratio of glycosyl azides; (d) sugars/chain.

A mannose-negative control was also synthesised to ensure that any binding effects observed were not simply due to density effects of galactose on the polymer chains. To generate an analogous homogenous polymer library, another master PPFMA polymer was synthesised with the same degree of polymerisation and molecular weight, confirmed by SEC. Three polymers were then synthesised targeting 7.5%, 15%, 22.5% displacement of PFP with DBCO-amine to obtain polymers with 4, 8, and, 12 cyclooctyne moieties and subsequently quenched with ethanolamine. Integrating the relative peaks of pentafluorophenol ester and free pentafluorophenol as before gives the percentage DBCO-amine substitution. A fourth polymer was substituted only with ethanolamine to give poly(hydroxyethyl methacrylamide) with identical molecular weight and dispersity as the glycopolymers, Figure 2.6. The results are summarised in Table 2.2

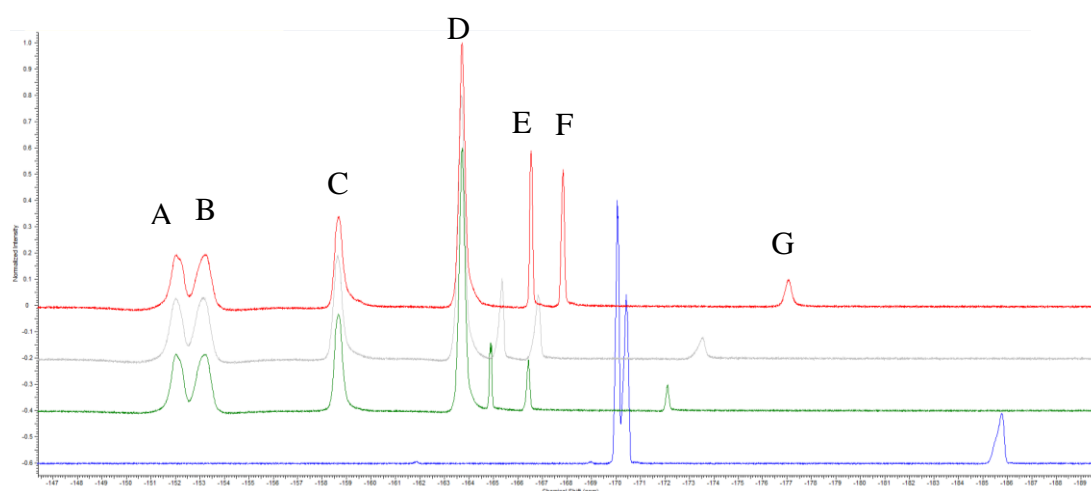


Figure 2.6: ¹⁹F NMR of PG₇₅ (red) PG₅₀ (grey) PG₂₅ (green) and HEMA (blue) post addition of DBCO (or ethanolamine for HEMA control). Peaks A, B, C, and D relate to fluorine atoms in the polymer repeat unit while peaks E, F and G relate to fluorine atoms in solvated pentafluorophenol.

Table 2.2: Summary of the DBCO-substitution of P(PFPMA).

Polymer	Target	Alkyne	Calculated	Alkyne	M_n	M_w/M_n^(a)	Gal^(b)
	Substitution		Substitution		(g.mol⁻¹)	(-)	(-)
P(HEMA)	100%		100%		8700	1.6	0
PG₂₅	7.5%		9.7%		8700		4.85
PG₅₀	15%		16%		8700		8
PG₇₅	22.5%		21.42%		8700		10.71

(a) Determined by SEC (DMF); (b) sugars/chain.

The inclusion of the azido-sugars was confirmed *via* infra-red spectroscopy using the disappearance of the azide associated peak in the purified glyco-polymers, Figure 2.7. Raman spectroscopy also indicated the lack of alkyne peak in the purified polymer.

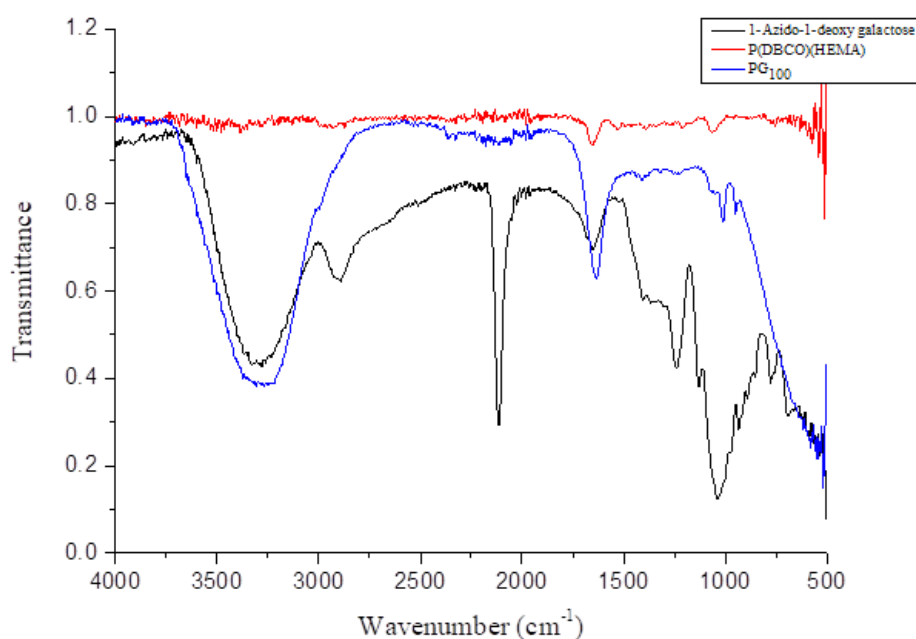


Figure 2.7: Infrared spectrum of 1-azido-1-deoxy galactose (black), P(DBCO)₁₅(HEMA)₃₅ (red) and PGal₁₀₀ (blue) showing the disappearance of the azide stretch at 2100cm⁻¹.

2.3.2. Competitive binding assay to determine inhibition

This panel of low density, heterogeneous and homogenous, glycopolymers were subsequently screened for inhibitory activity against cholera toxin B-subunit (CTxB) and *Ricinus communis agglutinin* 120 (RCA₁₂₀), a substitute for the biological warfare agent Ricin. CTxB is the pentameric subunit responsible for cell surface binding and subsequent internalisation, Figure 2.8A. The diameter of CTxB is approximately 60 Å³² with approximately 30 Å between binding domains (measured with Jmol using the protein data bank file (PDB) 1JR0). RCA₁₂₀ has two identical binding sites³³ that are 110 Å apart, Figure 2.8B. ^{34,35}

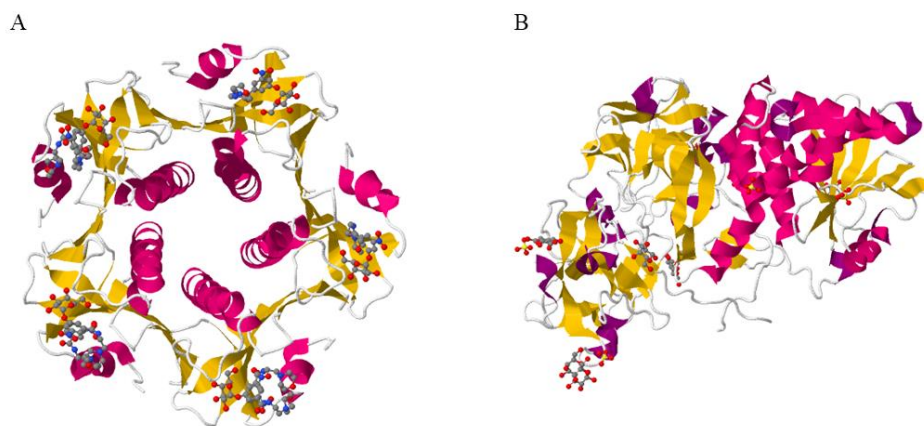


Figure 2.8: (A) The CtxB pentamer from PDB file 1JR0³⁶ (B) RCA₁₂₀ lectin from PDB file 1RZO.³⁷

By assuming a carbon-carbon bond length of 1.54 Å and a dihedral bond angle of 109.5° we can calculate an estimate for the maximum chain length of our DP50 polymers as 125.75 Å and therefore the average galactose spacing for each polymer is shown in Table 2.3.

Table 2.3: Table showing average galactose spacing for each polymer.

Polymer	Average Spacing between Galactose (Å)	Average Spacing between Sugars (Å)
P(HEMA)	N/A	N/A
PG₂₅	31.4	31.4
PG₅₀	15.7	15.7
PG₇₅	10.5	10.5
PG₂₅M₇₅	31.4	8.4
PG₅₀M₅₀	15.7	8.4
PG₇₅M₂₅	10.5	8.4
PG₁₀₀	8.4	8.4

These estimates for the average sugar spacing will not be representative of the conformation of the polymers in solution. They do, however, provide us with estimation for the physical spacing of the sugars, and even at the lowest density of galactose, the average spacing between sugars is sufficient to bridge the gap between binding sites for CTxB. However for RCA₁₂₀ the average spacing of the galactose moieties are far too small to bridge the distance between RCA₁₂₀ binding sites (110Å³⁵). While the entire polymer is large enough that sugars at either end of the polymer chain have the potential to span the binding sites; it is more likely

that we will be operating in a statistical rebinding regime with only one polymeric ligand per lectin binding site.

To generate a 'competitive' surface to perform the assay with, lipid coated "high-bind" 384-well plates were incubated for 16 hours with 1 mg.mL^{-1} of the galactose rich GM-1 ganglioside, the native ligand for CTxB, Figure 2.9. This allowed the GM-1 ganglioside to undergo lipid insertion and become bound to the 384-well surface.

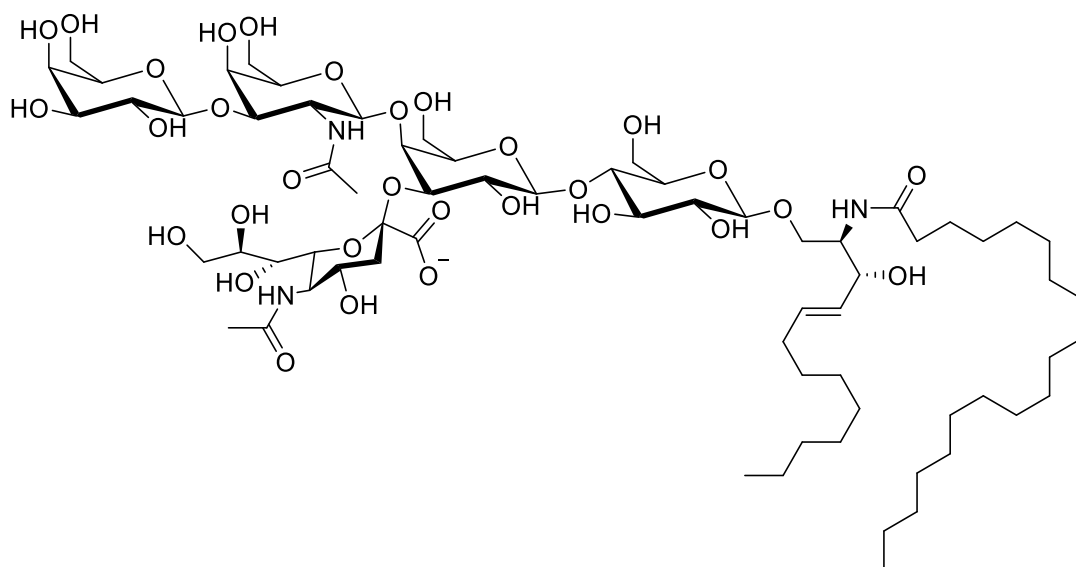


Figure 2.9: The GM-1 ligand, D-galactose- β (1-3)-N-acetyl-D-galactosamine- β (1-4)-D-galactose- (α (2-3)-neuraminic acid)- β (1-4)-D-glucose- β (1-1)- ceramide.

To perform the competitive binding assays, lectin binding assays were first performed to find the optimal lectin concentration. Serial dilutions of FITC-labelled RCA₁₂₀ and FITC-labelled CTxB were incubated with the GM-1 coated plates for 30 minutes at 37.5 °C. The middle of the dose-dependant binding curves were chosen, which gave concentrations of 0.13 mg.mL^{-1} and 0.05 mg.mL^{-1} for RCA₁₂₀ and CTxB respectively. The fluorescently labelled lectins were

then incubated with each polymer, before being applied to the (GM-1) microtitre (384 well) plate using an automated pipetting robot to increase throughput. After incubation and washing the total fluorescence was measured, Figure 2.10.

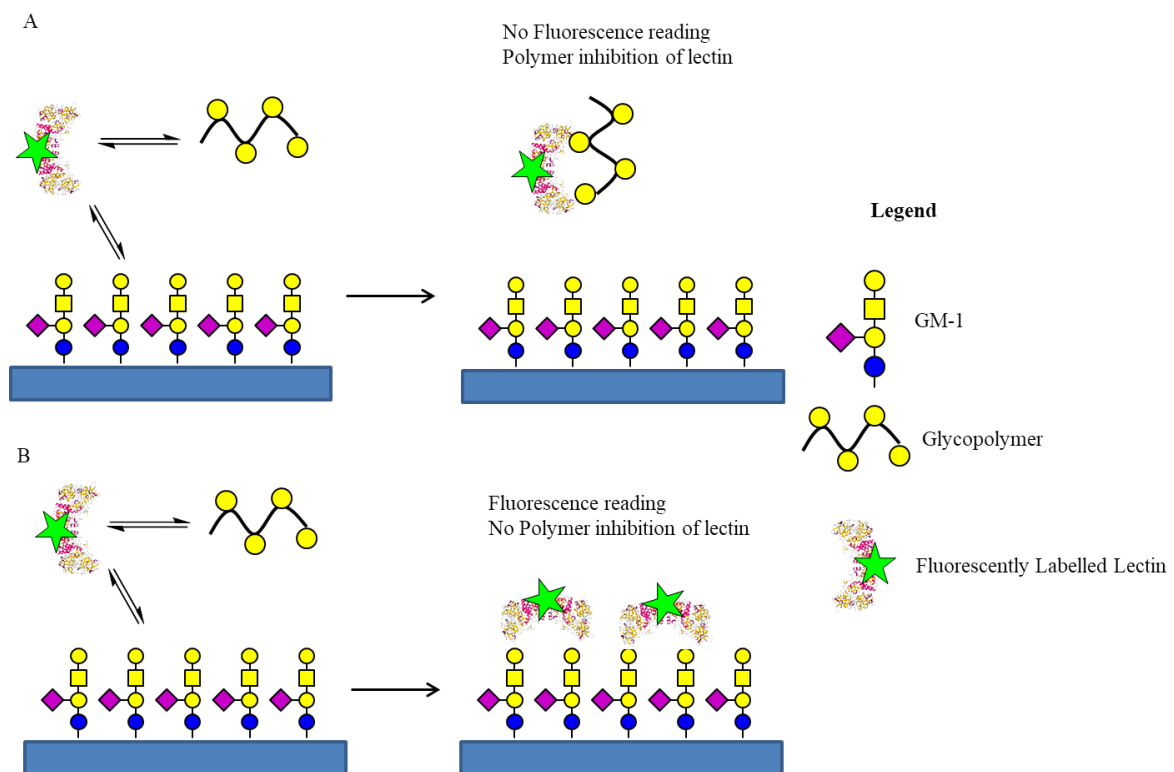


Figure 2.10: Schematic of inhibitory assay demonstrating the inverse relationship between inhibitory activity and fluorescence readout. In (A), glycopolymer binding out competes binding of the lectin to the GM-1 surface, leading to the formation of lectin-polymer complex that is then removed by washing, resulting in no fluorescence reading. In (B) the GM-1 surface out competes binding with the glycopolymer, which is then removed by washing, leaving only fluorescently labelled lectin bound to the surface.

In this assay, less fluorescence corresponds to more inhibition. As none of the polymer concentrations tested result in 100% inhibition and this assay lacks a positive control, the

results are reported as the relative IC_{50} . We have defined the relative IC_{50} as the mid-point between the estimates for the upper and lower plateaus, rather than the more often used absolute IC_{50} which defines the point at which 50% inhibition has been achieved.³⁸ While the relative IC_{50} value is less preferable to the absolute, it still allowed us to evaluate the trends in inhibition and what effect, if any, the heterogeneity had upon the inhibition. The results of the assay against RCA_{120} and CTxB are shown in Figure 2.11.

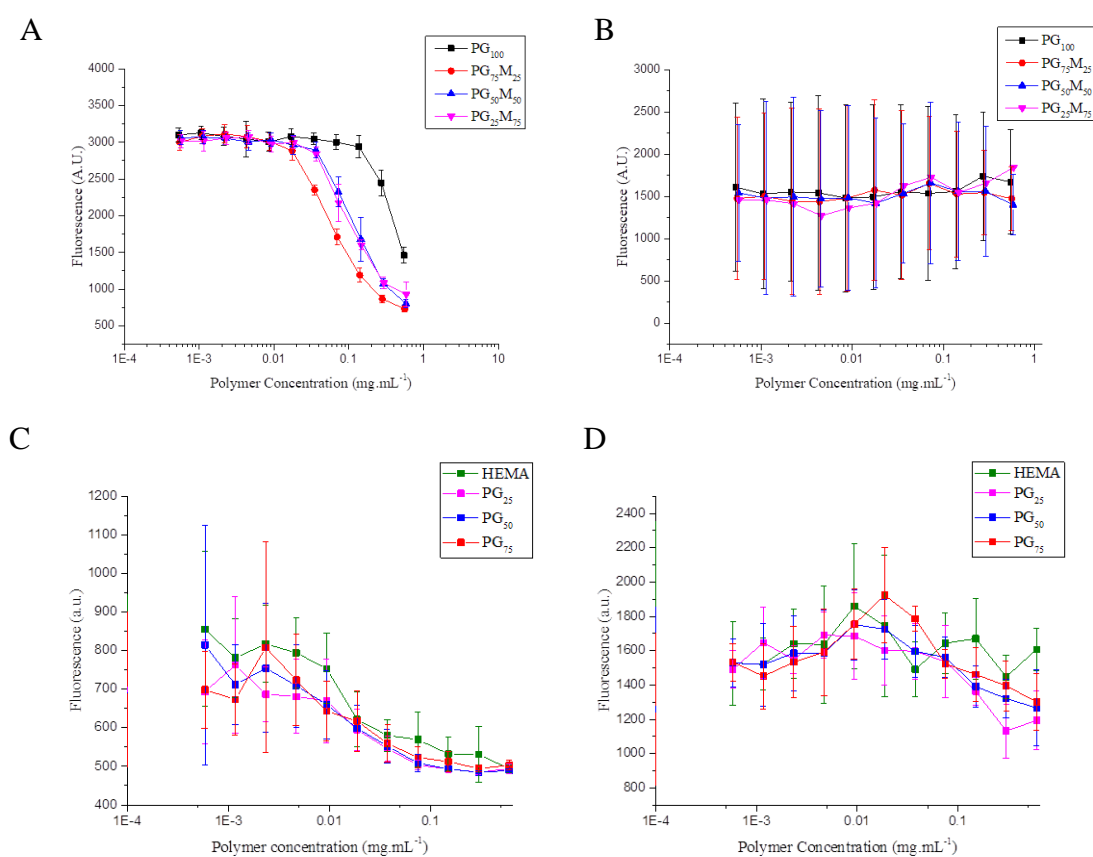


Figure 2.11: Fluorescence linked inhibitory assay results. (A) Heterogeneous polymers vs RCA₁₂₀ inhibition, n=18 (B) Heterogeneous polymers vs CTxB inhibition n=3 (C) Homogeneous polymers vs RCA₁₂₀, n= 6 (D) Homogeneous polymers vs CTxB, n=6. Error bars are one standard deviation.

The heterogeneous polymers demonstrate inhibitory activity towards RCA₁₂₀, however, against CTxB no inhibition was observed, which was surprising as there are several reports of galactose rich polymers which inhibit CTxB. Meanwhile the homogeneous polymers display only weak inhibitory activity against RCA₁₂₀ and negligible activity towards CTxB.

2.3.2.1 Inhibition of RCA₁₂₀ Discussion

To determine the percentage inhibition, the fluorescence value at zero polymer concentration (Y_0) is taken to be the total possible binding. The percentage inhibition is therefore given by Equation 2.1:

$$\theta = \frac{(Y_0 - Y)}{Y_0} \quad 2.1$$

Plotting the maximum inhibition obtained for each polymer shows that the heterogeneous polymers achieve much higher inhibition than the homogenous, 20 percentage points more than PG₁₀₀ and by 50 percentage points more than PG₂₅₋₇₅, which achieve only a similar level of inhibition as the non-glycosylated pHEMA negative control, Figure 2.12.

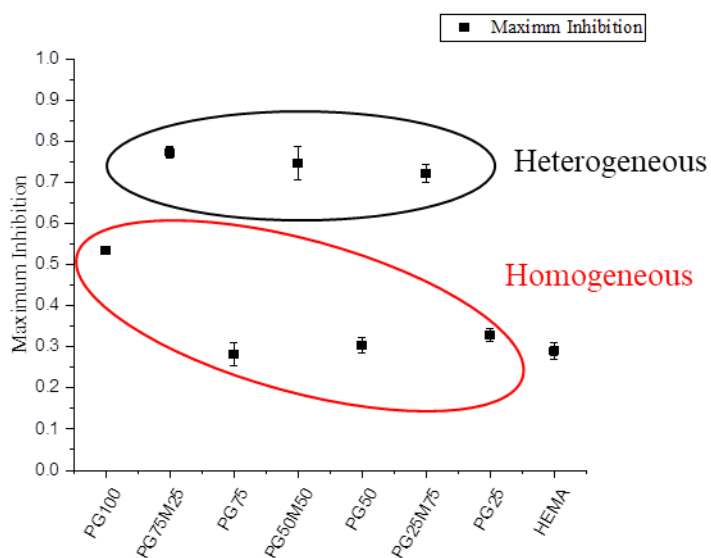


Figure 2.12: Maximum inhibition achieved by heterogeneous (black) and homogenous (red) polymer libraries.

The binding curves were then plotted individually and fit with a logistic curve fit to determine the mid-point and relative IC₅₀ value, Figure 2.13. As the entire binding curve for PG₁₀₀ was not obtained within the concentration range tested, the relative IC₅₀ could only be determined to be greater than the maximum concentration tested.

To enable comparison of any avidity enhancement due to multivalency, the relative IC₅₀ values were also calculated in galactose concentration, by correcting for the valency of each polymer and plotting the curves against the total galactose concentration, see Appendix 1. This is assuming the observed binding was due to the galactose units alone. The relative IC₅₀ values determined for both polymer concentration (mg.mL⁻¹) and galactose concentration (M) are shown in Table 2.4.

Table 2.4: Summary of relative IC₅₀ values obtained.

Polymer	IC₅₀ (mg.mL⁻¹)	Error	IC₅₀ Gal (M)	Error
PG₁₀₀	>0.54	N/A	>632.64 x10 ⁻⁶	N/A
PG₇₅M₂₅	59.96x10 ⁻³	2.25x10 ⁻³	55.77x10 ⁻⁶	2.09x10 ⁻⁶
PG₇₅	17.46x10 ⁻³	4.56x10 ⁻³	21.99x10 ⁻⁶	5.75x10 ⁻⁶
PG₅₀M₅₀	122.25x10 ⁻³	5.08x10 ⁻³	75.81x10 ⁻⁶	3.14x10 ⁻⁶
PG₅₀	20.25x10 ⁻³	3.44x10 ⁻³	19.06 x10 ⁻⁶	3.24x10 ⁻⁶
PG₂₅M₇₅	105.26x10 ⁻³	4.32x10 ⁻³	34.06 10 ⁻⁶	1.39x10 ⁻⁶
PG₂₅	21.18x10 ⁻³	5.76x10 ⁻³	12.09x10 ⁻⁶	3.28x10 ⁻⁶
PHEMA	25.08x10 ⁻³	6.73x10 ⁻³	N/A	N/A

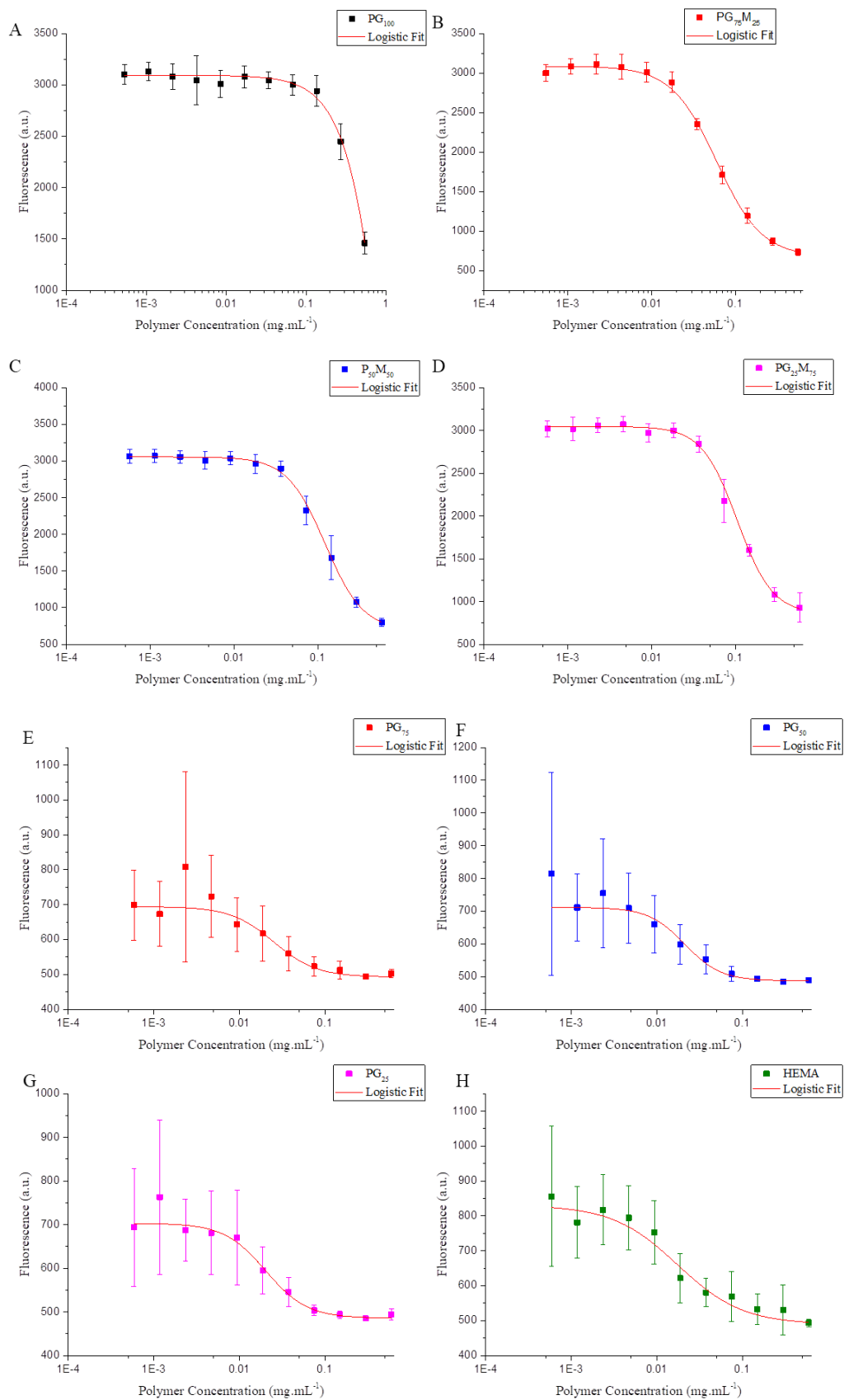


Figure 2.13: Fitted curves of heterogeneous (A-D) and homogeneous libraries (E-H) binding with RCA₁₂₀.

All heterogeneous polymers were potent inhibitors of RCA₁₂₀ compared to galactose monosaccharide alone (no inhibition observable) with IC₅₀ values in the μM range. Interestingly, going from 100% to 75% gal, 50% gal, and 25% gal, (15 to 12, 8 and 4 Gal per chain) gave an 11, 8, and 18-fold enhancement in activity per galactose respectively. This revealed that simply increasing the density of homo-multivalent polymers will not necessarily lead to the best inhibitors. On a polymer basis the lowest IC₅₀ was PG₇₅M₂₅, however, when valency corrected the lowest IC₅₀ was PG₂₅M₇₅, demonstrating an increased inhibitory effect per galactose in the presence of mannose. Comparing this result with the homogenous polymers to determine if this decrease in IC₅₀ is due to the mannose or simply a density effect gave some surprising results.

Despite the lower maximum inhibitory activity observed (as discussed earlier), when compared only by the relative IC₅₀ values, the homogeneous polymers appear to be better inhibitors of RCA₁₂₀, than the heterogeneous polymers. Unexpectedly, when measured in polymer concentration, the IC₅₀ stays relatively constant (within error) as galactose density changes. However, on a valency corrected basis the IC₅₀ increases as galactose density decreases, such that PG₂₅ has the lowest IC₅₀ value. Figure 2.14. This implies that the lower sugar density overall and lower galactose density in particular is having a contribution towards the decreased IC₅₀ values observed, but the presence of mannose is resulting in an increased inhibitory activity of the polymer.

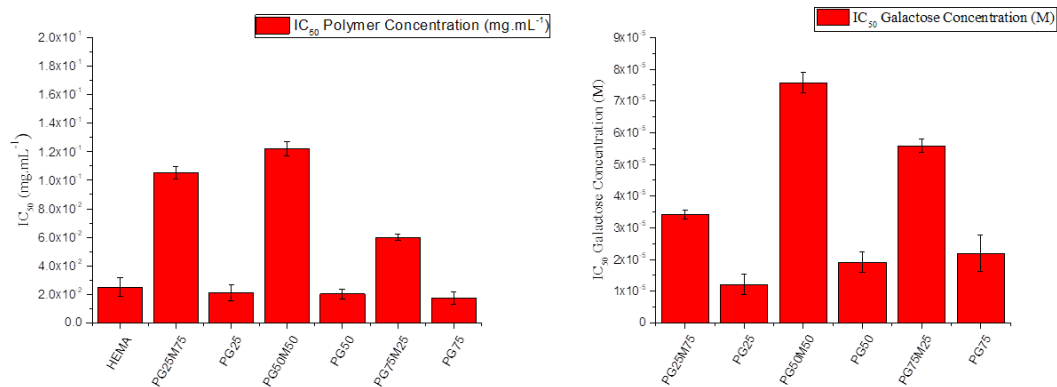


Figure 2.14: Relative IC₅₀ values in (A) polymer concentration and (B) galactose concentration.

To determine if there are any differences in the cooperativity of the binding between the heterogeneous and homogeneous libraries the Hill binding coefficients were extracted from plots of: the percentage of specific binding (binding between polymer and RCA₁₂₀) against the polymer concentration, Appendix Figure S3. These curves can be fit with the Hill-Waud Equation:³⁹

$$\theta = \frac{I_{Max}[P]^n}{k_h^n + [P]^n} \quad 2.2$$

Where θ = Specific binding, *i.e.* the percentage inhibition, $[P]$ = Polymer concentration, k_h = the ligand concentration that results in half occupation, I_{max} = maximum inhibition and n = Hill cooperativity constant. The results of which are shown in Table 2.5.

Table 2.5: Hill Cooperativity Coefficients.

Polymer	n	Error
PG₇₅M₂₅	1.69	0.10
PG₇₅	1.87	0.83
PG₅₀M₅₀	2.13	0.31
PG₅₀	1.88	0.55
PG₂₅M₇₅	1.98	0.13
PG₂₅	1.41	0.26

The Hill Cooperativity Coefficient is a measure of the cooperativity of the system, i.e. the extent to which initial binding is either synergistic (resulting in a value of $n > 1$), antagonistic ($n < 1$) or additive ($n = 1$) towards further binding events. All the polymers show positive cooperativity ($n > 1$) toward RCA₁₂₀. This is in contrast to previous reports that have seen negative cooperativity of multivalent binders and lectins.^{24,40} With the exception of PG₇₅M₂₅ the heterogeneous polymers display greater cooperativity than the homogenous polymers, but the difference is much smaller than might be expected from the relative steepness of the binding curves.

Contrasting this increased inhibitory activity for the heterogeneous polymers with the apparent lower relative IC₅₀ values of the homogenous polymers shows the importance of the roles of the relative rates of association and dissociation occurring within the assay. The

percentage inhibition achieved at any concentration is due to the formation of protein-polymer complexes in solution. It is therefore a function of the forward and backward rate constants for the formation and dissociation of the protein-polymer complex during the initial incubation period, and for the formation and dissociation of the protein-competitor (GM-1) complex in the second incubation period.

The results of this assay imply that the interplay between the rates for the competing reactions result in the homogenous polymers forming a higher concentration of protein-polymer complex at lower concentrations, relative to the heterogeneous polymers. However the formation of protein-polymer complex plateaus quickly for the homogenous polymers, resulting in a lower maximum inhibition. Therefore in the case of RCA₁₂₀ it appears that the inclusion of low-affinity secondary sugars actually enhances inhibitory activity.

2.3.2.2. Inhibition of CTxB

In contrast to RCA₁₂₀, against CTxB both sets of glycopolymers showed very weak inhibitory activity, Figure 2.15.

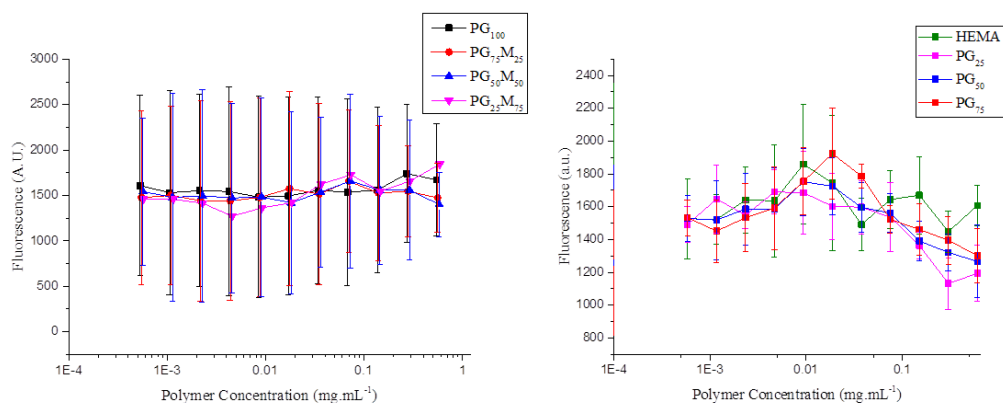


Figure 2.15: Results of the inhibitory assay against CTxB for (A) Heterogenous polymers (B) Homogenous polymers.

We attribute this to the nature of the CTxB binding pocket(s). CTxB binding of GM-1 involves the interaction of two binding domains: a deep binding domain interacts with a galactose and a shallower secondary domain that interacts with a neuramic acid. These two interactions have intrinsic dissociation constants of $K_d = \sim 50$ mM and 210 mM respectively⁴¹. The other carbohydrates of the GM-1 pentasaccharide restrict the conformations possible, to the extent that the CTxB-GM-1 complex has one of the highest affinities known for a protein-carbohydrate interaction⁴²; 1.9×10^{-10} M ($\pm 0.9 \times 10^{-10}$).⁴³ Experiments have shown the importance of the role of the linker and 3 dimensional arrangement.^{20,44} We therefore attribute the lack of CTxB inhibition observed to be a result of the conjugation chemistry resulting in a relatively inaccessible galactose (for the deep CTxB binding pocket), as well as being out-competed by the GM-1 carbohydrate. This means that lack of inhibition does not mean lack of binding. Further binding analysis is included later in this chapter.

2.3.3. Biolayer interferometry analysis of glycopolymer binding

The observations that the incorporation of a low-affinity sugar enhanced the inhibitory activity against RCA₁₂₀ is initially counter intuitive. However, in nature, native glycan ligands are often branched carbohydrates enabling presentation of multiple monosaccharides which undergo separate (or allosteric) interactions.²⁴ To probe in detail the molecular basis for these observations, biolayer interferometry (BLI) was employed.⁴⁵ First, the optimal loading conditions for each protein were established by testing the loading density of each protein at pH4, 5, and 6 HEPES at 25 and 50 $\mu\text{g.mL}^{-1}$. It was determined that 25 $\mu\text{g.mL}^{-1}$ at pH 5 gave the best loading density for both polymers. CTxB and RCA₁₂₀ were then immobilised *in situ* and exposed to the glycopolymers. An example of the binding curves obtained for PG₁₀₀ vs RCA₁₂₀ is shown in Figure 2.16 with the characteristic association and dissociation phases.

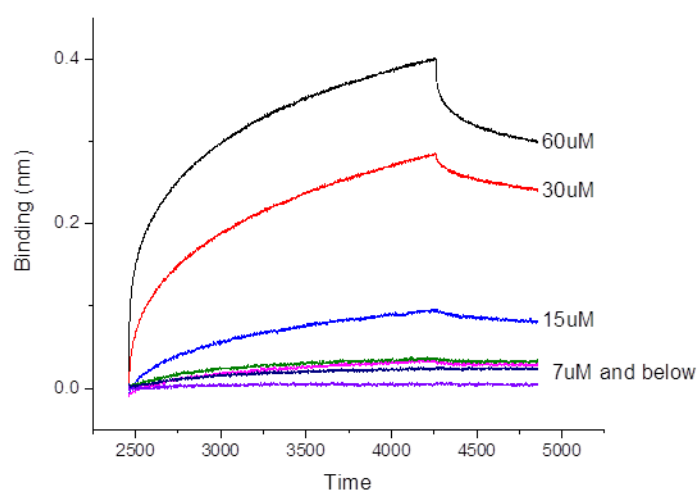


Figure 2.16: BLI response of PG₁₀₀ showing the characteristic association phase, followed by the dissociation phase starting at $t \approx 4250s$.

During the association phase we observe the binding that results from the equilibrium between association (k_{on}) and dissociation (k_{off}), while in the dissociation phase we only observe the loss of binding resulting from dissociation. This is because the BLI technique utilises low concentrations and high levels of mixing to ensure that re-association cannot occur during the dissociation phase. By fitting the association and dissociation curves we can obtain values for the observed rate during the association phase (k_{obs}) and a value for k_{off} from the dissociation phase. The observed rate k_{obs} is related to k_{on} and k_{off} by Equation 2.3:

$$k_{obs} = (k_{on} + k_{off})[Ligand\ Concentration] \quad 2.3$$

Therefore by extracting k_{obs} and k_{off} from the binding curves, a value for k_{on} can be calculated and therefore, from the ratio between k_{off}/k_{on} , the dissociation constant K_d .

Choosing which fitting model to apply can therefore have a huge impact on the outcome. In this instance RCA₁₂₀ and CTxB are multivalent receptors, bivalent and pentavalent respectively, interacting with the disperse multivalent glycopolymers. This is a highly complex system that is impossible to model with complete accuracy, and so some simplifications must be made. The heterogeneous binding model treats the binding curve as resulting from the simultaneous competition of two binders, which in this system are galactose and mannose, Figure 2.17.

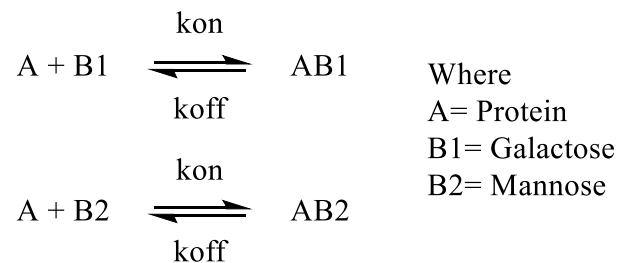


Figure 2.17: The heterogeneous binding model.

However, as previously mentioned this system is complicated by the presence of multiple protein binding sites and dispersity in the polymer. For RCA₁₂₀ a more realistic list of the interactions taking place is shown in Figure 2.18.

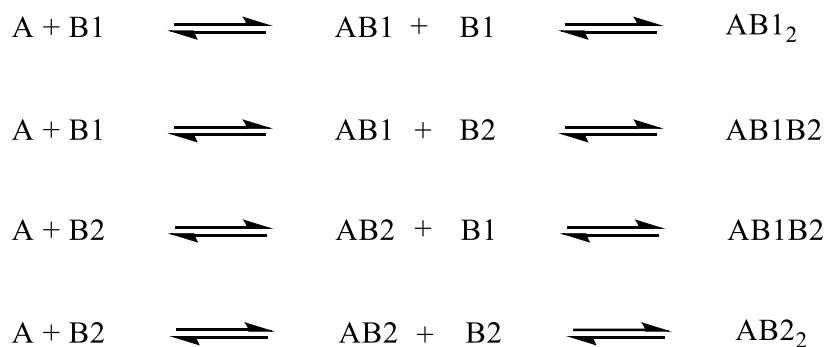


Figure 2.18: A more realistic depiction of the interactions taking place between bivalent RCA_{120} and the glycopolymers. Pentameric CTxB will have an associated increase in complexity. Furthermore, there will also be polymer-polymer interactions in solution and polymer backbone – protein interactions; however, as these should be essentially equal for each polymer they can be discounted.

This means that the two K_d s calculated by this model will be amalgamations of the galactose and mannose binding rates and primary and secondary binding events. An alternative method of analysis will be to generalise these interactions as shown in Figure 2.19.

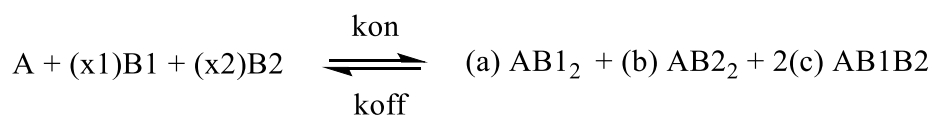


Figure 2.19: Where the ratio of (x1):(x2) varies as the heterogeneity of the polymers change. As the BLI method measures the size of the bound layer onto the tip, we can gain a value for the K_d of the formation of all the protein-polymer complexes by plotting the end points of the dissociation curves vs polymer concentration.

2.3.3.1. Bilayer interferometry of RCA₁₂₀

The K_{dS} , on rates (k_{on}), and, off rates (k_{off}) are summarised in Table 2.6 and shown in Figure 2.20 below. All rate constants are expressed in molar concentration of polymer. As the rate constants are functions of both galactose and mannose binding, it does not make sense to valency correct these rates constants and would bias the data.

Table 2.6: Summary of rate constants and R^2 and χ^2 values associated with the fitting.

Polymer	K_{d1} (M)	K_{d2} (M)	K_{on1} (M ⁻¹ S ⁻¹)	K_{on2} (M ⁻¹ S ⁻¹)	K_{off1} (S ⁻¹)	K_{off2} (S ⁻¹)	R^2 ^(a)	χ^2 ^(b)
PG₁₀₀	1.8×10^{-6}	$<1.0 \times 10^{-12}$	980	30	1.8×10^{-3}	$<1.0 \times 10^{-7}$	0.99	0.32
PG₇₅M₂₅	1.0×10^{-4}	3.9×10^{-6}	19	2400	1.9×10^{-3}	$<1.0 \times 10^{-7}$	0.99	3.70
PG₅₀M₅₀	1.9×10^{-8}	1.9×10^{-8}	78	78	1.5×10^{-6}	1.5×10^{-6}	0.86	9.42
PG₂₅M₇₅	3.3×10^{-5}	$<1.0 \times 10^{-12}$	70	11000	2.3×10^{-3}	$<1.0 \times 10^{-7}$	0.99	0.73
PG₇₅	3.2×10^{-7}	$<1.0 \times 10^{-12}$	8900	220	2.9×10^{-3}	$<1.0 \times 10^{-7}$	0.81	2.83
PG₅₀	2.8×10^{-7}	$<1.0 \times 10^{-12}$	15000	230	4.1×10^{-3}	$<1.0 \times 10^{-7}$	0.97	0.90
PG₂₅	4.1×10^{-7}	$<1.0 \times 10^{-12}$	9700	85	4.0×10^{-3}	$<1.0 \times 10^{-7}$	0.99	1.68

(a) Values closer to 1 indicate a better fit, values greater than 0.80 are considered acceptable

(b) Values closer to 0 indicate a better fit, values less than 3 are considered acceptable.

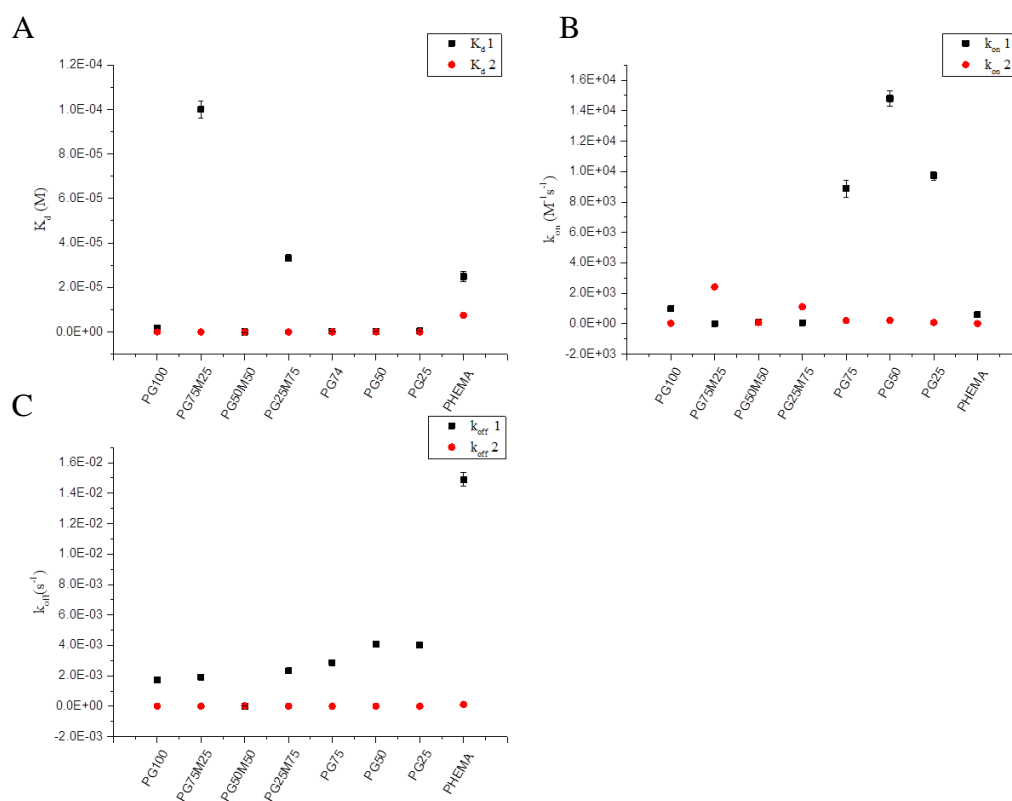


Figure 2.20: Calculated values of (A) K_d , (B) k_{on} , and (C) k_{off} , as determined by the heterogeneous fitting model applied to BLI binding curves.

As may be predicted for a bivalent protein and multivalent binder, one K_d is considerably smaller than the other in most cases, reflecting the increased affinity resulting from the chelate effect. Interestingly for PG₅₀M₅₀, the rate constants are identical for K_d , k_{on} and k_{off} . This is likely an artefact of the fitting; the relative concentrations of galactose and mannose are the same, therefore both galactose and mannose binding contribute equally to the competing rates and are modelled as the same value. However, care must be taken as the fitting model was poor, $R^2 = 0.86$ and $\chi^2 = 9.42$.

The first thing to note is that the heterogeneous polymers PG₂₅M₇₅ and PG₇₅M₂₅ have a K_d value considerably higher than the other polymers tested and that the K_d values do not follow the trends for relative IC₅₀ nor the percentage inhibition observed from the inhibition assays. It is important to remember that in a multivalent or competitive binding scenario, of which both are true here, the K_d does not relate to the concentration that produces 50% inhibition and is only the ratio of the forward and backward reaction rate constants. All the homogeneous polymers (excluding PG₁₀₀), have similar K_d 's, correlating with the similar relative IC₅₀ and inhibition values, but drastically different on and off rates.

While we cannot assign individual interactions to the rate constants calculated, we can make generalisations about the binding events taking place. The difference in the K_{d1} values of PG₇₅M₂₅ and PG₂₅M₇₅ are due to the k_{on1} rate only. The two polymers have almost identical k_{off1} rates, but PG₂₅M₇₅ has a k_{on1} rate 3.6x faster, resulting in a K_{d1} value a factor of ten smaller. For the homogeneous polymers, the k_{on1} rate does increase with decreasing galactose valency (up to a point, at PG₂₅ the rate decreases again); however, we also see the trend is mirrored in the k_{off} rates, see Figure 2.21B and C. This symmetry in the on and off rates is not present in the heterogeneous polymers. For PG₂₅M₇₅ and PG₇₅M₂₅, the binding event with the fastest on rate has the slowest off rate and *vice versa*, see Figure 2.22B and C. The highest affinity K_d (K_{d2}) for both PG₇₅M₂₅ and PG₂₅M₇₅ are the same ($<1 \times 10^{-12}$), which we can assume to be the secondary binding event. Therefore we would expect the inhibition to be determined by the lower affinity K_d . However, looking at the K_{d1} s alone, it would be expected that PG₂₅M₇₅ would be the better inhibitor of the two. PG₂₅M₇₅ does achieve a lower IC₅₀, when measured in galactose concentration, however, it is PG₇₅M₂₅ that has a lower relative IC₅₀ value when measured by concentration of polymer. Both polymers achieve similar inhibition of 77% and 72%. The k_{off1} for both of these polymers are essentially the

same (1.92×10^{-3} and 2.32×10^{-3} respectively) so the difference in the inhibition activity of these polymers must be determined by the difference in the k_{on1} rate constant, which for $PG_{25}M_{75}$ is 3.6x larger than $PG_{75}M_{25}$.

Therefore it seems that the addition of mannose to the polymers results in an increased k_{on} rate, and therefore an increased relative IC_{50} per galactose. However this is clearly offset by other factors as the galactose density increases, to give similar overall inhibition.

It is apparent therefore that the galactose density and orientation is playing a role in the binding rates of the polymers. For both homogeneous and heterogeneous polymers higher density multivalent glycopolymers are not necessarily better inhibitors, and that in heterogeneous multivalent systems, calculation of K_d alone may not be an indicator for a good inhibitor or not.

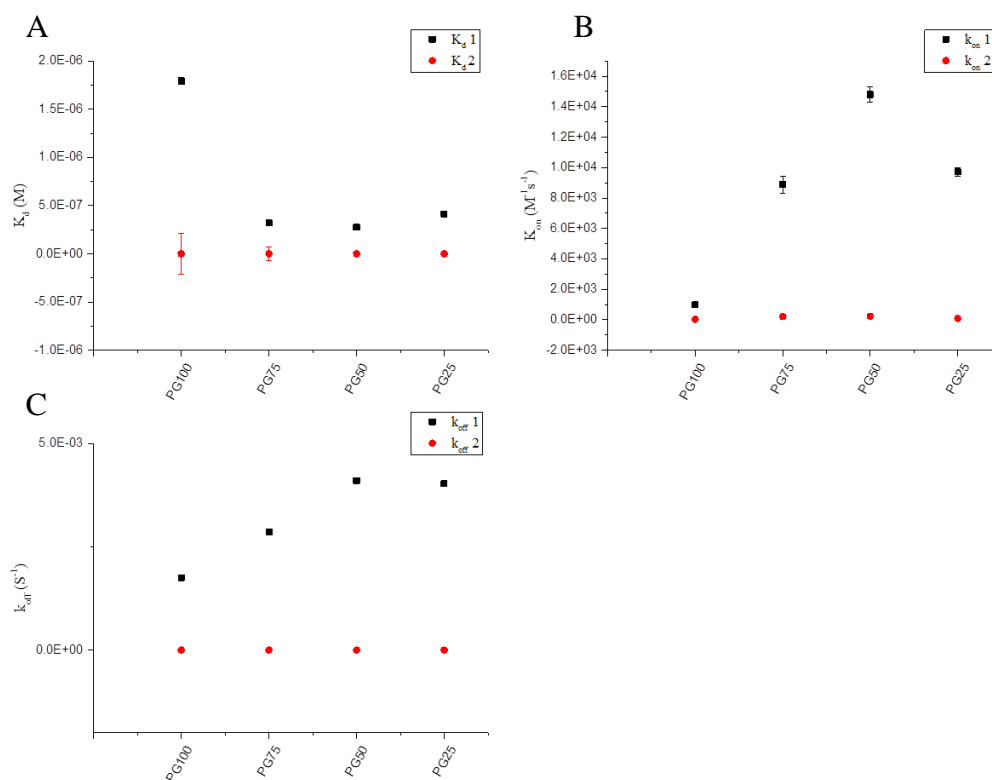


Figure 2.21: Homogeneous polymers: (A) K_d (B) k_{on} (C) k_{off} .

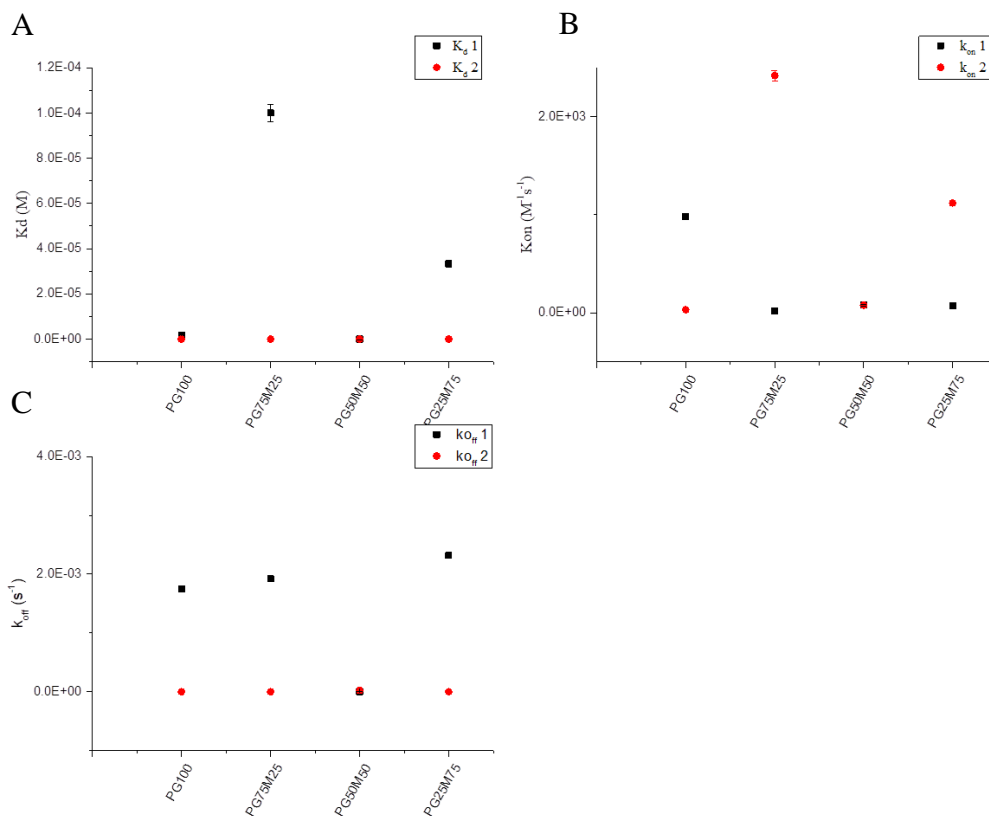


Figure 2.22: Heterogeneous polymers: (A) K_d (B) k_{on} (C) k_{off} .

An alternative method to extract an overall K_d for the process is to perform an end point analysis of the BLI binding curves. As the curves decay quickly and plateau the binding mass of the curves can be directly related to the formation of polymer-protein complex on the surface of the BLI sensor. By fitting just the dissociation curve for the end point and plotting the end points against polymer concentration, a value for the steady state K_d can be obtained, an example of which is shown in Figure 2.23. All the other curves are in the Appendix.

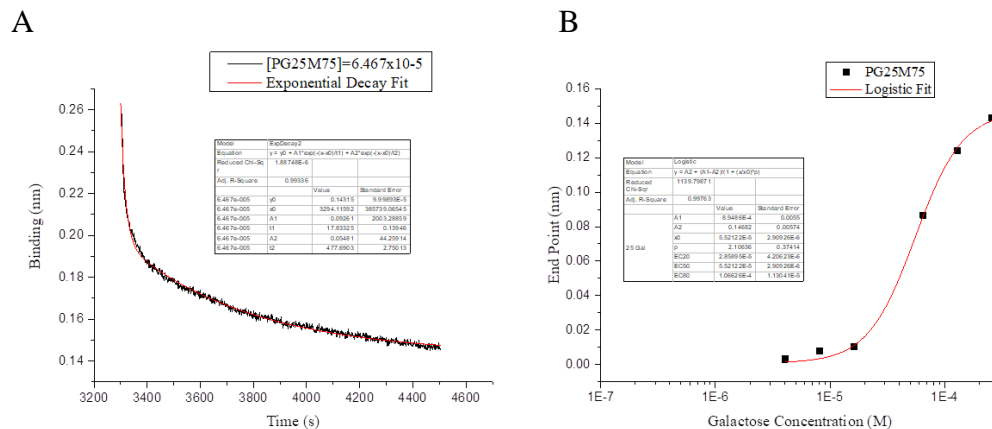


Figure 2.23: For PG₂₅M₇₅: (A) Fitting of the dissociation phase to extract the end point (B) End point vs Concentration fit to extract an overall K_d .

The results of this method are summarised in Table 2.7. However when this method was used to analyse the binding of the homogeneous curves, the fitting was very poor, and for PG₇₅M₂₅, no fit could be obtained, Figure 2.24.

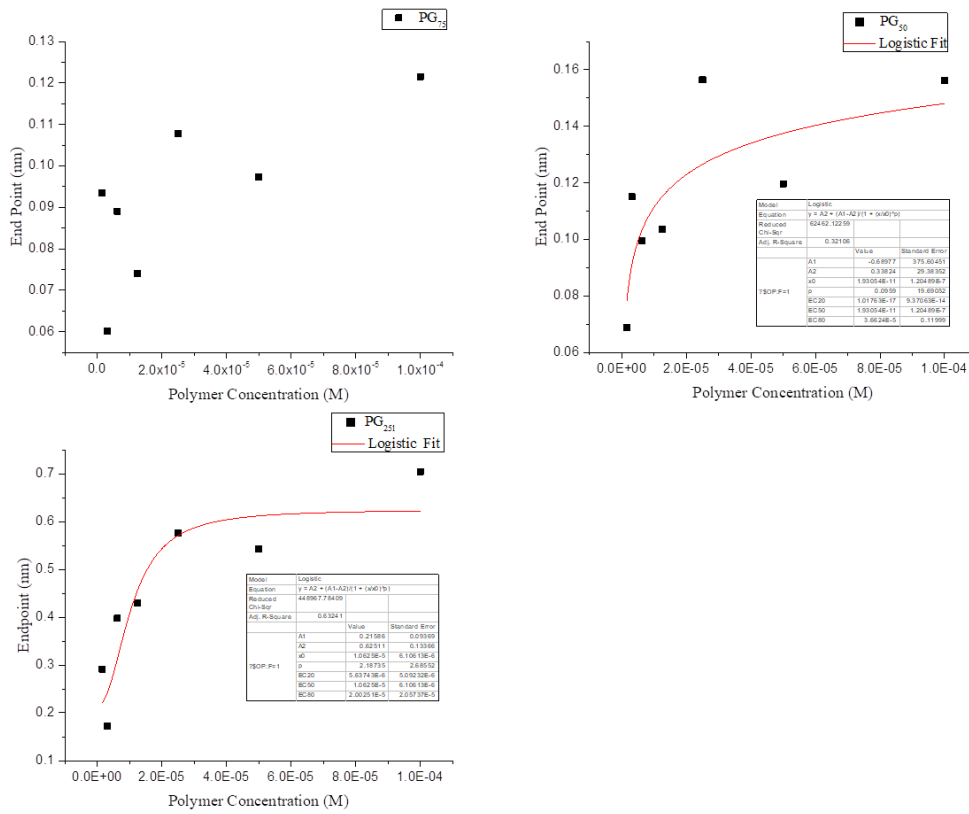


Figure 2.24: Attempted fits of homogeneous polymers steady state K_d .

Table 2.7: Steady state K_d against RCA₁₂₀ in polymer concentration (M).

Polymer	K_d [Polymer] (M)	K_d Error	K_d [Galactose] (M)	Kd err
PG ₂₅ M ₇₅	1.38×10^{-5}	7.27×10^{-7}	5.52×10^{-5}	2.90×10^{-6}
PG ₅₀ M ₅₀	2.18×10^{-5}	6.23×10^{-8}	1.52×10^{-4}	4.36×10^{-7}
PG ₇₅ M ₂₅	5.95×10^{-6}	5.22×10^{-6}	6.54×10^{-5}	5.74×10^{-5}
PG ₁₀₀	2.19×10^{-5}	1.01×10^{-7}	3.29×10^{-4}	1.51×10^{-6}
PG ₂₅ ^(a)	1.06×10^{-5}	6.10×10^{-6}	4.79×10^{-5}	2.75×10^{-5}
PG ₅₀ ^(b)	1.93×10^{-11}	1.20×10^{-7}	1.54×10^{-10}	9.63×10^{-7}
PG ₇₅	Could not fit	Could not fit	Could not fit	Could not fit

(a) Obtained from fit with $R^2 = 0.6$ (b) Obtained from fit with $R^2=0.8$

The K_d s obtained in this way match the trend observed with the relative IC_{50} values obtained *via* the competitive binding assay performed in section 2.2. Figure 2.25. This further points to the inclusion of mannose resulting in an effective increased affinity per galactose due to the heterocluster effect.

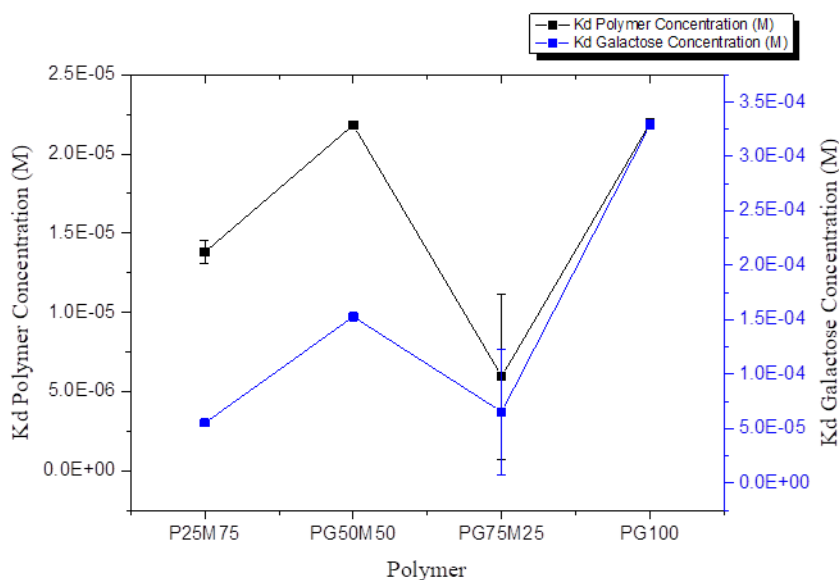


Figure 2.25: Steady State K_d for RCA_{120} .

2.3.3.2. Biolayer interferometry of CTxB

BLI analysis of the polymer series $PG_{25}M_{75} - PG_{100}$ showed that despite any evidence of inhibition from the competitive binding assay, binding to CTxB was occurring, and for all heterogenous polymers a BLI response was observed. BLI of the homogeneous library against CTxB was not performed. The resulting association and dissociation curves were fit to the heterogeneous binding model as described in section 2.2.3. and the results are summarised in Table 2.8. One of the first things to note is that the heterogeneous binding model fits to the CTxB data with a higher confidence, with $R^2=0.99$ and $\chi^2 < 3$ in all cases. The reason for this increased accuracy in fitting the CTxB binding data (with its five binding sites and associated increase in complexity) over the RCA_{120} binding is unknown.

Table 2.8: Summary of BLI derived rate constants against CTxB.

Polymer	K_d1 (M)	K_d2 (M)	K_{on1} (M ⁻¹ S ⁻¹)	K_{on2} (M ⁻¹ S ⁻¹)	K_{off1} (S ⁻¹)	K_{off2} (S ⁻¹)	R^2 ^(a)	χ^2 ^(b)
PG₁₀₀	6.67x10 ⁻⁵	<1x10 ⁻¹²	44.8	183	2.99x10 ⁻³	<1x10 ⁻⁷	0.99	0.10
PG₇₅M₂₅	4.9x10 ⁻⁵	3.05x10 ⁻⁶	603	59.2	29.5x10 ⁻³	1.8x10 ⁻⁴	0.99	0.03
PG₅₀M₅₀	1.07x10 ⁻⁵	2.64x10 ⁻⁶	1760	71.9	18.9x10 ⁻³	1.9x10 ⁻⁴	0.99	0.04
PG₂₅M₇₅	1.13x10 ⁻⁵	3.52x10 ⁻⁶	1760	72.8	19.8x10 ⁻³	2.56x10 ⁻⁴	0.99	0.02

(a) Values closer to 1 indicate a better fit, values greater than 0.80 are considered acceptable

(b) Values closer to 0 indicate a better fit, values less than 3 are considered acceptable.

As seen against RCA₁₂₀, the two binding events probed by the heterogeneous binding model will in this case be an accumulation of galactose vs mannose binding and primary vs secondary binding events. However, we can make some general observations. It appears that there is a lower avidity event ($K_d 1$) and a higher avidity one ($K_d 2$). The low avidity event is most likely is mostly due to the primary binding event. As the mannose density increases the avidity increases, due to a 39-fold increase in $k_{on 1}$ while $k_{off 1}$ only sees a ~6.5 fold increase. This increase plateaus at PG₅₀M₅₀ (8 Mannose per chain) and PG₂₅M₇₅ (4 Mannose per chain), Figure 2.26.

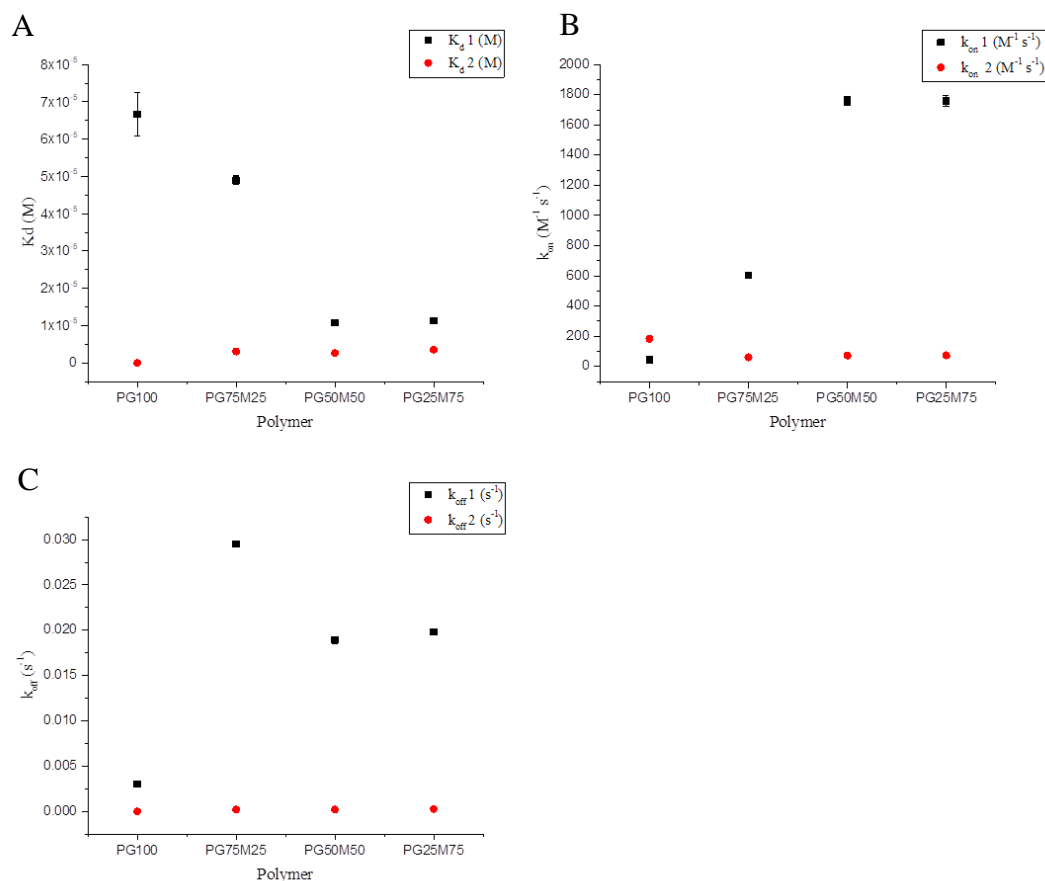


Figure 2.26: For the binding of heterogenous polymers with CTxB (A) Dissociation constants (K_d) (B) Association rate constants (k_{on}) (C) Dissociation rate constants (k_{off})

This demonstrates that despite showing no activity in the inhibitory assay, the heterogenous polymers do display affinities against CtxB in the tens of μM range, which could not out-compete the CTxB-GM-1 interaction ($K_d = 1.9 \times 10^{-10} M$)⁴³ in the inhibitory test. We also see further evidence that an increased density of mannose results in faster rates of both association and dissociation; however the increase in association outcompetes the increase in dissociation to provide an overall lower avidity.

The same end point analysis of the dissociation curves was also performed as before, see Appendix, and the results are shown in Table 2.9.

Table 2.9: Steady state K_d against CTxB in polymer concentration

Polymer	K_d [Polymer] (M)	K_d Error	K_d [Galactose] (M)	K_d Error
PG ₂₅ M ₇₅	1.19×10^{-5}	2.49×10^{-6}	4.76×10^{-5}	9.97×10^{-6}
PG ₅₀ M ₅₀	8.75×10^{-6}	4.63×10^{-6}	6.12×10^{-5}	3.24×10^{-5}
PG ₇₅ M ₂₅	3.76×10^{-5}	4.75×10^{-6}	4.14×10^{-4}	5.23×10^{-5}
PG ₁₀₀	2.45×10^{-5}	1.83×10^{-6}	3.67×10^{-4}	3.37×10^{-5}

The values obtained from the end point analysis are in good agreement with the values obtained *via* BLI, with the exception of PG₇₅M₂₅, somewhat validating the method, Figure 2.27.

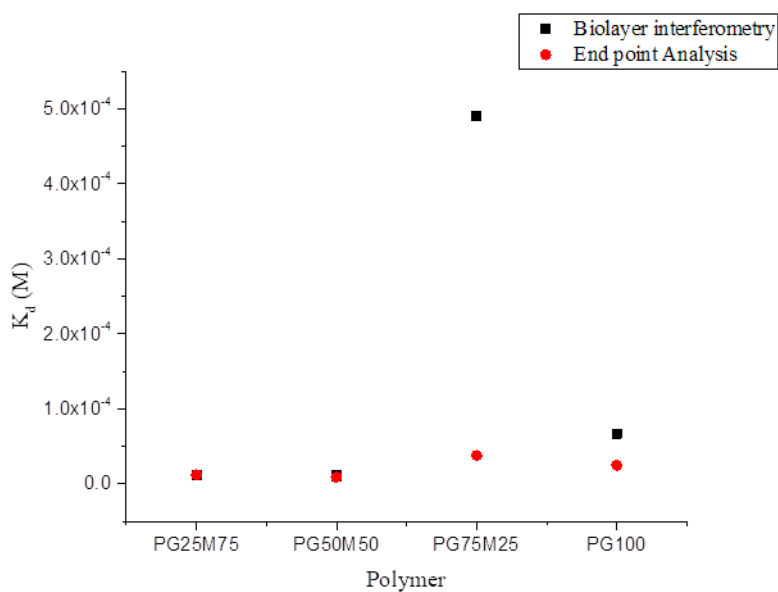


Figure 2.27: Comparison of K_d 's obtained from either the BLI method or end point analysis method.

2.4. Conclusions and further work

In conclusion we have shown that increasing glyco-conjugate density does not necessarily correlate with increased affinity, or increased inhibition. The inclusion of the nominally non-binding mannose, appears to result in a decrease in avidity, but an increase in the inhibition of RCA₁₂₀ compared to the isovalent homogenous polymers. There was not a linear relationship between the mannose density and inhibition or avidity observed for RCA₁₂₀ binding, with the highest affinity per galactose being PG₂₅M₇₅, the lowest galactose density polymer tested. This was attributed to the increased association rate, while the dissociation rate stayed constant. This fits with a mechanism of binding whereby the weaker binding sugar does not pay as large an entropic penalty for binding due to its increased degrees of freedom relative to a more specific interaction. Once bound the entropic penalty for binding of the polymer as a whole has largely been paid and the bind and slide mechanism results in increased re-binding and movement of the polymer to find the optimal binding configuration. However it should be stressed that sufficient evidence for this mechanism is not presented here and further work is required. However this does highlight the need to consider every aspect of the system under investigation.

Meanwhile for CtxB, no inhibitory activity was detected at all. We attribute this to the inability of the glycosylated polymers to outcompete the very strong GM-1 interaction. BLI analysis revealed that the polymers do bind to CTxB with tens of μM avidity. The observed avidity decreased with increasing mannose density up to a plateau at PG₅₀M₅₀ (8 Gal and 8 Man per chain). Again this was due to an increased rate of association with increased mannose density, while the rate of disassociation did not increase to the same extent and fits with the proposed model for RCA₁₂₀ and previous observations of the heterocluster effect.

The use of asialoganglioside GM1, a GM-1 isomer that does not contain the neuraminic acid used by CTxB as a secondary binding site as an alternative competitive binder for inhibitory assays may allow access to competitive binding behaviour for CTxB, however, any IC_{50} or inhibitory data for assays of this type are highly dependent upon the system and so would have to be considered separately to the already obtained data here for RCA₁₂₀.

To extend this work further the use of further parameterized fitting model to better fit the BLI kinetic data could allow for the extraction of rate constants that relate directly to the interactions resulting from galactose or mannose binding, as well as the primary and secondary binding states of RCA₁₂₀. Furthermore the use of isothermal titration microcalorimetry (ITC) would allow for the determination of the thermodynamic parameters associated with the binding. However this is ultimately beyond the scope of what was achievable within the timeframe of this work.

2.5. Experimental

2.5.2. Materials

2-Chloro-1,3-dimethylimidazolium chloride, and GM-1 Ganglioside was purchased from Carbosynth. D-(+)-galactose was purchased from MP Biomedicals. D-(+)-Mannose, trimethylamine, sodium azide, pentafluorophenol, methacryloyl chloride, 2-cyano-2-propyl benzodithioate, 4,4'-azobis(4-cyanovaleric acid), 1,4-dioxane, dichloromethane, DBCO-amine, DMF, 2-aminoethan-1-ol, Greiner 384-well "high-binding" microtitre plates, PBS, HEPES (10 mM HEPES (0.48 g), 0.15 M NaCl (1.75 g), 0.1 mM CaCl₂ (2 mg), 0.01 mM MnCl₂ (0.2 mg) in 200mL DI water), FITC-labelled CtxB, and unlabelled CTxB, were purchased from Sigma-Aldrich. 2,6-lutidine 99% was purchased from Acros Organics. FITC-labelled RCA₁₂₀ and RCA₁₂₀ was purchased from Vector labs. Amine reactive 2nd Generation BLI sensors, EDC, NHS, from Bioforte. Ultrapure milli Q water was obtained from a Merk Milli-Q water purifier at 18.2 MΩ.cm resistivity at 25 °C. 3500 MWCO 'snakeskin' dialysis tubing was purchased from Thermofisher (UK).

2.5.2. Analytical methods

^1H , ^{13}C NMR, and ^{19}F spectra were recorded on Bruker HD-300, HD-400, and AV-500 spectrometers using deuterated solvents purchased from Sigma-Aldrich. Chemical shifts are reported relative to residual non-deuterated solvent. Mass spectrometry was performed on an Agilent 6130B single Quad (ESI). FTIR spectra were acquired using a Bruker Vector 22 FTIR spectrometer with a Golden Gate diamond attenuated total reflection cell. Raman spectra were collected on a Reinshaw inVia Reflex Raman using a 442 nm HeCd laser. Liquid handling was performed by Gilson Pipette Max. 96-well plates were read using a Biotek Synergy plate reader set at 25 °C. UV-Vis spectra were obtained on an Agilent Cary spectrometer. Biolayer interferometry was performed using a ForteBio Octet 96 RED interferometer, with the indicated probes. DMF SEC was performed on a Varian 390-LC MDS system equipped with a PL-AS RT/MT autosampler, a PL-gel 3 μm (50 x 7.5 mm) guard column, two PL-gel 5 μm (300 x 7.5 mm) mixed-D columns using DMF with 5 mM NH_4BF_4 at 50 °C as eluent at a flow rate of 1.0 $\text{mL}\cdot\text{min}^{-1}$. The SEC system was equipped with ultraviolet (UV)/visible (set at 280 and 461 nm) and differential refractive index (DRI) detectors. Narrow molecular weight PMMA standard (200 – 1.0 x 10⁶ $\text{g}\cdot\text{mol}^{-1}$) were used for calibration using a second order polynomial fit.

Bilayer Interferometry

Amine reactive 2nd Generation BLI sensors from ForteBio were pre-soaked for 10 minutes in MilliQ water before activation with an EDC/NHS solution. After 10 minutes the sensors were moved to a solution containing the lectin at 25 $\mu\text{g}\cdot\text{mL}^{-1}$ in pH 5 HEPES. After 10 minutes the sensors were quenched with ethanolamine, placed in HEPES buffer at the corresponding pH to baseline for 10 minutes, and tested against 5 serial dilutions of polymer solution for 30 minutes. The sensors were then placed into HEPES buffer for 10 minutes to measure dissociation. The raw data was processed using ForteBio analysis software heterogenous ligand model. To measure the pseudo steady state K_d 's the dissociation steps only were plotted and fit with an exponential decay in Origin to extract the end point deflection. The end points were then plotted vs both polymer and galactose concentration and fit with logistic curves to extract a midpoint value.

Competitive Binding Assays

384-well high-binding microtitre plates were incubated for 16 hours with 50 μL of 1 $\text{mg}\cdot\text{mL}^{-1}$ GM-1 Ganglioside dissolved in phosphate buffered saline solution, per well. Unattached GM-1 was removed by washing extensively with PBS buffer.

Due to the relatively low solubility of the polymers, polymers were dissolved in HEPES buffered saline, and any undissolved material removed by centrifugation. Exact concentrations were determined by the DBCO absorbance at 292 nm, using a calculated value for the extinction co-efficient ϵ as 2.00628 $\text{mL}\cdot\text{mg}^{-1}\text{cm}^{-1}$.

Table S1: Glycopolymer Concentrations used for serial dilutions

Polymer	Concentration (mg.mL⁻¹)
PG₁₀₀	0.90
PG₇₅M₂₅	0.93
PG₅₀M₅₀	0.96
PG₂₅M₇₅	0.97

To perform the competitive binding assays, lectin binding assays were first performed to find the optimal concentration. Serial dilutions of FITC-labelled RCA and FITC-labelled CTx in HEPES buffered saline were made and incubated in a GM-1 coated 384 well plate for 30 minutes at 37 °C. After this time, the plates were washed extensively with buffer to remove unbound lectin and the fluorescence. The middle of the dose-dependent binding curves were chosen, which gave concentrations of 0.13 mg.mL⁻¹ and 0.05 mg.mL⁻¹ for RCA₁₂₀ and CTx respectively.

Polymer solutions were made up as serial dilutions in HEPES from saturated stock solutions to give a volume of 180 µL in each well. 120 µL FITC labelled lectin in HEPES was added to 180 µL of each polymer solution and incubated for 30 minutes at 37 °C. 45 µL of the polymer FITC-labelled lectin solutions were then added to the GM-1 surfaces and incubated at 37 °C for 30 mins. Fluorescence was then measured at excitation/emission wavelengths of 485/528

nm. All RCA experiments were carried out 18 times, CTx B experiments were carried out in triplicate. MIC₅₀ values were calculated using logistic fitting in Origin.

2.5.3. Synthetic Procedures

Synthesis of Azido-Monosaccharides

2-Chloro-1,3-dimethylimidazolium chloride (2.82 g, 16.7 mmol) was added to a solution of galactose/mannose (1.00 g, 5.6 mmol), trimethylamine (7.7 mL, 55 mmol) and sodium azide (3.61 g, 55.5 mmol) dissolved in ultrapure milli Q water (20 mL), sitting on ice. The solution was stirred for 40 minutes on ice before removing the solvent *in vacuo*. Ethanol (40 mL) was added to precipitate NaN₃, filtered, and the solvent removed (repeat to ensure complete removal of NaN₃). The resulting solid was then dissolved in ultrapure milli Q water (10 mL) and washed three times with dichloromethane. The water layer was freeze dried to give a yellow solid. The product was then purified on a silica column using 5:1 chloroform:methanol (R_f = 0.3) to give an off-white product. Yield: 0.98 g 86%

1-Azido-1-deoxy-galactose

^1H NMR (D_2O) 400MHz, ppm: 5.57 (1H, d, $J_{1-2} = 4.40\text{Hz}$, H1, α anomer 23.7%), 4.67 (1H, d, $J_{1-2} = 8.68\text{Hz}$, H1, β anomer 76.3%), 3.96 (1H, d, $J_{1-2} = 3.30\text{Hz}$, H5), 3.79-3.78 (1H, m, H4), 3.77-3.75 (2H, m, H6), 3.70 (1H, dd $J_{1-2} = 3.42$, $J_{3-4} = 9.78\text{Hz}$, H3) 3.53 (1H, t, $J_{1-2} = 9.78$, H2)

^{13}C NMR (D_2O) 75MHz, ppm: 90.55 (β C1), 89.44 (α C1) 77.21 (β C4), 75.88, 75.13, 74.23, 73.06, 72.64 (β C3), 71.20 70.32 (β C2), 69.19, 68.51(β C5), 68.20, 64.20, 63.46, 61.17, 60.94 (β C6)

MS (ESI +): Observed: 228.00 Expected: 228.17 $[\text{M}+\text{Na}]^+$

IR: 2107cm^{-1} ($-\text{N}_3$)

1-Azido-1-deoxy-mannose

^1H NMR (D_2O) 400MHz, ppm: 5.46 (1H, d, $J_{1-2} = 1.71\text{ Hz}$, alpha 100%) 3.92 (1H, d, $J = 10.27\text{ Hz}$) 3.86 (1H, dd, $J_{1-2} = 1.96$, $J_{3-4} = 3.18\text{ Hz}$, H^2) 3.78, (2H, m) 3.75-3.72 (2H, m), 3.64 (1H, t, $J_{1-2} = 9.54\text{Hz}$)

^{13}C NMR (D_2O) 75MHz, ppm: Major Anomer (100%): 90.57 (C1), 78.47 (C5), 70.36 (C2), 70.37 (C3), 66.60 (C4), 61.10(C6)

Mass Spec: Observed: 228.00 Expected: 228.17 $[\text{M}+\text{Na}]^+$

IR: 2107cm^{-1} ($-\text{N}_3$)

Synthesis of Pentafluorophenyl Methacrylate

Pentafluorophenol (5.4 g, 29.3 mmol) and lutidine (3.5 ml, 30.0 mmol) were added to a round bottom flask of dichloromethane (50 mL) on ice. Methacryloyl chloride (3.0 mL, 31.0 mmol) was slowly added. The reaction was stirred for 3 hours on ice, before leaving at room temperature overnight. The lutidine HCl precipitate was filtered and the filtrate was washed twice with water (30 mL), dried with MgSO₄, and the solvent removed *in vacuo*. The product was then passed through a silica column in petroleum ether 40-60 (R_f = 0.3) to give a colourless liquid, Yield 4.7 g.

¹H NMR (CDCl₃) 400MHz, ppm: 6.37 (1H, s), 5.83 (1H, s), 2.01 (3H, s)

¹⁹F NMR (CDCl₃) 376MHz, ppm: -152.89 (2F, dd, J₁₋₂ = 16.35 Hz, J₃₋₄ = 6.81 Hz) -158.34 (1F, td, J₁₋₂ = 21.80, J₃₋₄ = 9.53 Hz) -162.63 (2F, m)

¹³C NMR (CDCl₃) 100MHz, ppm: 163.04 (C4, C=O), 142.52, 140.67, 140.14, 139.14, 138.16 (C5-10, Aromatics), 133.68 (C3, Me-C(=CH₂)-CO)), 129.91(C2, =CH₂) 18.18 (C1, -Me)

Mass Spec: Observed: 253.1 Expected 253.1 [M+H]⁺

IR: 1760 cm⁻¹ (ester), 1517 cm⁻¹ (unsaturated C=C), 1086 cm⁻¹ (C-O), 994 cm⁻¹ (C-F)

Synthesis of Poly(Pentafluorophenol Methacrylate)

PFMA (4.7 g, 18.6 mmol), 2-Cyano-2-propyl benzodithioate (55.3 mg, 0.25 mmol) and 4,4'-Azobis(4-cyanovaleric acid) (35.0 mg, 0.12 mmol) were dissolved in dioxane (9 mL). A sample was removed for NMR analysis. The solution was degassed with N₂ for 30 minutes. The reaction was then heated to 90 °C and left for 90 minutes. The polymerisation was quenched in liquid nitrogen and precipitated three times from pentane into THF to give a pink solid, 2.3 g 50% yield. 62% Conversion by NMR. SEC (THF): M_w = 15250 Đ = 1.7.

¹H NMR (CDCl₃) 400MHz, ppm: 2.42 (2H, br, CH₂) 1.72 (NC-C(CH₃)₂-) 1.54 (3H, br, CH₃)

¹⁹F NMR (CDCl₃) 376MHz, ppm: -150.35 (1F, br s), -151.44 (1F, br s), -156.97 (1F, br s), -162.11 (1F, br s)

IR (cm⁻¹): 950 (C-F) 1050 (C-O) 1600 (C=O) 1700 (C=C)

Post-polymerisation modification of Poly(Pentafluorophenol Methacrylate)

For the synthesis of PG₂₅M₇₅, PG₅₀M₅₀, PG₇₅M₂₅, PG₁₀₀.

P(PFPMA) (0.260 g, 0.12 mmol) and DBCO-amine (72 mg, 0.26 mmol) were dissolved in 3 mL DMF and left at 50°C overnight under N₂. Reaction completion was confirmed via fluorine NMR, ratio of pentafluorophenol peaks to polymeric pentafluorophenol ester peaks was 33%. Without further workup, a large excess of 2-aminoethan-1-ol (0.5 mL, 8.3 mmol) was added, and left for a further 16 hours at 50 °C. Reaction completion was again confirmed *via* fluorine NMR observation of only pentafluorophenol peaks. The reaction was then diluted into ultrapure milli Q water and dialysed for 3 days. 0.10 g of white polymer was isolated. No fluorine was observed in the NMR of the final product. DOSEY was carried out to further confirm the conjugation of the DBCO unit to the polymer.

^1H NMR (MeOD) 500MHz, ppm: 7.5-7.0 (br, Benzyl) 4.42 (br, cyclooctyne ring CH_2) 3.65 (br, $\text{NH-CH}_2\text{-CH}_2\text{-}$), 3.28 (br, $\text{-NH-CH}_2\text{-CH}_2\text{-}$), 2.5-1.5 (br, Backbone CH_2) 1.5-1.0 (br, backbone Me)

DOSEY NMR (MeOD) 500MHz, $\log(\text{m}^2\text{s}^{-1}) = -9.25$, ppm: 7.5-7.0, (Benzyl) 4.42 (br, cyclooctyne ring CH_2) 3.65 (br, $\text{NH-CH}_2\text{-CH}_2\text{-}$), 3.28 (br, $\text{-NH-CH}_2\text{-CH}_2\text{-}$), 2.5-1.5 (br, Backbone CH_2) 1.5-1.0(br, backbone Me)

^{13}C NMR (MeOD) 500MHz: 179.42 (br, C=O) 141.16 (Benzyl No H), 136.93 (Benzyl No H), 132-128 (benzyl H), 63.02, 61.31 ($\text{NH-CH}_2\text{-CH}_2\text{-OH}$), 61.08 ($\text{NH-CH}_2\text{-CH}_2\text{-OH}$), 60.09, 59.61, 56.93, 52.49 (Cyclooctyne Ring CH_2), 46.95 ($\text{NH-CH}_2\text{-CH}_2\text{-C(=O)-DBCO}$), 46.56 ($\text{NH-CH}_2\text{-CH}_2\text{-C(=O)-DBCO}$), 43.77 (Backbone CH_2), 43.14 (Backbone CH_2) 30.93 (backbone CH_3)

Raman (cm^{-1}): 1614 (Aromatic C-C) 2159 (Alkyne)

For the synthesis of PG₂₅, PG₅₀, and PG₇₅

The same synthetic procedure as above, but with the number of equivalents of DBCO adjusted to give target substitutions of 7.5%, 15% and 22.5%.

^1H NMR (MeOD) 500MHz, ppm: 7.5-7.0 (br, Benzyl) 4.42 (br, cyclooctyne ring CH_2) 3.65 (br, $\text{NH-CH}_2\text{-CH}_2\text{-}$), 3.28 (br, $\text{-NH-CH}_2\text{-CH}_2\text{-}$), 2.5-1.5 (br, Backbone CH_2) 1.5-1.0 (br, backbone Me)

^{13}C NMR (MeOD) 500MHz: 179.42 (br, C=O) 141.16 (Benzyl No H), 136.93 (Benzyl No H), 132-128 (benzyl H), 63.02, 61.31 ($\text{NH-CH}_2\text{-CH}_2\text{-OH}$), 61.08 ($\text{NH-CH}_2\text{-CH}_2\text{-OH}$), 60.09, 59.61, 56.93, 52.49 (Cyclooctyne Ring CH_2), 46.95 ($\text{NH-CH}_2\text{-CH}_2\text{-C(=O)-DBCO}$), 46.56 ($\text{NH-CH}_2\text{-CH}_2\text{-C(=O)-DBCO}$), 43.77 (Backbone CH_2), 43.14 (Backbone CH_2) 30.93 (backbone CH_3)

Raman (cm^{-1}): 1614 (Aromatic C-C) 2159 (Alkyne)

Synthesis of Glycopolymers PG₂₅M₇₅, PG₅₀M₅₀, PG₇₅M₂₅, PG₁₀₀

Using stock solutions of $1 \text{ mg}\cdot\text{mL}^{-1}$ sugar azide ($4.87 \times 10^{-3} \text{ mL}^{-1}$), 2.75 ml of each of; [Gal]:[Man], 100:0, 75:25, 50:50 and 25:75 (V:V) solutions were prepared. For each glycopolymer, 2.75 mL of the corresponding azido-sugar solution was added to p(DBCO)₁₅(HEMA)₃₅ (5 mg, 357 nmol) in a vial. The reaction was left at room temperature overnight. To remove excess sugar the solutions were passed through a 1000MWCO centrifugal filter and re-suspended in water three times. The resulting solution was then freeze dried. IR and Raman of final polymers showed no presence of alkyne or azide peak.

N.B. To give a 2.5x excess of sugar-azide to polymer-alkyne, the number of moles of polymer was multiplied by 15 (for each alkyne unit) and 2.5 (to give an excess of sugar)

Synthesis of Glycopolymers PG₂₅, PG₅₀, and PG₇₅

To 50mg of p(DBCO)_{4.85}(HEMA)_{45.15}, p(DBCO)₈(HEMA)₄₂ and p(DBCO)_{10.71}(HEMA)_{39.29} each, was added 1-azido-1-deoxy galactose, (7.5mg, 12mg and 15mg respectively) and 2.75mL of DI water added. The reaction was left at room temperature overnight. To remove excess sugar the solutions were passed through a 1000MWCO centrifugal filter and re-suspended in water three times. The resulting solution was then freeze dried. Raman of final polymers showed no presence of Alkyne peak.

¹H NMR (MeOD) (500MHz): 7.5-7.0 (br, Benzyl) 4.59, 4.59 (br, cyclooctyne ring CH₂) 3.65 (br, NH-CH₂-CH₂-), 3.28 (br, -NH-CH₂-CH₂-), 2.5-1.5 (br, Backbone CH₂) 1.5-1.0 (br, backbone Me)

¹³C NMR (MeOD) 500MHz: 179.42 (br, C=O) 141.16 (Benzyl No H), 136.93 (Benzyl No H), 132-128 (benzyl H), 63.02, 61.31 (NH-CH₂-CH₂-OH), 61.08 (NH-CH₂-CH₂-OH), 60.09,

59.61, 56.93, 52.49 (Cyclooctyne Ring CH₂), 46.95 (NH-CH₂-CH₂-C(=O)-DBCO), 46.56 (NH-CH₂-CH₂-C(=O)-DBCO), 43.77 (Backbone CH₂), 43.14 (Backbone CH₂) 30.93 (backbone CH₃)

DOSEY NMR (MeOD) 500MHz, $\log(\text{m}^2\text{s}^{-1}) = -4.8$, 7.5-7.0, (Benzyl) 4.42 (br, cyclooctyne ring CH₂) 3.65 (br, NH-CH₂-CH₂-), 3.28 (br, -NH-CH₂-CH₂-), 2.5-1.5 (br, Backbone CH₂) 1.5-1.0(br, backbone Me)

2.6 References

- 1 T. R. Branson and W. B. Turnbull, *Chem. Soc. Rev.*, 2013, **42**, 4613–22.
- 2 G. E. Soto and S. J. Hultgren, *J. Bacteriol.*, 1999, **181**, 1059–71.
- 3 J. D. Esko and N. Sharon, *Microbial Lectins: Hemagglutinins, Adhesins, and Toxins*, Cold Spring Harbor Laboratory Press, 2009.
- 4 C. M. Thorpe, *Clin. Infect. Dis.*, 2004, **38**, 1298–1303.
- 5 C. D. Herbert, *Toxic. Rep. Ser.*, 1993, **37**, 1-D3.
- 6 L. A. Lasky, *Annu. Rev. Biochem.*, 1995, **64**, 113–140.
- 7 P. M. Rudd, *Science*, 2001, **291**, 2370–2376.
- 8 R. O. Hynes, *Cell*, 1992, **69**, 11–25.
- 9 M. Ambrosi, N. R. Cameron and B. G. Davis, *Org. Biomol. Chem.*, 2005, **3**, 1593–608.
- 10 T. K. Dam and C. F. Brewer, *Biochemistry*, 2008, **47**, 8470–8476.
- 11 J. J. Lundquist and E. J. Toone, *Chem. Rev.*, 2002, **102**, 555–578.
- 12 A. Bernardi, J. Jiménez-Barbero, A. Casnati, C. De Castro, T. Darbre, F. Fieschi, J. Finne, H. Funken, K.-E. Jaeger, M. Lahmann, T. K. Lindhorst, M. Marradi, P. Messner, A. Molinaro, P. V Murphy, C. Nativi, S. Oscarson, S. Penadés, F. Peri, R. J. Pieters, O. Renaudet, J.-L. Reymond, B. Richichi, J. Rojo, F. Sansone, C. Schäffer, W. B. Turnbull, T. Velasco-Torrijos, S. Vidal, S. Vincent, T. Wennekes, H. Zuilhof and A. Imberty, *Chem. Soc. Rev.*, 2013, **42**, 4709–27.

- 13 S. Won, S.-J. Richards, M. Walker and M. I. Gibson, *Nanoscale Horiz.*, 2017, **3**, 1593–1608.
- 14 N. Sharon, *Biochim. Biophys. Acta*, 2006, **1760**, 527–37.
- 15 P. I. Kitov, J. M. Sadowska, G. Mulvey, G. D. Armstrong, H. Ling, N. S. Pannu, R. J. Read and D. R. Bundle, *Nature*, 2000, **403**, 669–72.
- 16 C. R. Becer, M. I. Gibson, J. Geng, R. Ilyas, R. Wallis, D. A. Mitchell and D. M. Haddleton, *J. Am. Chem. Soc.*, 2010, **132**, 15130–15132.
- 17 A. Muñoz, D. Sigwalt, B. M. Illescas, J. Luczkowiak, L. Rodríguez-Pérez, I. Nierengarten, M. Holler, J.-S. Remy, K. Buffet, S. P. Vincent, J. Rojo, R. Delgado, J.-F. Nierengarten and N. Martín, *Nat. Chem.*, 2015, **8**, 50–57.
- 18 M. L. Huang, M. Cohen, C. J. Fisher, R. T. Schooley, P. Gagneux and K. Godula, *Chem. Commun.*, 2015, **51**, 5326–9.
- 19 M. W. Jones, L. Otten, S.-J. Richards, R. Lowery, D. J. Phillips, D. M. Haddleton and M. I. Gibson, *Chem. Sci.*, 2014, **5**, 1611.
- 20 S.-J. Richards, M. W. Jones, M. Hunaban, D. M. Haddleton and M. I. Gibson, *Angew. Chemie. Int. Ed.*, 2012, **51**, 7812–7816.
- 21 K. W. Moremen, M. Tiemeyer and A. V. Nairn, *Nat. Rev. Mol. Cell Biol.*, 2012, **13**, 448–462.
- 22 M. Ortega-Muñoz, F. Perez-Balderas, J. Morales-Sanfrutos, F. Hernandez-Mateo, J. Isac-García and F. Santoyo-Gonzalez, *European J. Org. Chem.*, 2009, **2009**, 2454–2473.
- 23 S. Zhang, Q. Xiao, S. E. Sherman, A. Muncan, A. D. M. Ramos Vicente, Z. Wang, D.

- A. Hammer, D. Williams, Y. Chen, D. J. Pochan, S. Vértesy, S. André, M. L. Klein, H.-J. Gabius and V. Percec, *J. Am. Chem. Soc.*, 2015, **137**, 13334-13344.
- 24 N. C. Worstell, P. Krishnan, J. D. Weatherston and H. J. Wu, *PLoS One*, 2016, **11**, e0153265.
- 25 S.-J. Richards, L. Otten and M. I. Gibson, *J. Mater. Chem. B*, 2016, **4**, 3046–3053.
- 26 M. Mammen, S.-K. Choi and G. M. Whitesides, *Angew. Chemie Int. Ed.*, 1998, **37**, 2754–2794.
- 27 L. L. Kiessling, J. E. Gestwicki and L. E. Strong, *Angew. Chemie Int. Ed.*, 2006, **45**, 2348–2368.
- 28 M. Eberhardt, R. Mruk, R. Zentel and P. Théato, *Eur. Polym. J.*, 2005, **41**, 1569–1575.
- 29 M. I. Gibson, E. Fröhlich and H.-A. Klok, *J. Polym. Sci. Part A Polym. Chem.*, 2009, **47**, 4332–4345.
- 30 N. J. Agard, J. A. Prescher and C. R. Bertozzi, *J. Am. Chem. Soc.*, 2004, **126**, 15046–7.
- 31 N. Vinson, Y. Gou, C. R. Becer, D. M. Haddleton and M. I. Gibson, *Polym. Chem.*, 2011, **2**, 107–113.
- 32 D. Cabral-Lilly, G. E. Sosinsky, R. A. Reed, M. R. McDermott and G. G. Shipley, *Biophys. J.*, 1994, **66**, 935–941.
- 33 S. Sharma, S. Bharadwaj, A. Surolia and S. K. Podder, *Biochem. J.*, 1998, **333 (Pt 3)**, 539–42.
- 34 V. Wittmann and R. J. Pieters, *Chem. Soc. Rev.*, 2013, **42**, 4492.
- 35 S. G. Spain and N. R. Cameron, *Polym. Chem.*, 2011, **2**, 1552.

- 36 J. C. Pickens, E. A. Merritt, M. Ahn, C. L. M. J. Verlinde, W. G. J. Hol and E. Fan, *Chem. Biol.*, 2002, **9**, 215–24.
- 37 A. G. Gabdoulkhakov, Y. Savochkina, N. Konareva, R. Krauspenhaar, S. Stoeva, S. V. Nikonov, W. Voelter, C. Betzel and A. M. Mikhailov, *doi.org*.
- 38 J. L. Sebaugh, *Pharm. Stat.*, 2011, **10**, 128–134.
- 39 D. R. Waud, in *Advances in General and Cellular Pharmacology*, Springer US, Boston, MA, 1976, pp. 145–178.
- 40 Tarun K. Dam, René Roy, and Daniel Pagé and C. Fred Brewer, *Biochem.* 2002,**41**, 1351-1358.
- 41 H.-A. Tran, P. I. Kitov, E. Paszkiewicz, J. M. Sadowska and D. R. Bundle, *Org. Biomol. Chem.*, 2011, **9**, 3658.
- 42 W. Bruce Turnbull, Bernie L. Precious and Steve W. Homans, 2004.
- 43 A. T. Aman, S. Fraser, E. A. Merritt, C. Rodighiero, M. Kenny, M. Ahn, W. G. Hol, N. A. Williams, W. I. Lencer and T. R. Hirst, *Proc. Natl. Acad. Sci. U. S. A.*, 2001, **98**, 8536–41.
- 44 P. Cheshev, L. Morelli, M. Marchesi, C. Podlipnik, M. Bergström and A. Bernardi, *Chem. - A Eur. J.*, 2010, **16**, 1951–1967.
- 45 G. Volkers, L. J. Worrall, D. H. Kwan, C.-C. Yu, L. Baumann, E. Lameignere, G. A. Wasney, N. E. Scott, W. W. Wakarchuk, L. J. Foster, S. G. Withers and N. C. J. Strynadka, *Nat. Struct. Mol. Biol.*, 2015, **22**, 627–635.

Chapter Three

Semi-Automated Assembly of Heterogeneous Glycosylated Gold Nanoparticles for High- Throughput Screening

Declarations

The work submitted in this chapter was performed by myself except where specified: 1-(8-azidooctyl)-1-deoxy mannose was kindly provided by Martina Lahmann, University of Bangor. GalNH₂-HEAA₂₅Au₄₀ was synthesised by Sarah Jane Richards, Gibson Group, University of Warwick. TEM images were obtained by Gemma Louise Davies and George Henry Lee, Davies Group, University of Warwick.

3.1. Abstract

Carbohydrate binding proteins, which include lectins, play a vital role in many biological processes including pathogen binding at the initial stages of infection. Tools which can detect pathogenic lectins may enable the development of point-of-care diagnostics to help prevent the spread of diseases, detecting biological warfare agents and also to enable fundamental glycobiology studies as mimics of complex cell surfaces. Further to this, a greater understanding of lectin interactions may play a role in developing anti-adhesion therapies as alternatives to traditional antibiotics. This chapters introduces the development of scalable methods for assembling glycosylated nanoparticle libraries containing both homogenous and heterogeneous glycan coatings that is simple, compatible with automated liquid handling robots and generates a binding signal without additional labels, allowing native (unlabelled) lectins to be studied. Figure 3.1.

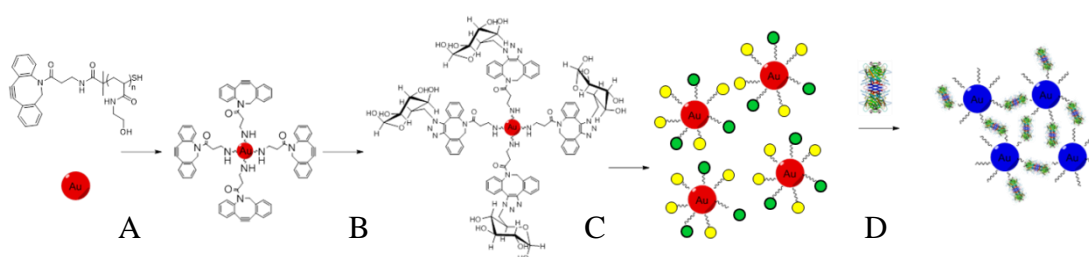


Figure 3.1: Overall schematic for the robotic assembly and label-free detection of lectins. A. Formation of a azide reactive polymer coated gold nanoparticle precursor B and C. Homo and heterogeneous functionalisation of the nanoparticle with azide-modified sugars in a statistical manner. D. Lectin induced aggregation results in a reduced gold nanoparticle separation distance and produces a blue colour.

3.2. Introduction

Carbohydrates play a key role in the adhesion of pathogenic species¹⁻⁴, cancer progression^{2,5-7}, inflammation^{1,8} and a host of other processes¹. It is estimated that up to 50% of proteins in the human body are glycosylated⁹ and the mapping of this ‘glycome’ remains a huge challenge. The proteins that decipher this glycan-information are termed lectins. Lectins non-covalently bind to their specified carbohydrate targets dependant on the carbohydrate stereochemistry, branching pattern and functional isomerism. Individual protein-monosaccharide interactions are usually very weak; however, the interaction with multiple clustered saccharides is much greater than the sum of the individual affinities. This multivalent effect is termed “the cluster glycoside effect”.^{10,11} This effect is well documented, with a wide number of lectins and carbohydrate ligands studied; a prime example is the use of rational design to create a sub-nanomolar inhibitor of shiga toxins I and II by Kitov *et al.* Shiga toxins are AB₅ toxins consisting of an A domain that gains entry to mammalian cells after the adhesion of the homopentameric B subdomain. By synthesising a pentameric multivalent carbohydrate ligand (named STARFISH), inhibition of shiga toxins I and II was increased by more than 1 million fold over the carbohydrate ligand alone.¹² However, most studies using multivalent scaffolds have focused on homogenous structures – i.e. using a single glycan. Cell surfaces, however, present a heterogeneous array of glycans and lectins themselves are often termed pattern recognition domains.¹³ Therefore, any synergistic or antagonistic effects that may arise within such a heterogeneous environment, that would help to understand affinity *in vivo*, may be missed. Work by Hartmann and co-workers investigated the effects of heterogeneity in glyco oligomers. It was shown that for the Mannose binding lectin Con A, a glucose-mannose-glucose trimer had twice the inhibitory activity (0.4µM), compared to the mannose only trimer (0.8µM), while the galactose-mannose-galactose trimer had comparable activity (1.0µM).¹⁴ This is despite Con

A having an affinity 4 times greater for mannose than glucose, and no affinity for galactose. They found that the galactose residues in this instance do not participate in the binding to Con A, but they promote steric shielding giving an increase in affinity. This highlights the complexity in understanding multivalent modes of binding the difficulty in rationally designing inhibitors.

Therefore it is important to develop widely applicable, robust, easily synthesised screening techniques to probe lectin binding in heterogeneous environments.

One of the difficulties in synthesising heterogeneous multivalent glyco-libraries is maintaining control over the positioning of the two (or more) sugars relative to each other in the heterogeneous assembly. There have been two main approaches to this problem: (1) Low density glyco-clusters utilizing multiple protecting group and/or orthogonal chemical strategies to develop well defined glyco-environments at a cost of greater synthetic complexity and the associated drawbacks or (2) High density glyco-clusters utilizing a statistical approach to lectin binding.

To move towards 'glycomics' research in the same vain as proteomics, large scale robust screening libraries are required. To achieve this several aspects need to be addressed:

- Straightforward, robust synthesis
- Facile purification to allow large scale production
- High throughput output
- Straight forward analysis

Gold nanoparticles offer a convenient route to a high through-put colourimetric assay. Monodisperse solutions of gold nanoparticles are highly coloured, this is due to the electromagnetic field of incident light inducing an oscillation of the free electrons in the

conduction band of the metal. This oscillation of electrons at the particles surface induces a dipole and the frequency at which this oscillation occurs is known as the surface plasmon resonance (SPR peak), which for gold occurs around 520 nm.¹³ The SPR causes a strong absorption of incident light, and the intensity and wavelength of the absorption is dependent on factors that affect the electron charge density at the surface of the particle. As such, changing the particles size changes the absorption of the SPR peak and so the colour of the nanoparticle solution. At smaller wavelengths the SPR peak absorbs in the blue-green portion of the spectrum and so the particles appear red. As the nanoparticle size increases, the SPR absorption is red shifted and so the solution takes on a blue hue. This makes gold nanoparticles ideal for a colorimetric assay based on aggregation of the gold nanoparticles that can be analysed using UV-Vis spectrometry.¹⁵⁻²¹

On top of this, colourimetric assays of this type have potential applications in point of care diagnosis work.^{20,22,23} The thermal stability of gold nanoparticles allows easy transportation to areas of the world where refrigeration is difficult or not an option, and while UV-Vis spectrometry is a relatively cheap analysis technique (compared to other options such as SPR assays) efforts have been made to allow analysis of colourimetric assays using mobile phones.²⁴⁻²⁶ While this is outside the scope of this work, assays based on this technique have the ability to expand into practical diagnostic roles from the outset.

To give gold nanoparticles the stability against salts required for protein buffers and biological conditions they must be stabilised with a steric coating.²³ Polymers offer an easy method to provide this coating and provide chemical functionality. In particular polymers produced via reversible addition fragmentation chain transfer polymerisation (RAFT) are perfect as they contain a thiol end group that is reactive towards gold. RAFT polymerisation allows the synthesis of polymers with high control over the molecular weight and dispersity to ensure repeatability and control over the particle stability. Figure 3.2.

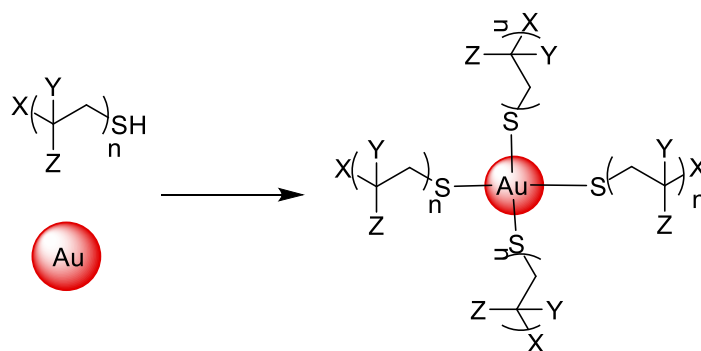


Figure 3.2: Assembly of functionalised gold nanoparticles using raft polymerisation, where X, Y and Z are potential chemical functionality that can be incorporated. This figure ignores co-polymer effects.

To assemble our ‘modular’ nanoparticle we have chosen to use the strained cyclooctyne DBCO, Figure 3.3. This allows us to utilise the strain promoted alkyne azide cyclisation reaction, also known as copper-free click in reference to the well-known copper catalysed azide alkyne cycloaddition popularised by Sharpless.²⁷

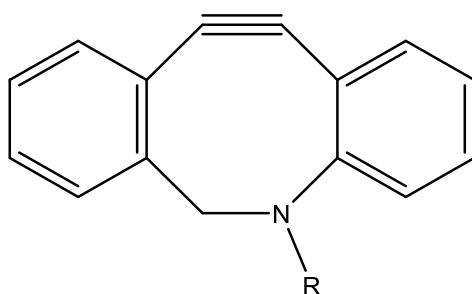


Figure 3.3: DBCO.

This reaction is fast and has 100% atom efficiency resulting in very little work up, making it ideal for large scale combinatorial chemistry. Further to this it introduces a large hydrophobic face close to the binding ligand which may help increase the rigidity of the system and reduce the entropic cost of binding.

All of these synthetic components together are compatible with large scale liquid handling robots and biological assay consumables such as 384-well plates, giving the assays built in scale-ability for high throughput processing.

To test the effectiveness of the AuNP library, 5 lectins were screened against, Table 3.1.

Table 3.1: Lectin and stated specificity.

Lectin	Stated Binding Ligand
<i>Dolichos biflorus</i> agglutinin (DBA)	<i>N</i> -Acetyl galctosamine
Peanut agglutinin (PNA)	Galactose
Soy bean agglutinin (SBA)	<i>N</i> -Acetyl galctosamine
Wheat germ agglutinin (WGA)	<i>N</i> -Acetyl glucosamine
<i>Ricinus communis</i> Agglutinin I (RCA ₁₂₀)	Galactose

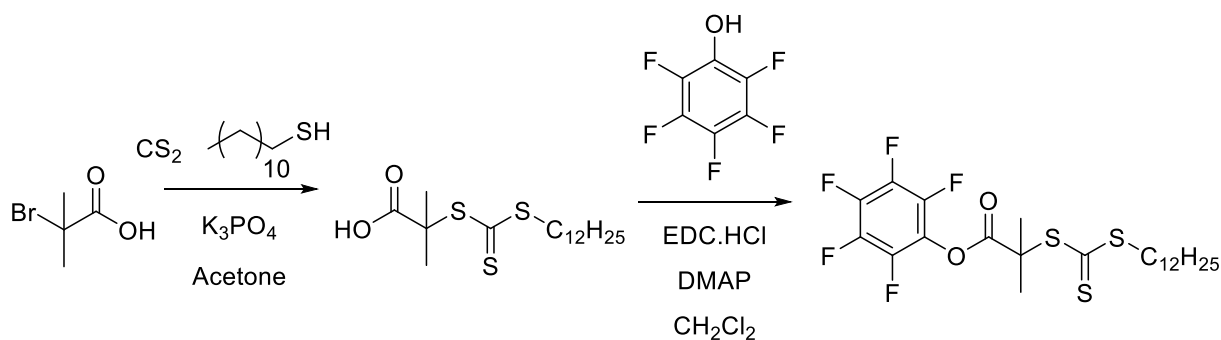
Despite having similar stated binding specificities, in practise they have quite different binding behaviours. PNA is known to bind to lactose²⁸. All five lectins are easy to work with and obtain.

To this end, a gold nanoparticle based carbohydrate screening library was developed, which utilises the multivalency effect as a means of both interrogating lectin binding and as method for circumventing time consuming purification steps. This library is easily adapted to give any glyco-environment required; homo- or heterogeneous and is compatible with high throughput liquid handling and analytical techniques.

3.3. Results and discussion

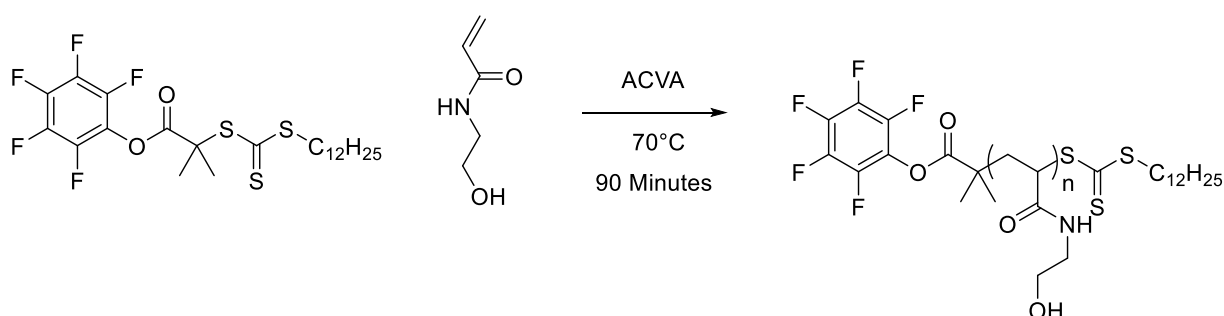
3.3.1. Polymerisation

To generate the heterogeneous library the polymer coating must fulfil several criteria. It must be water soluble, sufficiently stabilise the gold particles against protein buffer solution, not stabilise the particles so much that the reaction times are prohibitively long and allow further functionalisation to generate the heterogeneous library. In line with previous work by Richards *et al*, hydroxyethyl acrylamide (HEAA) was chosen as an appropriate stabiliser²⁹. In order to maintain control over the polymer chain length and therefore have control over the assay reaction time, 2-(dodecylthiocarbonothioylthio)-2-methylpropionic acid pentafluorophenyl ester was synthesised using a modified method by Phillips *et al*,³⁰ Scheme 3.1. ¹⁹F NMR confirmed the presence of the PFP group, and ¹H NMR and Mass spec confirmed the structure in line with previous reports.



Scheme 3.1: Two step synthesis of 2-(dodecylthiocarbonothioylthio)-2-methylpropionic acid pentafluorophenyl ester.

A trithiocarbonate-based RAFT agent was chosen as they give good molecular weight control over acrylamide monomers and are convenient to synthesise. This allowed us to polymerise acrylamides with high molecular weight control and low dispersity, and to install the pentafluorophenol-ester at the alpha end of any generated polymer. The raft agent was synthesised in a two-step procedure and the resulting yellow liquid characterised using ^1H NMR spectroscopy, and used as a RAFT agent for the polymerisation of hydroxyethyl acrylamide.



Scheme 3.2: Polymerisation of PFP-HEAA synthetic scheme.

Hydroxyethyl acrylamide was prepared using RAFT polymerisation with a targeted degree of polymerisation of 25, 50, 75 and 100, Scheme 3.2. PFP-DMP was used as the RAFT agent (CTA) as previously discussed, and 4,4'-azobis(4-cyanovaleric acid) (ACVA) was chosen as the radical initiator. The polymer was isolated by precipitation. The isolated yellow solids were characterised by ^1H NMR, and size exclusion chromatography (SEC), Figure 3.4.

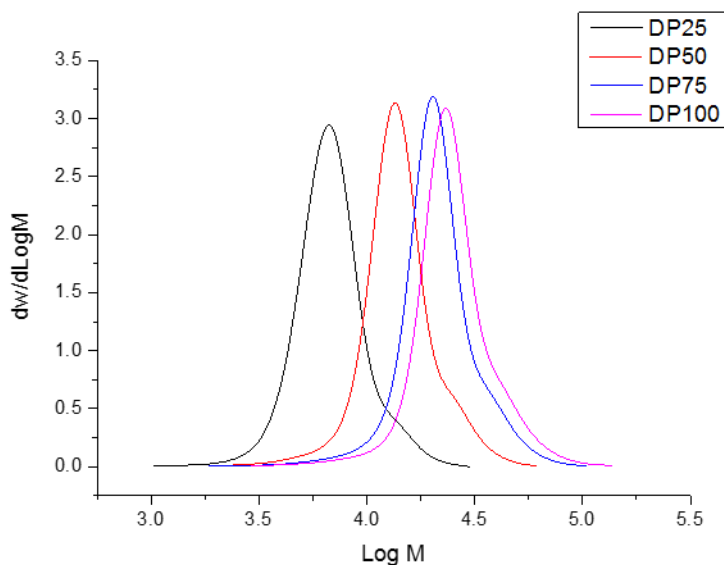


Figure 3.4: SEC trace of pHEAA-PFP at different degrees of polymerisation.

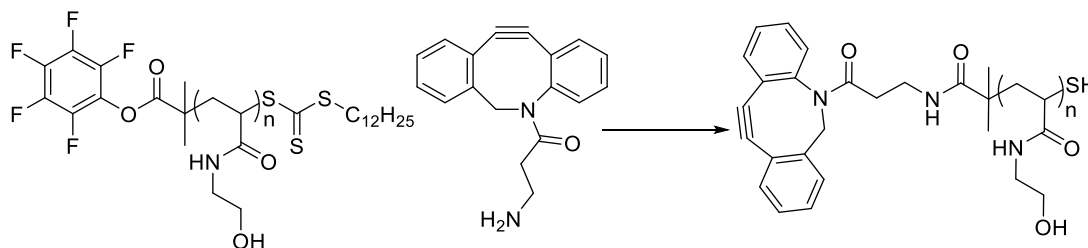
The degree of polymerisation was calculated using ^1H NMR spectroscopy by determining the relative monomer concentration before the reaction is initiated and after the reaction has been quenched, relative to an internal mesitylene standard.

Table 3.2: Characterisation of p(hydroxyethyl acrylamide) pentafluorophenol ester.

Polymer ^(a)	[HEAA]:[CTA]	Conversion(%) ^(b)	M_n Theo	M_n SEC	M_w/M_n ^(c)
pHEAA ₂₅ -PFP	25:1	97	3300	6300	1.15
pHEAA ₅₀ -PFP	50:1	96	6100	12900	1.17
pHEAA ₇₅ -PFP	75:1	85	7900	19100	1.19
pHEAA ₁₀₀ -PFP	100:1	90	10900	22500	1.20

^apHEAA-PFP = p(hydroxyethyl acrylamide) pentafluorophenol ester; ^bDetermined by ^1H NMR spectroscopy relative to an internal standard (mesitylene); ^c Determined by SEC (DMF) relative to PMMA standards.

After the polymerisation, the α -end group of PHEAA₂₅-PFP was modified via nucleophilic addition of dibenzocyclooctyne-amine (DBCO-amine) to the pentafluorophenol ester, as shown in Scheme 3.3 PHEAA₂₅-PFP was chosen for this step as this has previously been identified as an ideal chain length for stabilising 30-60nm gold nanoparticles while ensuring the agglutination assay still occurred rapidly.²⁹



Scheme 3.3: Nucleophilic addition of DBCO-amine to the amine reactive PFP-endgroup.

The reaction was monitored using ¹⁹F NMR spectroscopy, and the presence of the DBCO alkyne was confirmed using Raman spectroscopy, showing the aromatic C-C and alkyne peak at 1600cm⁻¹ and 2159 cm⁻¹ respectively, Figure 3.5.

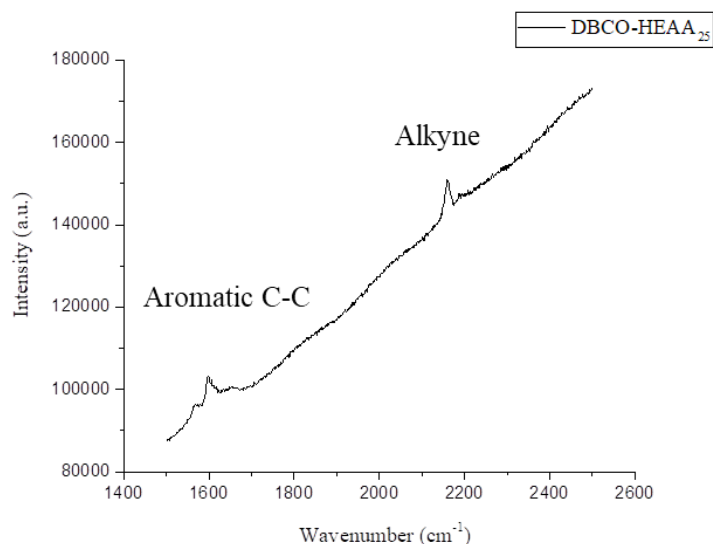


Figure 3.5: Solid phase Raman spectra of PHEAA₂₅-DBCO.

3.3.2. Synthesis of gold nanoparticles *via* one-pot citrate reduction

The AuNPs were synthesised using the citrate reduction method,³¹ varying the ratio of HAuCl₄ to citrate to allow control of the size. Originally 60 nm gold particles were targeted, as this had previously been shown to give an effective response within a reasonable timeframe.²³ However these particles were found to be unstable during a period of 24-48 hours post coating with HEAA₂₅-DBCO, which would make them non applicable for screening applications, where a stock of stable particles is essential. This can be explained if we assume that 60 nm gold and pHEAA with a degree of polymerisation of 25 is on the boundary of stability for the nanoparticles not providing a sufficient steric shield. Therefore, variations in the dispersity of either the gold nanoparticles or the polymer stabiliser will have an impact upon the stability of the system. It was decided to use a smaller size of gold nanoparticle.

A molar ratio of 1:3.5 gold:citrate gave nanoparticles with diameter 32 nm, as measured by the Haiss method³² with UV-Vis and by dynamic light scattering, Table 3.3. The resulting

particles were also characterised by transmission electron spectroscopy (TEM), the resulting images were processed in imageJ³³ to obtain a histogram of nanoparticle size, Figure 3.6.

The gold particles were then coated with the DBCO-pHEAA at a concentration of 1 mg/ml overnight, and excess polymer was removed by repeated centrifugation-resuspension cycles. UV-Vis and DLS characterisation are shown below, Figure 3.7 and summarised in Table 3.3.

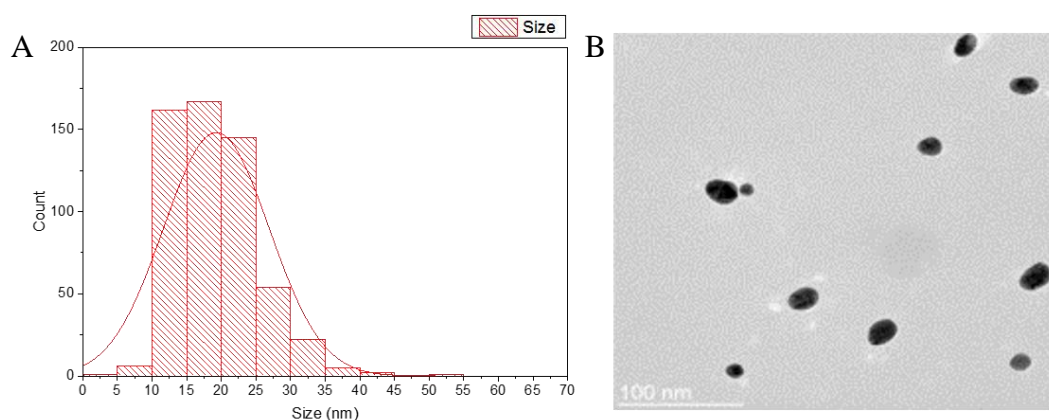


Figure 3.6: (A) Histogram of AuNP size, $n= 567$, $d=19.2\pm 7.6$ (B) Example TEM showing nanoparticle morphology.

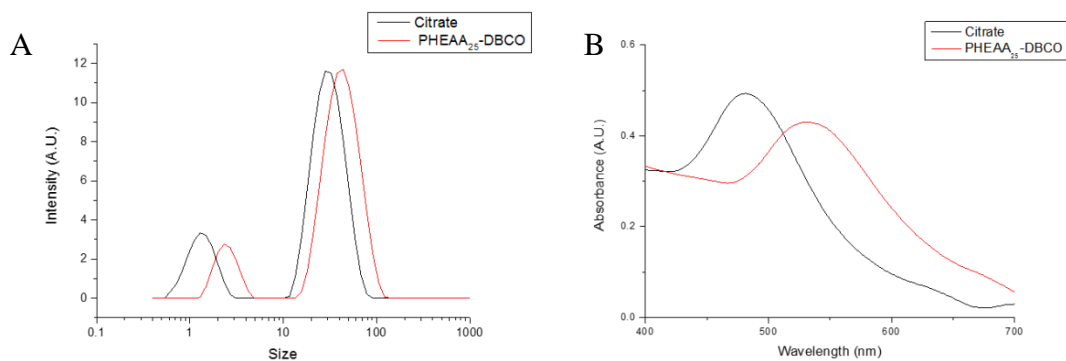


Figure 3.7: (A) DLS trace of Citrate and PHEAA₂₅-DBCO-stabilised polymers N.B. small intensity peak at very low size. (B) UV-Vis of Citrate and PHEAA₂₅-DBCO-HEAA stabilised particles.

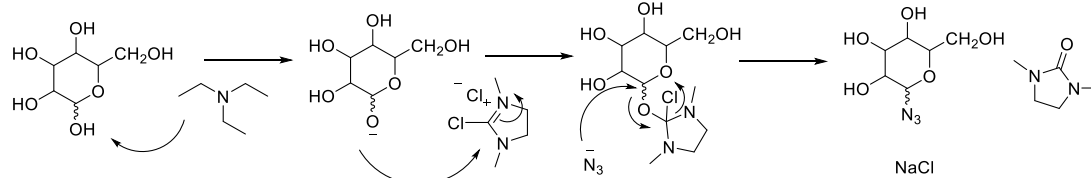
Table 3.3 Summary of UV-Vis and DLS characterisation.

Coating	Size ^(a) (nm)	Size ^(b) (nm)	Size (nm) ^(c)
Citrate	32	32 ±0.2	19.2 ±7.6
DBCO-HEAA ₂₅	54	47 ±1.7	N/A

(a) UV-Vis (b) Dynamic light scattering (c) TEM

The DLS trace showed a small intensity peak ~3-5nm in size. This peak could be due to gold seed particles that did not grow during the synthesis. However, it is more likely that these are artefacts arising from glancing-angle light scattering causing a false peak.

3.3.3. Synthesis of azido-sugars and assembling a heterogeneous library



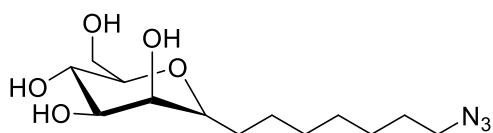
Scheme 3.4: General synthesis for forming 1-azido-1-deoxy hexoses.

In order to construct a heterogeneous library, 1-azido-1-deoxy galactose and 1-azido-1-deoxy mannose were synthesised, as shown in Scheme 3.4, using the synthetic scheme reported by Vinson *et al.*³⁴ 2-Chloro-1,3-dimethylimidazolium chloride (DMC) which specifically activates the anomeric centre rather than the other hydroxyls, due to its lower pK_a , enables nucleophilic attack by sodium azide without the use of protecting groups. IR and MS confirmed installation of the azide.

Galactose was chosen as this is the stated primary binding partner for the lectins (PNA and RCA, while DBA and SBA bind *N*-Acetyl galactosamine, WGA binds *N*-Acetyl glucosamine) we intended to screen against, while mannose is a nominally non-binding sugar. However as shown in chapter two, there is evidence to suggest that mannose can act to improve the binding of nominally galactose binding lectins such as RCA₁₂₀ by acting as a weak but rapid binder to drive lectin association .

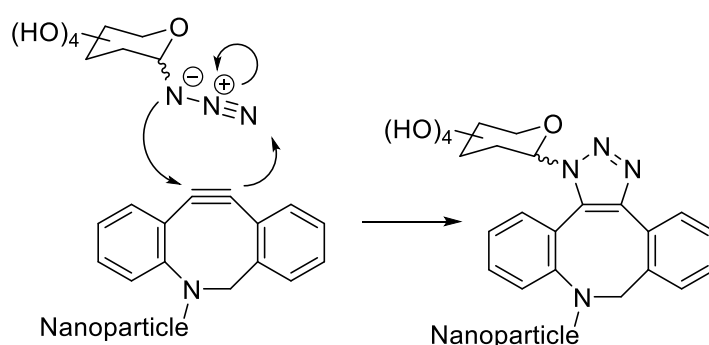
In addition to this, 2-azido-2-deoxy glucose, 2-azido-2-deoxy galactose, 6-azido-6-deoxy glucose, and, 6-azido-6-deoxy galactose were also purchased from a commercial source (Carbosynth Ltd), while 1-(8-azido-octyl)-1-deoxy mannose (mannose-C8-azide), Scheme 3.5, was obtained from Martina Lahmann at Bangor University, Wales to provide a glycan with a longer linker. As the monosaccharides all have azido groups on them, they will

undergo spontaneous cycloaddition with the strained cyclooctyne at the polymer terminus, on the gold nanoparticle surface.



Scheme 3.5 : The structure of 1-(8-azido-octyl)-1-deoxy mannose (mannose-C8-azide)

To assemble the heterogeneous nanoparticle library, Scheme 3.6, solutions containing the molar percentage ratios of the intended final sugar concentration of each sugar combination to be tested were prepared in milliQ water and added to the alkyne-functional gold nanoparticles.



Scheme 3.6: The strain promoted azide alkyne coupling reaction

For example, to obtain a particle with an 80:20 ratio of 2-azido-2-deoxy galactose to 6-azido-6-deoxy glucose, a solution containing an 8:2 molar ratio of 2-azido-2-deoxy galactose to 6-azido-6-deoxy glucose was made. The total number of moles of both sugars was 2.5x the number of moles of polymer added to coat the particles. The particles were left overnight and purified by centrifugation at 3,000g for 30 minutes, three times. During these purification cycles it was noted that a large proportion of the gold nanoparticles formed aggregated

clusters that would not re-suspend without sonication, a step we were keen avoid due to potential damage to the polymer coating and a loss of material. The new concentration of gold was determined *via* UV-Vis to be 6.7×10^{-11} M, using the Beer Lambert law (Equation 3.1) a value of ϵ_{450} of $3.21 \times 10^9 \text{ M}^{-1} \text{ cm}^{-1}$ ³² and a path length of 0.274 cm^{-1} .

$$A = \epsilon lc \quad \mathbf{3.1}$$

The first library to be tested used 2-azido-2-deoxy glucose, 2-azido-2-deoxy galactose, 6-azido-6-deoxy glucose, and, 6-azido-6-deoxy galactose in molar percentage ratios of 100:0, 80:20, 60:40, 40:60, 20:80 and 0:100. For these initial investigations we chose to limit the library to bi-functional nanoparticles (2 different sugars per particle). With these conditions, 36 unique sugar coated gold nanoparticles could be made, as shown in Table 3.4

Table 3.4: Heterogenous AuNP library formed with 2-azido-2-deoxy glucose, 2-azido-2-deoxy galactose, 6-azido-6-deoxy glucose, and, 6-azido-6-deoxy galactose.

Sample	Ratio (mol %)	Sugar 1	Sugar 2
A1	100:0	2-Azido-2-deoxy Glucose	2-Azido-2-deoxy Galactose
A2	80:20	2-Azido-2-deoxy Glucose	2-Azido-2-deoxy Galactose
A3	60:40	2-Azido-2-deoxy Glucose	2-Azido-2-deoxy Galactose
A4	40:60	2-Azido-2-deoxy Glucose	2-Azido-2-deoxy Galactose
A5	20:80	2-Azido-2-deoxy Glucose	2-Azido-2-deoxy Galactose
A6	0:100	2-Azido-2-deoxy Glucose	2-Azido-2-deoxy Galactose
B1	100:0	2-Azido-2-deoxy Glucose	6-Azido-6-deoxy Glucose
B2	80:20	2-Azido-2-deoxy Glucose	6-Azido-6-deoxy Glucose
B3	60:40	2-Azido-2-deoxy Glucose	6-Azido-6-deoxy Glucose
B4	40:60	2-Azido-2-deoxy Glucose	6-Azido-6-deoxy Glucose
B5	20:80	2-Azido-2-deoxy Glucose	6-Azido-6-deoxy Glucose
B6	0:100	2-Azido-2-deoxy Glucose	6-Azido-6-deoxy Glucose
C1	100:0	2-Azido-2-deoxy Glucose	6-Azido-6-deoxy Galactose
C2	80:20	2-Azido-2-deoxy Glucose	6-Azido-6-deoxy Galactose
C3	60:40	2-Azido-2-deoxy Glucose	6-Azido-6-deoxy Galactose
C4	40:60	2-Azido-2-deoxy Glucose	6-Azido-6-deoxy Galactose
C5	20:80	2-Azido-2-deoxy Glucose	6-Azido-6-deoxy Galactose
C6	0:100	2-Azido-2-deoxy Glucose	6-Azido-6-deoxy Galactose
D1	100:0	2-Azido-2-deoxy Galactose	6-Azido-6-deoxy Glucose
D2	80:20	2-Azido-2-deoxy Galactose	6-Azido-6-deoxy Glucose
D3	60:40	2-Azido-2-deoxy Galactose	6-Azido-6-deoxy Glucose
D4	40:60	2-Azido-2-deoxy Galactose	6-Azido-6-deoxy Glucose
D5	20:80	2-Azido-2-deoxy Galactose	6-Azido-6-deoxy Glucose
D6	0:100	2-Azido-2-deoxy Galactose	6-Azido-6-deoxy Glucose
E1	100:0	2-Azido-2-deoxy Galactose	6-Azido-6-deoxy Galactose
E2	80:20	2-Azido-2-deoxy Galactose	6-Azido-6-deoxy Galactose
E3	60:40	2-Azido-2-deoxy Galactose	6-Azido-6-deoxy Galactose
E4	40:60	2-Azido-2-deoxy Galactose	6-Azido-6-deoxy Galactose
E5	20:80	2-Azido-2-deoxy Galactose	6-Azido-6-deoxy Galactose
E6	0:100	2-Azido-2-deoxy Galactose	6-Azido-6-deoxy Galactose
F1	100:0	6-Azido-6-deoxy Glucose	6-Azido-6-deoxy Galactose
F2	80:20	6-Azido-6-deoxy Glucose	6-Azido-6-deoxy Galactose
F3	60:40	6-Azido-6-deoxy Glucose	6-Azido-6-deoxy Galactose
F4	40:60	6-Azido-6-deoxy Glucose	6-Azido-6-deoxy Galactose
F5	20:80	6-Azido-6-deoxy Glucose	6-Azido-6-deoxy Galactose
F6	0:100	6-Azido-6-deoxy Glucose	6-Azido-6-deoxy Galactose

3.3.4. Assay of 35nm gold nanoparticle library

With our heterogeneous library in hand we proceeded to investigate lectin binding against each gold nanoparticle sample. The reported lectin specificities are shown in Table 3.5.

Table 3.5: Lectin binding specificities.

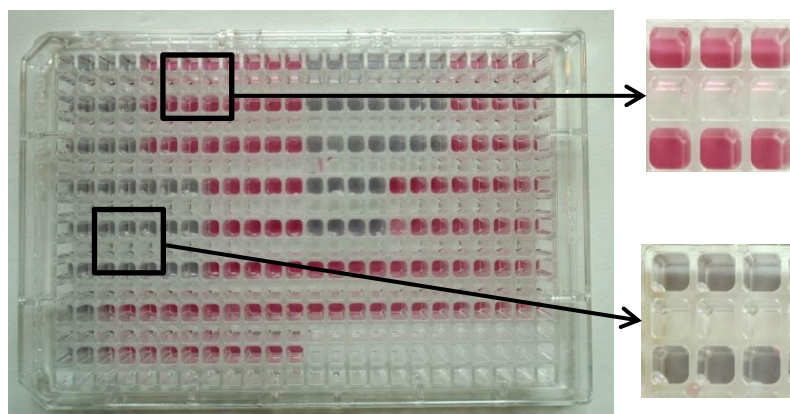
Lectin	Stated binding ligand
DBA	<i>N</i> -Acetyl galctosamine
PNA	Galactose
SBA	<i>N</i> -Acetyl galctosamine
WGA	<i>N</i> -Acetyl glucosamine
RCA ₁₂₀	Galactose

The five lectins, DBA, PNA, RCA, SBA and WGA were reconstituted in HEPES buffered saline at 0.1 mg.mL⁻¹(containing 0.1 mM Ca²⁺ and 0.01 mM Mn²⁺), with 12 serial dilutions from 0.1 mg.mL⁻¹ to 97 ng.mL⁻¹ plus a control at 0 mg.mL⁻¹. It is crucial to note that PBS was not used, as unwanted calcium phosphate precipitation can complicate lectin binding results due to the removal of Ca²⁺ necessary for lectin binding.

This gives 2160 individual experiments from our single starting nanoparticle coating. In triplicate this is 6480 individual lectin-binding events, demonstrating the potential for evolution of complex data sets using scalable methods. In this first iteration this step was performed by hand.

10uL of the AuNP to be tested was added to a well containing 10ul of Lectin solution, incubated at 37.5°C for 30 minutes, then placed into a UV-Vis plate reader and scanned from 450nm to 700nm. An example 384 well plate is shown below in Figure 3.8.

A



B

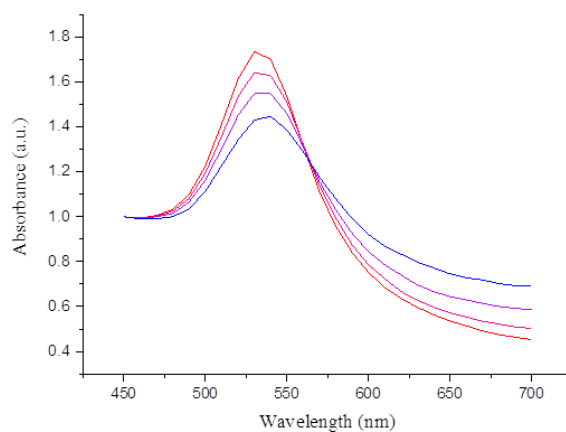


Figure 3.8: (A) Example of 384 well plate. Red indicates no binding has occurred while blue shows lectin binding induced aggregation of the gold nanoparticles. Note: This image is for illustrative purposes only, due to loss of gold during the purification steps, the actual absorbance intensity was much lower, and as such the colour of the solutions very faint. This is discussed in more detail in the main text. (B) Example binding curve showing the change in the absorption spectrum for galactosylated AuNP induced aggregation by SBA. The decrease in absorbance at the SPR peak at $\lambda=530$ nm and increase in absorbance at 700nm are clearly seen.

With no lectin present or in the presence of a non-binding lectin the solution stays red and there is a strong SPR peak at around 530 nm. If binding occurs then the solution turns blue and there is a reduction in the SPR peak and an increase in absorption at 700 nm. The absorbance at 530 nm vs lectin concentration for each lectin is shown in Figures 3.10 to 3.40

It is clear from the changes in absorbance that each particle set and lectin combination does display different trends in lectin-induced aggregation as glycan composition varies, particularly at the highest concentrations of lectin binding. However, it is apparent that the assay has a low resolution. As discussed in section 3.3.3. purification of the gold led to a reduction in the gold concentration, due to aggregation. This has a proportional effect in reducing the absorption of the gold solution and potentially reducing the resolution of the assay. Plotting the raw absorbance data confirms this, as the absorption curves become rough and stepped, suggesting the absorption value at each wavelength is changing by amounts lower than the resolution of the instrument, Figure 3.9.

Therefore, in order to improve this, the limit of detection for the assay was determined, as discussed in section 3.3.5.

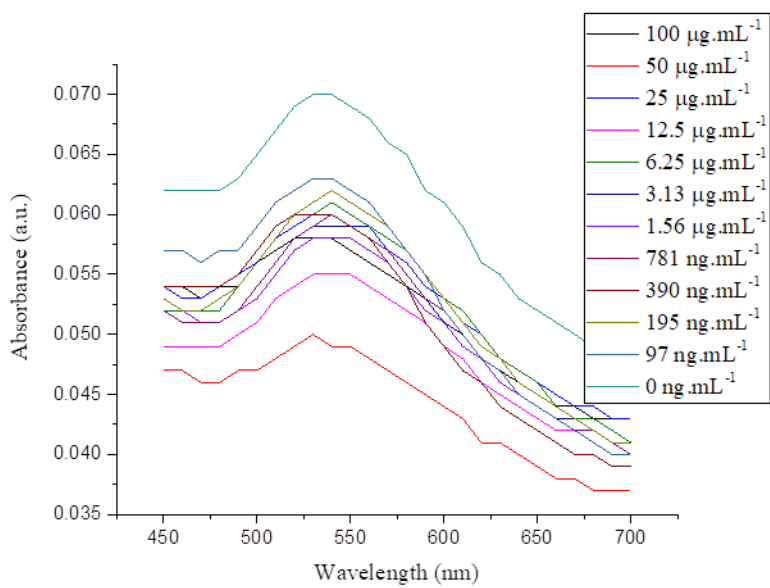


Figure 3.9 Raw UV-Vis spectra for each lectin concentration of the binding between Sample F6 (6-AzGal-pHEAA₂₅AuNP₃₅) and DBA.

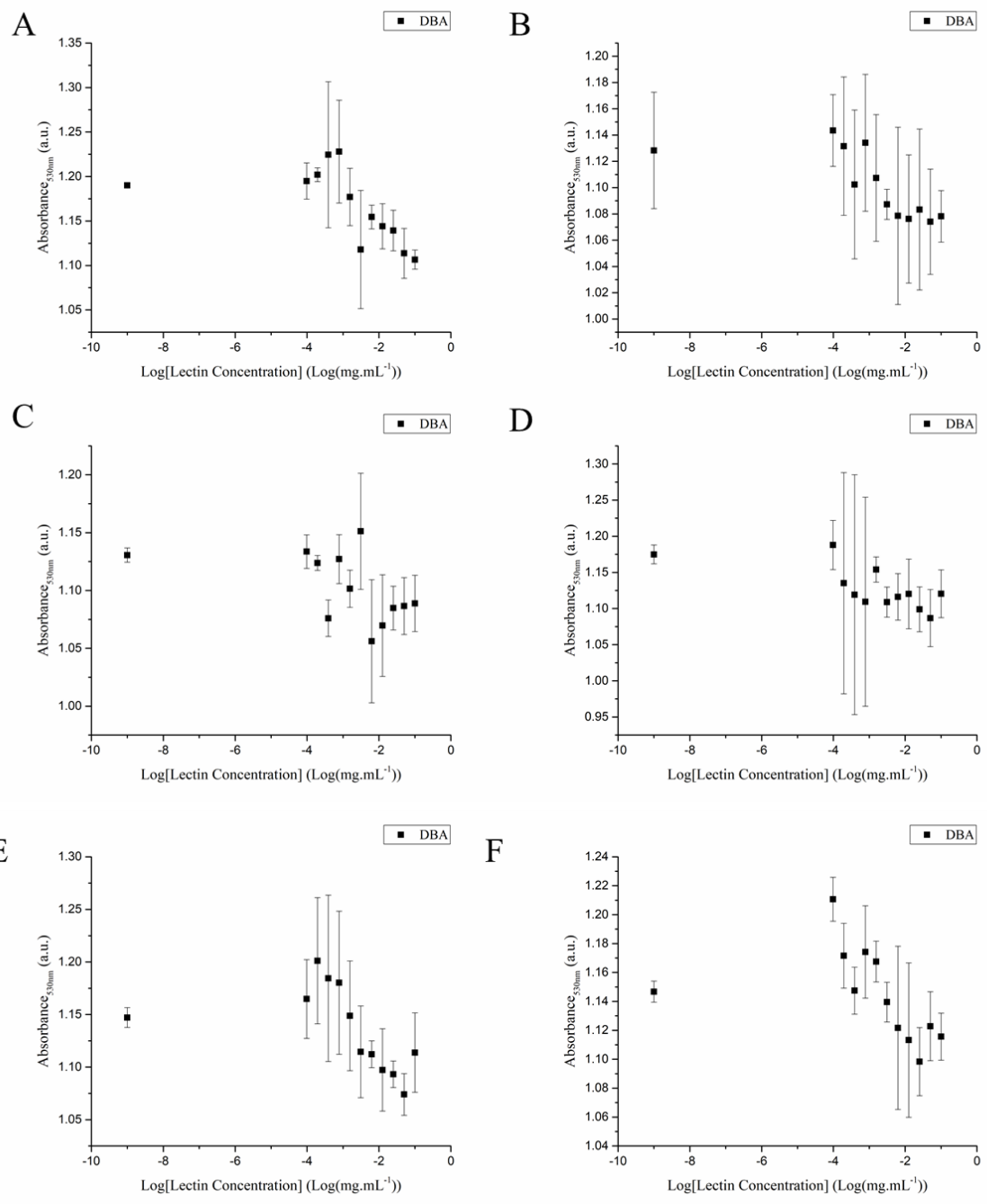


Figure 3.10: DBA binding to Nanoparticle group A containing sugars 2-Azido-2-deoxy Glucose and 2-Azido-2-deoxy Galactose (A) 100:0 2-Azido-2-deoxy Glucose: 2-Azido-2-deoxy Galactose (B) 80:20 2-Azido-2-deoxy Glucose : 2-Azido-2-deoxy Galactose (C) 60:40 2-Azido-2-deoxy Glucose : 2-Azido-2-deoxy Galactose (D) 40:60 2-Azido-2-deoxy Glucose : 2-Azido-2-deoxy Galactose (E) 20:80 2-Azido-2-deoxy Glucose : 2-Azido-2-deoxy Galactose (F) 0:100 2-Azido-2-deoxy Glucose : 2-Azido-2-deoxy Galactose.

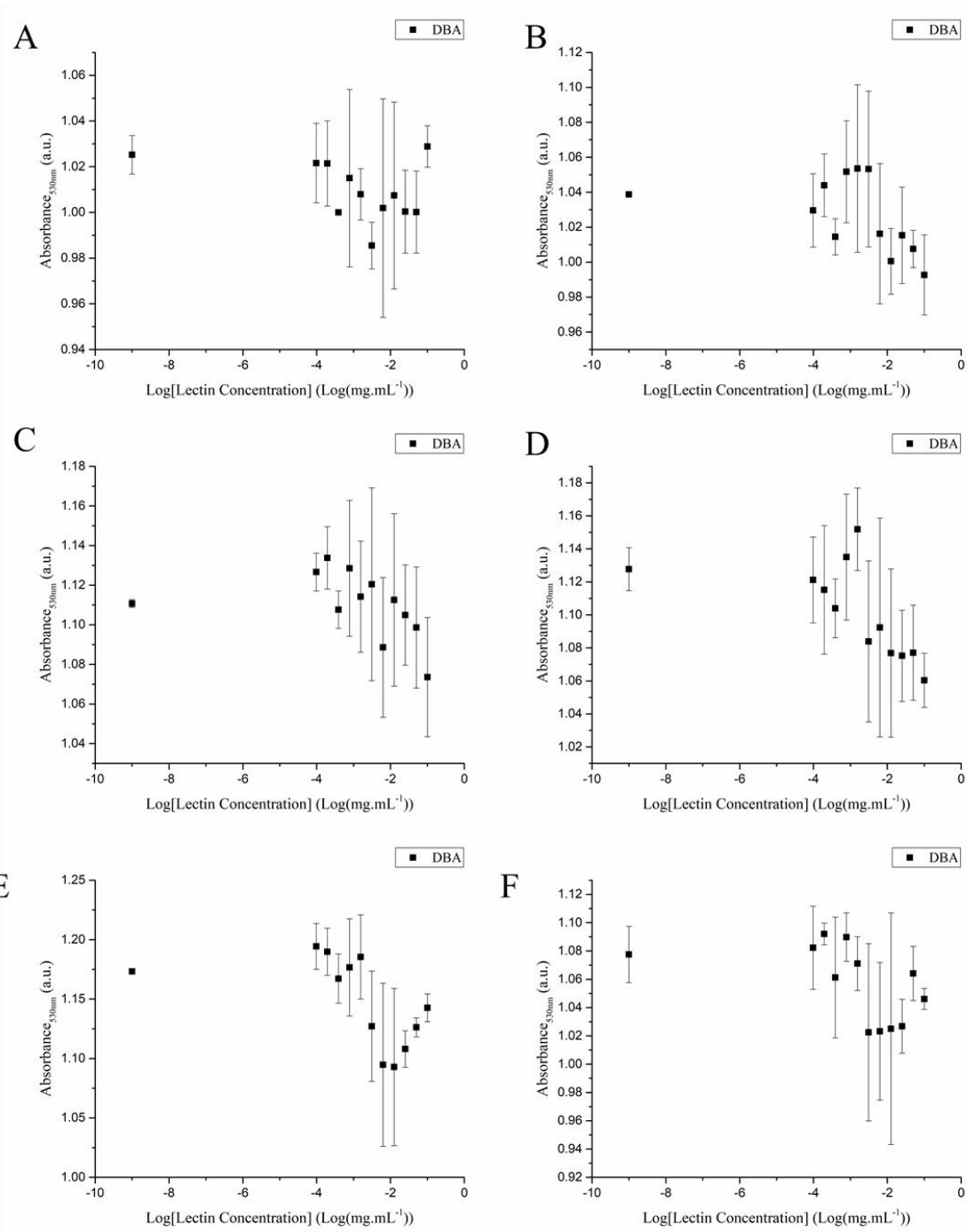


Figure 3.11: DBA binding to nanoparticle group B; containing sugars 2-Azido-2-deoxy Glucose and 6-Azido-6-deoxy Glucose. (A) 100:0 2-Azido-2-deoxy Glucose : 6-Azido-6-deoxy Glucose (B) 80:20 2-Azido-2-deoxy Glucose : 6-Azido-6-deoxy Glucose (C) 60:40 2-Azido-2-deoxy Glucose : 6-Azido-6-deoxy Glucose (D) 40:60 2-Azido-2-deoxy Glucose : 6-Azido-6-deoxy Glucose (E) 20:80 2-Azido-2-deoxy Glucose : 6-Azido-6-deoxy Glucose (F) 0:100 2-Azido-2-deoxy Glucose : 6-Azido-6-deoxy Glucose

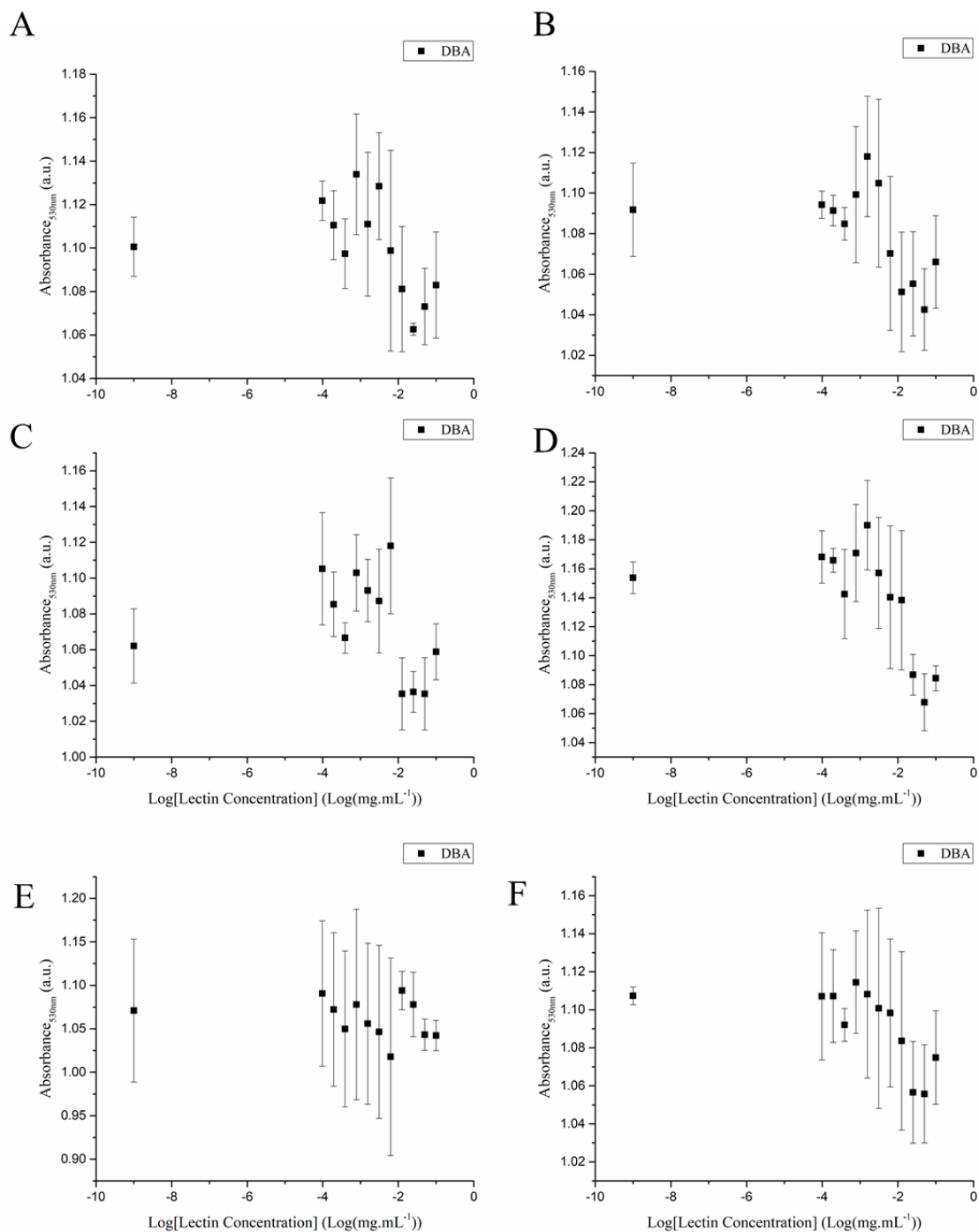


Figure 3.12: DBA binding to nanoparticle group C; containing sugars 2-Azido-2-deoxy Glucose and 6-Azido-6-deoxy Galactose (A) 100:0 2-Azido-2-deoxy Glucose : 6-Azido-6-deoxy Galactose (B) 80:20 2-Azido-2-deoxy Glucose : 6-Azido-6-deoxy Galactose (C) 60:40 2-Azido-2-deoxy Glucose : 6-Azido-6-deoxy Galactose (D) 40:60 2-Azido-2-deoxy Glucose : 6-Azido-6-deoxy Galactose (E) 20:80 2-Azido-2-deoxy Glucose : 6-Azido-6-deoxy Galactose (F) 0:100 2-Azido-2-deoxy Glucose : 6-Azido-6-deoxy Galactose

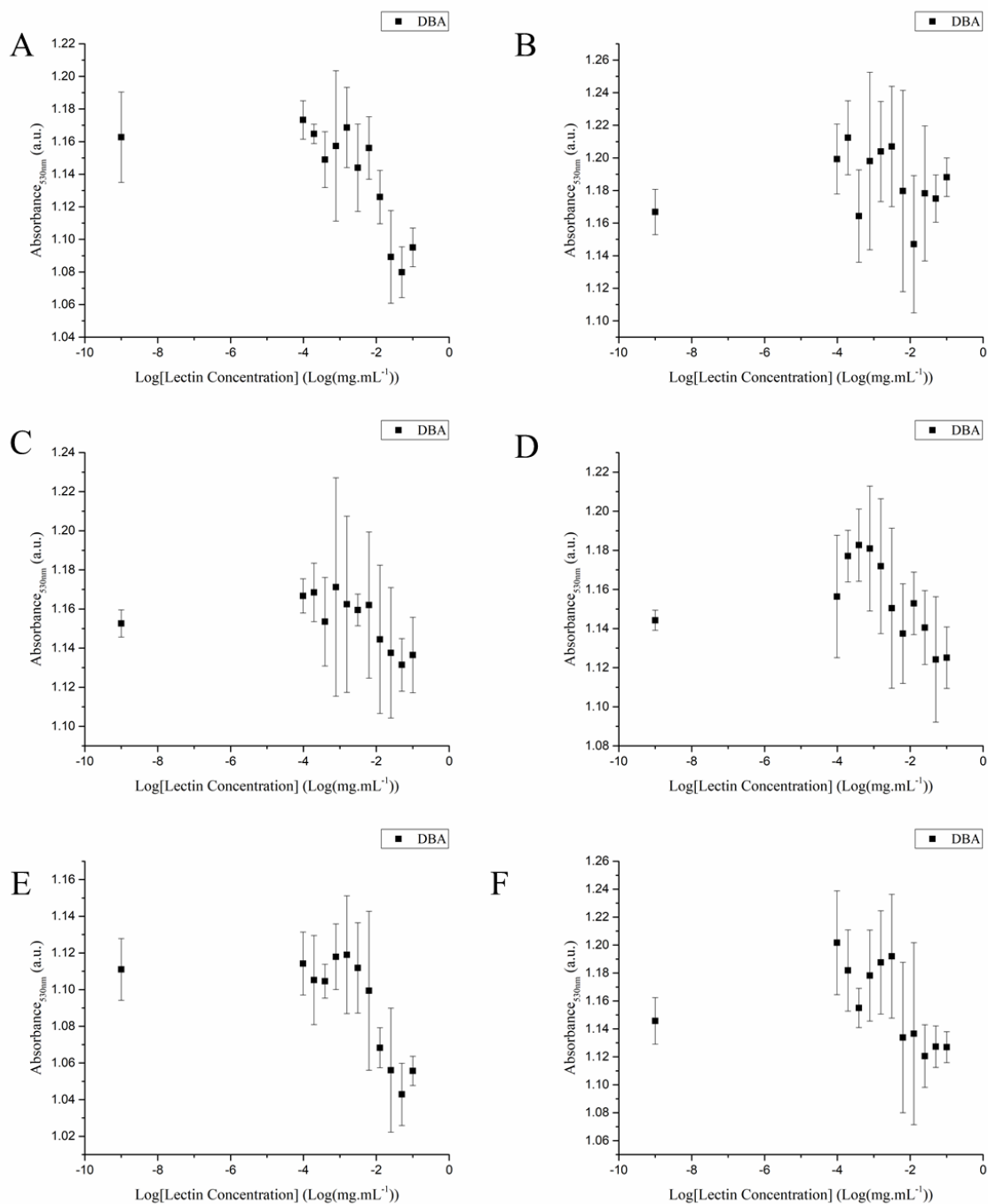


Figure 3.13: DBA binding to nanoparticle group D; containing sugars 2-Azido-2-deoxy Galactose and 6-Azido-6-deoxy Glucose (A) 100:0 2-Azido-2-deoxy Galactose : 6-Azido-6-deoxy Glucose (B) 80:20 2-Azido-2-deoxy Galactose : 6-Azido-6-deoxy Glucose (C) 60:40 2-Azido-2-deoxy Galactose : 6-Azido-6-deoxy Glucose (D) 40:60 2-Azido-2-deoxy Galactose : 6-Azido-6-deoxy Glucose (E) 20:80 2-Azido-2-deoxy Galactose : 6-Azido-6-deoxy Glucose (F) 0:100 2-Azido-2-deoxy Galactose : 6-Azido-6-deoxy Glucose

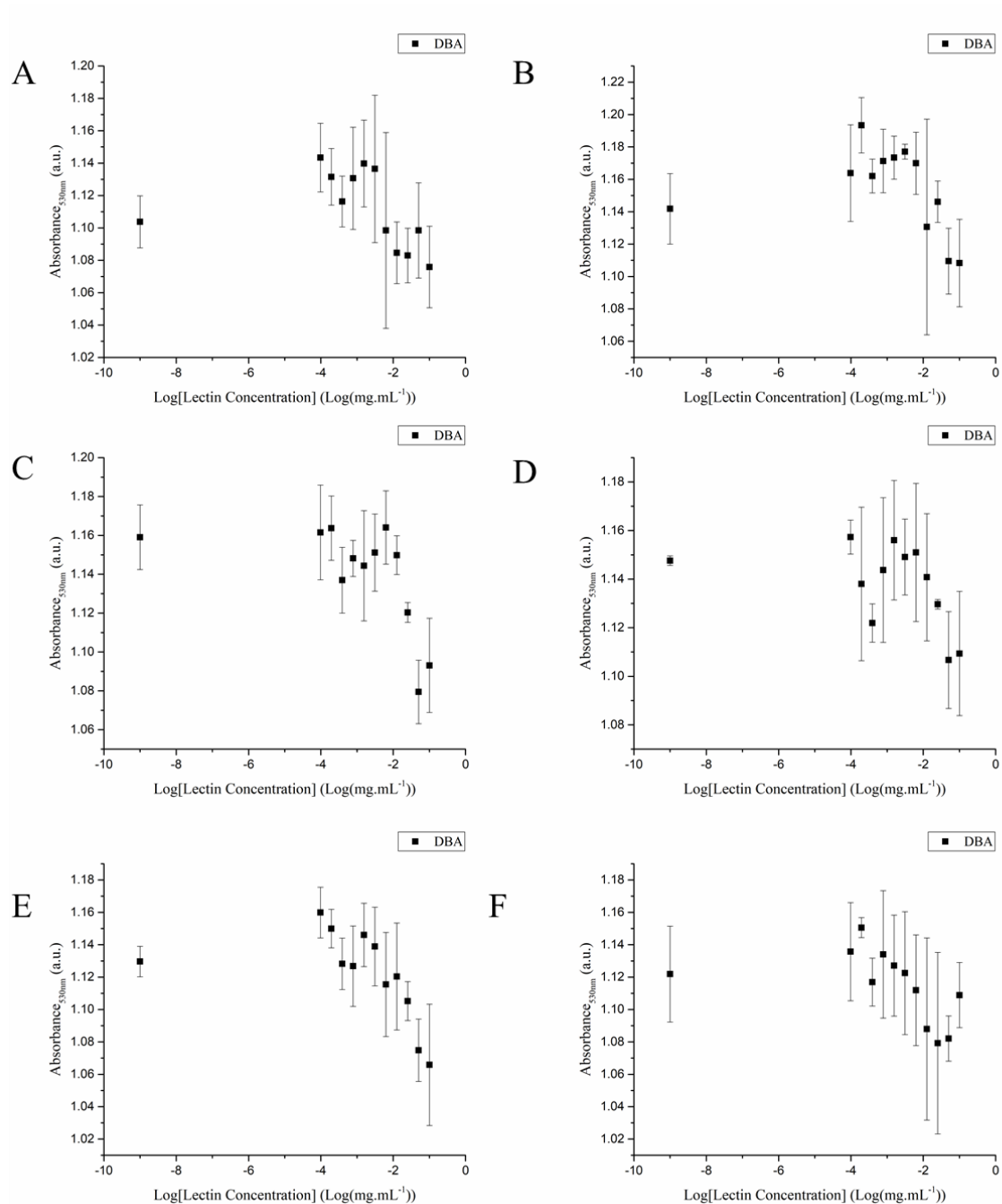


Figure 3.14: DBA binding to nanoparticle group E; containing sugars 2-Azido-2-deoxy Galactose and 6-Azido-6-deoxy Galactose (A) 100:0 2-Azido-2-deoxy Galactose : 6-Azido-6-deoxy Galactose (B) 80:20 2-Azido-2-deoxy Galactose : 6-Azido-6-deoxy Galactose (C) 60:40 2-Azido-2-deoxy Galactose : 6-Azido-6-deoxy Galactose (D) 40:60 2-Azido-2-deoxy Galactose : 6-Azido-6-deoxy Galactose (E) 20:80 2-Azido-2-deoxy Galactose : 6-Azido-6-deoxy Galactose (F) 0:100 2-Azido-2-deoxy Galactose : 6-Azido-6-deoxy Galactose

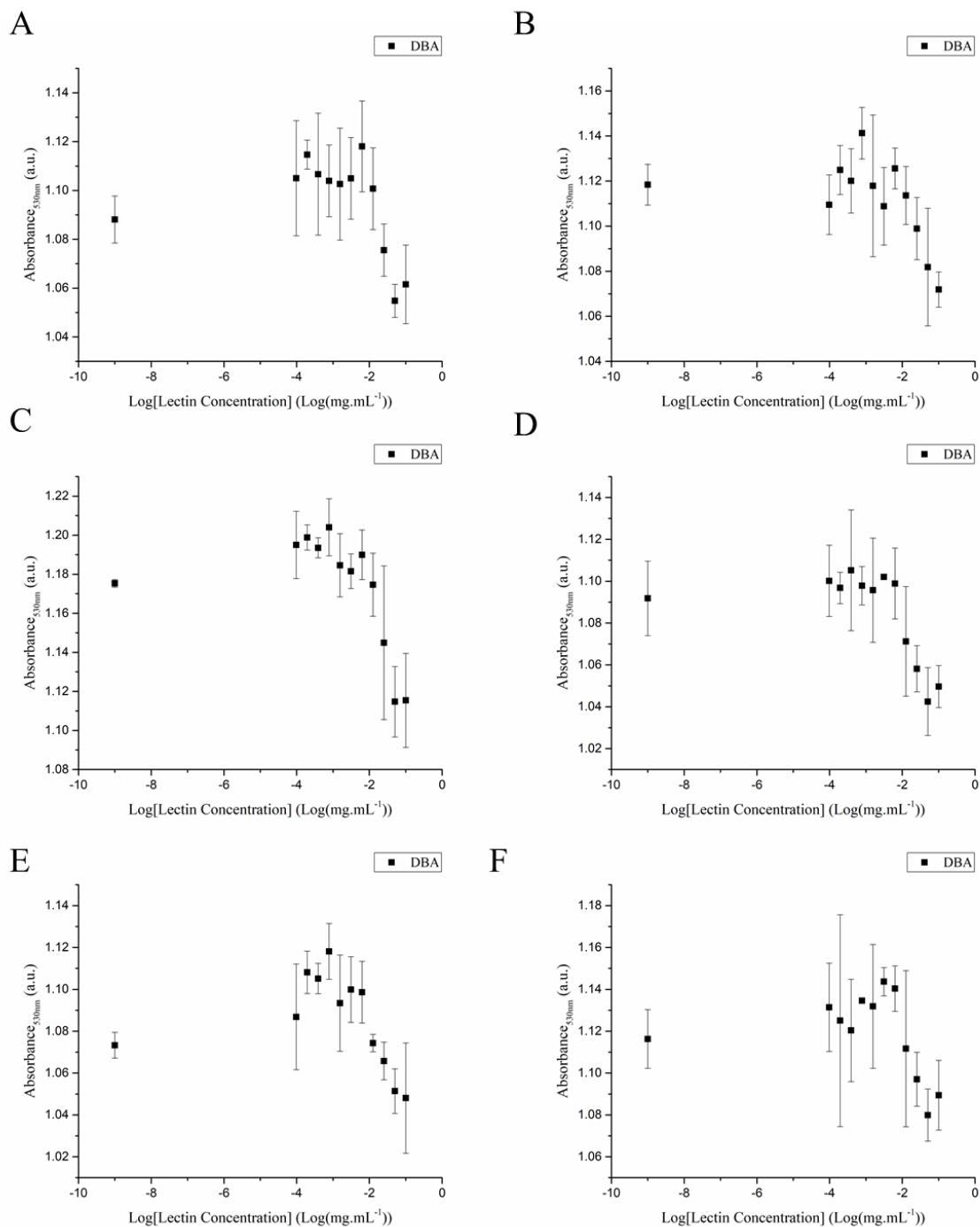


Figure 3.15: DBA binding to nanoparticle group F; containing sugars 6-Azido-6-deoxy Glucose and 6-Azido-6-deoxy Galactose (A) 100:0 6-Azido-6-deoxy Glucose : 6-Azido-6-deoxy Galactose (B) 80:20 6-Azido-6-deoxy Glucose : 6-Azido-6-deoxy Galactose (C) 60:40 6-Azido-6-deoxy Glucose : 6-Azido-6-deoxy Galactose (D) 40:60 6-Azido-6-deoxy Glucose : 6-Azido-6-deoxy Galactose (E) 20:80 6-Azido-6-deoxy Glucose : 6-Azido-6-deoxy Galactose (F) 0:100 6-Azido-6-deoxy Glucose : 6-Azido-6-deoxy Galactose

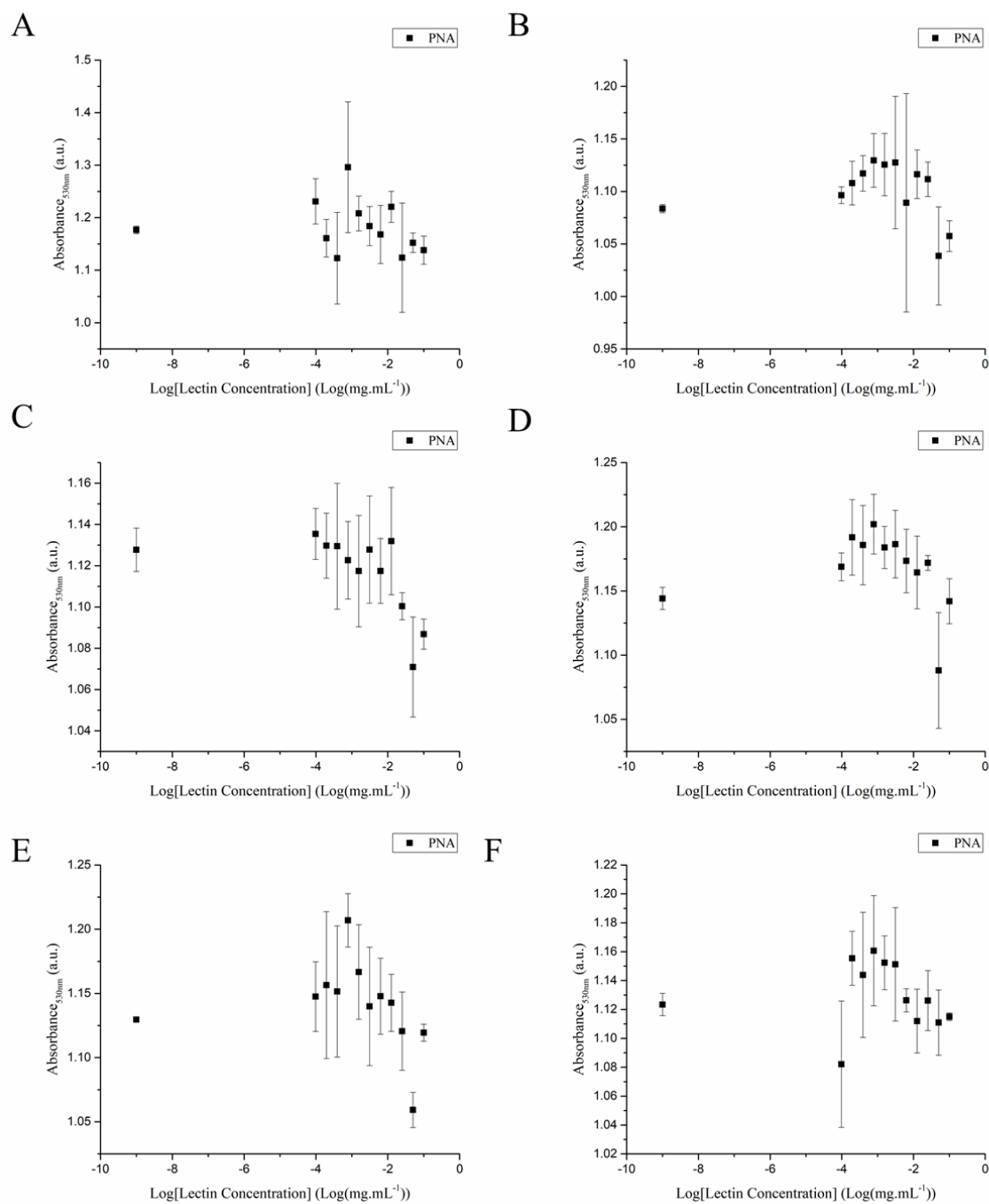


Figure 3.16: PNA binding to nanoparticle group A containing sugars 2-Azido-2-deoxy Glucose and 2-Azido-2-deoxy Galactose (A) 100:0 2-Azido-2-deoxy Glucose: 2-Azido-2-deoxy Galactose (B) 80:20 2-Azido-2-deoxy Glucose : 2-Azido-2-deoxy Galactose (C) 60:40 2-Azido-2-deoxy Glucose : 2-Azido-2-deoxy Galactose (D) 40:60 2-Azido-2-deoxy Glucose : 2-Azido-2-deoxy Galactose (E) 20:80 2-Azido-2-deoxy Glucose : 2-Azido-2-deoxy Galactose (F) 0:100 2-Azido-2-deoxy Glucose : 2-Azido-2-deoxy Galactose.

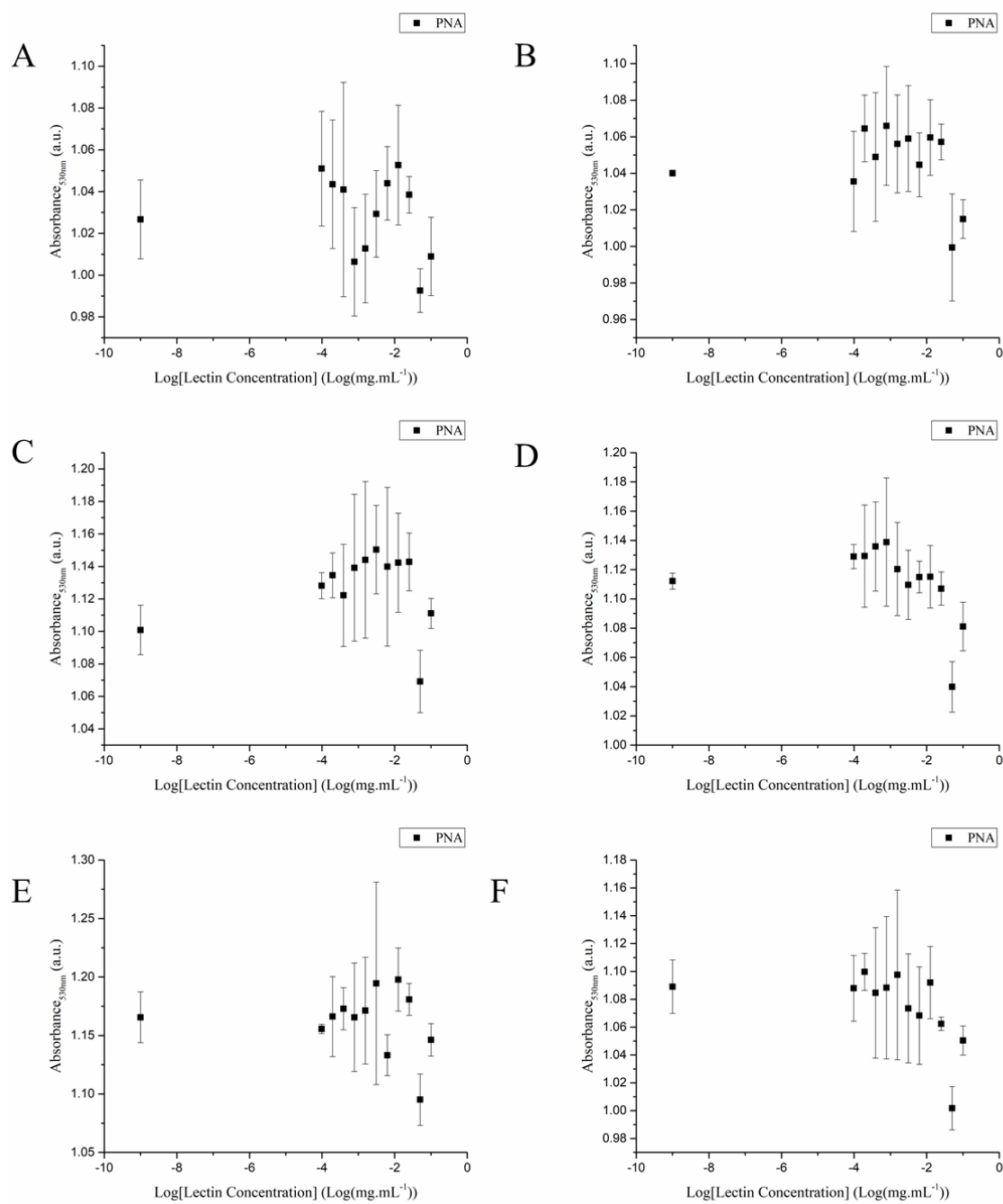


Figure 3.17: PNA binding to nanoparticle group B; containing sugars 2-Azido-2-deoxy Glucose and 6-Azido-6-deoxy Glucose. (A) 100:0 2-Azido-2-deoxy Glucose : 6-Azido-6-deoxy Glucose (B) 80:20 2-Azido-2-deoxy Glucose : 6-Azido-6-deoxy Glucose (C) 60:40 2-Azido-2-deoxy Glucose : 6-Azido-6-deoxy Glucose (D) 40:60 2-Azido-2-deoxy Glucose : 6-Azido-6-deoxy Glucose (E) 20:80 2-Azido-2-deoxy Glucose : 6-Azido-6-deoxy Glucose (F) 0:100 2-Azido-2-deoxy Glucose : 6-Azido-6-deoxy Glucose

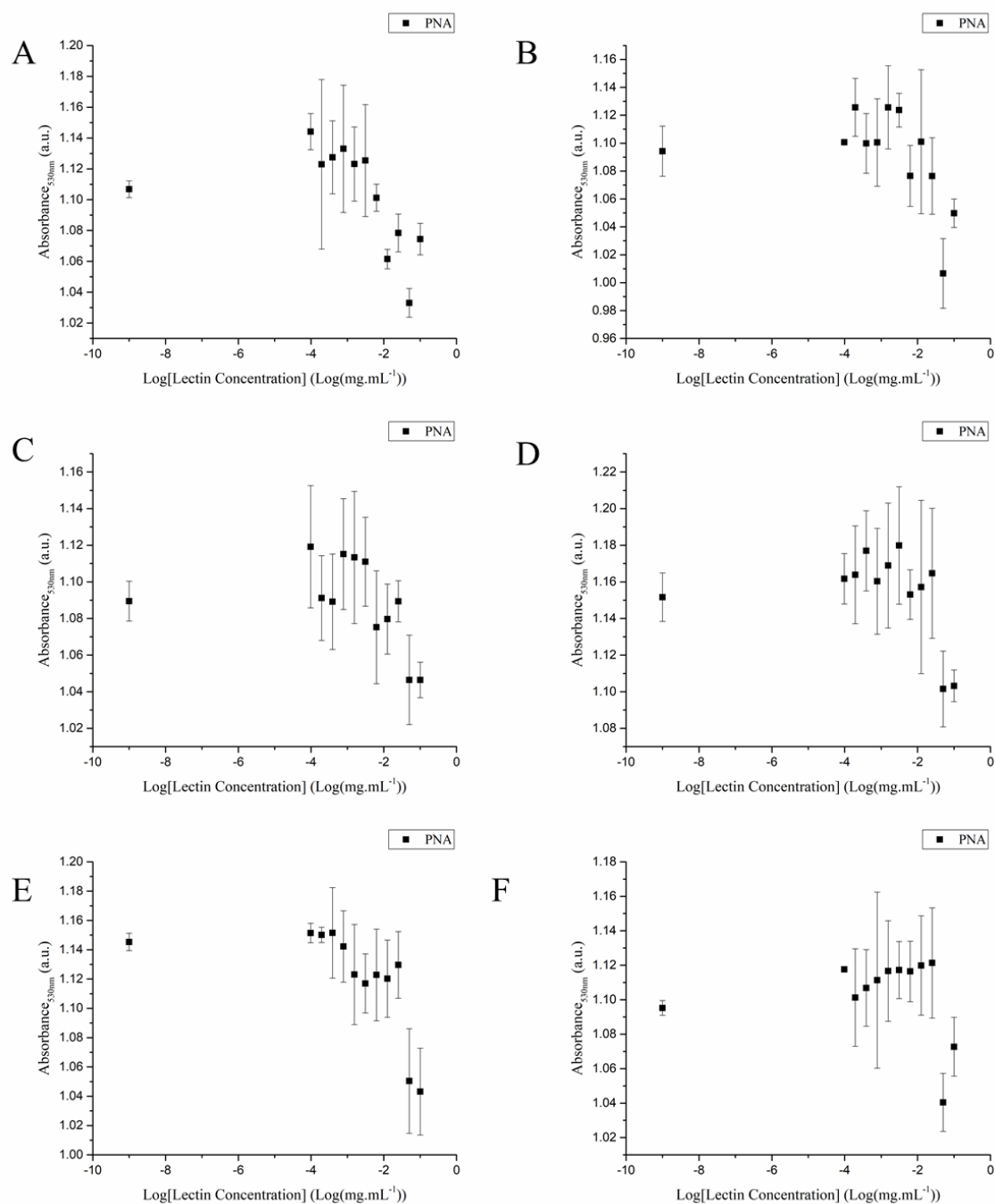


Figure 3.18: PNA binding to nanoparticle group C; containing sugars 2-Azido-2-deoxy Glucose and 6-Azido-6-deoxy Galactose (A) 100:0 2-Azido-2-deoxy Glucose : 6-Azido-6-deoxy Galactose (B) 80:20 2-Azido-2-deoxy Glucose : 6-Azido-6-deoxy Galactose (C) 60:40 2-Azido-2-deoxy Glucose : 6-Azido-6-deoxy Galactose (D) 40:60 2-Azido-2-deoxy Glucose : 6-Azido-6-deoxy Galactose (E) 20:80 2-Azido-2-deoxy Glucose : 6-Azido-6-deoxy Galactose (F) 0:100 2-Azido-2-deoxy Glucose : 6-Azido-6-deoxy Galactose

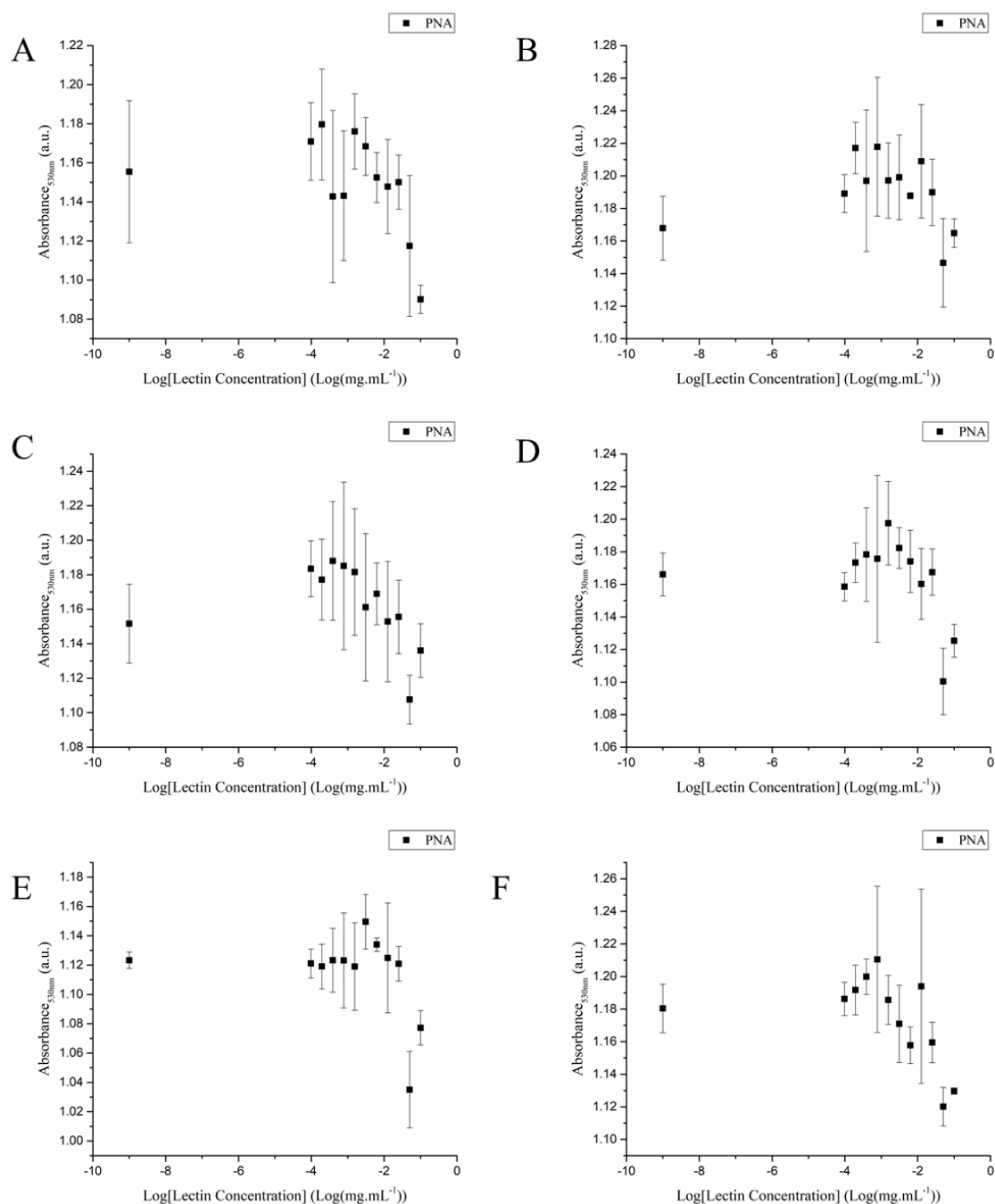


Figure 3.19: PNA binding to nanoparticle group D; containing sugars 2-Azido-2-deoxy Galactose and 6-Azido-6-deoxy Glucose (A) 100:0 2-Azido-2-deoxy Galactose : 6-Azido-6-deoxy Glucose (B) 80:20 2-Azido-2-deoxy Galactose : 6-Azido-6-deoxy Glucose (C) 60:40 2-Azido-2-deoxy Galactose : 6-Azido-6-deoxy Glucose (D) 40:60 2-Azido-2-deoxy Galactose : 6-Azido-6-deoxy Glucose (E) 20:80 2-Azido-2-deoxy Galactose : 6-Azido-6-deoxy Glucose (F) 0:100 2-Azido-2-deoxy Galactose : 6-Azido-6-deoxy Glucose

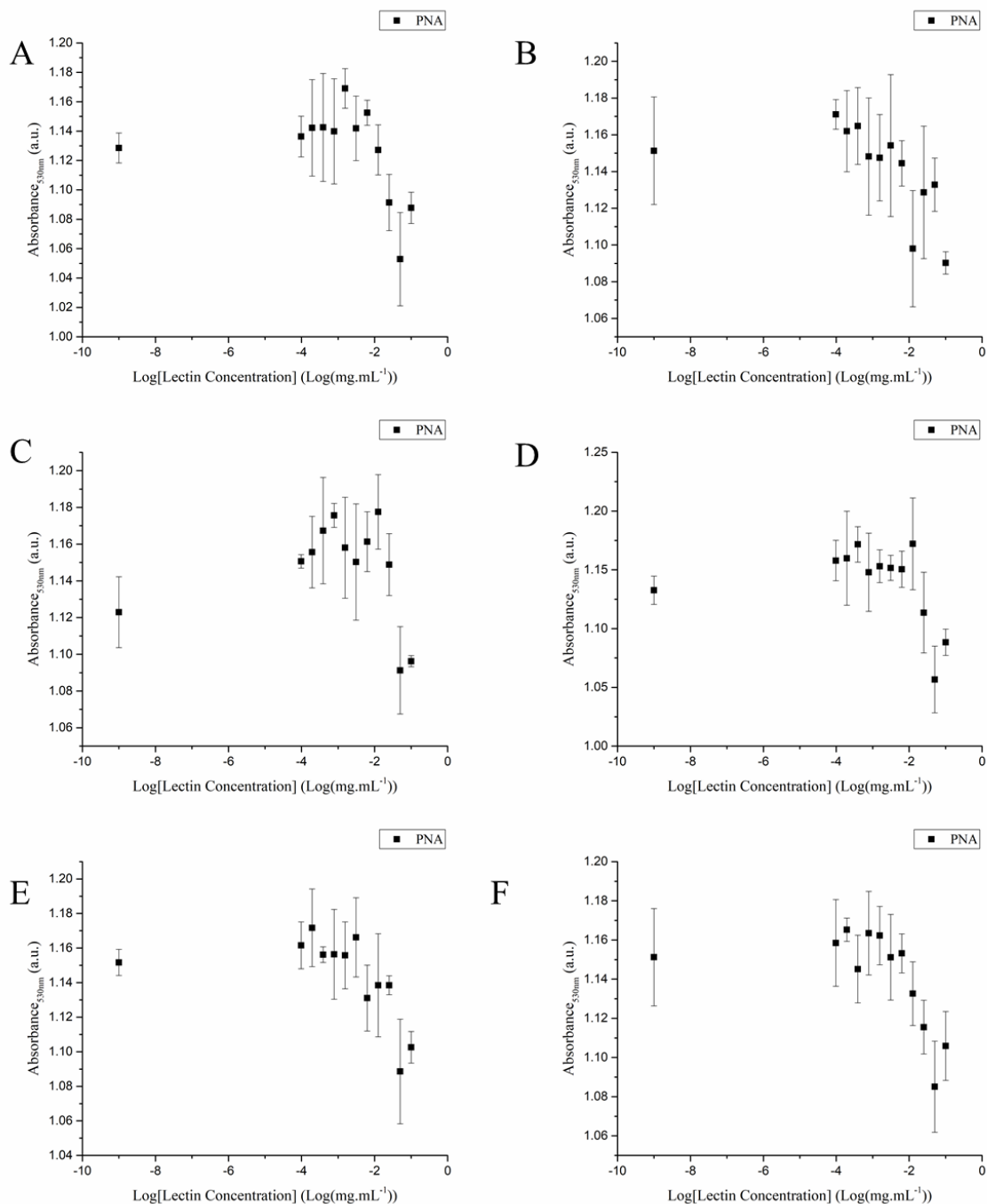


Figure 3.20: PNA binding to nanoparticle group E; containing sugars 2-Azido-2-deoxy Galactose and 6-Azido-6-deoxy Galactose (A) 100:0 2-Azido-2-deoxy Galactose : 6-Azido-6-deoxy Galactose (B) 80:20 2-Azido-2-deoxy Galactose : 6-Azido-6-deoxy Galactose (C) 60:40 2-Azido-2-deoxy Galactose : 6-Azido-6-deoxy Galactose (D) 40:60 2-Azido-2-deoxy Galactose : 6-Azido-6-deoxy Galactose (E) 20:80 2-Azido-2-deoxy Galactose : 6-Azido-6-deoxy Galactose (F) 0:100 2-Azido-2-deoxy Galactose : 6-Azido-6-deoxy Galactose

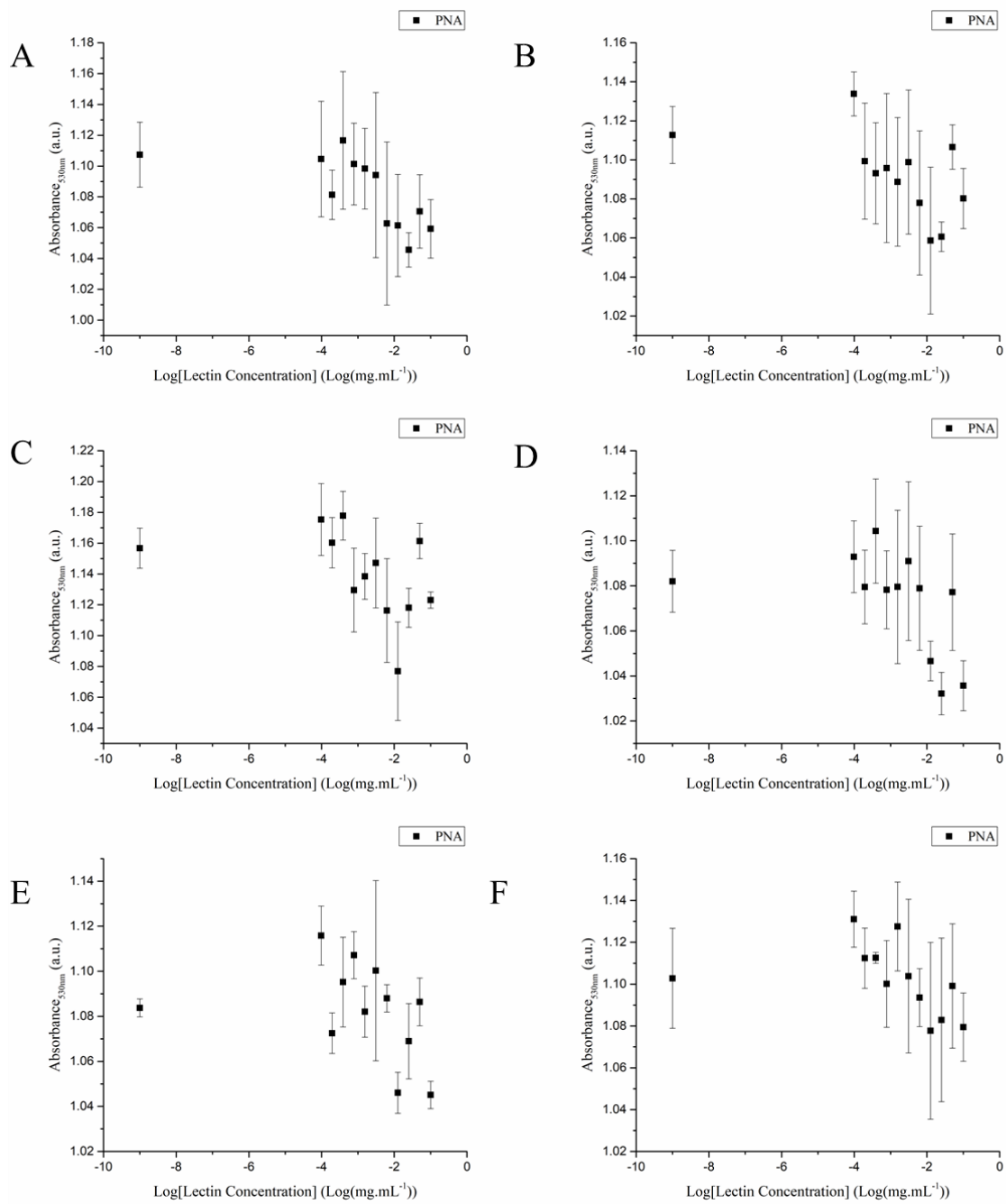


Figure 3.21: PNA binding to nanoparticle group F; containing sugars 6-Azido-6-deoxy Glucose and 6-Azido-6-deoxy Galactose (A) 100:0 6-Azido-6-deoxy Glucose : 6-Azido-6-deoxy Galactose (B) 80:20 6-Azido-6-deoxy Glucose : 6-Azido-6-deoxy Galactose (C) 60:40 6-Azido-6-deoxy Glucose : 6-Azido-6-deoxy Galactose (D) 40:60 6-Azido-6-deoxy Glucose : 6-Azido-6-deoxy Galactose (E) 20:80 6-Azido-6-deoxy Glucose : 6-Azido-6-deoxy Galactose (F) 0:100 6-Azido-6-deoxy Glucose : 6-Azido-6-deoxy Galactose

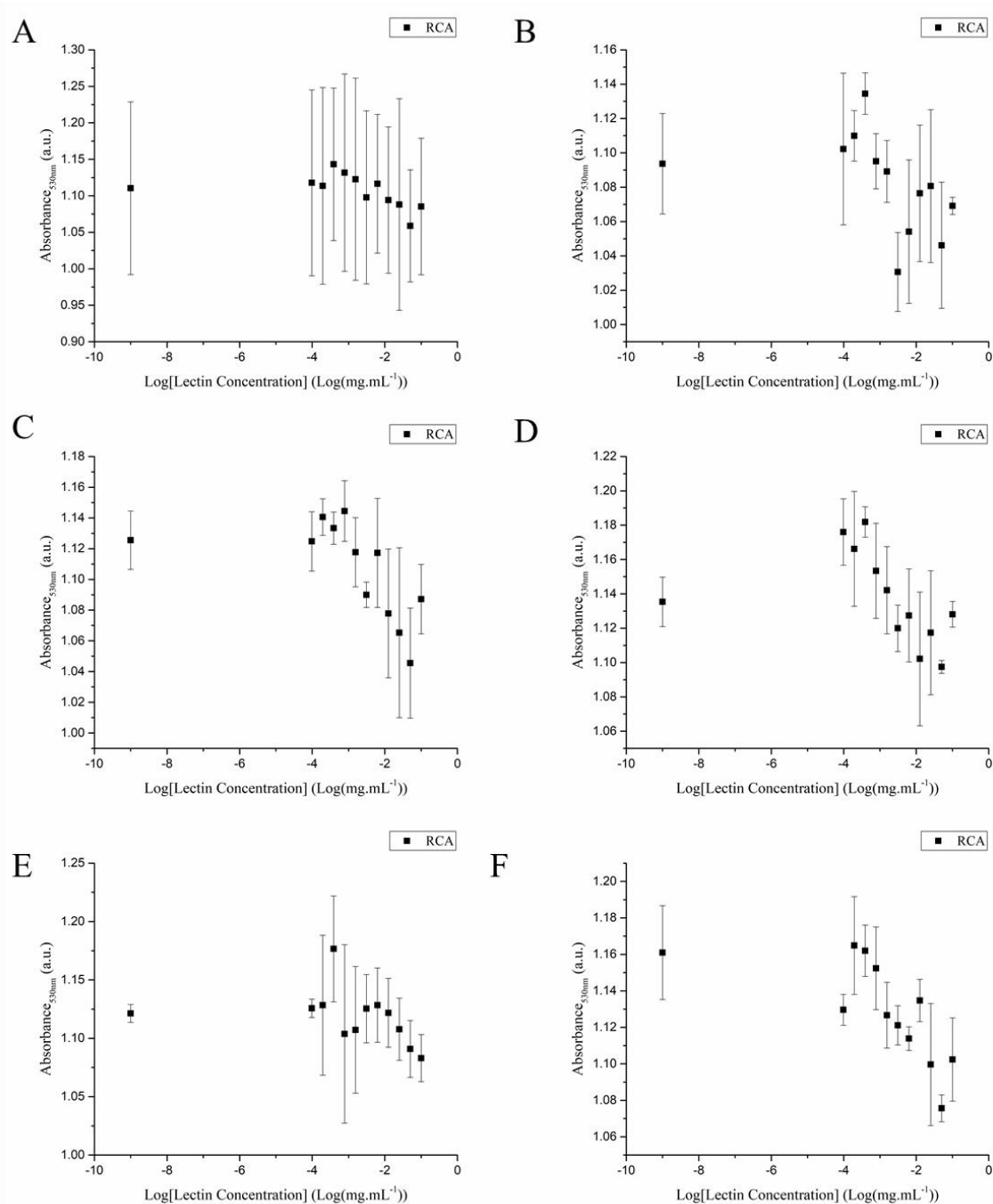


Figure 3.22: RCA binding to nanoparticle group A containing sugars 2-Azido-2-deoxy Glucose and 2-Azido-2-deoxy Galactose (A) 100:0 2-Azido-2-deoxy Glucose: 2-Azido-2-deoxy Galactose (B) 80:20 2-Azido-2-deoxy Glucose : 2-Azido-2-deoxy Galactose (C) 60:40 2-Azido-2-deoxy Glucose : 2-Azido-2-deoxy Galactose (D) 40:60 2-Azido-2-deoxy Glucose : 2-Azido-2-deoxy Galactose (E) 20:80 2-Azido-2-deoxy Glucose : 2-Azido-2-deoxy Galactose (F) 0:100 2-Azido-2-deoxy Glucose : 2-Azido-2-deoxy Galactose.

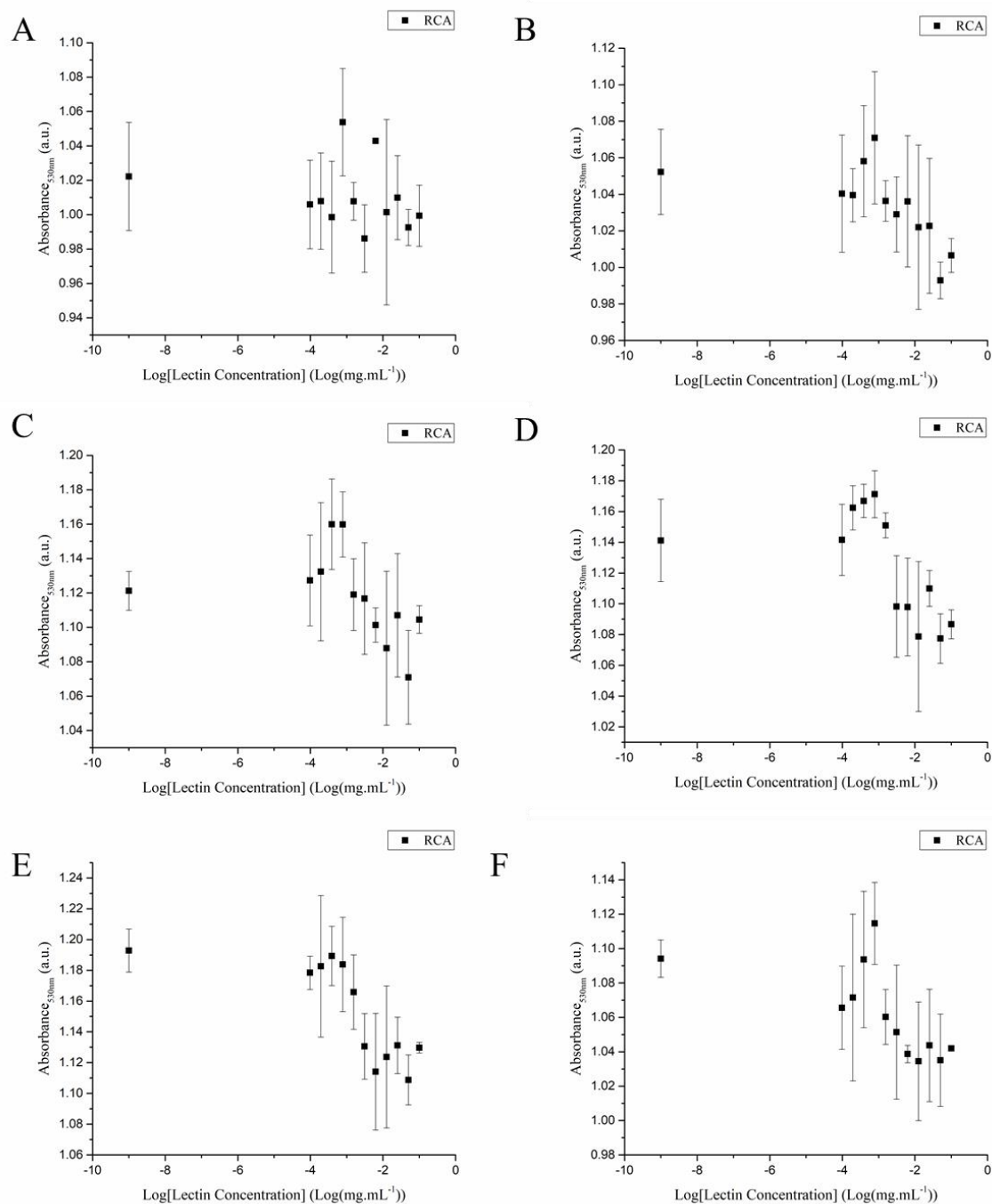


Figure 3.23: RCA binding to nanoparticle group B; containing sugars 2-Azido-2-deoxy Glucose and 6-Azido-6-deoxy Glucose. (A) 100:0 2-Azido-2-deoxy Glucose : 6-Azido-6-deoxy Glucose (B) 80:20 2-Azido-2-deoxy Glucose : 6-Azido-6-deoxy Glucose (C) 60:40 2-Azido-2-deoxy Glucose : 6-Azido-6-deoxy Glucose (D) 40:60 2-Azido-2-deoxy Glucose : 6-Azido-6-deoxy Glucose (E) 20:80 2-Azido-2-deoxy Glucose : 6-Azido-6-deoxy Glucose (F) 0:100 2-Azido-2-deoxy Glucose : 6-Azido-6-deoxy Glucose

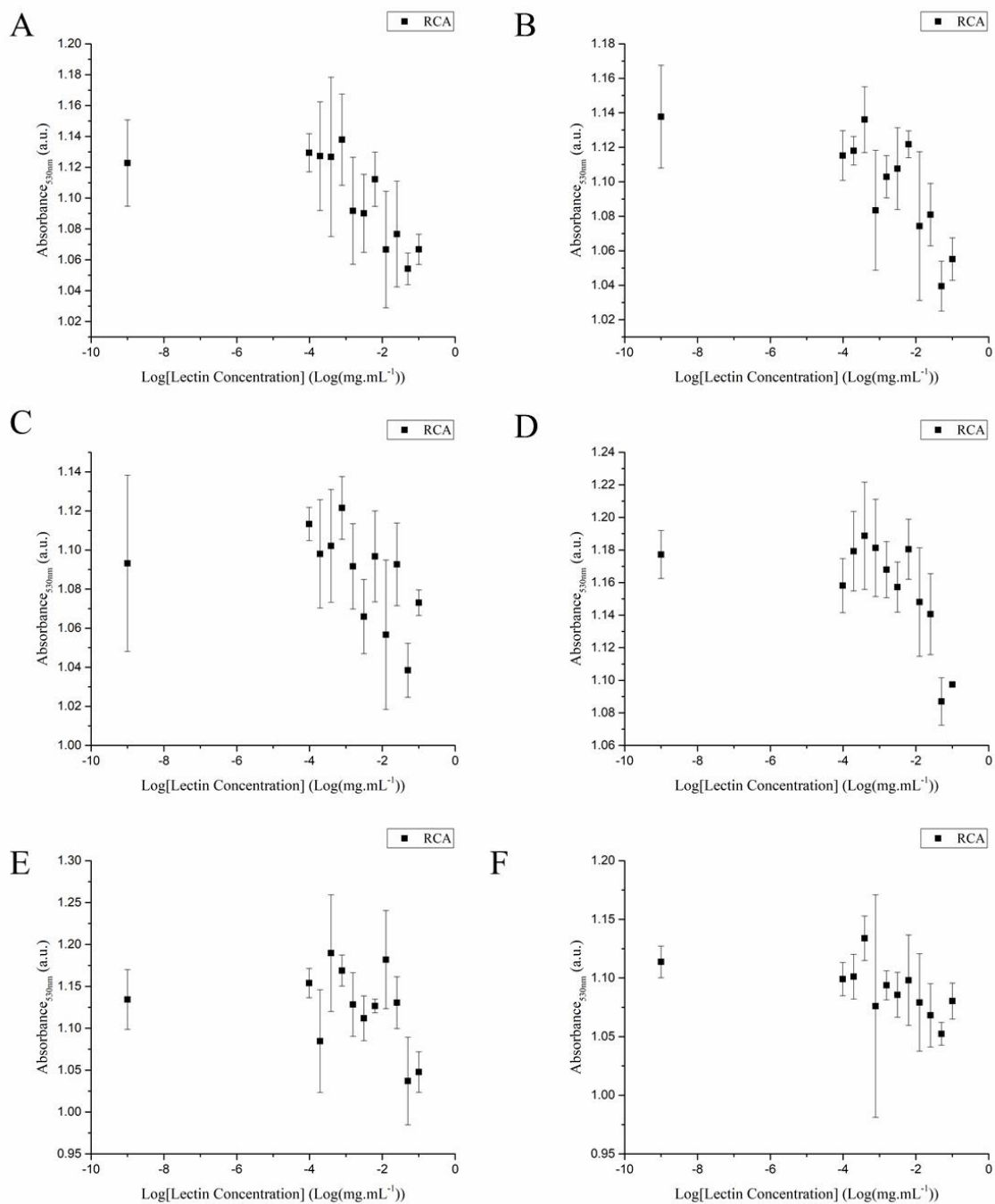


Figure 3.24: RCA binding to nanoparticle group C; containing sugars 2-Azido-2-deoxy Glucose and 6-Azido-6-deoxy Galactose (A) 100:0 2-Azido-2-deoxy Glucose : 6-Azido-6-deoxy Galactose (B) 80:20 2-Azido-2-deoxy Glucose : 6-Azido-6-deoxy Galactose (C) 60:40 2-Azido-2-deoxy Glucose : 6-Azido-6-deoxy Galactose (D) 40:60 2-Azido-2-deoxy Glucose : 6-Azido-6-deoxy Galactose (E) 20:80 2-Azido-2-deoxy Glucose : 6-Azido-6-deoxy Galactose (F) 0:100 2-Azido-2-deoxy Glucose : 6-Azido-6-deoxy Galactose

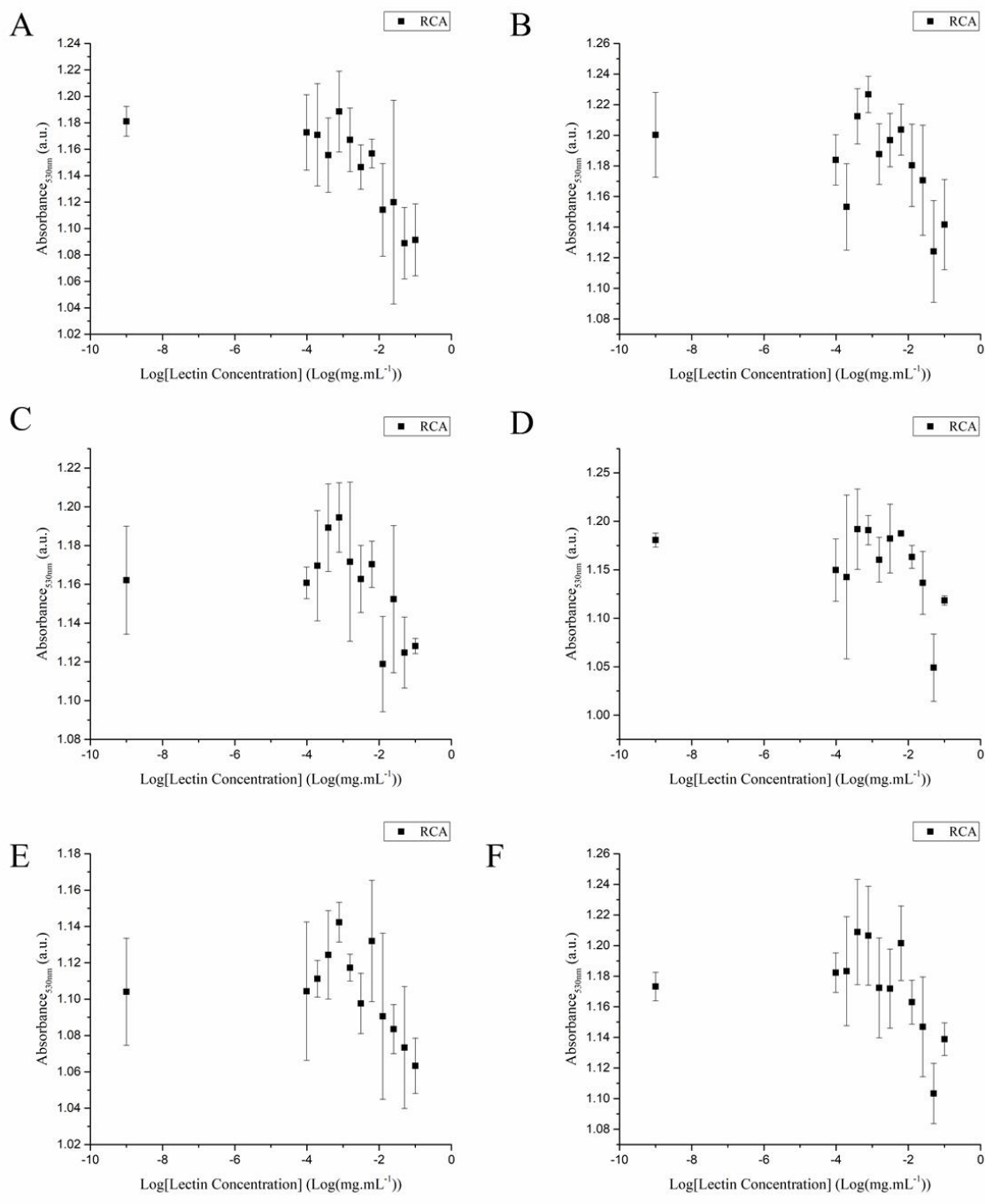


Figure 3.25: RCA binding to nanoparticle group D; containing sugars 2-Azido-2-deoxy Galactose and 6-Azido-6-deoxy Glucose (A) 100:0 2-Azido-2-deoxy Galactose : 6-Azido-6-deoxy Glucose (B) 80:20 2-Azido-2-deoxy Galactose : 6-Azido-6-deoxy Glucose (C) 60:40 2-Azido-2-deoxy Galactose : 6-Azido-6-deoxy Glucose (D) 40:60 2-Azido-2-deoxy Galactose : 6-Azido-6-deoxy Glucose (E) 20:80 2-Azido-2-deoxy Galactose : 6-Azido-6-deoxy Glucose (F) 0:100 2-Azido-2-deoxy Galactose : 6-Azido-6-deoxy Glucose

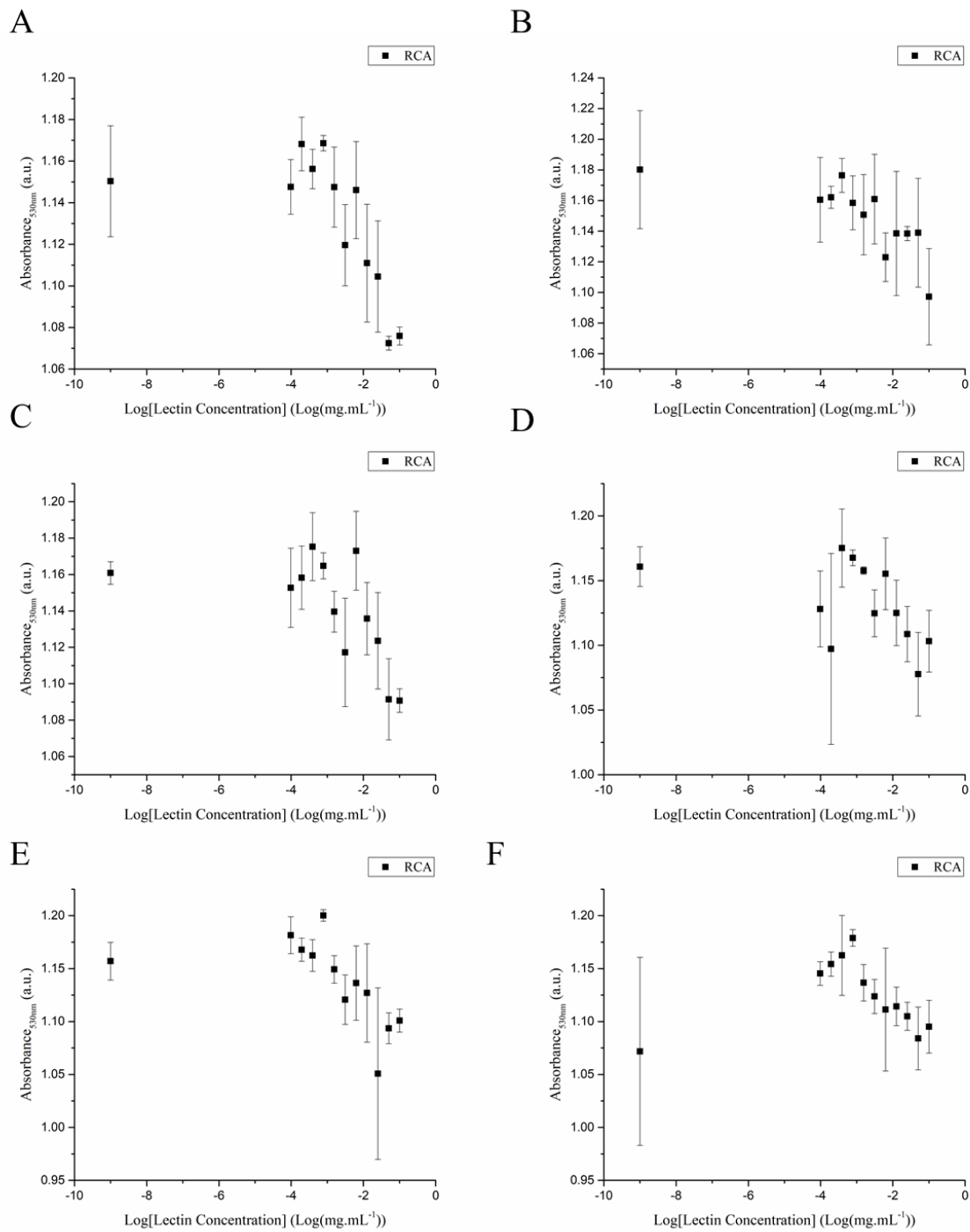


Figure 3.26: RCA binding to nanoparticle group E; containing sugars 2-Azido-2-deoxy Galactose and 6-Azido-6-deoxy Galactose (A) 100:0 2-Azido-2-deoxy Galactose : 6-Azido-6-deoxy Galactose (B) 80:20 2-Azido-2-deoxy Galactose : 6-Azido-6-deoxy Galactose (C) 60:40 2-Azido-2-deoxy Galactose : 6-Azido-6-deoxy Galactose (D) 40:60 2-Azido-2-deoxy Galactose : 6-Azido-6-deoxy Galactose (E) 20:80 2-Azido-2-deoxy Galactose : 6-Azido-6-deoxy Galactose (F) 0:100 2-Azido-2-deoxy Galactose : 6-Azido-6-deoxy Galactose

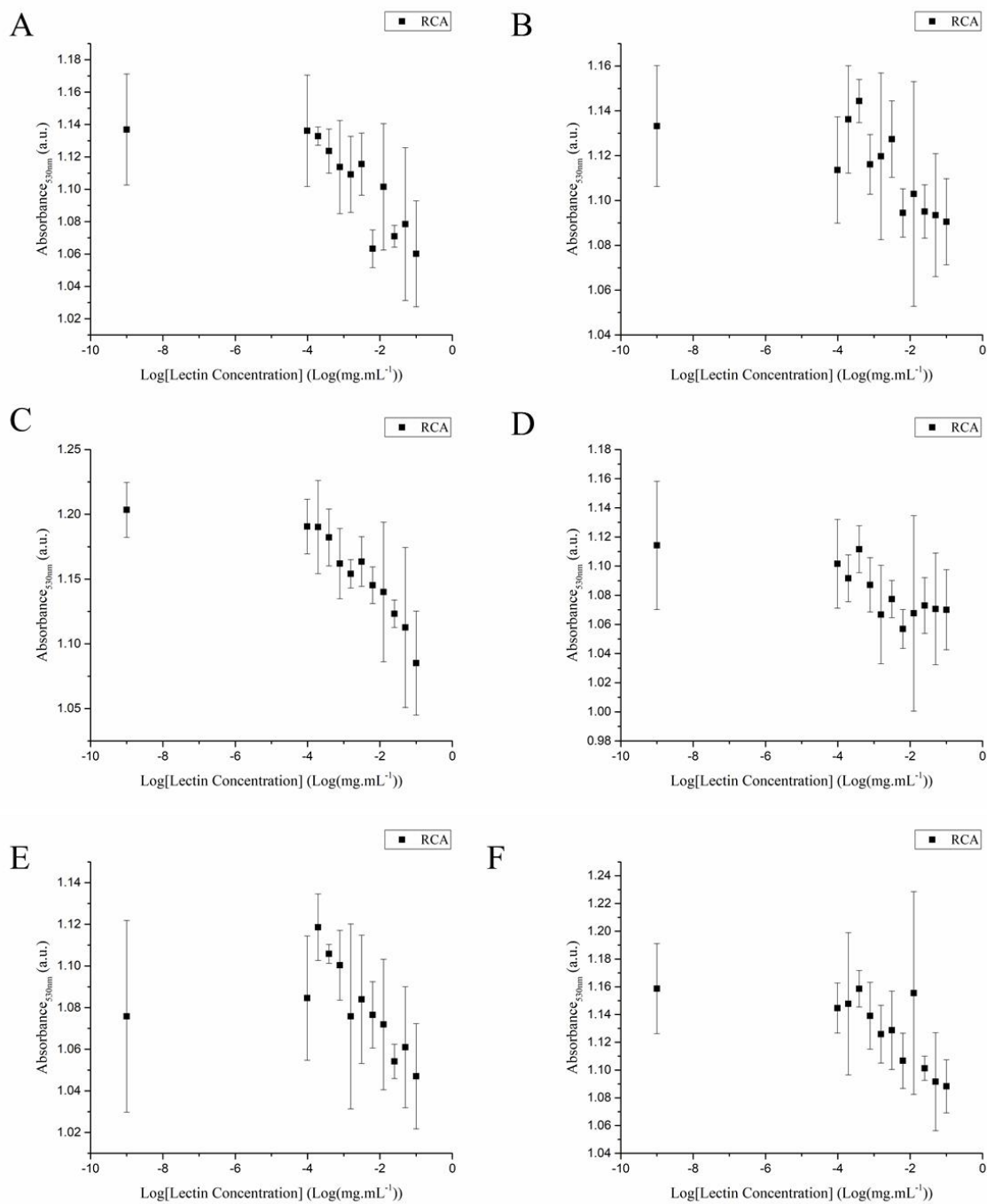


Figure 3.27: RCA binding to nanoparticle group F; containing sugars 6-Azido-6-deoxy Glucose and 6-Azido-6-deoxy Galactose (A) 100:0 6-Azido-6-deoxy Glucose : 6-Azido-6-deoxy Galactose (B) 80:20 6-Azido-6-deoxy Glucose : 6-Azido-6-deoxy Galactose (C) 60:40 6-Azido-6-deoxy Glucose : 6-Azido-6-deoxy Galactose (D) 40:60 6-Azido-6-deoxy Glucose : 6-Azido-6-deoxy Galactose (E) 20:80 6-Azido-6-deoxy Glucose : 6-Azido-6-deoxy Galactose (F) 0:100 6-Azido-6-deoxy Glucose : 6-Azido-6-deoxy Galactose

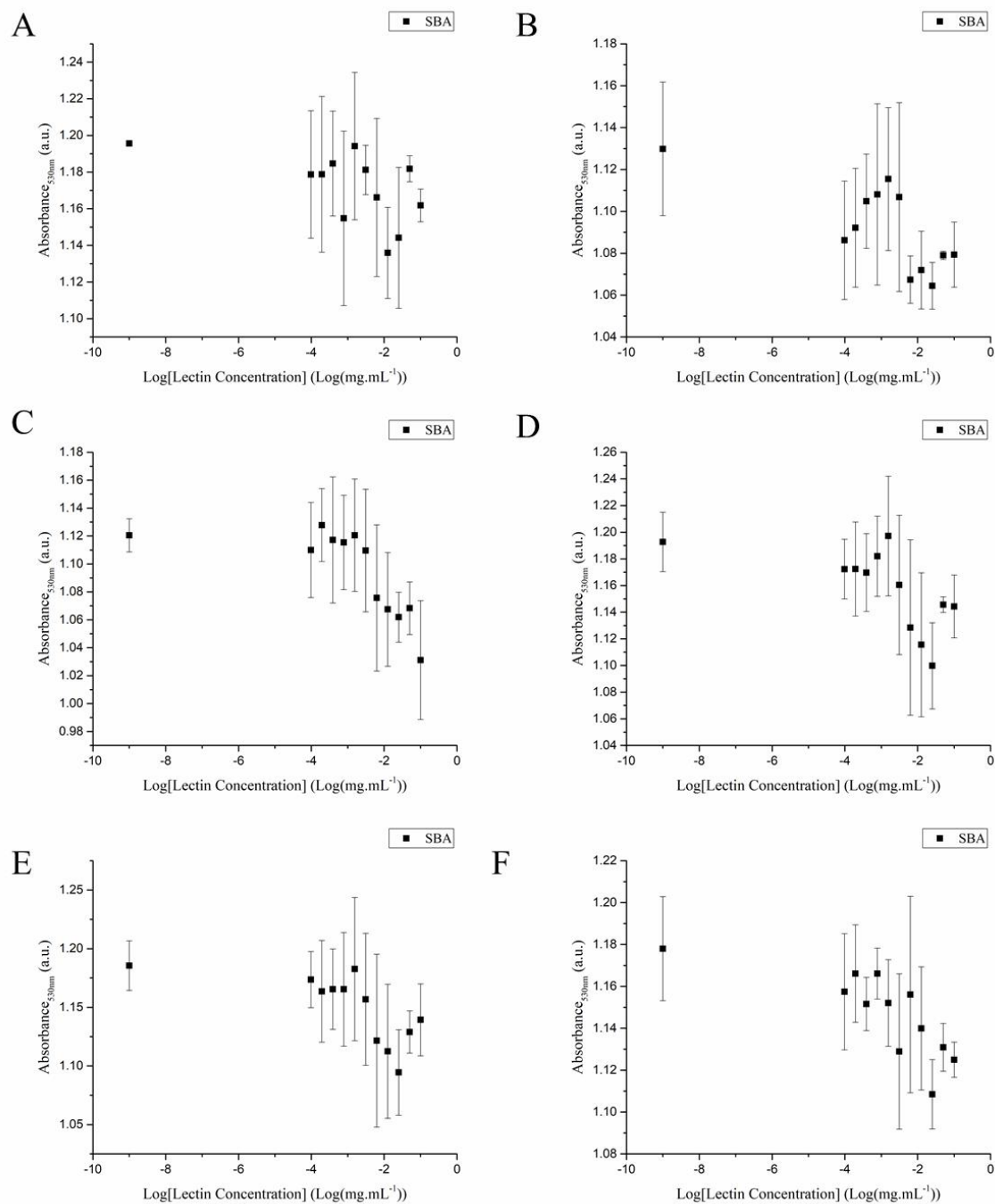


Figure 3.28: SBA binding to nanoparticle group A containing sugars 2-Azido-2-deoxy Glucose and 2-Azido-2-deoxy Galactose (A) 100:0 2-Azido-2-deoxy Glucose: 2-Azido-2-deoxy Galactose (B) 80:20 2-Azido-2-deoxy Glucose : 2-Azido-2-deoxy Galactose (C) 60:40 2-Azido-2-deoxy Glucose : 2-Azido-2-deoxy Galactose (D) 40:60 2-Azido-2-deoxy Glucose : 2-Azido-2-deoxy Galactose (E) 20:80 2-Azido-2-deoxy Glucose : 2-Azido-2-deoxy Galactose (F) 0:100 2-Azido-2-deoxy Glucose : 2-Azido-2-deoxy Galactose.

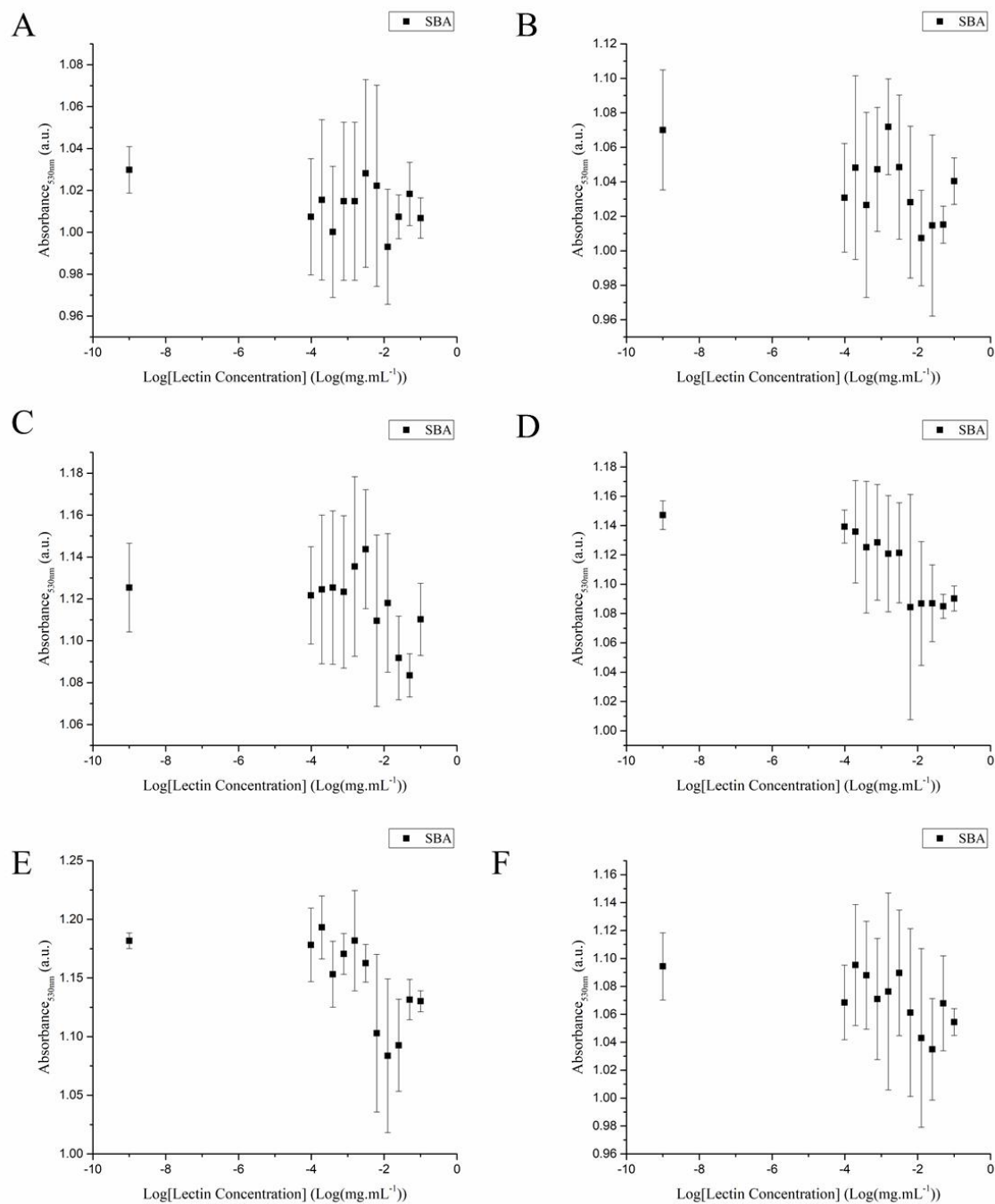


Figure 3.29: SBA binding to nanoparticle group B; containing sugars 2-Azido-2-deoxy Glucose and 6-Azido-6-deoxy Glucose. (A) 100:0 2-Azido-2-deoxy Glucose : 6-Azido-6-deoxy Glucose (B) 80:20 2-Azido-2-deoxy Glucose : 6-Azido-6-deoxy Glucose (C) 60:40 2-Azido-2-deoxy Glucose : 6-Azido-6-deoxy Glucose (D) 40:60 2-Azido-2-deoxy Glucose : 6-Azido-6-deoxy Glucose (E) 20:80 2-Azido-2-deoxy Glucose : 6-Azido-6-deoxy Glucose (F) 0:100 2-Azido-2-deoxy Glucose : 6-Azido-6-deoxy Glucose

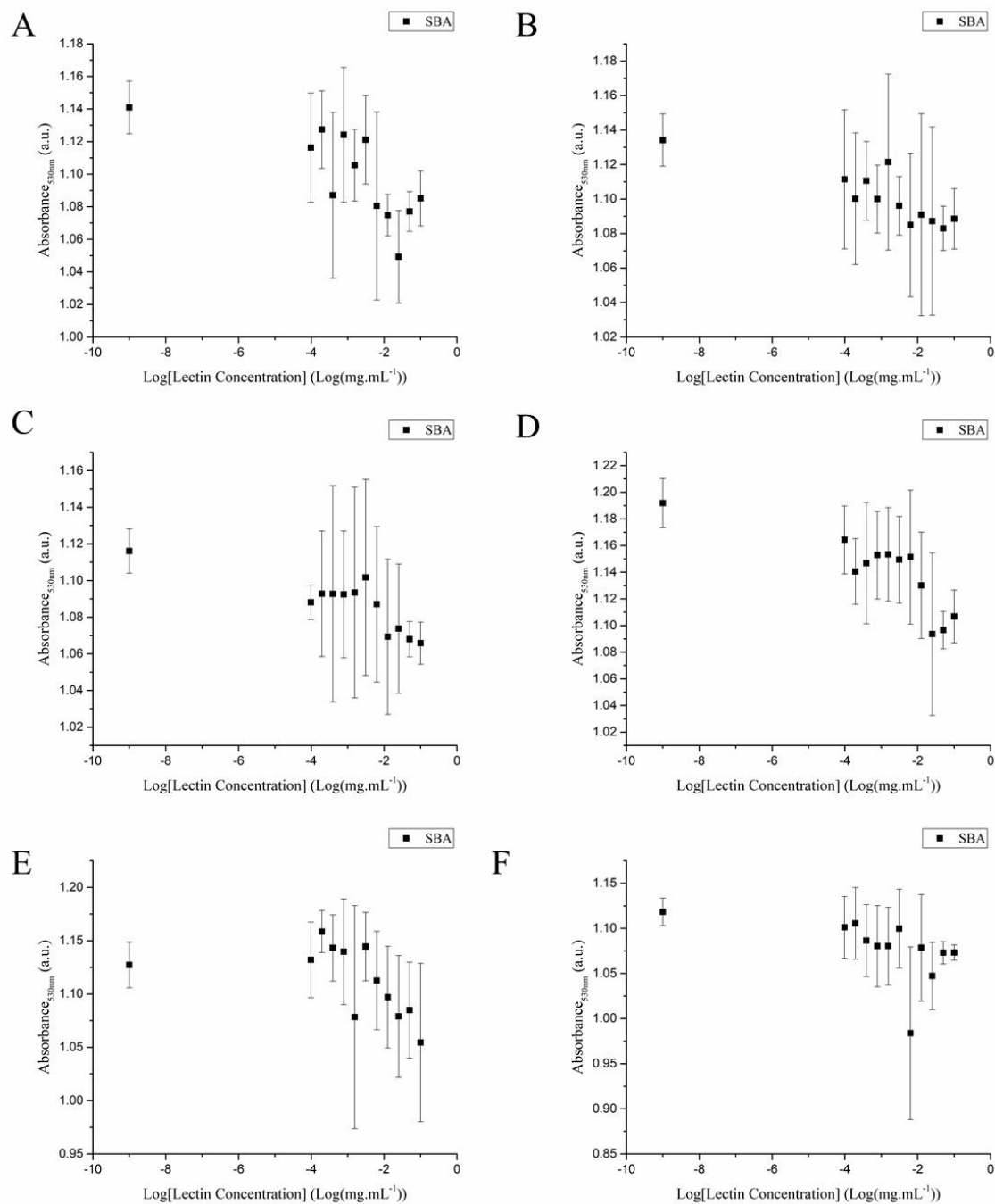


Figure 3.30: SBA binding to nanoparticle group C; containing sugars 2-Azido-2-deoxy Glucose and 6-Azido-6-deoxy Galactose (A) 100:0 2-Azido-2-deoxy Glucose : 6-Azido-6-deoxy Galactose (B) 80:20 2-Azido-2-deoxy Glucose : 6-Azido-6-deoxy Galactose (C) 60:40 2-Azido-2-deoxy Glucose : 6-Azido-6-deoxy Galactose (D) 40:60 2-Azido-2-deoxy Glucose : 6-Azido-6-deoxy Galactose (E) 20:80 2-Azido-2-deoxy Glucose : 6-Azido-6-deoxy Galactose (F) 0:100 2-Azido-2-deoxy Glucose : 6-Azido-6-deoxy Galactose

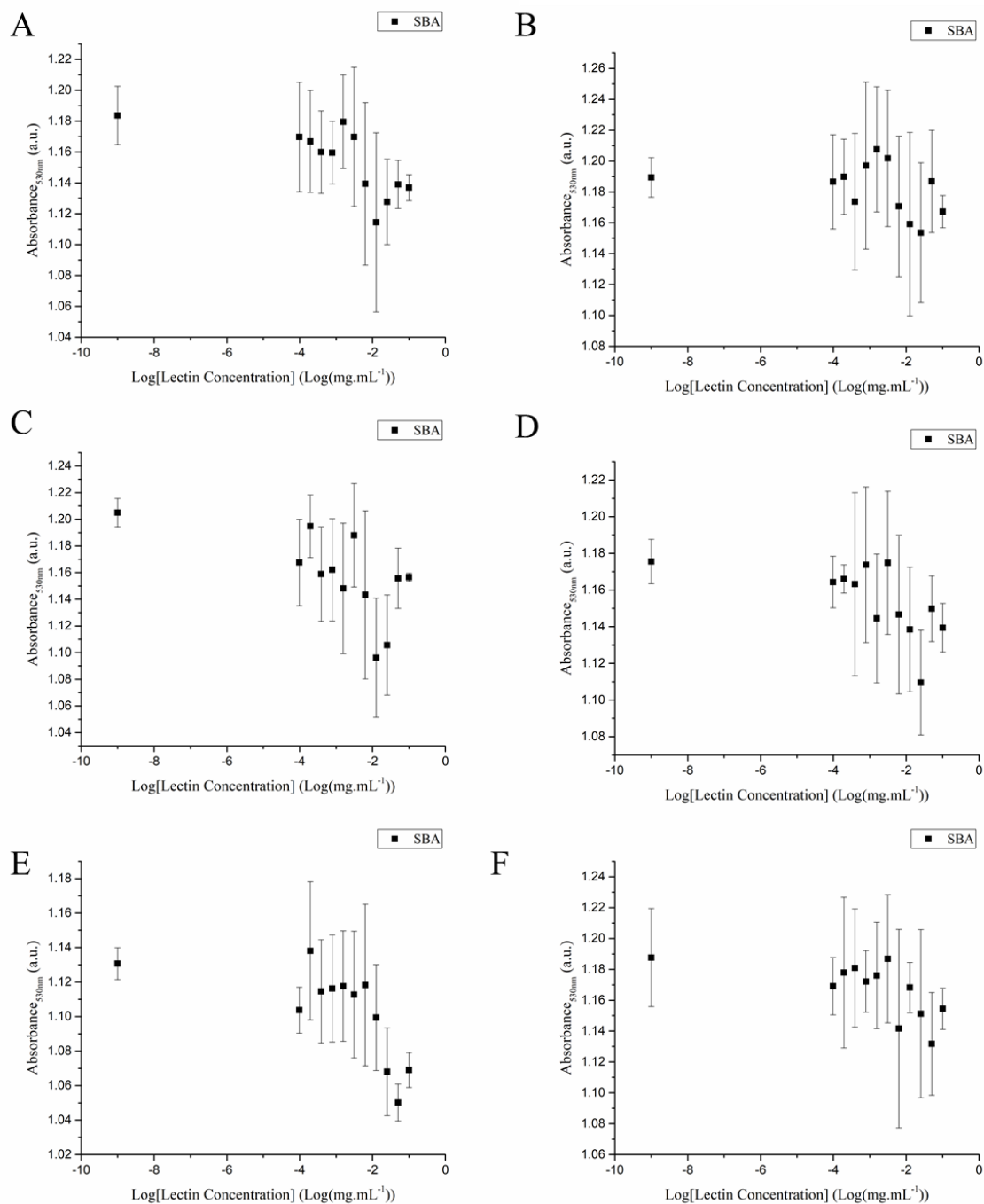


Figure 3.31: SBA binding to nanoparticle group D; containing sugars 2-Azido-2-deoxy Galactose and 6-Azido-6-deoxy Glucose (A) 100:0 2-Azido-2-deoxy Galactose : 6-Azido-6-deoxy Glucose (B) 80:20 2-Azido-2-deoxy Galactose : 6-Azido-6-deoxy Glucose (C) 60:40 2-Azido-2-deoxy Galactose : 6-Azido-6-deoxy Glucose (D) 40:60 2-Azido-2-deoxy Galactose : 6-Azido-6-deoxy Glucose (E) 20:80 2-Azido-2-deoxy Galactose : 6-Azido-6-deoxy Glucose (F) 0:100 2-Azido-2-deoxy Galactose : 6-Azido-6-deoxy Glucose

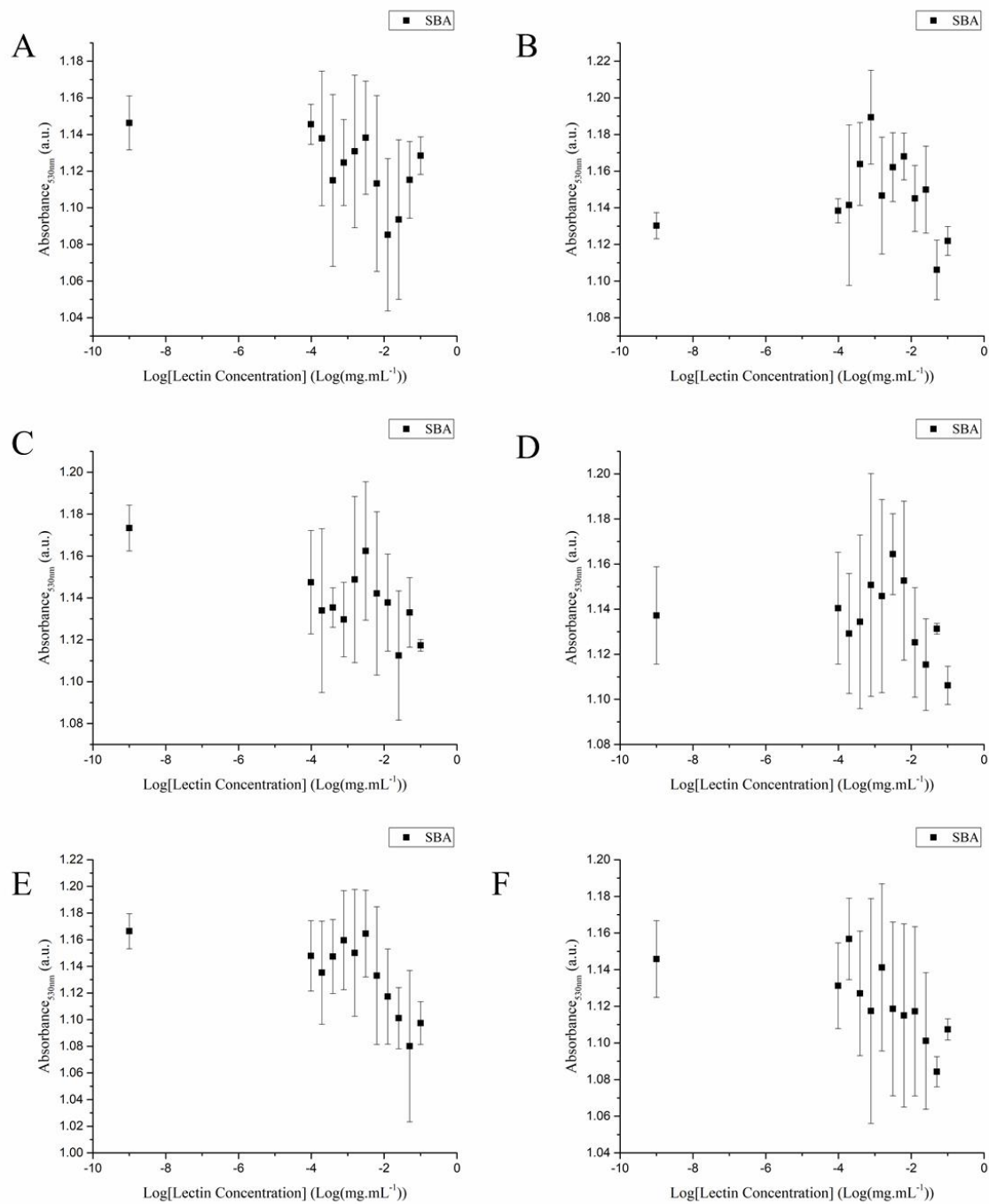


Figure 3.32: SBA binding to nanoparticle group E; containing sugars 2-Azido-2-deoxy Galactose and 6-Azido-6-deoxy Galactose (A) 100:0 2-Azido-2-deoxy Galactose : 6-Azido-6-deoxy Galactose (B) 80:20 2-Azido-2-deoxy Galactose : 6-Azido-6-deoxy Galactose (C) 60:40 2-Azido-2-deoxy Galactose : 6-Azido-6-deoxy Galactose (D) 40:60 2-Azido-2-deoxy Galactose : 6-Azido-6-deoxy Galactose (E) 20:80 2-Azido-2-deoxy Galactose : 6-Azido-6-deoxy Galactose (F) 0:100 2-Azido-2-deoxy Galactose : 6-Azido-6-deoxy Galactose

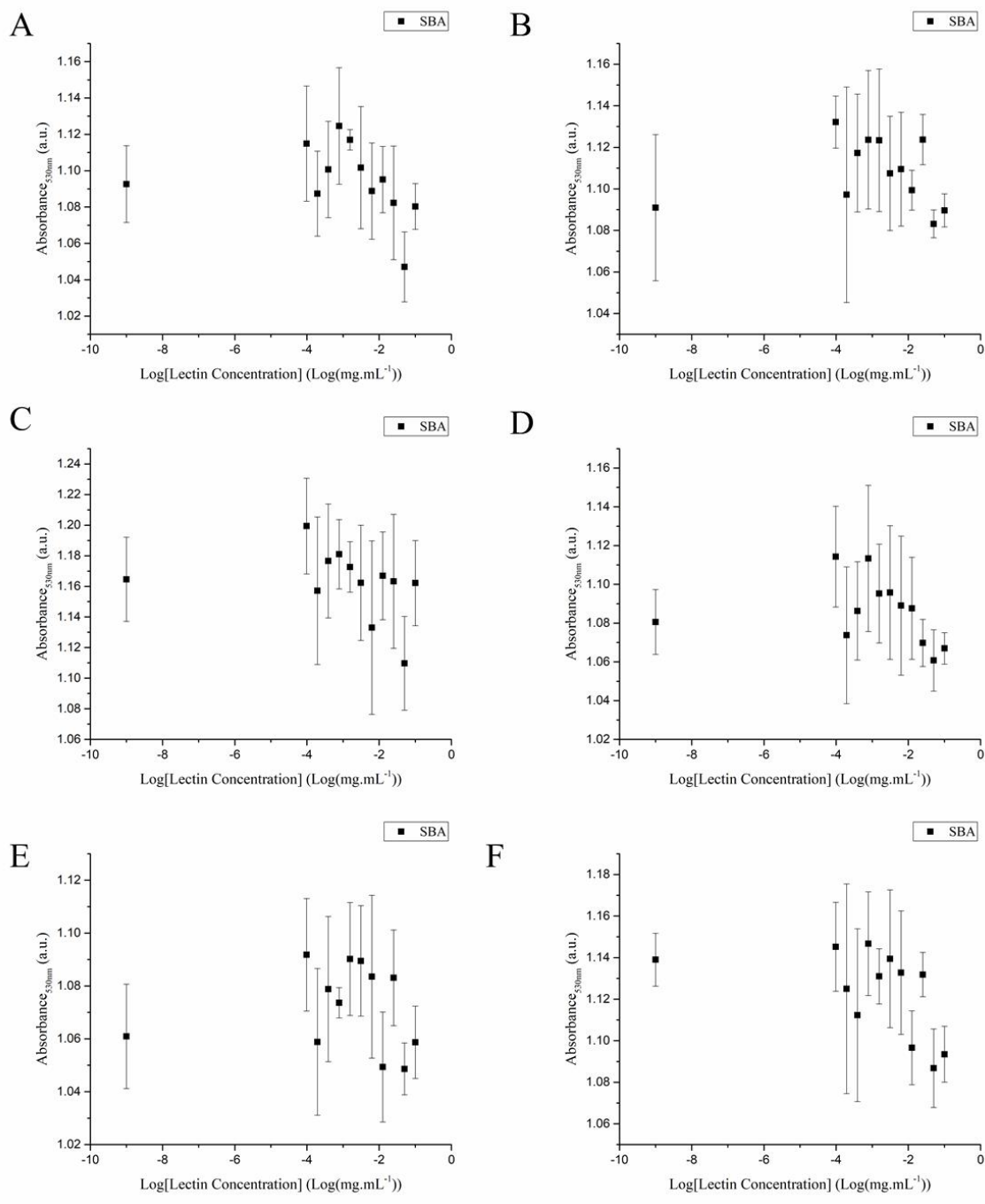


Figure 3.33: SBA binding to nanoparticle group F; containing sugars 6-Azido-6-deoxy Glucose and 6-Azido-6-deoxy Galactose (A) 100:0 6-Azido-6-deoxy Glucose : 6-Azido-6-deoxy Galactose (B) 80:20 6-Azido-6-deoxy Glucose : 6-Azido-6-deoxy Galactose (C) 60:40 6-Azido-6-deoxy Glucose : 6-Azido-6-deoxy Galactose (D) 40:60 6-Azido-6-deoxy Glucose : 6-Azido-6-deoxy Galactose (E) 20:80 6-Azido-6-deoxy Glucose : 6-Azido-6-deoxy Galactose (F) 0:100 6-Azido-6-deoxy Glucose : 6-Azido-6-deoxy Galactose

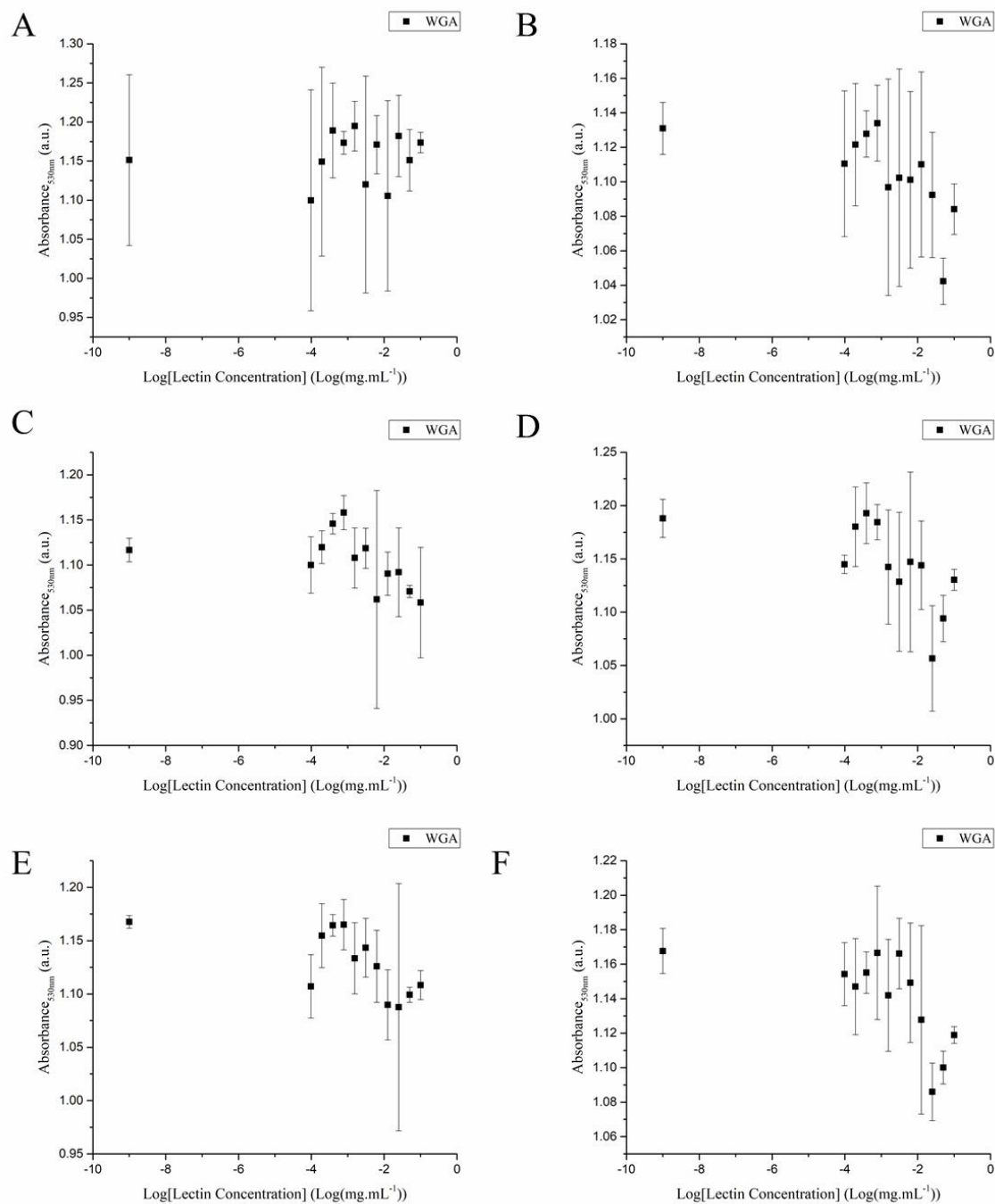


Figure 3.34: WGA binding to nanoparticle group A containing sugars 2-Azido-2-deoxy Glucose and 2-Azido-2-deoxy Galactose (A) 100:0 2-Azido-2-deoxy Glucose: 2-Azido-2-deoxy Galactose (B) 80:20 2-Azido-2-deoxy Glucose : 2-Azido-2-deoxy Galactose (C) 60:40 2-Azido-2-deoxy Glucose : 2-Azido-2-deoxy Galactose (D) 40:60 2-Azido-2-deoxy Glucose : 2-Azido-2-deoxy Galactose (E) 20:80 2-Azido-2-deoxy Glucose : 2-Azido-2-deoxy Galactose (F) 0:100 2-Azido-2-deoxy Glucose : 2-Azido-2-deoxy Galactose.

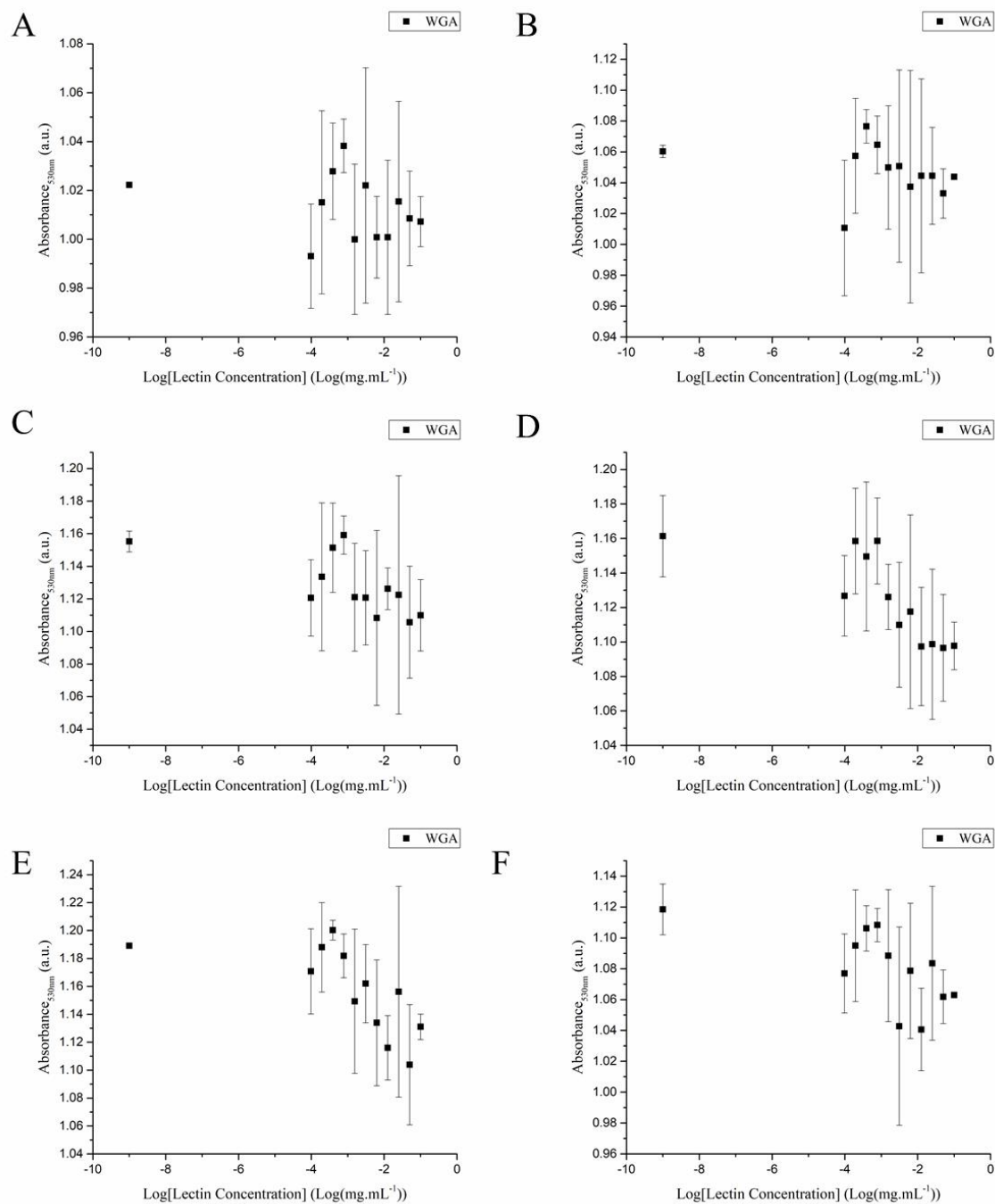


Figure 3.35: WGA binding to nanoparticle group B; containing sugars 2-Azido-2-deoxy Glucose and 6-Azido-6-deoxy Glucose. (A) 100:0 2-Azido-2-deoxy Glucose : 6-Azido-6-deoxy Glucose (B) 80:20 2-Azido-2-deoxy Glucose : 6-Azido-6-deoxy Glucose (C) 60:40 2-Azido-2-deoxy Glucose : 6-Azido-6-deoxy Glucose (D) 40:60 2-Azido-2-deoxy Glucose : 6-Azido-6-deoxy Glucose (E) 20:80 2-Azido-2-deoxy Glucose : 6-Azido-6-deoxy Glucose (F) 0:100 2-Azido-2-deoxy Glucose : 6-Azido-6-deoxy Glucose

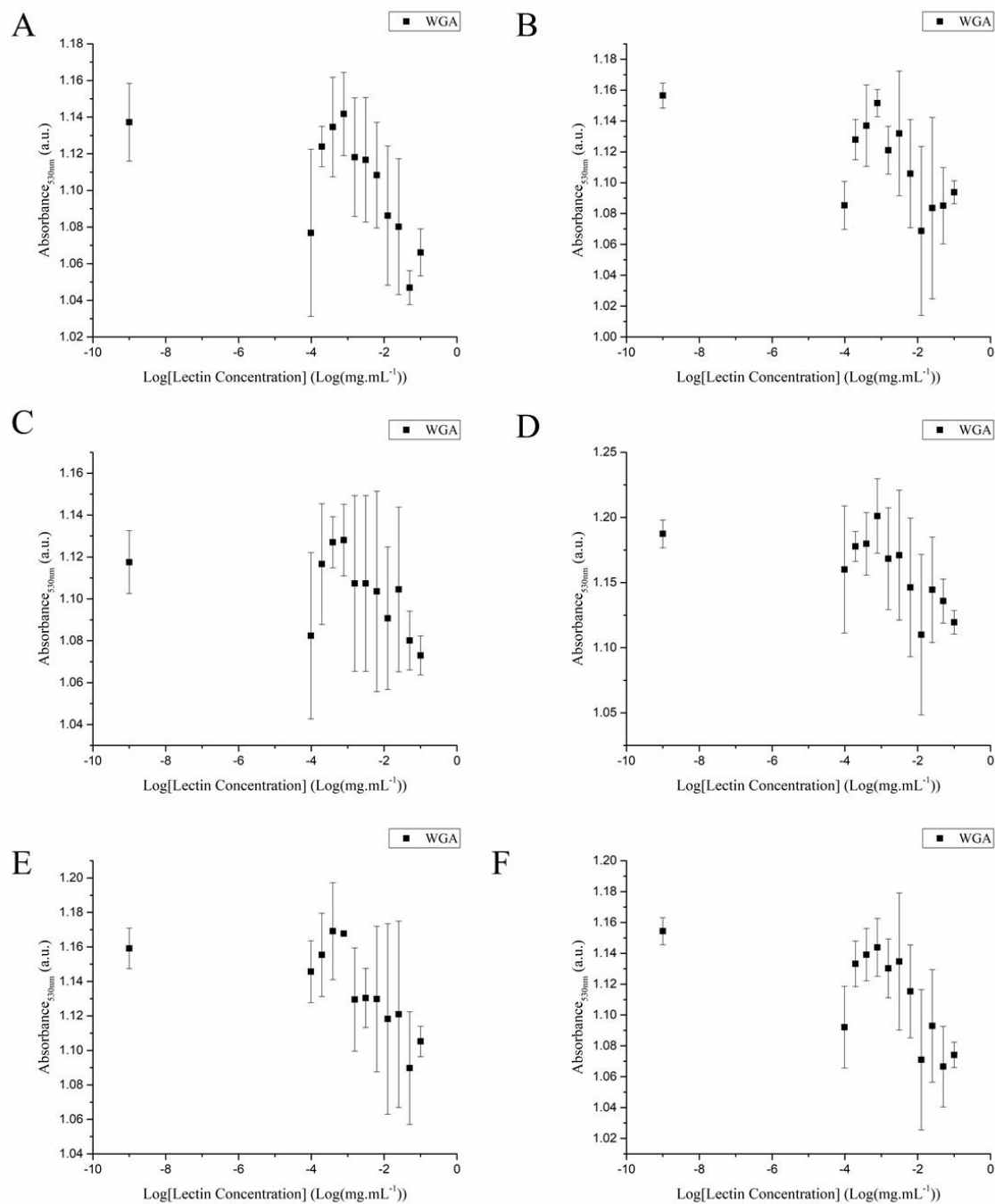


Figure 3.36: WGA binding to nanoparticle group C; containing sugars 2-Azido-2-deoxy Glucose and 6-Azido-6-deoxy Galactose (A) 100:0 2-Azido-2-deoxy Glucose : 6-Azido-6-deoxy Galactose (B) 80:20 2-Azido-2-deoxy Glucose : 6-Azido-6-deoxy Galactose (C) 60:40 2-Azido-2-deoxy Glucose : 6-Azido-6-deoxy Galactose (D) 40:60 2-Azido-2-deoxy Glucose : 6-Azido-6-deoxy Galactose (E) 20:80 2-Azido-2-deoxy Glucose : 6-Azido-6-deoxy Galactose (F) 0:100 2-Azido-2-deoxy Glucose : 6-Azido-6-deoxy Galactose

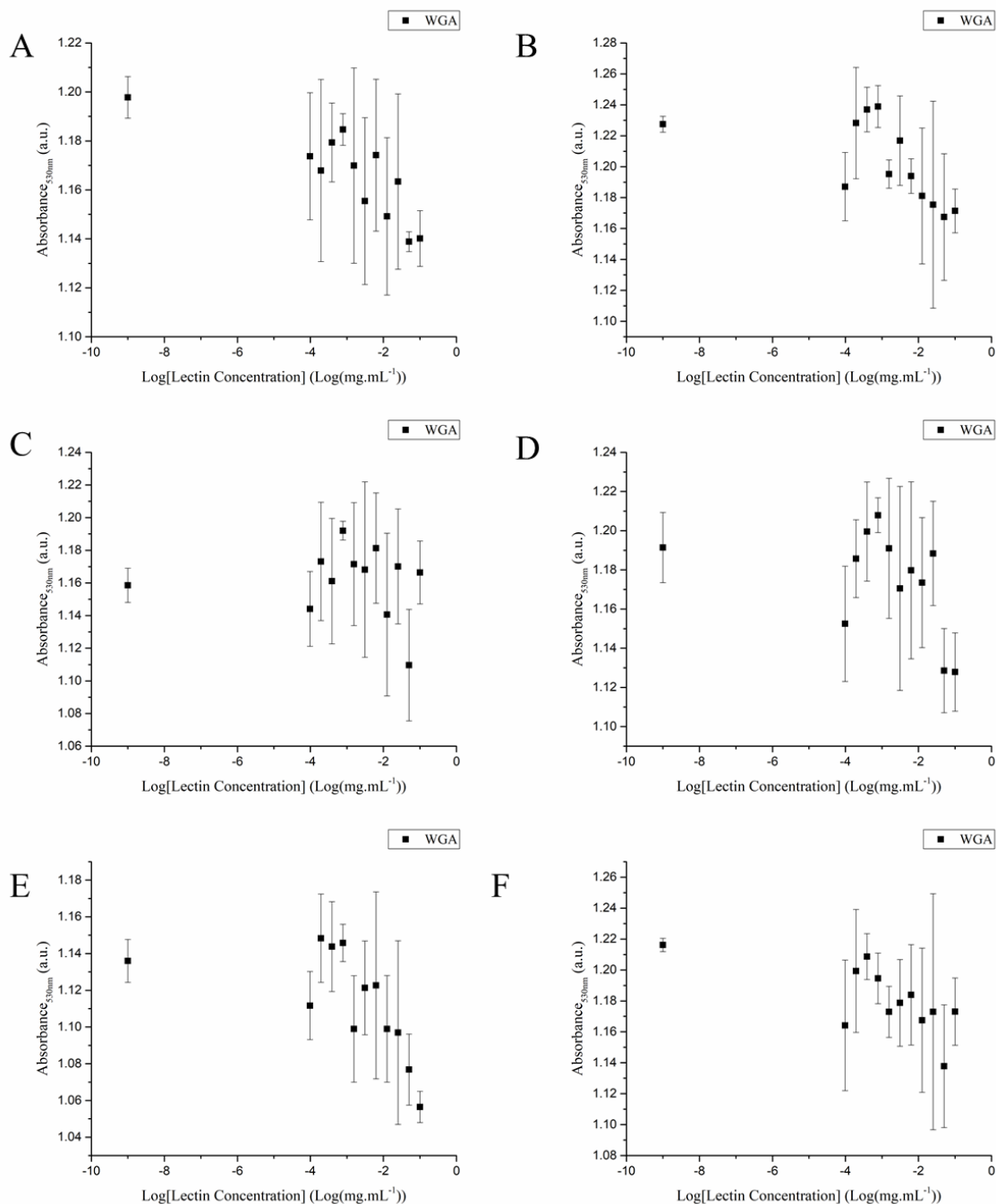


Figure 3.37: WGA binding to nanoparticle group D; containing sugars 2-Azido-2-deoxy Galactose and 6-Azido-6-deoxy Glucose (A) 100:0 2-Azido-2-deoxy Galactose : 6-Azido-6-deoxy Glucose (B) 80:20 2-Azido-2-deoxy Galactose : 6-Azido-6-deoxy Glucose (C) 60:40 2-Azido-2-deoxy Galactose : 6-Azido-6-deoxy Glucose (D) 40:60 2-Azido-2-deoxy Galactose : 6-Azido-6-deoxy Glucose (E) 20:80 2-Azido-2-deoxy Galactose : 6-Azido-6-deoxy Glucose (F) 0:100 2-Azido-2-deoxy Galactose : 6-Azido-6-deoxy Glucose

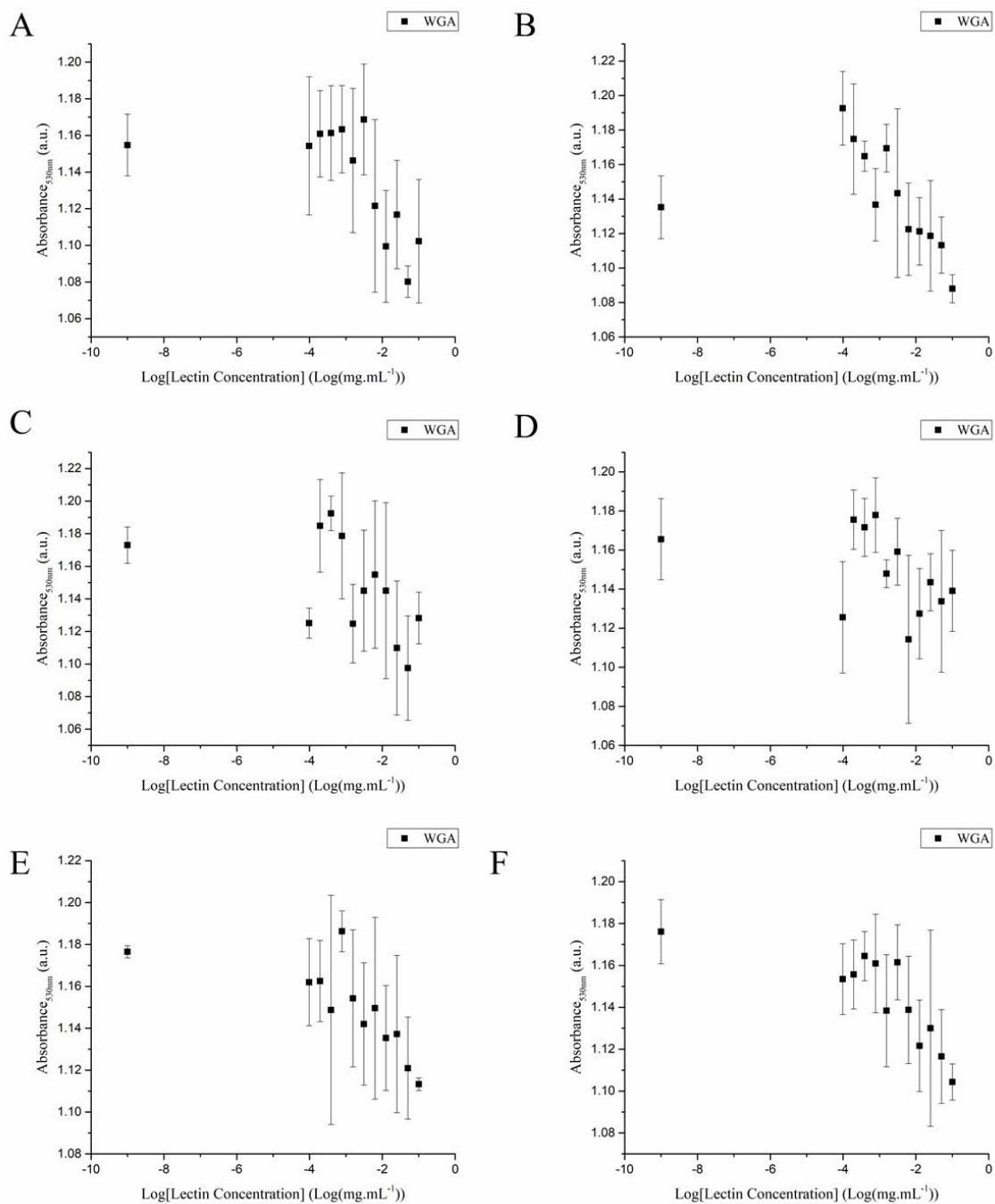


Figure 3.38: WGA binding to nanoparticle group E; containing sugars 2-Azido-2-deoxy Galactose and 6-Azido-6-deoxy Galactose (A) 100:0 2-Azido-2-deoxy Galactose : 6-Azido-6-deoxy Galactose (B) 80:20 2-Azido-2-deoxy Galactose : 6-Azido-6-deoxy Galactose (C) 60:40 2-Azido-2-deoxy Galactose : 6-Azido-6-deoxy Galactose (D) 40:60 2-Azido-2-deoxy Galactose : 6-Azido-6-deoxy Galactose (E) 20:80 2-Azido-2-deoxy Galactose : 6-Azido-6-deoxy Galactose (F) 0:100 2-Azido-2-deoxy Galactose : 6-Azido-6-deoxy Galactose

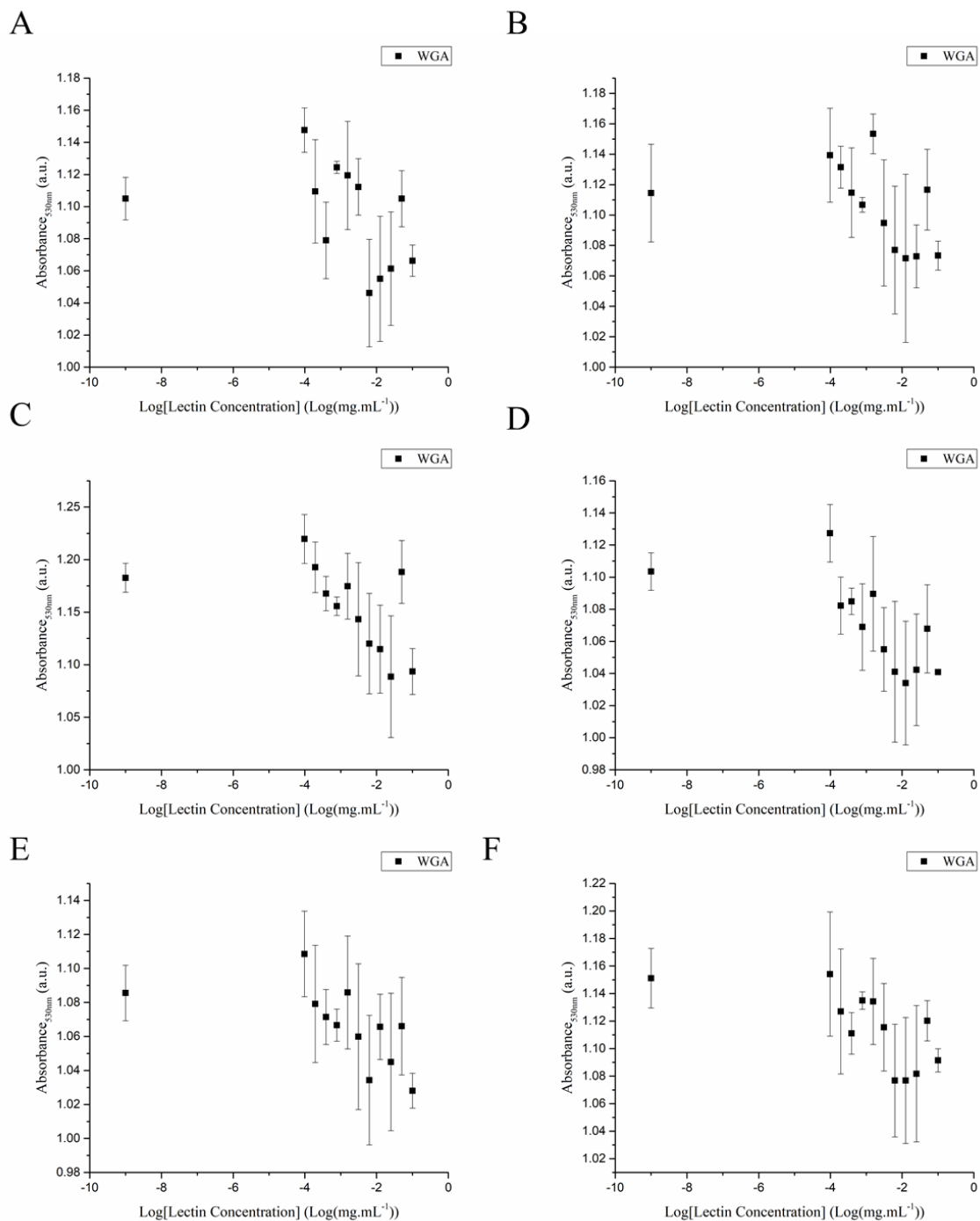


Figure 3.39: WGA binding to nanoparticle group F; containing sugars 6-Azido-6-deoxy Glucose and 6-Azido-6-deoxy Galactose (A) 100:0 6-Azido-6-deoxy Glucose : 6-Azido-6-deoxy Galactose (B) 80:20 6-Azido-6-deoxy Glucose : 6-Azido-6-deoxy Galactose (C) 60:40 6-Azido-6-deoxy Glucose : 6-Azido-6-deoxy Galactose (D) 40:60 6-Azido-6-deoxy Glucose : 6-Azido-6-deoxy Galactose (E) 20:80 6-Azido-6-deoxy Glucose : 6-Azido-6-deoxy Galactose (F) 0:100 6-Azido-6-deoxy Glucose : 6-Azido-6-deoxy Galactose

3.3.5. Determining the limit of detection

To determine if the high variability in the binding we observed was due to the low concentration of gold tested, a study was undertaken to determine the limit of detection of gold for this assay, a point that had not yet been addressed in the literature. To do so we chose to use a homo-sugar coated gold nanoparticle in a system that has been shown to work previously. In work previously conducted within our group, galactosylated particles have shown ideal binding behaviour with the lectin soybean agglutinin (SBA). GalNH₂-pHEA₂₅@AuNP₄₀ were incubated at 37 °C in the presence of a fixed SBA concentration, and the UV-Vis spectra recorded at 4 time points from 0 to 150 minutes. The resulting absorbance at 700nm was recorded and plotted, shown in Figure 3.40. At all concentrations the general shape of the gold absorbance was still visible in the UV-Vis spectra, including an identifiable SPR peak. However, below a concentration of $-10.5 \log(\text{Mol.L}^{-1})$, equal to $31 \times 10^{-12} \text{ Mol.L}^{-1}$, the assay sharply loses resolution.

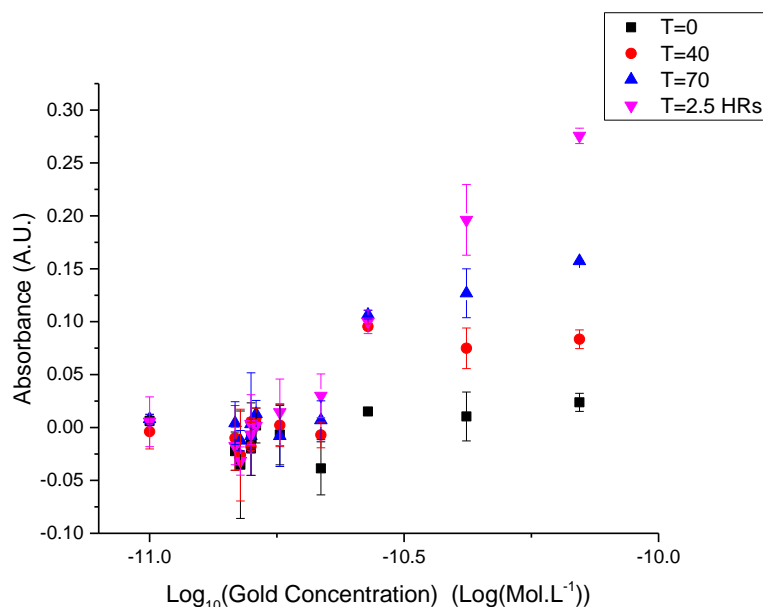


Figure 3.40: Incubation of GalNH₂-pHEAA₂₅@AuNP₄₀ particles with SBA at at 6.25×10^{-3} mg.mL⁻¹ in HEPES buffered saline, against varying gold concentrations to investigate the limit of detection. Error bars correspond to one standard deviation.

This is likely due simply to the decrease in the absorbance signal with concentration as described by the Beer-Lambert law, (Equation 3.1) therefore resulting in a lower signal to noise ratio, loss of resolution to the assay, and large error in the results. Compared to our earlier assay which was performed at a concentration of 6.7×10^{-11} Mol.L⁻¹ or $-10.2 \log(\text{Mol.L}^{-1})$, the assay was performed on the limit of the resolution.

To counteract this issue and prevent the loss of gold concentration during the purification process it we proposed that it would be possible to utilise the multivalent binding effect to our advantage. Due to the high efficiency of the strain promoted azide alkyne coupling between the azido-sugars and DBCO end group the concentration of sugar used to functionalise our particles was already low, $32 \mu\text{M}$ in Milli Q water. By forgoing any purification the vast difference in K_d between the multivalent lectin binding to our nanoparticle surface ($K_d \sim \text{nM}$)³⁵ and a simple monosaccharide ($K_d \sim \text{mM}$)³⁶ would render the purification step unnecessary. This would have the advantage of also improving the applicability of this method to large scale screening techniques, Figure 3.41.

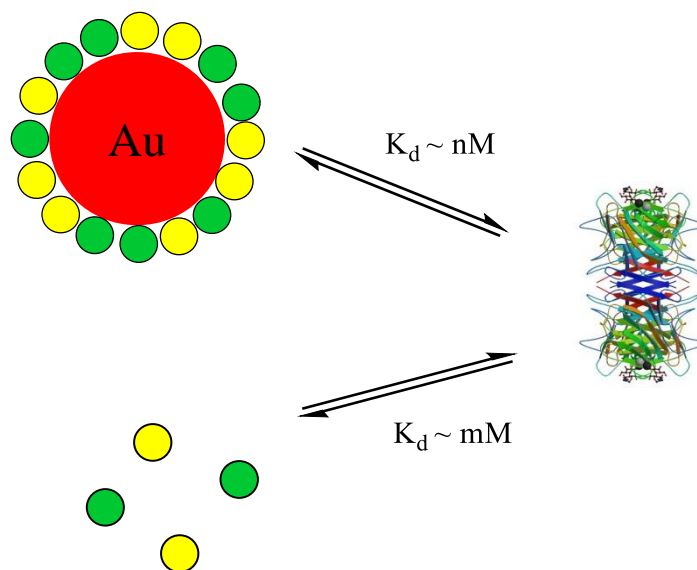


Figure 3.41: Multivalency effects should allow us to outcompete monosaccharide binding and eliminate the need for purification methods.

3.3.6. Synthesis of gold nanoparticles *via* step growth

In order to investigate the possibility of removing the purification steps a new nanoparticle library was synthesised. It was decided to move to a step growth synthesis for the gold nanoparticles as described by Bastús *et al.*³⁷ to gain better control and reproducibility. Particles of size 40nm were targeted and the nanoparticle growth was monitored by UV-Vis spectroscopy, Figure 3.42 and Table 3.6:

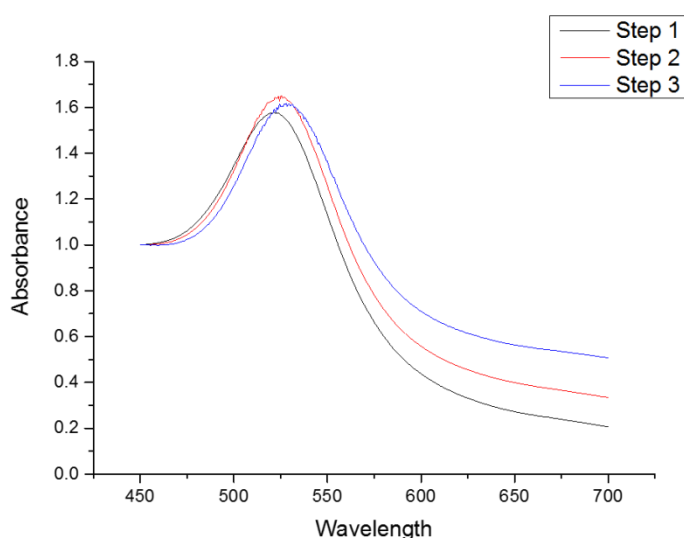


Figure 3.42: UV-Vis spectra of the step growth of gold nanoparticles.

Table 3.6: Determination of the size of gold nanoparticles by UV-Vis.

Step	λ_{spr} (nm)	A_{spr}/A_{450}	Diameter (nm) ^(a)
1	521.5	1.57	12 ^(b)
2	525.5	-	32
3	527.9	-	40

(a) As determined by comparison to Haiss *et al.*³² (b) For $\lambda_{\text{spr}} < 525.0$, A_{spr}/A_{450} is used to determine nanoparticle size.

The resulting particles were also characterised by transmission electron spectroscopy (TEM), the resulting images were processed in imageJ to obtain a histogram of nanoparticle size,

Figure 3.43

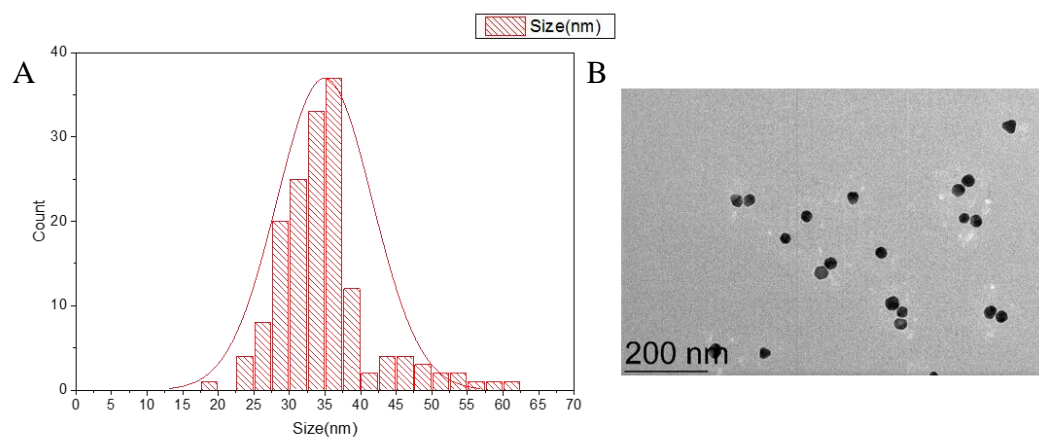


Figure 3.43: (A) Histogram of nanoparticle sizes obtained from TEM n=160 (B) TEM image showing gold nanoparticle morphology.

The nanoparticles were then coated with $p(\text{HEAA})_{25}\text{-DBCO}$, and used to generate a glycosylated nanoparticle library, as described in detail in the next section of this work. The polymer coating of the gold nanoparticles and subsequent addition of azido-hexoses was monitored using, UV-Vis, dynamic light scattering and zeta potential measurements, Table 3.7. The zeta potential of the AuNPs was negative, in line with other reports of surface modified gold.³⁸ The addition of both the polymer coating and then subsequent functionalisation with 1-azido-1-deoxy-galactose results in a change to the electrical double layer around the particle and results in an increase in the zeta potential (less negative).

Table 3.7: Dynamic light scattering and zeta potential.

Gold Coating	Size ^(a) (nm)	Size ^(b) (nm)	Size ^(c) (nm)	Zeta Potential ^(d) (mV)
Citrate	40	55 ±3.3	34.9 ±6.7	-38.1 ±1.0
DBCO-HEAA	62	76 ±0.9	N/A	-21.1 ±0.1
Gal-HEAA	62	76 ±3.5	N/A	-19.7 ±0.6

(a) UV-Vis (b) Dynamic Light Scattering, $\Delta=0.4$ (c) TEM (n=160) (d) Measured in milliQ water at pH=7.4

3.3.7. Synthesis of 1-azido-1-deoxy- sugar coated 40nm gold nanoparticle library

To follow on from work conducted in chapter one it was decided to investigate a heterofunctional galactose-mannose system. As such 1-azido-1-deoxy galactose and 1-azido-1-deoxy mannose were mixed in 10% molar increments as shown in Table 3.8.

Table 3.8: Heterofunctional library created using 1-azido-1-deoxy galactose, 1-azido-1-deoxy mannose and 1-(8-azidoethyl)-1-deoxy mannose.

Sample	Ratio	Sugar 1	Sugar 2
G₁₀₀AuNP₄₀	100:0	1-azido-1-deoxy galactose	1-azido-1-deoxy mannose
G₉₀M₁₀AuNP₄₀	90:10	1-azido-1-deoxy galactose	1-azido-1-deoxy mannose
G₈₀M₂₀AuNP₄₀	80:20	1-azido-1-deoxy galactose	1-azido-1-deoxy mannose
G₇₀M₃₀AuNP₄₀	70:30	1-azido-1-deoxy galactose	1-azido-1-deoxy mannose
G₆₀M₄₀AuNP₄₀	60:40	1-azido-1-deoxy galactose	1-azido-1-deoxy mannose
G₅₀M₅₀AuNP₄₀	50:50	1-azido-1-deoxy galactose	1-azido-1-deoxy mannose
G₄₀M₆₀AuNP₄₀	40:60	1-azido-1-deoxy galactose	1-azido-1-deoxy mannose
G₃₀M₇₀AuNP₄₀	30:70	1-azido-1-deoxy galactose	1-azido-1-deoxy mannose
G₂₀M₈₀AuNP₄₀	20:80	1-azido-1-deoxy galactose	1-azido-1-deoxy mannose
G₁₀M₉₀AuNP₄₀	10:90	1-azido-1-deoxy galactose	1-azido-1-deoxy mannose
M₁₀₀AuNP₄₀	0:100	1-azido-1-deoxy galactose	1-azido-1-deoxy mannose
C₈M₁₀₀AuNP₄₀	N/A	1-(8-azidoethyl)-1-deoxy mannose	N/A

In addition to this 1-(8-azido-octyl)-1-deoxy mannose was obtained from Martina Lahmann at the University of Bangor and used to generate a homofunctionalized nanoparticle to investigate the effect of the linker between the sugar and polymer coated particle, also shown in Table 3.8. It is well understood that secondary binding effects can play a role in lectin binding, and we hypothesised that the inclusion of the DBCO fused Pi-system close to the binding site may act as a large rigid hydrophobic domain that can play a role in lectin binding; alternatively, this large inflexible domain may inhibit binding by reducing the sugars ability to fit correctly into the lectin binding domain. Therefore, by introducing a flexible octyl linker and an extra 20Å distance (calculated assuming a carbon-carbon bond length of 1.54Å and sp³ hybridised bond angle of 109.5°) between the DBCO moiety and the binding site the increased flexibility and space may have allowed the sugars to more correctly orientate themselves into the binding site of the lectin. Conversely however, by introducing more degrees of rotational freedom to the system, we may be dis-advantaging binding by increasing the entropic penalty that must be paid upon binding.³⁹

3.3.8. Determining the effect of purification: can the multivalency effect out-compete monosaccharide binding?

With our second heterogeneous gold nanoparticle library in hand, we first attempted to determine if the additional purification steps can be removed from the synthesis and what effect that would have upon the binding results. Using homofunctionalized galactosyl nanoparticles the assay was carried out as before using particles that had been prepared by centrifuging at 3,000g and washing with deionised water three times, and particles that had not been further purified after the addition of the 1-azido-1-deoxy galactose for the strain promoted azide alkyne coupling. As can be seen from the resulting plots of absorbance vs lectin concentration in Figure 3.44, there is very little difference in the binding profiles of the two sets of nanoparticles.

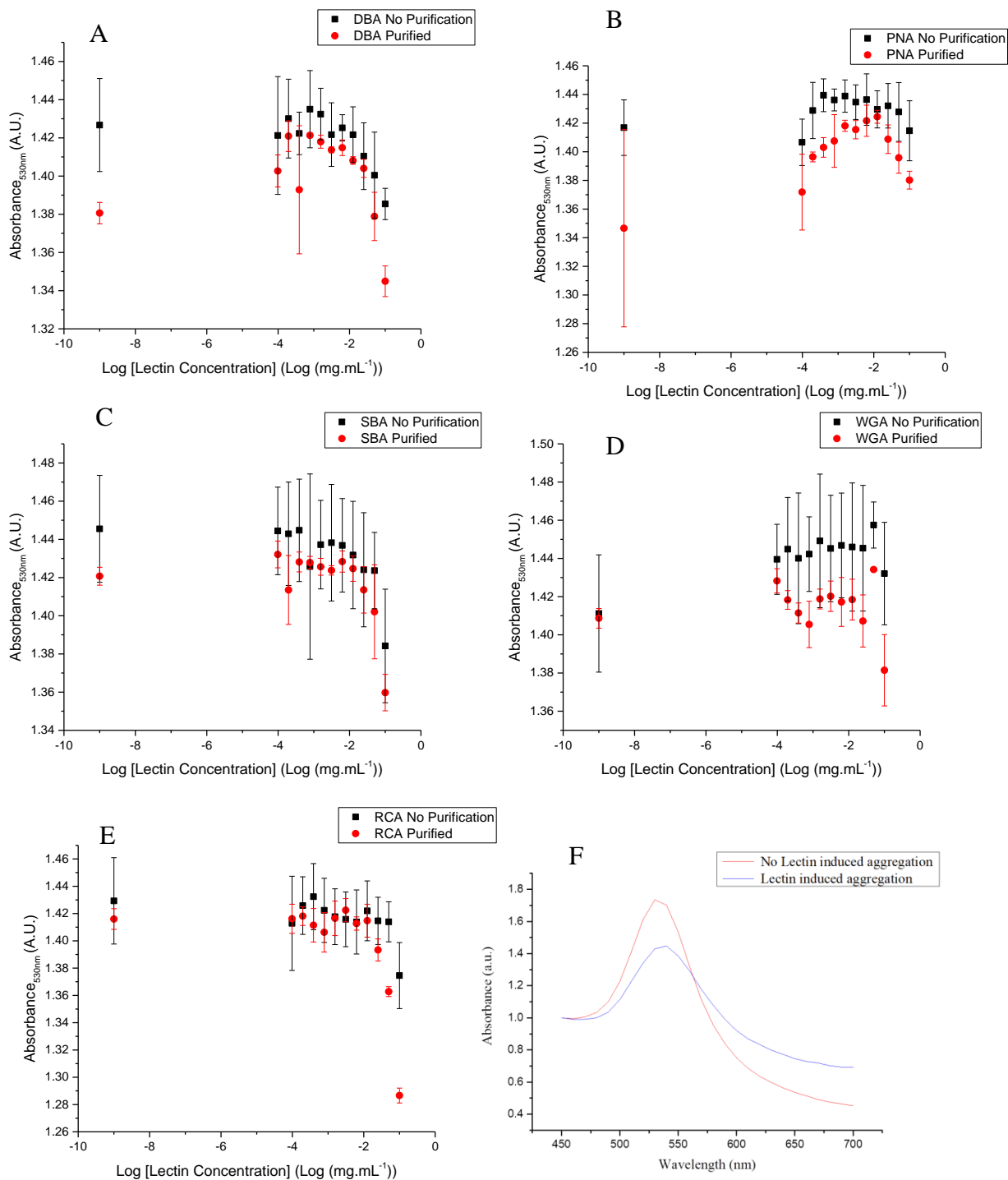


Figure 3.44: Effect of washed versus non-washed nanoparticles. Samples containing no lectin are represented at log -9. (A) DBA (B) PNA (C) SBA (D) WGA (E) RCA (F) Example UV-Vis trace showing the change in absorbance at 530nm, it is this value that is plotted for each concentration in (A) to (F).

To determine the significance of any differences between the preparation methods, a statistical T-test was carried out to determine if the mean absorbance value of each lectin concentration was equivalent between the washed and unwashed particles. The results of which can be seen for each lectin in Tables 3.9 to 3.13 below.

Table 3.9: T test to determine if washed and unwashed give statistically difference results in the binding of DBA.

DBA Concentration log(mg.mL ⁻¹)	T stat	P	T<T _{crit} ?	P > Alpha?	Accept or Reject null Hypothesis? ^(a)
-1	4.98	7.56×10^{-3}	NO	NO	Reject
-1.3	1.17	0.30	YES	YES	Accept
-1.6	0.49	0.64	YES	YES	Accept
-1.9	1.29	0.26	YES	YES	Accept
-2.2	1.83	0.13	YES	YES	Accept
-2.5	0.67	0.53	YES	YES	Accept
-2.8	1.47	0.21	YES	YES	Accept
-3.1	0.95	0.39	YES	YES	Accept
-3.4	1.18	0.30	YES	YES	Accept
-3.7	0.58	0.58	YES	YES	Accept
-4.0	0.82	0.45	YES	YES	Accept

(a)Null hypothesis: Hypothesised mean difference = 0. T_{Crit}=2.78, Alpha =0.05, Degrees of freedom = 4

Table 3.10: T test to determine if washed and unwashed give statistically difference results in the binding of PNA.

PNA Concentration log(mg.mL⁻¹)	T stat	P	T<T_{crit} ?	P > Alpha?	Accept or Reject null Hypothesis?^(a)
-1	2.23	0.09	YES	YES	Accept
-1.3	1.94	0.12	YES	YES	Accept
-1.6	1.78	0.14	YES	YES	Accept
-1.9	0.53	0.62	YES	YES	Accept
-2.2	0.99	0.37	YES	YES	Accept
-2.5	1.98	0.11	YES	YES	Accept
-2.8	2.45	0.06	YES	YES	Accept
-3.1	2.03	0.11	YES	YES	Accept
-3.4	3.85	0.01	NO	NO	Reject
-3.7	2.30	0.08	YES	YES	Accept
-4.0	1.58	0.18	YES	YES	Accept

(a) Null hypothesis: Hypothesised mean difference = 0, T_{Crit}=2.78, Alpha =0.05, Degrees of freedom = 4

Table 3.11: T test to determine if washed and unwashed give statistically difference results in the binding of SBA.

SBA Concentration log(mg.mL⁻¹)	T stat	P	T<T_{crit} ?	P > Alpha?	Accept or Reject null Hypothesis?^(a)
-1	1.10	0.33	YES	YES	Accept
-1.3	0.96	0.39	YES	YES	Accept
-1.6	0.46	0.66	YES	YES	Accept
-1.9	0.35	0.74	YES	YES	Accept
-2.2	0.47	0.65	YES	YES	Accept
-2.5	0.66	0.54	YES	YES	Accept
-2.8	0.69	0.52	YES	YES	Accept
-3.1	-0.06	0.95	YES	YES	Accept
-3.4	0.85	0.43	YES	YES	Accept
-3.7	1.27	0.26	YES	YES	Accept
-4.0	0.72	0.50	YES	YES	Accept

(a) Null hypothesis: Hypothesised mean difference = 0, T_{Crit}=2.78, Alpha =0.05, Degrees of freedom = 4

Table 3.12: T test to determine if washed and unwashed give statistically difference results in the binding of WGA.

WGA Concentration log(mg.mL⁻¹)	T stat	P	T<T_{crit} ?	P > Alpha?	Accept or Reject null Hypothesis?^(a)
-1	2.18	0.09	YES	YES	Accept
-1.3	2.72	0.05	YES	YES	Accept
-1.6	1.51	0.20	YES	YES	Accept
-1.9	1.10	0.33	YES	YES	Accept
-2.2	1.38	0.23	YES	YES	Accept
-2.5	1.22	0.28	YES	YES	Accept
-2.8	1.21	0.29	YES	YES	Accept
-3.1	2.26	0.08	YES	YES	Accept
-3.4	1.16	0.30	YES	YES	Accept
-3.7	1.36	0.24	YES	YES	Accept
-4.0	0.82	0.45	YES	YES	Accept

(a)Null hypothesis: Hypothesised mean difference = 0, T_{Crit}=2.78, Alpha =0.05, Degrees of freedom = 4

Table 3.13: T test to determine if washed and unwashed give statistically difference results in the binding of RCA.

RCA Concentration log(mg.mL⁻¹)	T stat	P	T<T_{crit} ?	P > Alpha?	Accept or Reject null Hypothesis?^(a)
-1	5.01	7.41x10 ⁻³	NO	NO	Reject
-1.3	4.78	8.73x10 ⁻³	NO	NO	Reject
-1.6	1.57	0.18	YES	YES	Accept
-1.9	0.40	0.70	YES	YES	Accept
-2.2	0.06	0.95	YES	YES	Accept
-2.5	-0.43	0.68	YES	YES	Accept
-2.8	0.06	0.94	YES	YES	Accept
-3.1	0.82	0.45	YES	YES	Accept
-3.4	1.08	0.33	YES	YES	Accept
-3.7	0.49	0.64	YES	YES	Accept
-4.0	-0.13	0.90	YES	YES	Accept

(a)Null hypothesis: Hypothesised mean difference = 0. T_{Crit}=2.78, Alpha =0.05, Degrees of freedom = 4.

As can be seen, for 3 of the 5 lectins there is essentially no difference in the binding profiles of the washed vs unwashed nanoparticle samples. In the case of PNA, at a concentration of $10^{-3.4}$ mg.mL⁻¹ there is a significant difference observed between the two nanoparticle sets, however this would likely not influence the interpretation of any assay result. Finally, for DBA and RCA, at the highest concentrations of lectin only there is a significant difference observed between the nanoparticle sets. Despite this the assay still performed well enough to distinguish between the different binding behaviours of the lectins. Therefore, as a first step screening method to determine heterogeneous surfaces of interest the unwashed particles performed satisfactorily.

3.3.9. Assay of heterogeneous 1-azido sugar coated 40nm gold nanoparticle library

Finally, the mannose-galactose heterogeneous library was screened as before, against the five lectins at a concentration of 0.1 mg.mL to 97ng.mL in order to observe the dose-dependent response. As this system is designed as a screening tool and we do not expect every sugar concentration to induce aggregation the aim was not to extract the dissociation constants (K_d). As such it does not matter if the full binding range has been covered. However, we can fit the resulting curves with a dose dependant response to extract an estimated K_d for the identification of potential inhibitors, the results of which are shown in Table 3.14, particles that did not show potential inhibition are not shown. Therefore, we have shown that this technique is suitable for the development of large scale, high throughput screening assays. The SPR values at 530nm are plotted versus log lectin concentration in Figures 3.45 to 3.49.

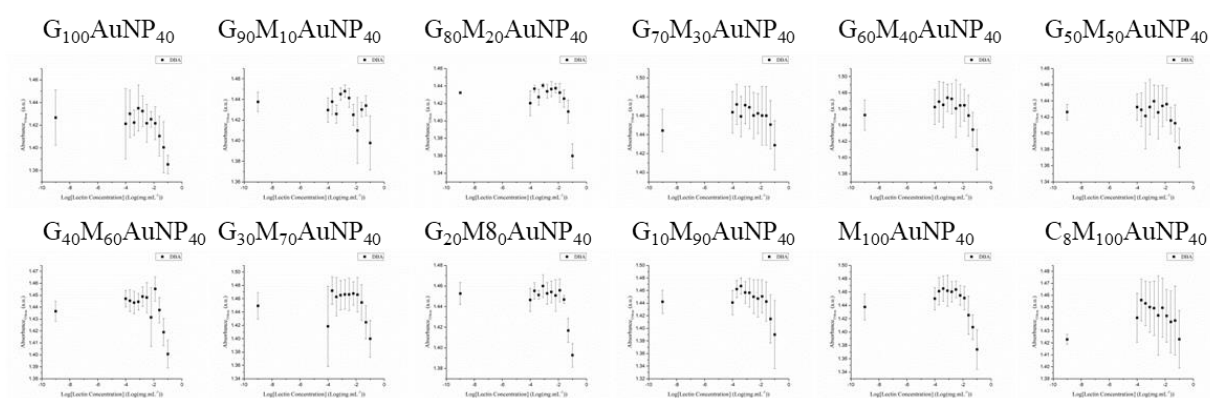


Figure 3.45: SPR absorbance value at 530nm plotted against log DBA concentration for the heterogeneous coated nanoparticles. Particles are labelled galactose percentage (G), mannose percentage (M), gold nanoparticle size (AuNP_{40nm}).

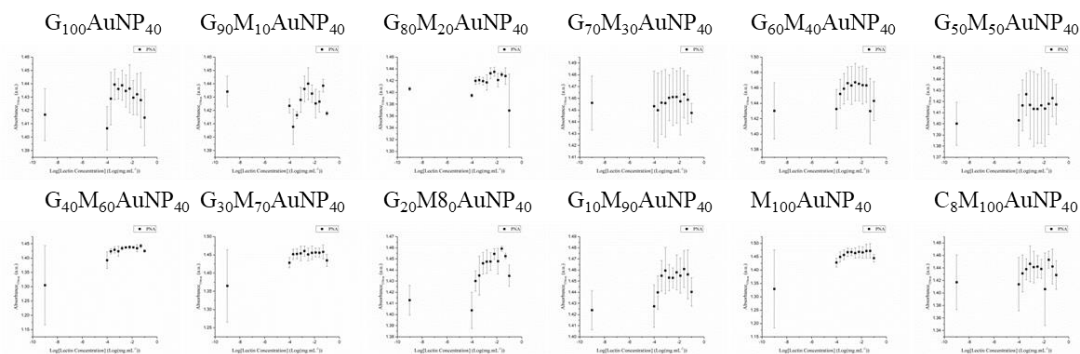


Figure 3.46: SPR absorbance value at 530nm plotted against log PNA concentration for the heterogeneous coated nanoparticles. Particles are labelled galactose percentage (G), mannose percentage (M), gold nanoparticle size (AuNP_{40nm}).

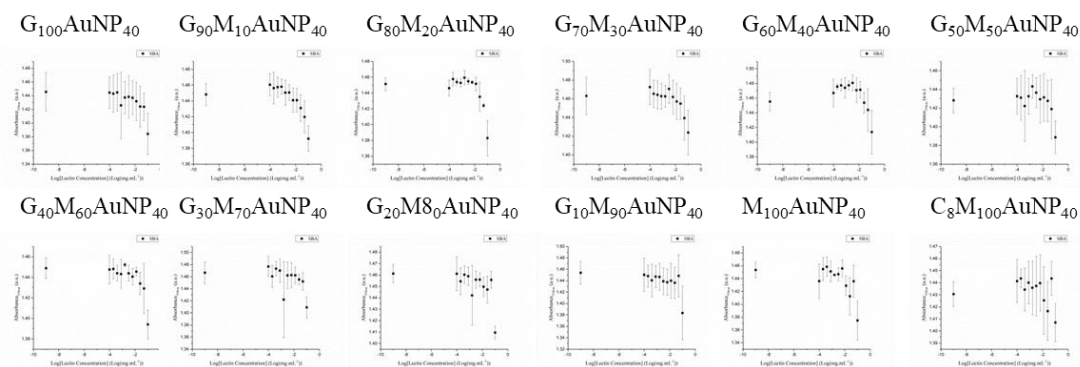


Figure 3.47: SPR absorbance value at 530nm plotted against log SBA concentration for the heterogeneous coated nanoparticles. Particles are labelled galactose percentage (G), mannose percentage (M), gold nanoparticle size (AuNP_{40nm}).

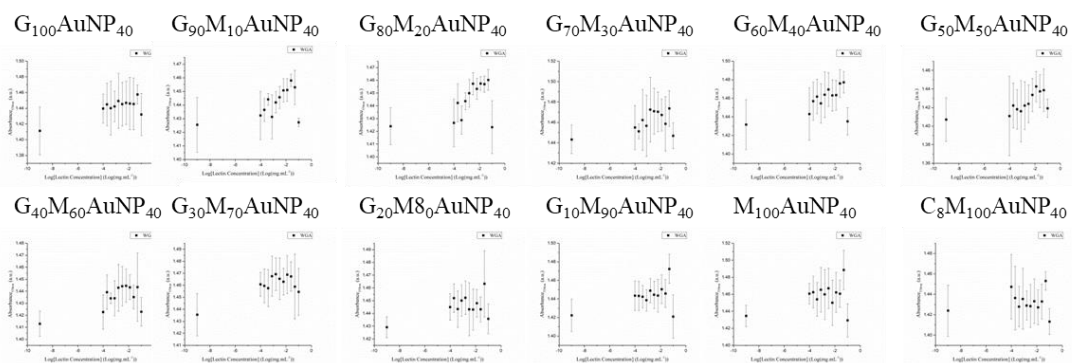


Figure 3.48: SPR absorbance value at 530nm plotted against log WGA concentration for the heterogeneous coated nanoparticles. Particles are labelled galactose percentage (G), mannose percentage (M), gold nanoparticle size (AuNP_{40nm}).

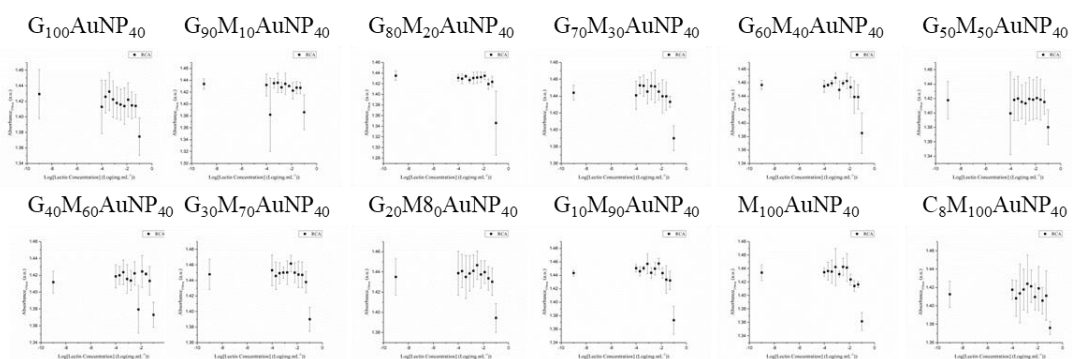


Figure 3.49: SPR absorbance value at 530nm plotted against log RCA concentration for the heterogeneous coated nanoparticles. Particles are labelled galactose percentage (G), mannose percentage (M), gold nanoparticle size (AuNP_{40nm}).

The lectins DBA, SBA and RCA all show improved binding towards nanoparticles with heterogeneous mixtures of galactose and mannose. DBA shows binding towards all nanoparticles regardless of composition, SBA has an increased avidity between 20 and 40% mannose density and RCA shows increased avidity towards particles containing 30% to 100% mannose, with the exception of the 50% mannose particle. The best activity was shown against DBA, the estimated K_d 's are shown in Figure 3.50.

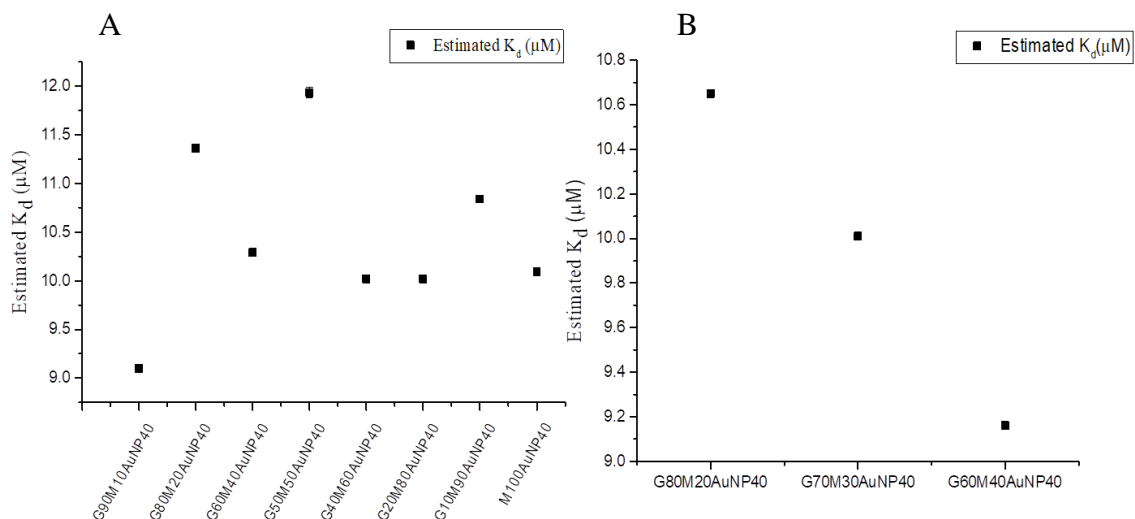


Figure 3.50: Estimated K_d 's for heterogeneous galactose-mannose particles against (A) DBA and (B) SBA. (K_d 's with error greater than 1SD removed).

As can be seen in Figure 3.50A, the particle that DBA had the highest affinity towards (lowest K_d) was G₉₀M₁₀Au₄₀, which has 10% mannose density. However all the mannose containing particles had improved affinity for DBA over the galactosylated particle. For SBA, affinity increased dramatically with increasing mannose density between 20 and 40% inclusion of mannose, Figure 3.50B while the other combinations didn't result in significant aggregation.

Table 3.14: Estimated K_d values extracted from fitting a dose-response curve. Particles that did not show potential inhibition are not shown. Estimated K_d is defined as the concentration of lectin predict to be at the midpoint of the dose dependent response curve.

Lectin	Sample	Estimated K_d (μM)	Error in Fitting
DBA	G ₁₀₀ AuNP ₄₀	9.91	54
DBA	G ₉₀ M ₁₀ AuNP ₄₀	9.10	0
DBA	G ₈₀ M ₂₀ AuNP ₄₀	11.36	1.57×10^{-3}
DBA	G ₇₀ M ₃₀ AuNP ₄₀	17.96	28.6
DBA	G ₆₀ M ₄₀ AuNP ₄₀	10.29	5.78×10^{-3}
DBA	G ₅₀ M ₅₀ AuNP ₄₀	11.93	5.38×10^{-2}
DBA	G ₄₀ M ₆₀ AuNP ₄₀	10.02	1.55×10^{-3}
DBA	G ₂₀ M ₈₀ AuNP ₄₀	10.02	6.33×10^{-4}
DBA	G ₁₀ M ₉₀ AuNP ₄₀	10.84	2.25×10^{-2}
DBA	M ₁₀₀ AuNP ₄₀	10.09	4.45×10^{-3}
SBA	G ₉₀ M ₁₀ AuNP ₄₀	223.74	10091.91
SBA	G ₈₀ M ₂₀ AuNP ₄₀	10.65	3.15×10^{-3}
SBA	G ₇₀ M ₃₀ AuNP ₄₀	10.01	9.84×10^{-3}
SBA	G ₆₀ M ₄₀ AuNP ₄₀	9.16	4.83×10^{-3}
SBA	G ₅₀ M ₅₀ AuNP ₄₀	17.09	20.6
SBA	G ₄₀ M ₆₀ AuNP ₄₀	15.09	4.49
RCA	G ₉₀ M ₁₀ AuNP ₄₀	8.33	0
RCA	G ₆₀ M ₄₀ AuNP ₄₀	1112.16	0
RCA	G ₄₀ M ₆₀ AuNP ₄₀	8.33	1.62×10^{10}

3.3.10. The role of the octyl-linker in the binding of mannosylated nanoparticles

The effect of the octyl linker on the binding with mannose is shown in Figure 3.51:

It is apparent that inclusion of the linker causes a decrease in the binding avidity towards the lectins compared to the mannose without linker. While none of the mannosylated particles have strong binding responses (as would be predicted by the stated binding targets for each

lectin) it is apparent that the presence of the linker substantially reduces the binding response and increases the error associated with the measurements. This is most likely due to the increased entropic cost associated with binding to a more flexible linker and the associated restriction in the degrees of freedom of the system. This highlights the importance to consider entropic effects when designing both inhibitors and sensor systems, and undermines any assumption that greater flexibility (to allow easier access to binding sites) leads to greater binding avidities. Instead, we must aim to develop methods that allow access to rigid scaffolds that match the target of interest. However, the use of generic systems to allow initial screening of a large number of ligands and proteins as presented here, will allow the identification of starting points for ligand synthesis that may not have been identified by traditional rational design.

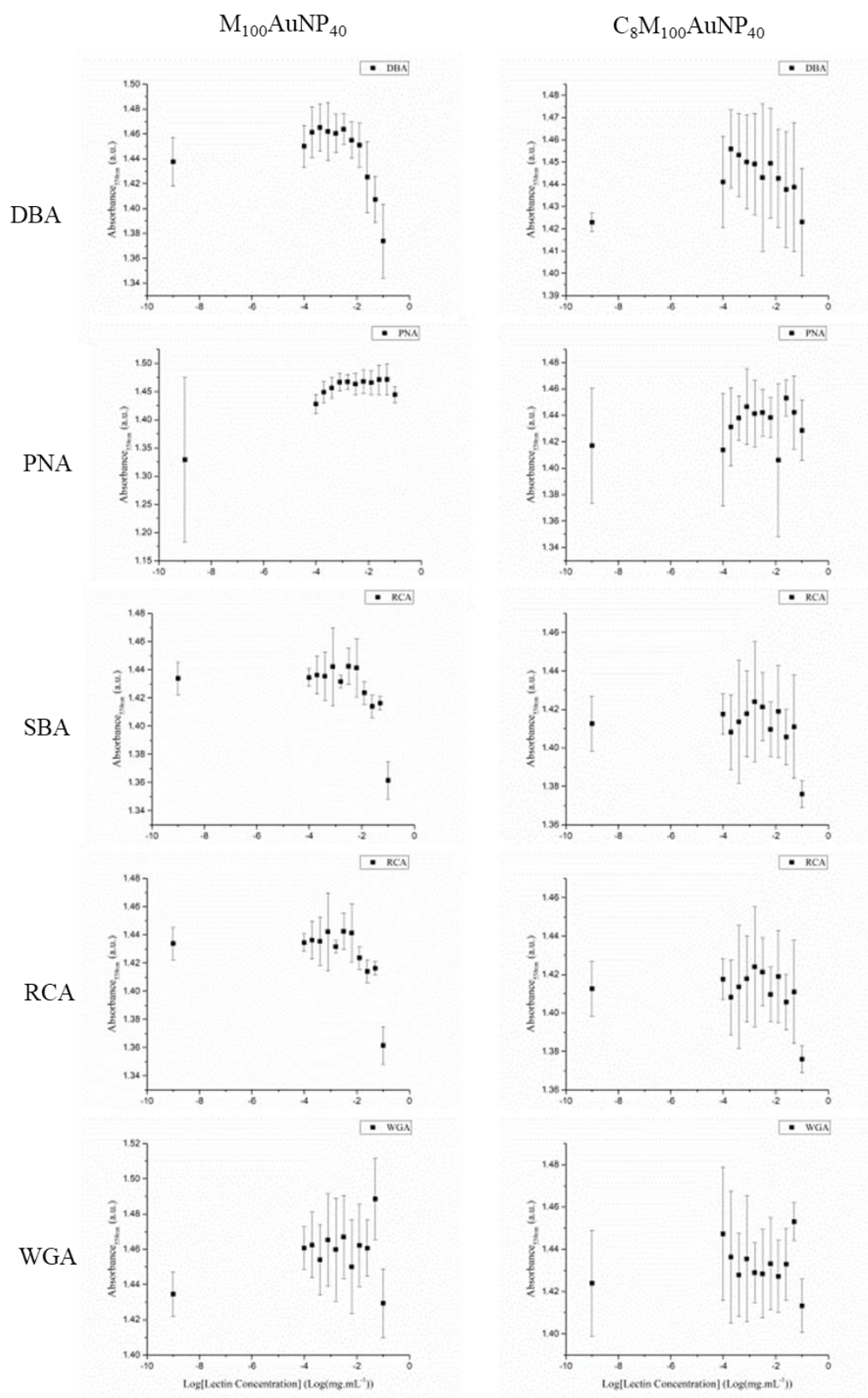


Figure 3.51 Binding curves for 100% mannosylated nanoparticles with and without octyl linker.

3.4. Conclusions and further work

We have shown the development of a high-throughput gold nanoparticle based, label free, screening system for the analysis of protein-carbohydrate interactions. The limit on the minimum concentration of gold was probed and determined to be at least $6.7 \times 10^{-11} \text{ Mol.L}^{-1}$. With this in mind, we investigated if multivalent binding effects could be used to out compete unreacted monosaccharides, and so reduce the need for purification steps. This is advantageous as it simplifies the synthesis and workflow, reduces the loss of gold due to purification, and, increases the applicability of this system to industrial, high-throughput use. It was shown that heterogeneous environments containing nominally non-binding sugar moieties can result in increased binding in a wide range of lectins, including in RCA₁₂₀, a possible chemical weapon. Furthermore it was shown that the inclusion of a flexible octyl linker between the sugar and polymer scaffold, resulted in reduced avidity, most likely due to the increase in entropic penalty that must be paid. These observations highlight the need to consider both the scaffold and binding ligand when developing inhibitors and biosensors. The use of large scale screening systems such as shown here may allow the identification of potentially effective inhibitors that may have unexpected structures and/or sugar compositions, as well as acting as a high through put method for the identification of unknown carbohydrate binding proteins.

To take this work further a greater number of lectins can be screened against, the role of different types of linker investigated and the work extended to probe more monosaccharides or more complex carbohydrates.

3.5. Experimental

3.5.1. Materials

2-Chloro-1,3-dimethylimidazolium chloride, and GM-1 Ganglioside was purchased from Carbosynth. D-(+)-Galactose was purchased from MP Biomedicals. D-(+)-Mannose, trimethylamine, sodium azide, pentafluorophenol, methacryloyl chloride, 2-cyano-2-propyl benzodithioate, 4,4'-azobis(4-cyanovaleric acid), 1,4-dioxane, dichloromethane, DBCO-amine, DMF, 2-aminoethan-1-ol, 2,6-lutidine 99% was purchased from Acros Organics. DBA, RCA, SBA, WGA and RCA₁₂₀ was purchased from Vector labs. Ultrapure milli Q water was obtained from a Merk Milli-Q water purifier at 18.2 MΩ.cm resistivity at 25 °C. 3500 MWCO 'snakeskin' dialysis tubing was purchased from Thermofisher (UK). Mannose-C8-N₃ obtained from Martin Lahmann. Galactose-amine coated gold nanoparticles obtained from Sarah Jane Richards.

3.5.2. Analytical methods

¹H, ¹³C NMR, and ¹⁹F spectra were recorded on Bruker HD-300, HD-400, and AV-500 spectrometers using deuterated solvents purchased from Sigma-Aldrich. Chemical shifts are reported relative to residual non-deuterated solvent. Mass spectrometry was performed on an Agilent 6130B single Quad (ESI). FTIR spectra were acquired using a Bruker Vector 22 FTIR spectrometer with a Golden Gate diamond attenuated total reflection cell. Raman spectra were collected on a Reinshaw inVia Reflex Raman using a 442 nm HeCd laser. Liquid handling was performed by Gilson Pipette Max. 96-well plates were read using a Biotech Synergy plate reader set at 25 °C. Uv-Vis spectra were obtained on an Agilent Cary spectrometer. DMF SEC was performed on a Varian 390-LC MDS system equipped with a PL-AS RT/MT autosampler, a PL-gel 3 μm (50 x 7.5 mm) guard column, two PL-gel 5 μm

(300 x 7.5 mm) mixed-D columns using DMF with 5 mM NH₄BF₄ at 50 °C as eluent at a flow rate of 1.0 mL.min⁻¹. The SEC system was equipped with ultraviolet (UV)/visible (set at 280 and 461 nm) and differential refractive index (DRI) detectors. Narrow molecular weight PMMA standard (200 – 1.0 x 10⁶ g.mol⁻¹) were used for calibration using a second order polynomial fit. TEM images were obtained on a JEOL 2000FX transmission electron microscope, 200 kV, LaB₆ instrument operated with a beam current of ~115 mA. Images were captured using a Gatan Orius 11 megapixel camera. Samples were prepared by deposition and drying of nanoparticle samples (10 µL of ethanol or water suspensions) onto formvar-coated 300 mesh copper Tem grids (Agar Scientific)

Assays

Lectin binding assay

For each gold sample in the library; 20 µL of each lectin made up in HEPES buffered saline solution was transferred by liquid handling robot to 3 separate wells of a 384-well micro-titre plate. The lectin was then serially diluted 11 times with HEPES buffer and a blank added to well 12. Next 10µL of gold sample was added to each well, and the plate incubated at 37°C for the duration of the assay. After incubation the plates were placed into an Agilent Cary spectrometer and full spectral scans from 400nm to 700nm were taken. This was repeated three times for each gold sample. The resulting scans were then normalised to the absorbance at 450nm and the mean absorbance value at the gold SPR peak of 530nm was recorded for each plate. Plots were then made using the mean and standard deviation of each plate mean.

Limit of detection assay

The concentration of SBA was fixed at 6.25x10⁻³ mg.mL⁻¹ in HEPES buffer. 20 µL of gold added to 384 microtitre plate and serially diluted 11 times and 12th well filled with blank.

Control with no lectin also plated. 10µL of Lectin was added and the plate incubated at 37 °C. UV-Vis spectra were taken at time-points T=30, 60 and 360 minutes. Gold concentration was calculated using Equation 3.2:

$$c = \frac{A_{450}}{\epsilon_{450} \times l} \quad 3.2.$$

Where A_{450} is the absorbance value at 450nm and experimentally determined. ϵ_{450} is the molar decadic extinction coefficient, taken from Haiss *et al.*³² ($4.92 \times 10^9 \text{ M}^{-1}\text{Cm}^{-1}$) and L is the path length, calculated to be 0.274 cm for 20 µl water in a 384 well plate.

Statistical determination of K_d Values

To determine the estimated K_d values the whole UV-Vis spectra were recorded on an Agilent Cary spectrometer and the data exported to a spreadsheet. Using the inbuilt spreadsheet functions the data was formatted to group sample's and repeats together. The data was then normalised to the absorption at 450nm. The average value and standard deviation of 530nm SPR peak was then calculated and the data transposed for exporting to origin.

3.5.3. Synthetic procedures

Synthesis of Azido-Monosaccharides

2-Chloro-1,3-dimethylimidazolium chloride (2.82 g, 16.7 mmol) was added to a solution of galactose/mannose (1.00 g, 5.6 mmol), trimethylamine (7.7 mL, 55 mmol) and sodium azide (3.61 g, 55.5 mmol) dissolved in ultrapure milli Q water (20 mL), sitting on ice. The solution was stirred for 40 minutes on ice before removing the solvent *in vacuo*. Ethanol (40 mL) was added to precipitate NaN₃, filtered, and the solvent removed (Repeat to ensure complete removal of NaN₃). The resulting solid was then dissolved in ultrapure milli Q water (10 mL) and washed three times with dichloromethane. The water layer was freeze dried to give a yellow solid. The product was then purified on a silica column using 5:1 chloroform: methanol (R_f = 0.3) to give an off-white product. Yield: 0.98 g 86%

1-Azido-1-deoxy-galactose

¹H NMR (MeOD) 400MHz, ppm: 5.57 (1H, d, J₁₋₂ = 4.40Hz, H1, α anomer 23.7%), 4.67 (1H, d, J₁₋₂ = 8.68Hz, H1, β anomer 76.3%), 3.96 (1H, d, J₁₋₂ = 3.30Hz, H5), 3.79-3.78 (1H, m, H4), 3.77-3.75 (2H, m, H6), 3.70 (1H, dd J₁₋₂ = 3.42, J₃₋₄ = 9.78Hz, H3) 3.53 (1H, t, J₁₋₂ = 9.78, H2)

¹³C NMR (MeOD) 75MHz, ppm: 90.55 (β C1), 89.44 (α C1) 77.21 (β C4), 75.88, 75.13, 74.23, 73.06, 72.64 (β C3), 71.20 70.32 (β C2), 69.19, 68.51(β C5), 68.20, 64.20, 63.46, 61.17, 60.94 (β C6)

MS (ESI +): Observed: 228.00 Expected: 228.17 [M+Na]⁺

IR: 2107cm⁻¹ (-N₃)

1-Azido-1-deoxy-mannose

^1H NMR (MeOD) 400MHz, ppm: 5.46 (1H,d, $J_{1-2} = 1.71$ Hz, alpha 100%) 3.92 (1H, d, $J=10.27$ Hz) 3.86 (1H, dd, $J_{1-2} = 1.96$, $J_{3-4} = 3.18$ Hz, H^2) 3.78, (2H, m) 3.75-3.72 (2H, m), 3.64 (1H, t, $J_{1-2} = 9.54$ Hz)

^{13}C NMR (MeOD) 75MHz, ppm: Major Anomer (100%): 90.57 (C1), 78.47 (C5), 70.36 (C2), 70.37 (C3), 66.60 (C4), 61.10(C6)

Mass Spec: Observed: 228.00 Expected: 228.17 $[\text{M}+\text{Na}]^+$

IR: 2107cm^{-1} ($-\text{N}_3$)

Synthesis of perfluorophenyl 2-(((dodecylthio)carbonothioyl)thio)-2-methylpropanoate (DMPPFP)

DMPPFP was synthesised using a method similar to that already reported^{40,41}. First 2-(dodecylthiocarbonothioylthio)-2-methylpropanoic acid (DMP) was synthesised as below. Dodecane thiol (4.00 g, 19.76 mmol) was added dropwise to a stirring suspension of K_3PO_4 (4.20g, 19.76 mmol) in acetone (60 mL) over 25 minutes. CS_2 (4.10 g, 53.85 mmol) was added and the solution turned bright yellow. After ten minutes 2-bromo-2-methylpropionic acid (3.00 g, 17.96 mmol) was added and KBr precipitation was observed. After stirring for 16 hours, the solvent was removed by rotary evaporation and the residue was extracted into Dichloromethane (DCM) (2 x 200 mL) from 1M HCl (200 mL). The organic extracts were washed with water (200 mL) and brine (200 mL) and further dried over MgSO_4 . The solvent was removed under reduced pressure and recrystallized from Hexane to give DMP as a bright yellow solid (3.71g, 56 %).

^1H NMR (400MHz): δ ppm: 3.26 (2H, t, $J_{12-11} = 7.16$ Hz, H12); 1.72 (6H, s, H13); 1.65(2H, m, Hz, H11); 1.63 (2H, m, H10); 1.56 (16H, m, H2-9); 0.86 (3H, t, $J_{1-2} = 6.03$ Hz, H1).

IR cm^{-1} : 2955 (alkyl-H stretch); 1712 (C=O stretch); 1066 (S-(C=S)-S stretch)

MS m/z (ESI-POS): 365 (M+H)

Following this DMPPFP was synthesised. DMP (3.7g, 10.13mmol), EDC HCl (2.91g, 15.20mmol), DMAP (1.86g, 15.20mmol) and 80.0mL of DCM were placed in a one-neck round bottom flask and sealed. The solution was stirred for 10 min under nitrogen atmosphere before Pentafluorophenol (PFP) (6.06g, 3.93mmol) dissolved in DCM was added via syringe, and then, stirred for overnight at RT. After that, the solution was washed in sequence with 3M HCl, 1M NaHCO_3 and 0.5 M NaCl aqueous solutions. The organic layer was dried with anhydrous MgSO_4 . The solvent was removed by rotary evaporation under vacuum to generate the product as a dark yellow viscous liquid (4.62g, 86.3%)

^1H NMR (400MHz): δ ppm: 3.26 (2H, t, $J_{12-11} = 7.16$ Hz, H12); 1.72 (6H, s, H13); 1.65(2H, m, Hz, H11); 1.63 (2H, m, H10); 1.56 (16H, m, H2-9); 0.86 (3H, t, $J_{1-2} = 6.03$ Hz, H1).

IR (cm^{-1}): 2955 (alkyl-H stretch); 1712 (C=O stretch); 1066 (S-(C=S)-S stretch) 1176 (C-F Stretch)

MS m/z (ESI-POS): 531 (M+H)

Synthesis of p(hydroxyethyl acrylamide) pentafluorophenol ester

HEAA (0.5g, 4.34mmol, 25eq) plus varied amounts of DMPPFP (1eq) and 4,4'-Azobis(4-cyanovaleric acid) (AVCA) as the initiator (0.5eq) were placed into a glass vial with 4.0mL of a 1:1 mix of Toluene and Methanol. 200 μ L of mesitylene as an internal NMR standard was added. A sample for NMR is taken and dissolved in deuterated chloroform. The glass vial was then sealed and degassed using N₂ for 30 minutes. Following this the reaction mixture is heated to 70 °C for 90 minutes at which time the reaction is quenched by exposure to air followed by cooling in liquid N₂. An NMR sample of the crude mix is made up in deuterated Methanol and the mixture is precipitated into Diethyl Ether from Methanol three times to give a yellow solid. Average: 92% conversion. \bar{D} =1.18

¹H NMR (MeOD) 300MHz, ppm: 3.65 (br, NH-CH₂-CH₂-), 3.28 (br, -NH-CH₂-CH₂-), 2.5-1.5 (br, Backbone CH₂)

¹⁹F NMR (CDCl₃) 376MHz, ppm: -150.35 (1F, br s), -151.44 (1F, br s), -156.97 (1F, br s), -162.11 (1F, br s)

Synthesis of p(hydroxyethyl acrylamide) dibenzocyclooctyne amide

Poly(HEAA) (1 eq), DBCO (10mg, 36.2 μ M, 1.05eq) and Triethylamine (TEA) (2eqs) are dissolved in 2 mL of deuterated methanol. The reaction mixture is then heated to 50°C for 16 hours. The solution is then concentrated to approximately 0.5mL and submitted for F19 NMR. Following this the mixture is diluted to 20mL of distilled H₂O and dialysed using dialysis tubing with an appropriate molecular weight cut off. The sample was then freeze-dried to afford the final product as a white powder, yield ~69%

¹H NMR (MeOD) 300MHz, ppm: 7.5-7.0 (br, Benzyl) 4.42 (br, cyclooctyne ring CH₂) 3.65 (br, NH-CH₂-CH₂-), 3.28 (br, -NH-CH₂-CH₂-), 2.5-1.5 (br, Backbone CH₂)

^{19}F NMR indicated no presence of fluorine left in sample

Raman (cm^{-1}): 1600 (Aromatic C-C) and 2159 (Alkyne)

Synthesis of Gold nanoparticles by one pot growth

Gold nanoparticles were synthesised using the citrate reduction method first proposed by Turkevich.³¹ The size of the nanoparticles can be tuned by varying the ratio of gold to citrate as shown by Frens.⁴² $\text{HAuCl}_4 \cdot 3\text{H}_2\text{O}$ (10mg, 1eq) is dissolved in 35mL of deionised water which is then heated to boiling. Following this trisodium citrate dehydrate (14.95mg, 2eqs) in 2ml of deionised water are added in one portion and the temperature maintained for 30 minutes. After ten minutes a deep red colour is observed. After 30 minutes the solution is allowed to cool slowly. To wash the Au NPs the solution is centrifuged at 3000g for 15 minutes, the supernatant decanted and the particles re-suspended in deionised water.

DLS: 32 ± 0.2 nm

UV-Vis: 32nm

TEM: 19.2 ± 7.6 nm

Synthesis of Gold nanoparticles by step growth

The 40nm gold nanoparticles used later in this work were synthesised using a step growth procedure described by Bastús *et al.*³⁷ Care must be taken to ensure extremely clean glassware and accurate temperature control throughout the synthesis.

A 25 mM stock solution of HAuCl_4 and a 60 mM stock of sodium citrate were prepared. 150 mL of 2.2 mM sodium citrate was brought to 100 °C in a three necked RBF, and 1 mL of stock HAuCl_4 solution was injected, to generate gold seeds of approximately 10nm in size at a concentration of $\sim 3 \times 10^{12}$ nanoparticles per mL. The solution immediately turns grey-blue

and deepens to a bright wine red colour over the course of approximately 5 minutes. This is labelled generation 0. The solution was then cooled to 90 °C and a further 1 mL of stock H_{Au}Cl₄ solution added. After 30 minutes nanoparticle growth for this step is finished. Another 1 mL of stock H_{Au}Cl₄ is added. After 30 minutes the sample is diluted by removing 55 mL of sample (used for analysis) and 53 mL of milli Q water and 2 mL of 60 mM sodium citrate (N.B. Keep both milli Q water and sodium citrate stock warmed at 90 °C to prevent temperature changes on addition). This solution is now generation 1 and the process is repeated until the desired gold nanoparticle size is achieved. Bastús *et al.* report successful synthesis of gold nanoparticles up to 180nm in size with this method.

Recorded nanoparticle step sizes using UV-Vis:

Step 1: 12nm

Step 2: 32nm

Step 3: 40nm

Gold Nanoparticle Coating with DBCO-HEAA Polymer

Gold nanoparticles were coated with polymer at a concentration of $1\text{mg}\cdot\text{mL}^{-1}$ polymer. 1.5 mL of stock gold nanoparticle solution was taken and 1.5 mg of DBCO-pHEAA₂₅ polymer was added. The reaction was allowed to proceed for 30 minutes at room temperature. The gold nanoparticles were washed three times by centrifugation at $3,000 \times g$ for 30 minutes before being re-suspended in 2 mL deionised water.

Appending Azido-Sugars to DBCO-HEAA Coated Gold Nanoparticles

A five times excess of sugar is used. A stock solution of each sugar was made up with 6.66mg ($32\mu\text{M}$) of sugars in 16.65 mL of deionised water. The Coated AuNPs were centrifuged at $3,000g$ for 30 minutes and 1.5 mL of water was removed. The stock sugar solutions were combined in 100:0,80:20,60:40,40:60,20:80 and 0:100 volume ratios to give a final volume of 1.5 mL, added to the centrifuged gold and left at room temperature overnight. The gold nanoparticles were then washed three times by centrifugation at 10,000rpm for 30 minutes before being re-suspended in 2 mL deionised water. For later work this washing step was removed, as discussed in the main text above. Characterisation shown in table 3.7, reproduced below.

Gold Coating	Size ^(a) (nm)	Size ^(b) (nm)	Size ^(c) (nm)	Zeta Potential ^(d) (mV)
Citrate	40	55 ± 3.3	34.9 ± 6.7	-38.1 ± 1.0
DBCO-HEAA	62	76 ± 0.9	N/A	-21.1 ± 0.1
Gal-HEAA	62	76 ± 3.5	N/A	-19.7 ± 0.6

(a) UV-Vis (b) Dynamic Light Scattering (c) TEM (n=160) (d) Measured in milliQ water at pH=7.4

3.6. References

- 1 A. Varki and J. B. Lowe, *Biological Roles of Glycans*, Cold Spring Harbor Laboratory Press, 2009.
- 2 Y.-Y. Zhao, M. Takahashi, J.-G. Gu, E. Miyoshi, A. Matsumoto, S. Kitazume and N. Taniguchi, *Cancer Sci.*, 2008, **99**, 1304–1310.
- 3 K. Ohtsubo and J. D. Marth, *Cell*, 2006, **126**, 855–867.
- 4 A. P. Moran, A. Gupta and L. Joshi, *Gut*, 2011, **60**, 1412–1425.
- 5 M. M. Fuster and J. D. Esko, *Nat. Rev. Cancer*, 2005, **5**, 526–542.
- 6 D. H. Dube and C. R. Bertozzi, *Nat. Rev. Drug Discov.*, 2005, **4**, 477–488.
- 7 K. S. Lau and J. W. Dennis, *Glycobiology*, 2008, **18**, 750–760.
- 8 Y. Kaneko, F. Nimmerjahn and J. V. Ravetch, *Science.*, 2006, **313**, 670–673.
- 9 J. Nicolas, E. Khoshdel, D. M. Haddleton, C. Peinado, S. Kelly, E. Fitzpatrick, S. D. Carrington, D. Brayden and D. M. Haddleton, *Chem. Commun.*, 2007, **553**, 1722.
- 10 Y. C. Lee and R. T. Lee, *Acc. Chem. Res.*, 1995, **28**, 321–327.
- 11 J. J. Lundquist and E. J. Toone, *Chem. Rev.*, 2002, **102**, 555–578.
- 12 P. I. Kitov, J. M. Sadowska, G. Mulvey, G. D. Armstrong, H. Ling, N. S. Pannu, R. J. Read and D. R. Bundle, *Nature*, 2000, **403**, 669–72.
- 13 T. K. Dam and C. F. Brewer, *Glycobiology*, 2010, **20**, 270–279.
- 14 D. Ponader, P. Maffre, J. Aretz, D. Pussak, N. M. Ninnemann, S. Schmidt, P. H. Seeberger, C. Rademacher, G. U. Nienhaus and L. Hartmann, *J. Am. Chem. Soc.*,

- 2014, **136**, 2008–2016.
- 15 M. I. Gibson, M. Danial and H.-A. Klok, *ACS Comb. Sci.*, 2011, **13**, 286–97.
- 16 G. J. Nusz, S. M. Marinakos, A. C. Curry, A. Dahlin, F. Höök, A. Wax and A. Chilkoti, *Anal. Chem.*, 2008, **80**, 984–989.
- 17 A. L. Parry, N. A. Clemson, J. Ellis, S. S. R. Bernhard, B. G. Davis and N. R. Cameron, *J. Am. Chem. Soc.*, 2013, **135**, 9362–9365.
- 18 S.-J. Richards, E. Fullam, G. S. Besra and M. I. Gibson, *J. Mater. Chem. B*, 2014, **2**, 1490–1498.
- 19 R. Elghanian, J. J. Storhoff, R. C. Mucic, R. L. Letsinger and C. A. Mirkin, *Science*, 1997, **277**, 1078–81.
- 20 M. Holzinger, A. Le Goff and S. Cosnier, *Front. Chem.*, 2014, **2**, 63.
- 21 S.-J. Richards, L. Otten and M. I. Gibson, *J. Mater. Chem. B*, 2016, **4**, 3046–3053.
- 22 P. Yager, G. J. Domingo and J. Gerdes, *Annu. Rev. Biomed. Eng.*, 2008, **10**, 107–144.
- 23 S.-J. Richards and M. I. Gibson, *ACS Macro Lett.*, 2014, **3**, 1004–1008.
- 24 A. K. Yetisen, J. L. Martinez-Hurtado, A. Garcia-Melendrez, F. Da Cruz Vasconcellos and C. R. Lowe, *Sensors Actuators B. Chem.*, 2014, **196**, 156–160.
- 25 S. K. Vashist, O. Mudanyali, E. M. Schneider, R. Zengerle and A. Ozcan, *Anal. Bioanal. Chem.*, 2014, **406**, 3263–77.
- 26 L. Shen, J. A. Hagen and I. Papautsky, *Lab Chip*, 2012, **12**, 4240.
- 27 Q. Wang, T. R. Chan, R. Hilgraf, V. V. Fokin, K. B. Sharpless and M. G. Finn, *J. Am. Chem. Soc.*, 2003, **125**, 3192–3193.

- 28 M. Gómez-García, J. M. Benito, A. P. Butera, C. Ortiz Mellet, J. M. García Fernández and J. L. Jiménez Blanco, *J. Org. Chem.*, 2012, **77**, 1273–88.
- 29 S.-J. Richards and M. I. Gibson, *ACS Macro Lett.*, 2014, **3**, 1004–1008.
- 30 D. J. Phillips, J. P. Patterson, R. K. O'Reilly and M. I. Gibson, *Polym. Chem.*, 2014, **5**, 126–131.
- 31 J. Turkevich, P. C. Stevenson and J. Hillier, *Discuss. Faraday Soc.*, 1951, **11**, 55.
- 32 W. Haiss, N. T. K. Thanh, J. Aveyard and D. G. Fernig, *Anal. Chem.*, 2007, **79**, 4215–21.
- 33 T. J. Collins, *Biotechniques*, 2007, **43**, 25–30.
- 34 N. Vinson, Y. Gou, C. R. Becer, D. M. Haddleton and M. I. Gibson, *Polym. Chem.*, 2011, **2**, 107–113.
- 35 K. Sakurai, Y. Hatai and A. Okada, *Chem. Sci.*, 2016, **7**, 702–706.
- 36 Rockefeller Institute for Medical Research. and American Society for Biochemistry and Molecular Biology., *The Journal of biological chemistry*, 1955, **214**, 839-852
- 37 N. G. Bastús, J. Comenge and V. Puentes, *Langmuir*, 2011, **27**, 11098–11105.
- 38 Z. Zhang, S. Maji, A. B. da F. Antunes, R. De Rycke, Q. Zhang, R. Hoogenboom and B. G. De Geest, *Chem. Mater.*, 2013, **25**, 4297–4303.
- 39 M. Mammen, S.-K. Choi and G. M. Whitesides, *Angew. Chemie Int. Ed.*, 1998, **37**, 2754–2794.
- 40 D. J. Phillips and M. I. Gibson, *Biomacromolecules*, 2012, **13**, 3200–8.
- 41 Z. Liu, J. Hu, J. Sun and G. Liu, *J. Polym. Sci. Part A Polym. Chem.*, 2010, **48**, 4922–

4928.

42 G. FRENS, *Nature*, 1973, **241**, 20–22.

Chapter Four

Remodelling Cell Surfaces with Synthetic Polymers by Tandem Glycan Metabolic Labelling and Copper-Free Click Conjugation

Declarations

The work submitted in this chapter was performed by myself, except for Cell culture experiments which were performed with assistance from Trisha Bailey, Gibson Group, University of Warwick. Trisha Bailey performed maintenance of the cell line, cytotoxicity assays and initial plating of cells. I performed the addition of the metabolic labelling reagents, washing, analysis and imaging.

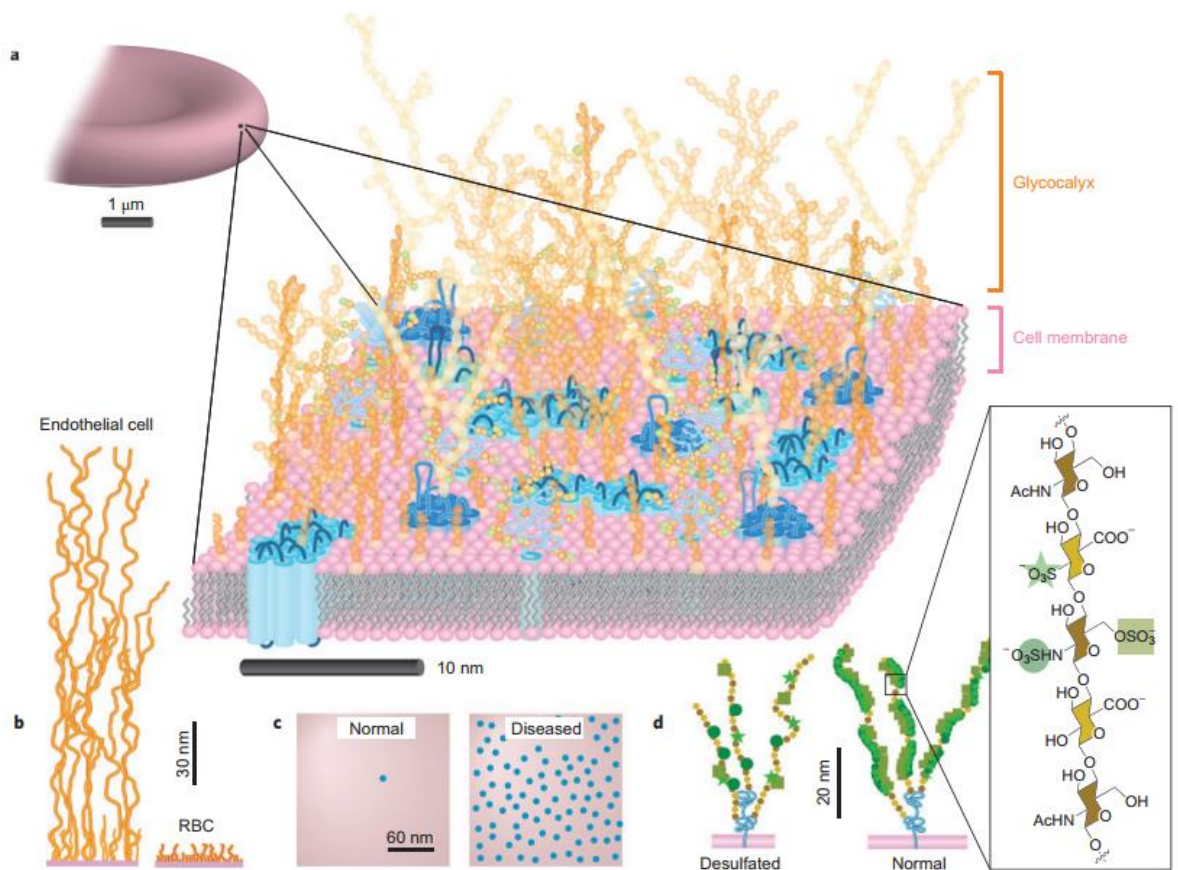
4.1. Abstract

Cell surfaces are coated with a dense layer of glycoproteins, glycans and glycolipids which constitute the glycocalyx. The glycocalyx directs cell-cell communication, is the first site of adhesion for pathogens, and defects are associated with cellular dysfunction. Chemical modifications to 'remodel' the glycocalyx are an essential tool to investigate its function, or as a scaffold for modifying cell surfaces for biotechnological or medical applications. As carbohydrates are a post-translational modification, genetic techniques to achieve this are rare, and challenging. Here we make use of the metabolic processing of azido-monosaccharides into cell surface azido *O*-linked glycans and azido-sialic acid residues and

'hijack' the systems to introduce azides onto the cell surface. These azides act as a bio-orthogonal handle to enable synthetic polymers to be grafted to the surface to chemically remodel the glycocalyx, providing a versatile tool to control this complex interface.

4.2. Introduction

Cell surfaces are multifunctional dynamic environments that provide vital communication pathways within the body. The cell surface assists in intracellular communication,¹ (non)self-recognition for the immune system,²⁻⁴ inflammation^{5,6} and more. The surface of the cell itself is a highly dynamic, consisting of lipids, proteins and carbohydrates, at various length scales and with diverse functionalities. Figure 4.1 shows a depiction of a cell surface.⁷



Reprinted by permission from Macmillan Publishers Ltd: Nature Chemistry⁷ copyright 2011.

Figure 4.1: (A) A representation of the cell surface showing the lipid membrane in pink, important proteins in blue and the glycocalyx in orange. Heterogeneity in the lipid membrane has been ignored for simplicity (B) Relative size of the glycocalyx. (C) Schematic of the over expression of HER2 protein in cancerous cells vs healthy cells.⁸ (D) Examples of the chemical modifications which the carbohydrates of the glycocalyx can undergo.

The glycocalyx of the cell surface is the outermost component, attached to the cell membrane and is therefore the first component of the cell encountered by external agents. Figure 4.1B demonstrates the relative sizes of the glycocalyx for an endothelial cell (more than 200 nm) and red blood cell (10 nm), demonstrating the vast difference in physical size the glycocalyx can exhibit depending on cell type. The cell surface also indicates the underlying cell physiology.^{4,9-14} Cancerous tissues exhibit modified cell surfaces,⁸ such as the overexpression

of HER2 protein as shown in Figure 4.1C, which can cover more than 15% of the surface area of the cell in cancerous tissue. Other modifications include the over-expression of sialic acid residues. In fact, hyper-silyation has been noted to confer increased resistance to chemo- and radio-therapy techniques in cancerous tissues, aids in immune evasion by the tumour decreasing the effectiveness of immunotherapy¹⁵ (such as Herceptin[®] to target HER2 overexpression) and is linked to poor prognosis.¹⁶ In addition, alternative strategies to common antibiotics, such as anti-adhesion therapy, offer a method to tackle the growing antibiotic resistance problem.^{17,18} To fully exploit anti-adhesion as a viable treatment option, the interaction of cell surfaces must be well characterised and understood. Therefore it will be necessary to develop new methods of probing these environments.

The ability to add abiotic functionality to the cell surface offers the chance to more effectively monitor the interactions taking place and the effect of any added external stimuli. Furthermore, the ability to structurally engineer the cell surface allows the introduction of a greater range of functionality to an already highly functional surface. This allows the creation of hybrid cells that can perform functions that differ greatly from their original intention, for use in tissue engineering,¹⁹ microelectronics fabrication,²⁰ and as biosensors.^{21,22}

One way of directly observing the glycosylation state of cells is metabolic glycan labelling. Developed by Bertozzi and co-workers,^{23,24,24-31} glycan labelling exploits intracellular biosynthetic pathways to re-engineer glycans. The sialic acid metabolic pathway from *N*-acetylmannosamine is very tolerant to modifications at the *N*-acetyl group enabling bulky substituents to be carried through all the way to sialic acid. As long as the chemical moiety used to tag the sugar is small it will be tolerated by the metabolic pathway and incorporated into glycans as if it were the native sugar. Wong *et al.* demonstrated that side chains up to 5 atoms long are tolerated by the sialic acid pathway of mannosamine.³² Several metabolic

pathways are open to investigation in this manner: *N*-acetylmannosamine, *N*-acetylglucosamine, *N*-acetylgalactosamine and the fucosylation pathway.

In particular the *N*-acetylgalactosamine (GalNAc) salvage pathway is of interest as it allows access to *O*-linked glycans. The two main forms of glycosylation of proteins are *N*-linked and *O*-linked glycans. *N*-linked glycans are attached to asparagine residues and are produced by the action of a single enzyme, oligosaccharyl transferase, that recognises a particular amino acid sequence (asparagine-X-serine/threonine, where X≠proline). This means that *N*-linked glycans can be predicted based upon analysis of the protein sequences and coupled with techniques like mutagenesis. *O*-linked glycans on the other hand, are attached through serine or threonine residues and are installed by a collection of transferases found within the Golgi apparatus of the cell. They are of interest as *O*-linked glycoproteins play an important role in several biological processes and disease states, including the Ebola glycoprotein required for the cytotoxicity of Ebola,^{33,34} the MUC1 tumor antigen present in the altered glycans of cancer cells,^{35,36} and the development of Alzheimer's disease.^{37,38}

By introducing the unnatural sugar of *N*-azidoacetylgalactosamine (GalNAz) into the *N*-acetylgalactosamine salvage pathway, Figure 4.2A, followed by the addition of an azide reactive probe such as an alkyne or Staudinger reagent, Figure 4.2B, direct conjugation to the glycocalyx can be achieved. This method has been utilised by Bertozzi *et al.*, to label and isolate *O*-linked glycosylated mucin-type proteins in Jurkat cells, separating them from other GalNAc metabolite products such as glycosphingolipids and chondroitin sulfate proteoglycans.³⁹ The technique has also been used less specifically to observe the evolution of glycans in developing zebra fish with fluorescent probes.⁴⁰⁻⁴³ It is possible for GalNAz to be epimerised into ManNAz *via* UDP-GlcNAc 2-epimerase and GlcNAc 2-epimerase enzymes, where upon ManNAz is incorporated into the terminal sialic acid residues of the glycocalyx.³⁹

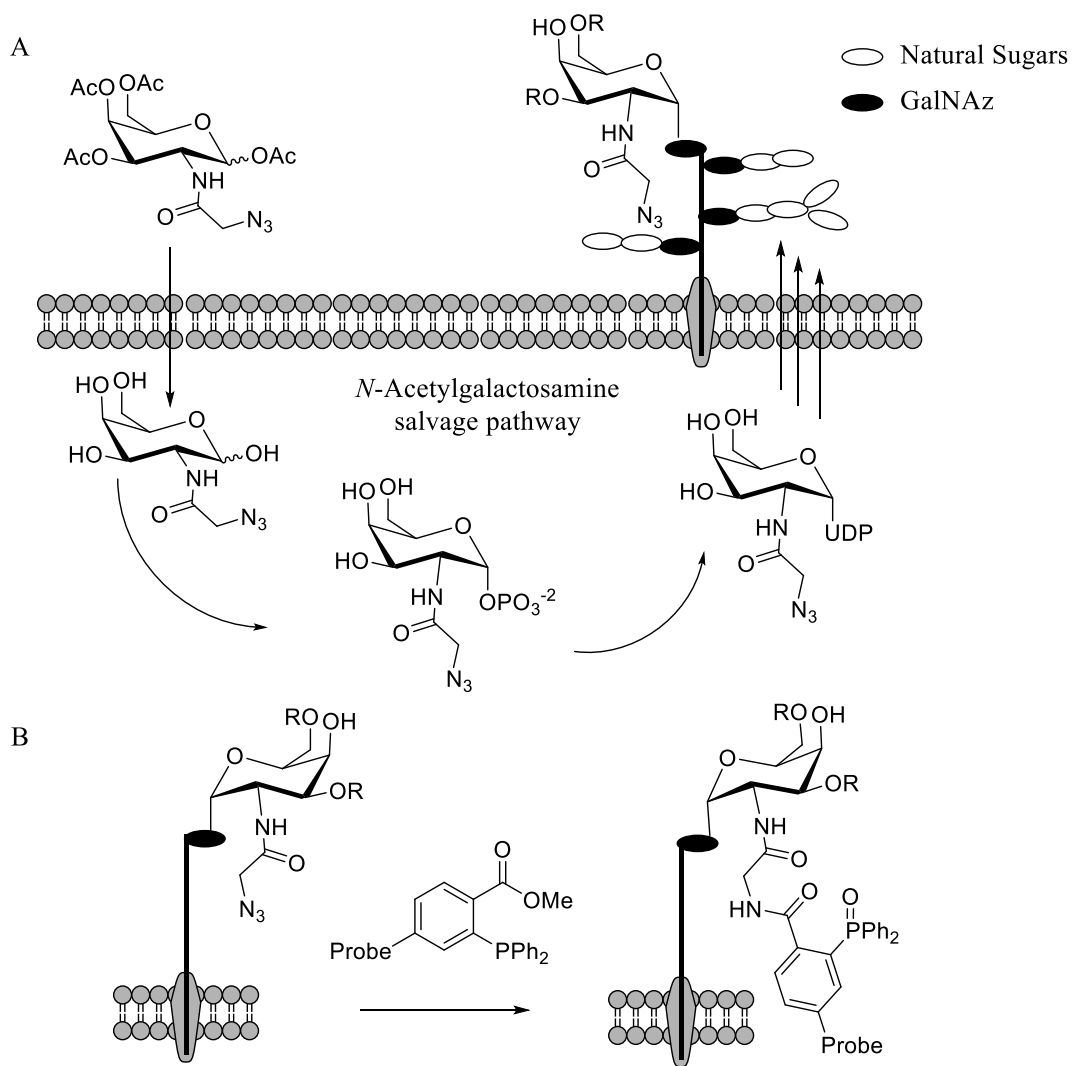
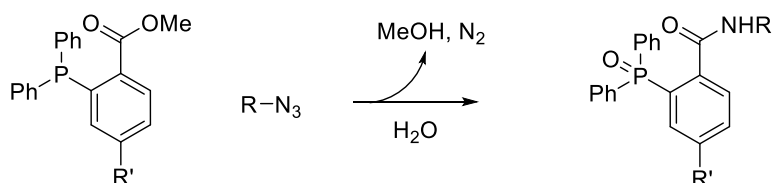


Figure 4.2: (A) Labelling the *N*-acetylgalactosamine salvage pathway with unnatural GalNAz (B) Introducing a probe to the labelled *O*-glycosylated proteins using the Staudinger ligation.

So far two main glycan labelling systems have been developed, the Staudinger Ligation,⁴⁴ Figure 4.3A and Copper-free alkyne-azide cycloaddition,⁴⁵ Figure 4.3B.

A

Staudinger Ligation



B

Strain promoted [3+2] Cycloaddition AKA Copper-free azide alkyne coupling

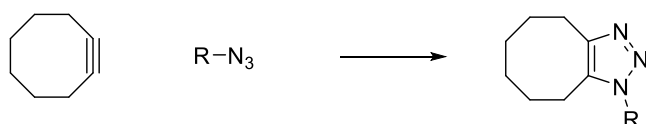


Figure 4.3: Bio-orthogonal reagents for metabolic labelling.

Both fulfil the requirements of a bio-orthogonal probe, they are non-toxic reagents that react selectively to produce chemically and biologically-inert products. However, the rate of reaction for the Staudinger ligation is too low compared to the rate at which the phenylphosphine based reagent is cleared from the body to give a good signal to noise ratio.⁴⁶

Bertozzi *et al.* developed cyclooctyne reagents to remove the need for toxic copper and allow the azide-alkyne coupling to occur *in vivo*.^{45,47-56} However, there are currently very few water-soluble cyclooctyne reagents available,⁵⁵ resulting in the need to use DMSO, and precluding their use in animals, including humans. Conjugating the cyclooctyne reagents to water soluble polymers might overcome this and have the benefit of improved

pharmacokinetics. One commercially available reagent is dibenzocyclooctyne (DBCO), see Figure 4.4, which has a comparable reaction rate to the fastest reported cyclooctyne reagent.⁵²

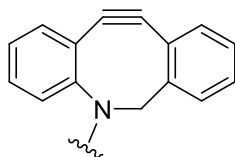
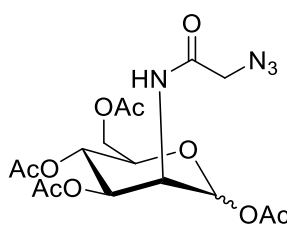
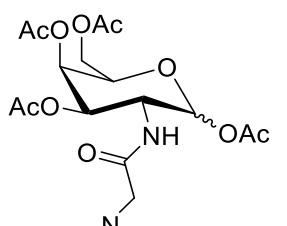
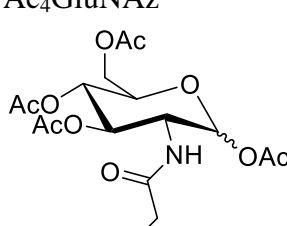
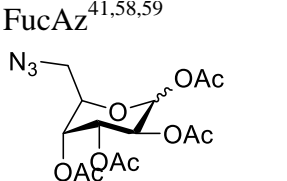
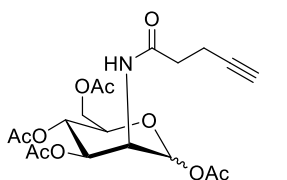


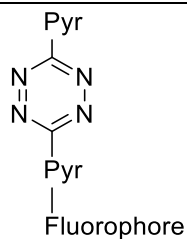
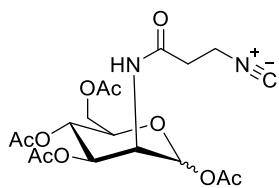
Figure 4.4: Dibenzocyclooctyne (DBCO).

Various other sugar modifications and bio-orthogonal reactions have been developed in recent years, an overview of which are shown below in Table 4.1.

Table 4.1: Summary of some of the unnatural sugars and probes used for metabolic glycan labelling.

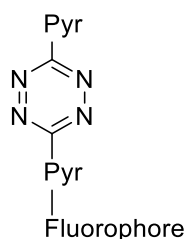
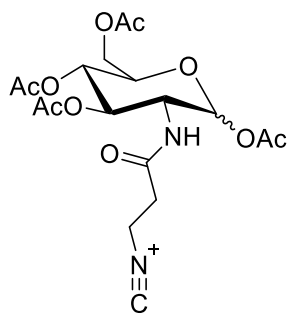
Label	Probe	Target
$\text{Ac}_4\text{ManNAz}^{57}$ 	Staudinger Ligation Cu-catalysed Alkyne Azide coupling Strain promoted Alkyne Azide coupling	Sialic Acids
$\text{Ac}_4\text{GalNAz}^{57}$ 	Staudinger Ligation Cu-catalysed Alkyne Azide coupling Strain promoted Alkyne Azide coupling	<i>O</i> -linked Glycans
$\text{Ac}_4\text{GluNAz}^{57}$ 	Staudinger Ligation Cu-catalysed Alkyne Azide coupling Strain promoted Alkyne Azide coupling	<i>N</i> -linked Glycans
$\text{FucAZ}^{41,58,59}$ 	Staudinger Ligation Cu-catalysed alkyne azide coupling Strain promoted alkyne azide coupling	Fucose salvage pathway
$\text{Ac}_4\text{ManNAI}^{32,60}$ 	Cu-catalysed alkyne azide coupling with biotin-azide	Sialic Acids

Nitrile Mannosamine⁶¹



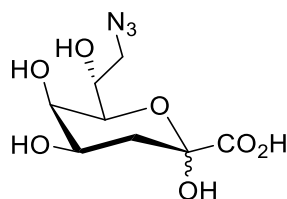
Sialic Acid
Pathway

Nitrile Glucosamine⁶¹



N-Linked
Glycans

3-deoxy-D-manno-
octulosonic acid⁵⁷

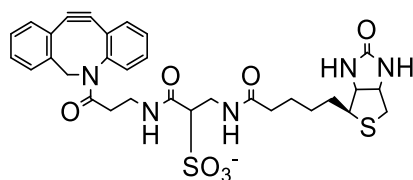
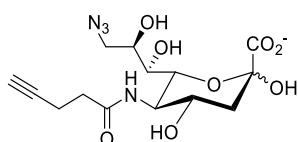


Cu-Catalysed Azide-Alkyne
coupling with Alkyne-
Alexafluor488

Labelling of gram
negative bacterial
membranes

Bifunctional Sialic
acids⁵⁷

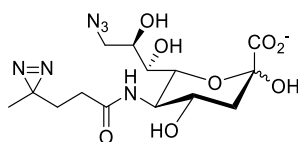
9-AzSiaNAI



Sialic Acids

Cu-Catalysed Alkyne Azide
coupling with BTTAA⁵⁷

9-AzSiaDaz



UV activated crosslinking

One of the biggest challenges to the wider applicability of this method is the insolubility of the acetylated sugars required to enable passage through the cell membrane (for mannose,

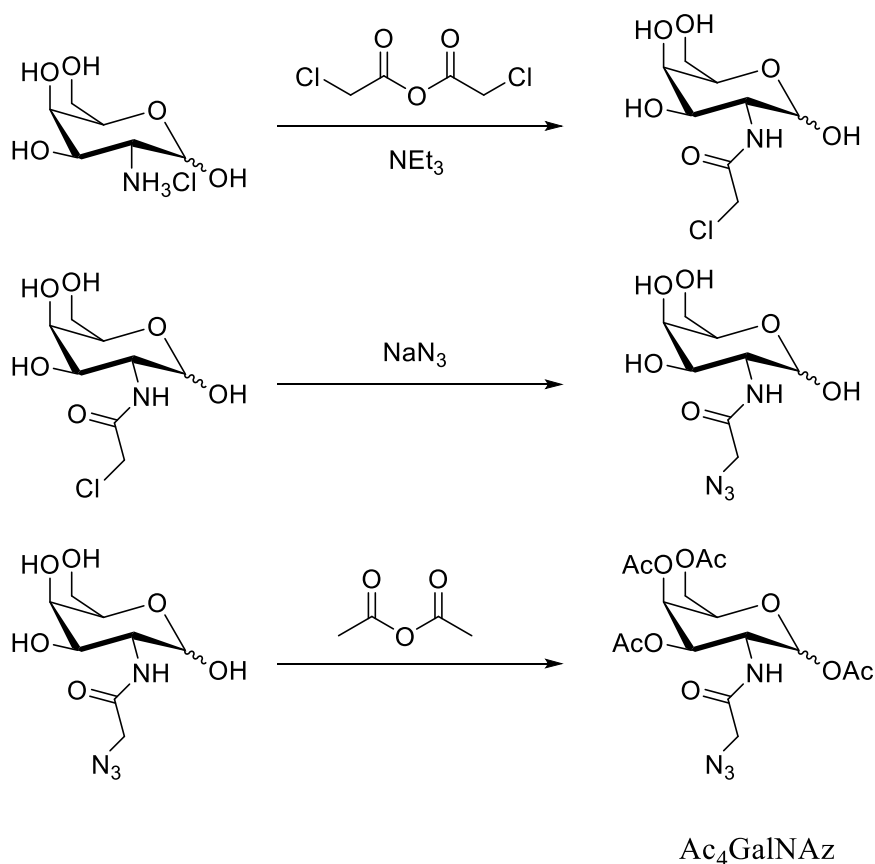
acetylation increases uptake over 100-fold⁵⁷) before subsequent de-acetylation by intracellular enzymes.^{31,46,62,63} Furthermore many fluorophores, other potential probe reagents, and abiotic functionality that researchers may want to introduce are hydrophobic and so precluded from use without the use of organic solvents such as DMSO, which is not passive and can damage cells. The ability to add polymers onto the cell surface can also be advantageous in and of itself. Work by Godula and co-workers has shown that synthetic neoproteoglycans based on an acrylamide backbone can be used to control stem cell differentiation by recruiting additional growth factors, which bind the synthetic materials immobilised onto the cell surface.⁶⁴ Bertozzi and co-workers utilised lipid-functionalised glycopolymers to investigate oligomerisation by galectins.⁶⁵ Hawker and co-workers have used the surface of yeast and mammalian Jurkat cells as a macro chain transfer agent for RAFT polymerisation performed directly on the cell surface.⁶⁶

The work in this chapter explores the use of water-soluble polymeric labelling reagents to enable both the visualisation of metabolically labelled glycans, but also as a new platform technology to enable the remodelling of cell surface using biocompatible, covalent chemistry.

4.3. Results and discussion

4.3.1. Synthesis of Ac₄GalNAz metabolic label

In order to introduce the orthogonal azide label into the cell surface, tetraacetylated galactosamine azide (Ac₄GalNAz) was synthesised using a procedure modified from Fűrinniss *et al*⁶⁷, shown below in Scheme 4.1:



Scheme 4.1: Synthesis of Ac₄GalNAz.

Galactosamine was first reacted with chloroacetic anhydride. Formation of the *N*-chloroacetic galactosamine was confirmed using mass spectroscopy and the crude product was used without further workup. The chlorine was then displaced by sodium azide [Caution: Care must be taken when handling NaN₃. Please read notes in experimental

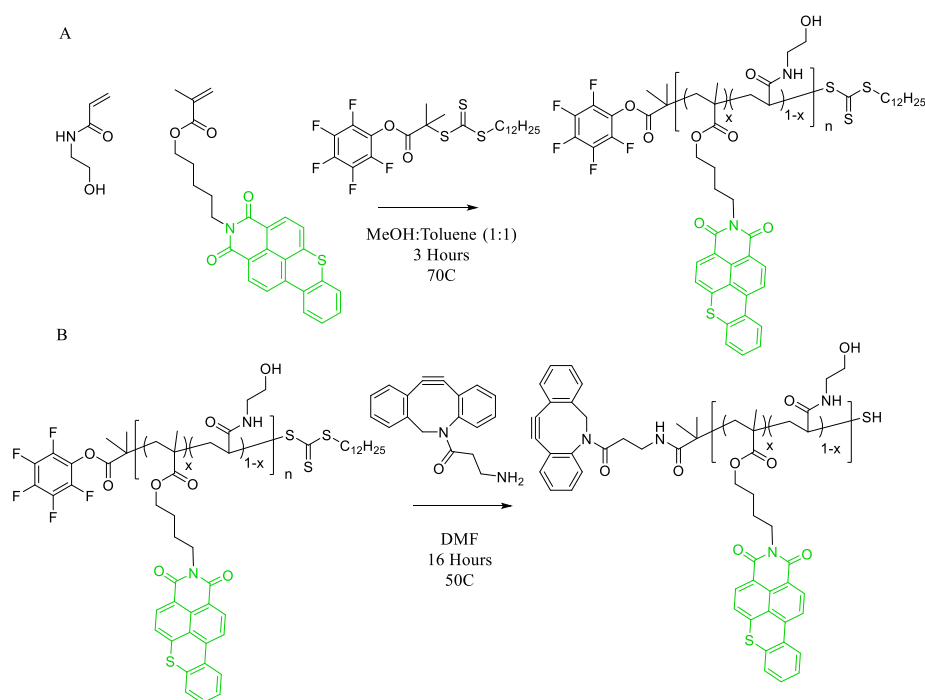
section]. The produced *N*-azidogalactosamine (GalNAz) was then directly acetylated using acetic anhydride and pyridine, again without isolation, to give the tetraacetylated product (Ac₄GalNAz), which was isolated *via* column chromatography. The presence of the azide was confirmed *via* infra red spectroscopy and the product characterised by nuclear magnetic resonance spectroscopy and mass spectrometry. In addition to the azido-monosaccharides, polymeric labelling reagents were also required. The design principle was to obtain a water-soluble polymer containing a fluorophore for labelling, and the necessary bio-orthogonal handle for cell-surface conjugation. To enable end group control, the polymer was synthesised as a copolymer using the RAFT polymerisation technique.

4.3.2. Synthesis of fluorescent polymers

A fluorescent monomer, hostasol methacrylate, Scheme 4.2, was chosen (kindly provided by the Haddleton Group, University of Warwick). By directly incorporating the dye into the polymer backbone, as opposed to the ω -end group, we could have multiple fluorescent units per polymer which means a greater total signal could be generated compared to traditional dyes which give a single fluorophore per conjugation. However, hostasol methacrylate is not water soluble, so it was copolymerized with *N*-hydroxyethyl acrylamide as it is a well-established, water soluble monomer which is non-cytotoxic (note lack of cytotoxicity does not prove, nor rule out, *in vivo* biocompatibility but shows it is suitable for cell-based studies). We chose to use RAFT polymerisation as our already prepared PFPDMP RAFT agent would be effective for polymerising both acrylamides and methacrylates, while installing the amine reactive PFP ester to the α -end group of our polymer, allowing the installation of DBCO-amine as the bio-orthogonal handle. DBCO is not compatible with controlled radical polymerisation hence this post-polymerisation approach is required. This would be difficult to achieve *via* another polymerisation method such as atom transfer radical

polymerisation (ATRP), as fine tuning the ligands to co polymerise both an acrylamide and methacrylate as a one pot reaction would be a time consuming task.^{68–71} Further, by choosing RAFT over ATRP we avoid the use of copper which would have needed complete removal prior to use with the cells. We chose 2 mol % hostasol methacrylate inclusion into polymers with a targeted degree of polymerisation of 25 and 75, giving polymers with a final dye incorporation of 0.5 and 1.5 per chain respectively. This allows us to see the effect of lower and higher fluorophore density on a single tag, and notice any quenching effects that may occur in a higher density probe.

Poly(*N*-hydroxyethyl acrylamide-co-hostasol methacrylate) was synthesised in a one-pot reaction as shown in Scheme 4.2.



Scheme 4.2: Reaction scheme for the synthesis of (A) the statistical copolymer PFP terminated Poly(*N*-hydroxyethyl acrylamide-co-hostasol methacrylate) (B) Functionalisation of end group with DBCO.

The resulting polymers were characterised by NMR spectroscopy and size exclusion chromatography (SEC), the results of which are summarised in Table 4.2. The SEC traces showed extremely strong fluorescence responses that align with the elution time of the polymers from the RI detector, saturating the detector at the 1 mg.mL⁻¹ concentration required for SEC analysis. This confirmed the inclusion of the hostasol fluorophore. It is important to note that although methacrylates and acrylamides have different reactivity ratios, the very low molar ratios means the challenges associated with statistical versus block copolymerisation are not relevant. Although the methacrylate will favour homopolymerisation, the raft agent favours acrylamide propagation, this should result in the distribution of methacrylate across the whole polymer backbone, with some favour towards the alpha end of the polymer and some block-like character. Determining the exact composition of the polymer however was beyond the scope of our aim to investigate to what extent we could modify the cell glycocalyx, and the subsequent effect on cell function.

Table 4.2: Table summarising characterisation of fluorescent polymers.

Polymer	[HEAA] :[HSM] :[CTA]	Conversion ^(a)	M _{theo}	Mn ^(b) (g.mol ⁻¹)	M _w /M _n
pHEAA ₂₅ -co-HMA _{0.5}	25:0.5:1	96.6%	3100	6500	1.23
pHEAA ₇₅ -co-HMA _{1.5}	75:1.5:1	88.3%	9300	13000	1.27

(a) Calculated by integration of HEAA vinyl peaks to mesitylene standard (b) DMF SEC

As a final step the DBCO-amine was installed at the α -end group by displacement of the pentafluorophenyl ester, using methods discussed in previous chapters, to give the final fluorescent water soluble co polymer shown in Scheme 4.2 Incorporation was confirmed by ¹⁹F NMR which enables monitoring of the release of the PFP group, as shown in Figure 4.5.

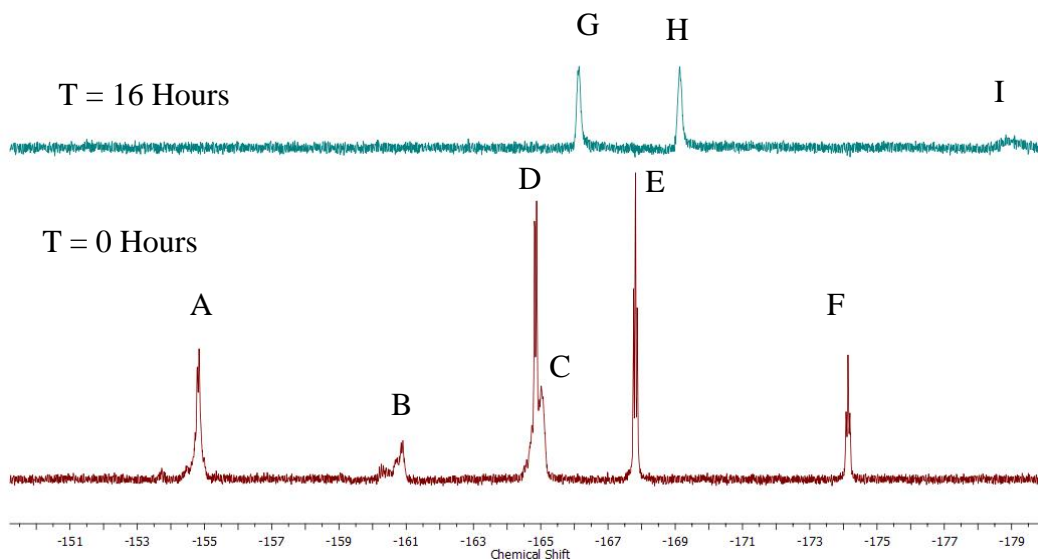


Figure 4.5: ^{19}F NMR of PFP-PHEAA₇₅-co-HMA_{1.5} on addition of DBCO at time = 0 (Red) and time = 16 hours (green). Note partial hydrolysis of the PFP end group is present even at time zero, we attribute this to the delay between taking the sample and the NMR spectrum being performed. Peaks A, B, and C correspond to fluorine in the polymer, Peaks D, E, and F correspond to solvated pentafluorophenol formed in the time = 0 sample before measurement. Peaks G, H and I correspond to solvated pentafluorophenol after 16 hours reaction time.

4.3.3. Testing the surface bound alkyne-azide coupling reaction with azide functionalised glass slides

With the above polymers with the necessary functionality; fluorescence read-out and DBCO-end group required for copper free click, a model system was set up to study the surface-binding properties. Azide coated glass slides were prepared as a simple mimic of a metabolically labelled cell surface. Glass slides were first cleaned using “Piranha solution”, a solution consisting of a 3:1 (v/v) mix of 98% H_2SO_4 and 30% H_2O_2 . [Note that Piranha

solution is extremely hazardous and should always be freshly prepared in small quantities; consult experimental section for further details]. After cleaning the glass slides were functionalised with (3-glycidyloxypropyl)trimethoxysilane before reacting them with sodium azide, Figure 4.6.

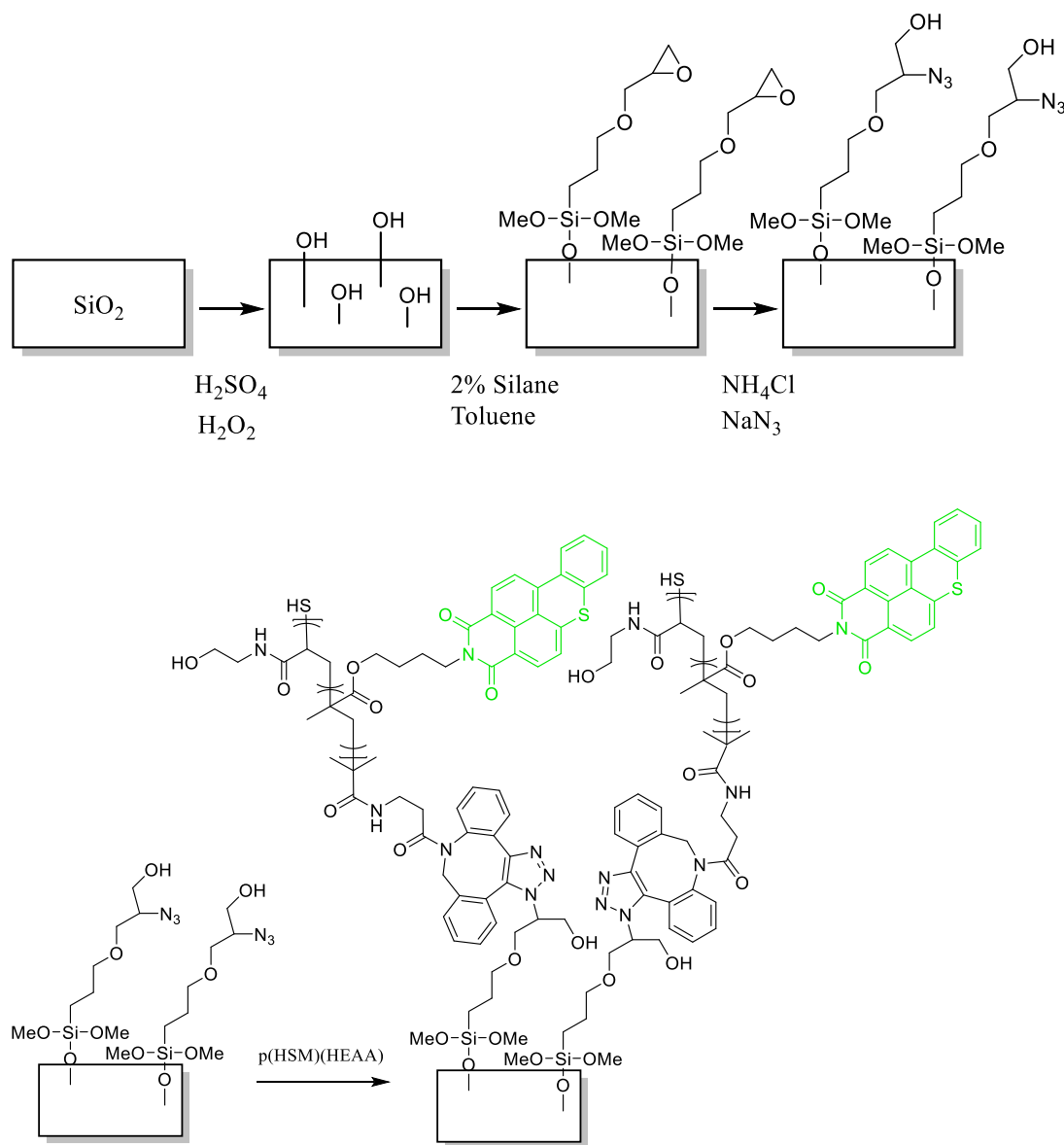


Figure 4.6: Synthetic procedure for the production of azide coated glass slides.

The successful incorporation of the azide onto the glass slide was confirmed using a drop shape analyser to confirm a change in the water contact angle between uncoated and coated slides, Figure 4.7 and Table 4.3:

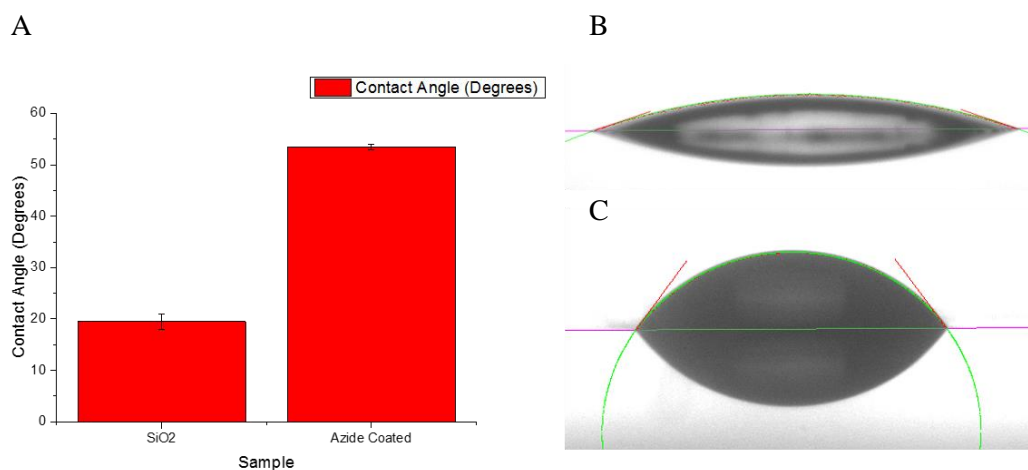


Figure 4.7: (A) Graph to show observed water contact angle measurements (B) Drop shape analysis of uncoated SiO₂ (C) Drop shape analysis of azide functionalised slide.

Table 4.3: Water contact angle measurements of coated and uncoated glass slides.

Slide	Water Contact angle (°)	Standard Deviation (°)
Uncoated SiO ₂	19.4 ^(a)	1.5
Azide-modified	53.4 ^(b)	0.6

(a) Average of 3 measurements (b) Average of 6 measurements

These azido-functional slides were used to investigate the surface binding reaction of PHEAA₂₅-co-HMA_{0.5}. The azide-reactive polymer was added to the glass slides at 0.1 mg.mL⁻¹ and 0.01mg.mL⁻¹ for 2 hours at room temperature. Following this the slides were washed copiously with de-ionised water and imaged using a micro array scanner. The array scanner images and analysis with ImageJ showed a clear localisation of the fluorescent polymers on the azido-slides, while uncoated glass slides showed no fluorescence (not shown due to lack of colour) post-washing, confirming the conjugation had occurred Figure 4.8.

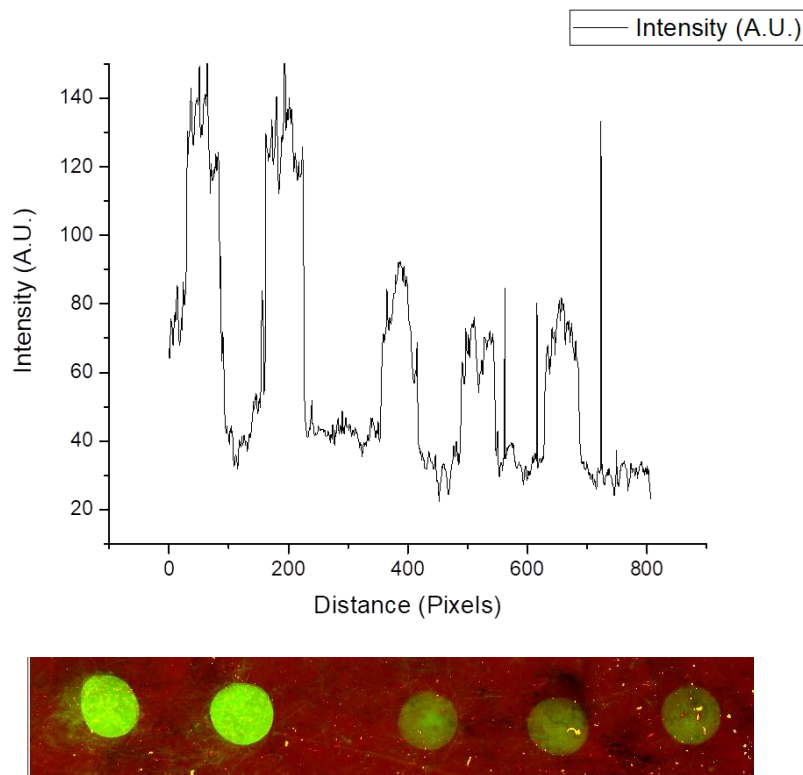


Figure 4.8: The localisation of PHEAA₂₅-co-HMA_{0.5} on the slide at 0.1 (Left two columns) and 0.01 (right three columns) mg.mL⁻¹. (Excitation at 532 nm and 633 nm).

4.3.4. Metabolic labelling of A549 carcinoma cells

Encouraged by the successful results on glass slides, a cell-based assay was devised for the metabolic labelling and capture to be explored. The immortalised human carcinoma A549 adherent cell line was chosen as the cell line to label as it is stable, well characterised⁷² and widely used in the research group. To screen for toxicity Ac₄GalNAz was drop cast from ethanol into collagen coated plates, to give final Ac₄GalNAz at concentrations of 0, 50 μM and 100 μM. A549 cells were then grown for 48 hours, after which the cells were observed for any morphological irregularities, stained with Alamar blue to check for cell viability and counted using a hemocytometer. No cytotoxicity was observed with cell viabilities above 90 % being obtained with the addition of the sugars. One way analysis of variance (ANOVA) showed no difference between the control and test groups (Null hypothesis mean variance =

0, null hypothesis accepted as calculated F (0.628) is less than or equal to F_{critical} (4.066). Morphological analysis also confirmed the cells were unaffected by the addition of the glycan. Figure 4.9.

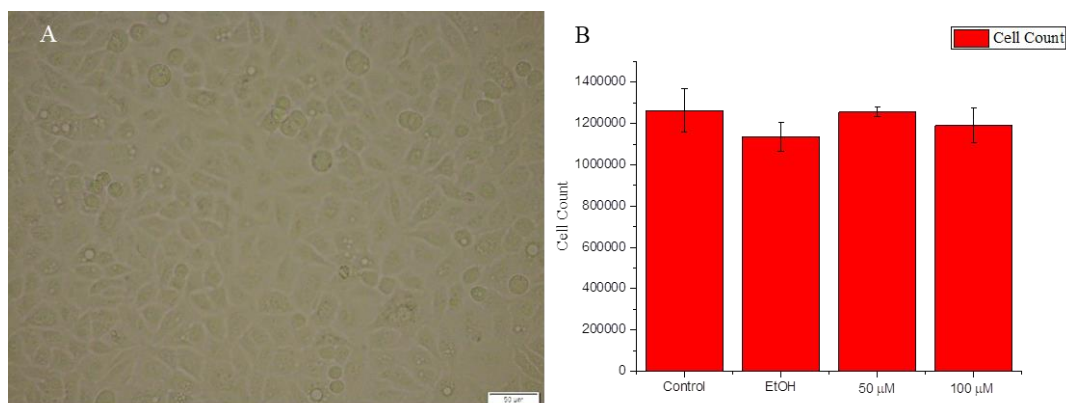


Figure 4.9: (A) 20x magnification brightfield image, showing healthy cell morphology (B) Cell counts, concentrations are of final plate concentration of Ac_4GalNAz .

Satisfied with the control experiment above that the Ac_4GalNAz sugar was not toxic we proceeded to metabolically label the cells. As before, Acetylated sugars were drop cast from ethanol onto the wells of a 96-well tissue culture plate to give a final concentration of 100 μM . *N*-acetylgalactosamine (GalNAc) was used as an azide-negative control. The cells were cultured to confluency over 48 hours in the presence of the sugar, after which serially diluted solutions of the fluorescent polymers, from 10 $\text{mg}\cdot\text{mL}^{-1}$ to 0.01 $\mu\text{g}\cdot\text{mL}^{-1}$ were added and incubated for a further 2 hours. Following this the cells were extensively washed with PBS to remove the excess unattached fluorescent polymer. It was found that at polymer concentrations greater than 0.6 $\text{mg}\cdot\text{mL}^{-1}$, the cells would detach from the plate and so PBS washes were kept to a minimum. This could be due to surface modification at higher concentrations reducing the cells ability to adhere to the plates. After washing, the fluorescence was recorded using a plate reader (excitation: 485 nm and emission: 528 nm) and the cells were also viewed under a fluorescence microscope. Typical microscopy images

along with a brightfield-fluorescence composite is shown in Figure 4.10. The cells appear normal and healthy with signs of epithelial-like morphology, as can be seen in Figure 4.10A. It is immediately apparent from Figure 4.10B and 4.10C that the highest fluorescence intensity appears localised to the cell membrane surface, consistent with successful labelling.

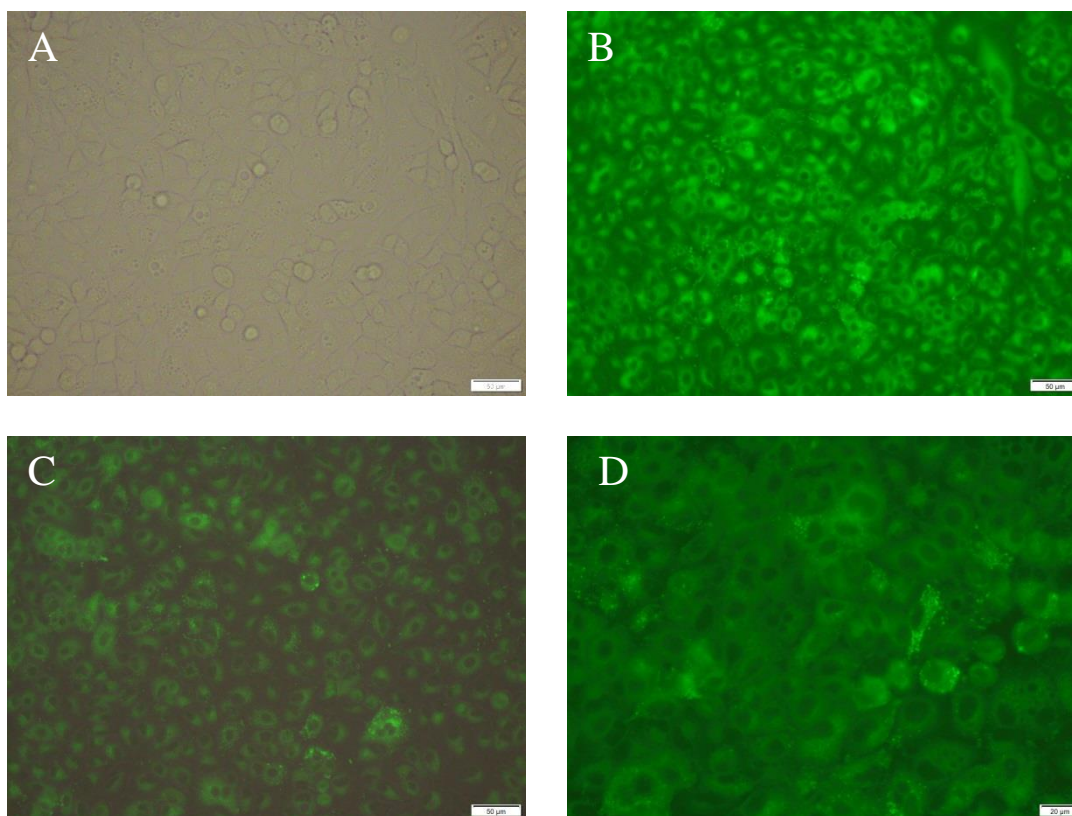


Figure 4.10: Microscope images of A549 cells metabolically labelled with PHEAA₂₅-co-HMA_{0.5} at a concentration of 0.31 mg.mL⁻¹ (A) 20x objective brightfield image, note the regular appearance of the cells (B) 20x objective fluorescence under blue filter, the fluorescence intensity appears localised to the cell membrane only (C) 20x objective composite overlay of green channel and brightfield performed in Image J. (D) 40x objective fluorescence under blue filter.

Whilst the imaging suggested we had successfully labelled the cell membrane, total fluorescence read by the plate reader showed conflicting results, as shown in Figure 4.11A and B. ANOVA analysis showed that there is no significant difference between the positive (Ac₄GalNAz) for azide and negative for azide (Ac₄GalNAc) experiments. This may be explained by two observations. First, at concentrations of 0.63 mg.mL⁻¹ and upwards, crystalline polymer regions forming during the incubation period that then would not wash

away were observed, Figure 4.12. Secondly, the polymer will non-specifically bind to the proprietary coating of the wells and to a certain extent the cells themselves. Any incomplete washing of polymer from the well will lead to variation in the fluorescence count but multiple wash steps lead to cell detachment. One method to overcome these issues in the future would be the use of flow cytometry to simultaneously count cells and observe the fluorescence. Unfortunately time and equipment restraints precluded this.

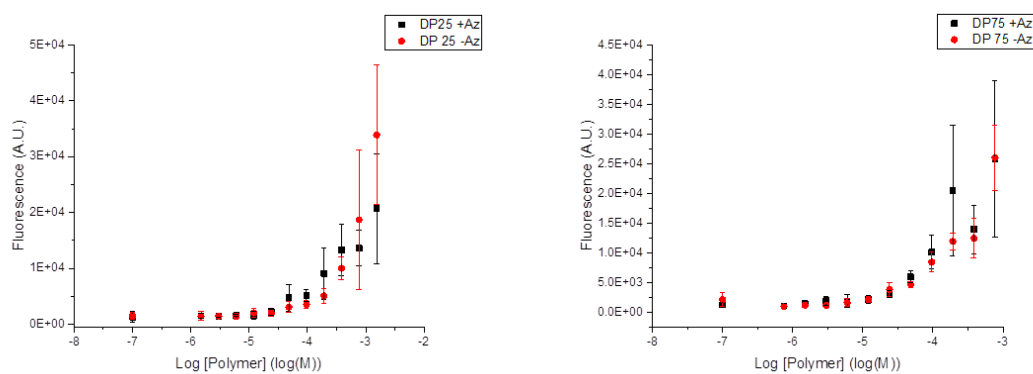


Figure 4.11: Left: PHEAA₂₅-co-HMA_{0.5}. Right: PHEAA₇₅-co-HMA_{1.5}. Concentration expressed in Log Molar with blank set to -7.

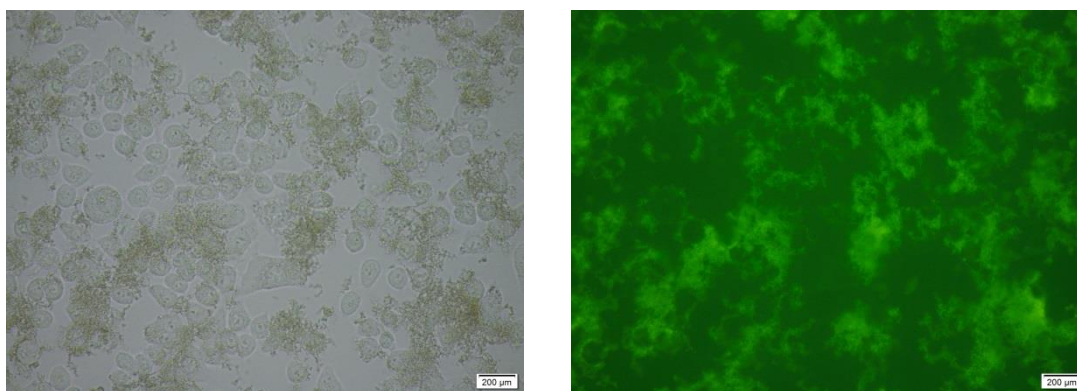


Figure 4.12: (A) 10x objective brightfield image (B) 10x objective fluorescence image with blue filter. Both images at a polymer concentration of 10 mg.mL⁻¹.

4.3.5. Titration of sugar concentration

Therefore, to attempt to confirm that metabolic labelling is occurring as expected a titration of sugar concentration was performed. It was hypothesised that in the presence of Ac₄GalNAz, a concentration dependent fluorescence response to the sugar would be observed, while the negative control would give a concentration independent response. This would also give an estimate for the background fluorescence occurring. To give the best chance of observing an effect, a wide concentration of sugar was used: 0, 10 μM, 100 μM, 250 μM, 500 μM, 1000 μM, and 5000 μM. This goes to a concentration considerably above the upper limit of toxicity previously tested, as we are not concerned if the cells lose viability due to the assay.

The cells were labelled with PHEAA₂₅-co-HMA_{0.5}, at a concentration of 0.6 mg.mL⁻¹. This concentration was chosen as it was within the range that we saw labelling under the microscope, but not so high that it appeared to be making the cells lose the ability to adhere. The same metabolic labelling protocol as before was used. The fluorescence intensity obtained by the plate reader is shown in Figure 4.13.

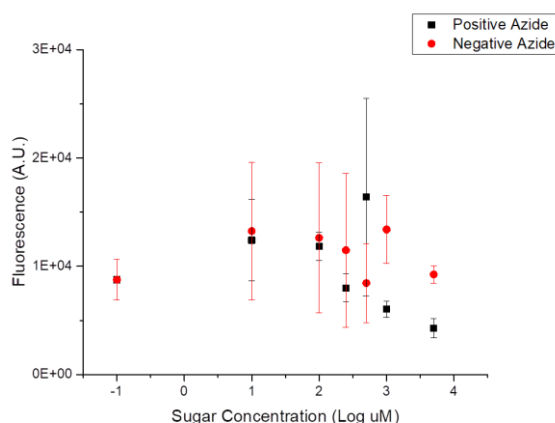


Figure 4.13: Plate reader obtained fluorescence data for titration of Ac₄GalNAz against pHEAA₂₅-co-HMA_{0.5}. Concentration expressed in Log Molar with blank set to -1.

It seems that when no azide is present, the fluorescence response is largely concentration independent, while in the presence of azide there is a concentration dependent response, however the fluorescence intensity decreases rather than increases. As before, as the concentration of sugar increases (and theoretically therefore an increased extent of labelling) the cell count observed in each well decreases substantially. To correct for the variation in the cell count between wells, 4x magnification images of the wells were processed using ImageJ software to count the cells, Figure 4.14.

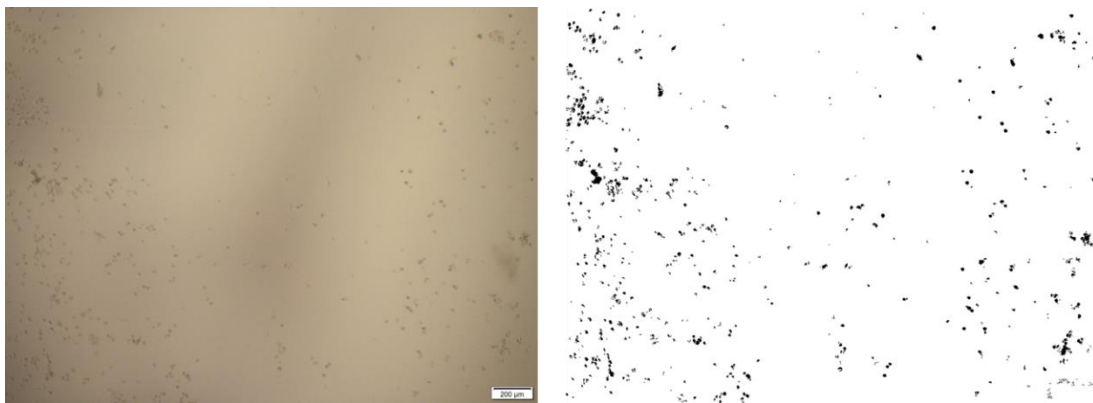


Figure 4.14: (A) Example of the reduced cell count observed in the higher concentration samples and (B) The output after processing with ImageJ to allow cell counts.

The average cell count for each concentration is shown in Figure 4.15A while there is considerable variation in the cell count between all concentrations in both the positive and negative azide experiment, there is a clear reduction in cell count at higher sugar concentrations in the case of the positive azide. It is possible that increased labelling is reducing the ability for the cells to adhere to the plate. Alternatively the reduced binding is a direct result of the increased sugar concentration, or a combination of the two. The

fluorescence per cell is shown in Figure 4.15B. ANOVA analysis of the data shows that there is statistically no significance between the positive and negative azide curves.

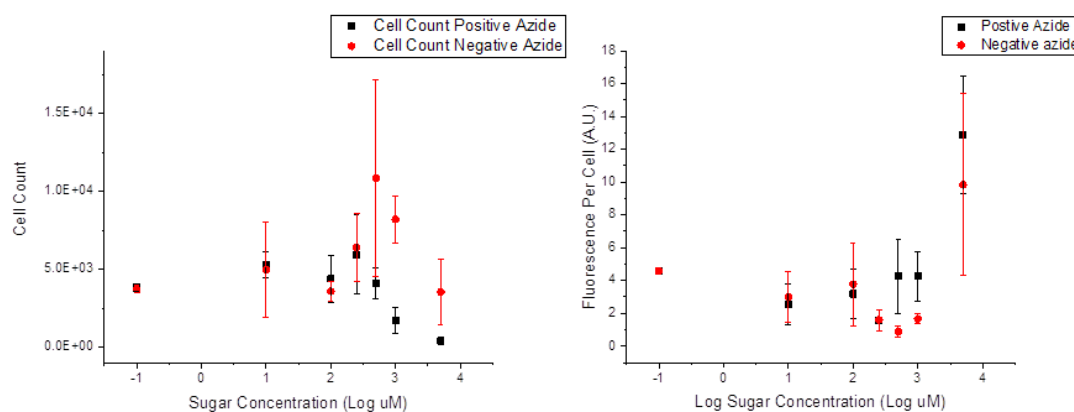


Figure 4.15: Results after incubation with pHEAA₂₅-co-HMA_{0.5} (A) Average cell counts (n=3). (B) The calculated average fluorescence per cell (n=3) In both cases concentration expressed in Log Molar with blank set to -1.

To evaluate if the surface labelling was occurring, the cells were imaged under a fluorescence microscope. To determine the extent to which the fluorescence was localised onto the cells (or not) fluorescence intensity slices were averaged over the area of the images, as shown in Figure 4.16. It is apparent that the fluorescence intensity is consistently localised only onto the cells in the experiments containing Ac₄GalNAz (Figure 4.16A, C, and, E), while in the negative control experiments containing Ac₄GalNAc (Figure 4.16 B, D, and, F), the fluorescence is delocalised across the whole image area, indicating non-specific adsorption of the polymer onto the well surface and to some extent the cells. This confirmed to us that the labelling had occurred successfully, and we had a method for easily modifying cell surfaces with polymers.

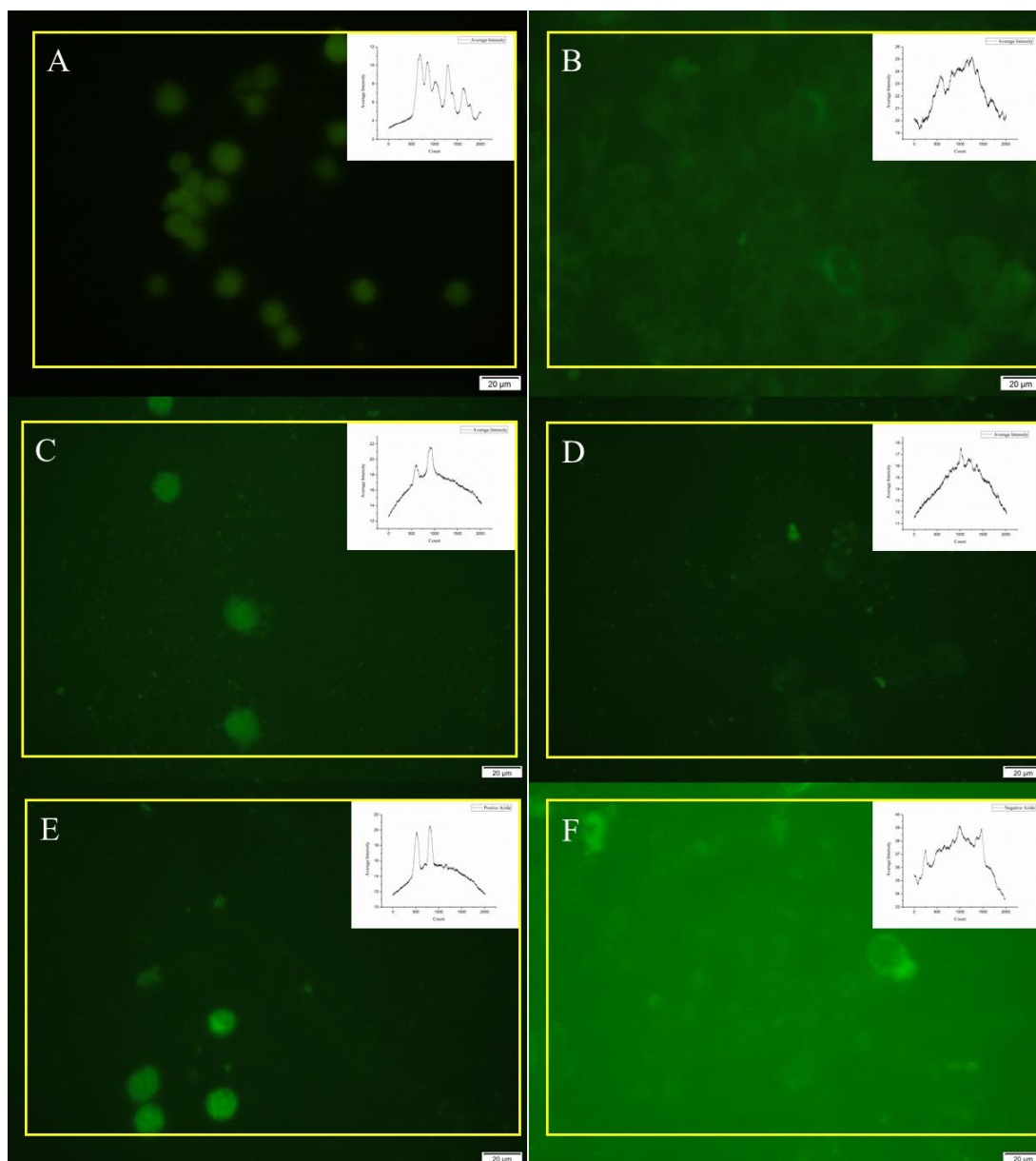


Figure 4.16: 40x fluorescence images of (A)(C) and (E) 5000 μ M positive azide and (B)(D) and (F) 5000 μ M negative azide after incubation with 0.6 mg.mL⁻¹ PHEAA₂₅-co-HMA_{0.5} for 2 hours. Each image is from a separate repeat. Inset: Slice of fluorescent intensity averaged from entire image area shown in yellow.

4.3.6. Investigating cell surface viability with fluorescently labelled WGA

Having confirmed that we had successfully modified the cell surface, we wished to determine the extent to which the labelling may be impacting cell function. Therefore an assay was developed to see to what extent the cell glycocalyx was still accessible, despite the steric hindrance of the polymer conjugations.

To do this fluorescein isothiocyanate-labelled wheat germ agglutinin (FITC-WGA) was used. WGA is known to bind to both terminal sialic acid residues and *O*-linked *N*-acetylgalactosamine residues on the cell glycocalyx.^{73,74} Ac₄GalNAz is metabolically incorporated primarily into *O*-linked *N*-acetylgalactosamine but will also access the sialic acid biosynthetic pathway. Therefore, by metabolically labelling the cells before the introduction of the FITC-WGA and monitoring the fluorescent output, we could determine if there was a reduction in fluorescence and consequently if access to the cell surface had been restricted. To minimise any interference that could arise from multiple fluorophores being present on the cell surface, such as quenching of the fluorescence intensity, pHEAA₂₅-DBCO and pHEAA₇₅-DBCO from chapter three were used as non-fluorescent analogues of the hostasol-dye polymers.

With these non-fluorescent polymers in hand, the first step was to perform a titration experiment using the FITC-WGA to determine what concentration to use on unlabelled cells. A549 cells were added to a 96 well plate at a concentration of 40,000 cells per well and left for 2 hours to allow adherence to the plate. Serially diluted solution of FITC-WGA was then added and the cells were incubated for 30 minutes as before. The cell media was then removed and the cells washed three times with PBS to ensure complete removal of any un-

adhered FITC-WGA and the fluorescence recorded, see Figure 4.18, the concentration of FITC-WGA used in later experiments is marked in red.

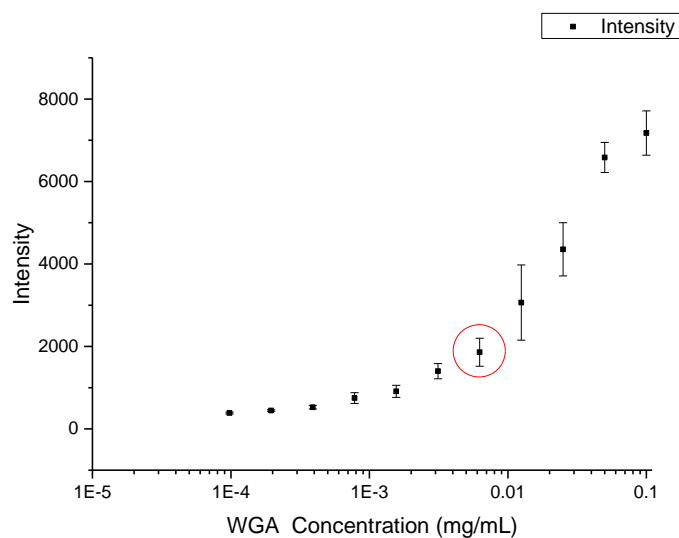


Figure 4.17: Titration curve of FITC-WGA against unlabelled A549 cells. Circled data point represents the concentration chosen for further experiments.

A concentration at the lower end of the binding curve was chosen to ensure that any inhibition of the cell surface was more likely to be observed.

A further batch of A549 cells were then metabolically labelled as before. After incubation for 48 hours the cell media was removed and pHEAA-DBCO solutions in cell media were added. The cells were incubated for 2 hours at 37°C before the media was removed and FITC-WGA solution added and incubated for a further 30 minutes, after which the cells were washed three times with PBS buffer and the fluorescence recorded. The resulting data is plotted below in Figure 4.18.

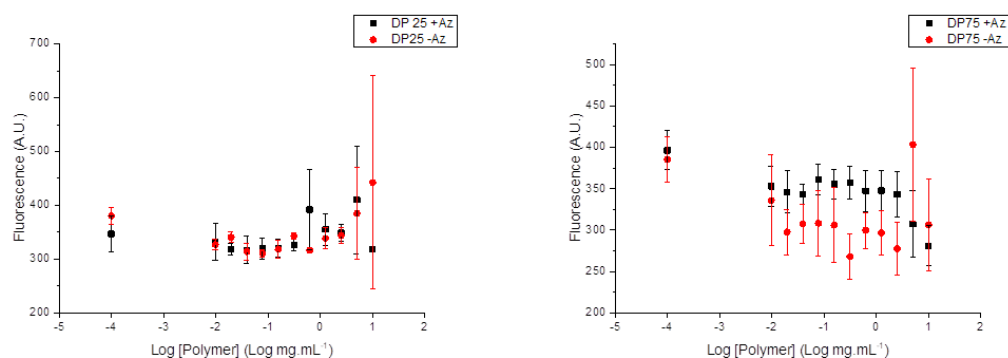


Figure 4.18: Fluorescent response of cells after incubation with pHEAA₂₅-DBCO or pHEAA₇₅-DBCO and subsequent addition of FITC-WGA.

There is no difference between the experiments performed in the presence of Ac₄GalNAz (positive azide) and Ac₄GalNAc (negative azide). This confirmed that although the cells are being labelled with the polymers, the function of the glycocalyx, essential for healthy cell growth, is being maintained and the modification is passive. This is consistent with relatively low levels of labelling, suggesting this could find application where additional functionality is needed, rather than for ‘turning off’ cell immunogenicity, for example. Such materials will find use in mapping cell surface glycans or by adding an additional, abiotic, layer of functionality to the cell surface.

4.4. Conclusions

We have shown that the polymeric modification of the cell glycoslyx is possible via metabolic engineering of *O*-linked glycans and sialic acid biosynthesis. However there are difficulties associated with quantifying the effects using fluorescent analysis methods that quantify an average over the area of a well. Flow cytometry may offer a way to circumvent this issue by coupling the fluorescence detection to cell count.

Coupling the metabolic labelling method with polymer chemistry is an attractive route to utilising the multiple metabolic pathways to tag particular regions of the glycocalyx with different polymeric functionality, either for later lysing and analysis or for probing the glycocalyx. Polymers offer the ability to introduce any bio-compatible chemical functional groups at controlled local density without worry for issues of solubility etc. This method circumvents the issues associated with cell-surface initiated polymer growth, such as maintaining cell viability while subjecting the cells to the conditions required for polymerisation. This method for the installation of polymers onto the glycocalyx could be coupled with knowledge of protein and glycan over-expression in certain disease states such as tumours and Alzheimer's as well as for fundamental study of glycocalyx interactions.

Further work requires a more complete study of the extent of labelling, using flow cytometry and confocal microscopy coupled with multiple stains to confirm the location of the cell labelling.

4.5. Experimental

4.5.1. Materials

d-(+)-Galactose was purchased from MP Biomedicals. Trimethylamine, sodium azide, 4,4'-azobis(4-cyanovaleric acid), 1,4-dioxane, dichloromethane, DBCO-amine, DMF, 2,6-lutidine 99% was purchased from Acros Organics. WGA was purchased from Vector labs. Ultrapure milli Q water was obtained from a Merk Milli-Q water purifier at 18.2 M Ω .cm resistivity at 25 °C. 3500 Da MWCO 'snakeskin' dialysis tubing was purchased from Thermofisher (UK). Chloroacetic anhydride, acetic anhydride, were purchased from Sigma-Aldrich. Hostasol methacrylate was synthesised by Julien Nicolas, the Haddleton Group at the University of Warwick^{75,76}, using hostasol dye provided by Clariant.

4.5.2. Analytical methods

¹H, ¹³C NMR, and ¹⁹F spectra were recorded on Bruker HD-300, HD-400, and AV-500 spectrometers using deuterated solvents purchased from Sigma-Aldrich. Chemical shifts are reported relative to residual non-deuterated solvent. Mass spectrometry was performed on an Agilent 6130B single Quad (ESI). FTIR spectra were acquired using a Bruker Vector 22 FTIR spectrometer with a Golden Gate diamond attenuated total reflection cell. Drop shape analysis was performed with a Krüss DSA 100. Solid state Raman spectra were collected on a Reinshaw inVia Reflex Raman using a 442 nm HeCd laser. 96-well plates were read using a Biotek Synergy plate reader set at 25 °C. Uv-Vis spectra were obtained on an Agilent Cary spectrometer. Glass slides were imaged using an Agilent Technologies 2 Colour Array Scanner using two lasers; a SHG-YAG laser (532 nm) and a helium-neon laser (633 nm). DMF SEC was performed on a varian 390-LC MDS system equipped with a PL-AS RT/MT autosampler, a PL-gel 3 μ m (50 x 7.5 mm) guard column, two PL-gel 5 μ m (300 x 7.5 mm)

mixed-D columns using DMF with 5 mM NH_4BF_4 at 50 °C as eluent at a flow rate of 1.0 mL.min⁻¹. The SEC system was equipped with ultraviolet (UV)/visible (set at 280 and 461 nm) and differential refractive index (DRI) detectors. Narrow molecular weight PMMA standard (200 - 1.0 x 10⁶ g.mol⁻¹) were used for calibration using a second order polynomial fit.

ImageJ analysis⁷⁷

To make overlays of fluorescence and brightfield images, the following operations were performed in ImageJ. First the images were converted to 8-bit, merged by colour and converted to RGB. To perform cell counting the images were converted to 8-bit. The background was subtracted using a rolling ball radius of 100 pixels. A threshold was applied to the image to give the greatest separation of cells from the background. The binary “Fill Holes” process was applied to solidify the cells to be counted. The image was converted to mask and “watershed” was applied. Finally the particle count was applied between the size of 8 to 1000 pixels.

To obtain profile slices, either a line or box was drawn over the area and “plot profile” used.

Cell culture

Human Caucasian lung carcinoma cells (A549 (ECACC 86012804)) were obtained from European Collection of Authenticated Cell Cultures (Public Health England, UK) and grown in 175 cm² Nunc cell culture flasks (ThermoFisher, Rugby, UK). Standard cell culture medium was composed of Ham's F-12K (Kaighn's) Medium (F-12K) (Gibco, Paisley, UK) supplemented with 10% USA-origin fetal bovine serum (FBS) purchased from Sigma Aldrich (Dorset, UK), 100 units/mL penicillin, 100 µg/mL streptomycin, and 250 ng/mL amphotericin B (PSA) (HyClone, Cramlington, UK). A549 cells were maintained in a

humidified atmosphere of 5% CO₂ and 95% air at 37 °C and the culture medium was renewed every 3–4 days. The cells were subcultured every 7 days or before reaching 90% confluency. To subculture, cells were dissociated using 0.25% trypsin plus 1 mM EDTA in balanced salt solution (Gibco) and reseeded at $1.87 \cdot 10^5$ cells per 175 cm² cell culture flasks.

Cell toxicity screening

Prior to plating cells, 100 uL of either ethanol or sugar solution was added to 6-well plates (ThermoFisher) and left to dry to allow ethanol to evaporate, control wells received no added solution. Cells were then seeded at 5×10^5 cells per well in 2 mL of cell culture medium. Cells were allowed to attach to the entire free surface of the bottom of the well and formed a confluent layer not greater in height than one cell. Cells were incubated for 48h in a humidified atmosphere of 5% CO₂ and 95% air at 37 °C. After the incubation period, cells were then dissociated using 0.25% trypsin plus 1 mM EDTA in balanced salt solution. The number of viable cells was determined by counting with a hemocytometer (Sigma Aldrich) at room temperature after 1:1 dilution of the sample with 0.4% trypan blue solution (Sigma Aldrich). The initial cell medium was discarded such that any non-attached cells were not included in the assessment. The fold change of recovered cells was calculated by dividing the number of recovered cells with intact membranes by the number of cells initially plated.

Statistical analysis

Data were analyzed with a one-way analysis of variance (ANOVA) on ranks followed by comparison of experimental groups with the appropriate control group (Holm–Sidak method) followed by Tukey’s post hoc test. Excel 2013 (Microsoft, Redmond, WA) and R (R Foundation for Statistical Computing, Vienna, Austria) were used for the analyses.

Plate Coating procedure

Ac₄GalNAz (4.3mg) and Ac₄GalNAc (3.8mg), as a negative control, were dissolved in 5 mL ethanol to give 2mM solutions. 10 µL of sugar solution was added to each well and ethanol was allowed to evaporate off for a minimum of 30 minutes to give a final concentration of 100 µM in 200 µL of cell media. Plates were not stored and used immediately.

Analysis of A549 cells

Cells were seeded at 0.2×10^4 cells per well in 200 µL of cell culture medium in 96-well sugar-coated plates (ThermoFisher). Cells were incubated for 48 h in a humidified atmosphere of 5% CO₂ and 95% air at 37 °C. Cell media was then removed and 100 µL of polymer solution added. The plates were returned to the incubator for another 2 hours. For the cell surface viability tests the polymer solutions were removed and FITC-WGA in cell media added and the plate incubated for a further 30 minutes, before removing the FITC-WGA solution. Otherwise the plate was then washed with PBS buffer and fluorescence recorded using a Biotek Synergy plate reader, with excitation and emission values set to, 485 nm and 525 nm, with gain set to 75. Finally the wells were imaged on an Olympus cxx41 microscope with camera xc30 and processed using Olympus CellSens software.

FITC-WGA Activity Test

WGA-FITC was serially diluted from 0.1 mg.mL to 4.88×10^{-5} mg.mL⁻¹ (11 serial dilutions plus a blank) with cell media and sterile filtered.

A549 Cells (40,000 per well) were added to a 96 well plate in 200 µL of cell media (F12K, with 10% FBS, 1x PSA) and incubated for 2 hours to allow adherence to the plate. The cell media was then removed and the WGA solutions added. The plate was incubated for 30

minutes in a humidified atmosphere of 5% CO₂ and 95% air at 37 °C. The cell media was then removed and the wells washed with PBS buffer three times. Fluorescence was then measured using a Biotek Synergy plate reader, with excitation and emission values set to 485 nm and 525 nm, with gain set to 75. Following this the cells were then imaged under an Olympus ckx41 microscope with camera xc30 and processed using Olympus CellSens software. This was repeated three times, the data plotted and a midpoint of the curve chosen as the WGA concentration to be used in further experiments.

4.5.3. Synthetic Procedures

Synthesis of tetraacetyl N-azidoacetylgalactosamine

Sodium methanolate (30% w/w NaOMe in MeOH, 1.66 mL, 4.64 mmol, 1.00 equivalent) was added to a solution of d-galactosamine hydrochloride (1.00 g; 4.64 mmol) in 50 mL of methanol. The mixture was left at room temperature for 30 min until complete dissolution. Triethylamine (0.47 g; 4.64 mmol, 1.00 equiv) and chloroacetic anhydride (871 mg; 5.10 mmol, 1.10 equiv) were added and the reaction was stirred at room temperature overnight. The solvent was removed under vacuum and the resulting *N*-chloroacetylgalactosamine solid was used in the following reaction without any further workup.

The *N*-chloroacetylgalactosamine was dissolved in a 20 mL:2 mL methanol:water mix and sodium azide (1.06 g; 16.24 mmol, 3.50 equiv) was added. The solution was stirred for 5 h at 65 °C. Following this the solvent was removed under vacuum. The resulting solid was then fully suspended in 20 mL pyridine and cooled on ice with an air condenser in place. 20 mL of acetic anhydride was then slowly added to the solution and left overnight. The solvent was then removed under vacuum and re-dissolved in 50 mL of ethyl acetate. The solution was washed with 50 mL of 1 M hydrochloric acid, 50 mL of sodium hydrogen carbonate and 50 mL of brine, and dried with magnesium sulphate. The crude product was then purified by silica gel column chromatography using 1:1 cyclohexane:ethyl acetate to give the final product as an oil that solidified after freeze drying under high-vacuum on a schlenk line. 0.48 g (25%)

¹H NMR (400MHz): δppm: 1.83 (3H, S) 1.94 (3H, S) 1.96 (3H, S) 1.97 (3H, S) 2.05 (3H, S) 2.05 (3H, S) 2.11 (3H, S) 2.12 (3H, S) 3.87 (S), 3.97-4.28 (M) 4.37 (dt, *J*=11.04, 9.03), 4.64 (M), 5.18 (M), 5.33(dd, *J*=8.03, 2.67) 5.34 (d, *J*=2.01)

^{13}C NMR (75MHz): δ ppm: 169.61, 169.17, 168.61, 168.21 (Carbonyl) 150.02 (Amide) 142.88 (C1) 69.66, 69.02, 67.16 (C3,4, 5) 60.89 (CH₂) 49.57 (C2) 19.66, 19.63, 19.14 (Me)

IR (cm⁻¹): 3353 (N-H Stretch) 2109 (-N₃) 1739 (Ester C=O) 1689 (Amide C=O)

1534 (Amide N-H Bend) 1040 (Ester C-O)

MS m/z (ESI-POS): Expected: 430 Observed: 453 (M+Na⁺)

Synthesis of p(hydroxyethylacrylamide)

HEAA (0.5g, 4.34mmol, 25eq) plus varied amounts of DMPPFP (1eq) and 4,4'-Azobis(4-cyanovaleric acid) (AVCA) as the initiator (0.5eq) were placed into a glass vial with 4.0mL of a 1:1 mix of Toluene and Methanol. 200ul of Mesitylene as an internal NMR standard was added. A sample for NMR is taken and dissolved in deuterated Chloroform. The glass vial was then sealed and degassed using N₂ for 30 minutes. Following this the reaction mixture is heated to 70°C for 90 minutes at which time the reaction is quenched by exposure to air followed by cooling in liquid N₂. An NMR sample of the crude mix is made up in deuterated Methanol and the mixture is precipitated into Diethyl Ether from Methanol three times to give a yellow solid. 92% conversion. $\bar{M}_n = 1.18$

^1H NMR (MeOD) 300MHz, ppm: 3.65 (br, NH-CH₂-CH₂-), 3.28 (br, -NH-CH₂-CH₂-), 2.5-1.5 (br, Backbone CH₂)

^{19}F NMR (CDCl₃) 376MHz, ppm: -150.35 (1F, br s), -151.44 (1F, br s), -156.97 (1F, br s), -162.11 (1F, br s)

Synthesis of p(hydroxyethyl acrylamide) dibenzocyclooctyne amide

Poly(HEAA) (1 eq), DBCO (10 mg, 36.2 μ M, 1.05 eq) and triethylamine (TEA) (2 eqs) are dissolved in 2 mL of deuterated methanol. The reaction mixture is then heated to 50 °C for 16 hours. The solution is then concentrated to approximately 0.5mL and submitted for ^{19}F NMR. Following this the mixture is diluted to 20 mL of distilled H_2O and dialysed using dialysis tubing with an appropriate molecular weight cut off. The sample was then freeze-dried to afford the final product as a white powder, yield ~69%

^1H NMR (MeOD) 300MHz, ppm: 7.5-7.0 (br, Benzyl) 4.42 (br, cyclooctyne ring CH_2) 3.65 (br, $\text{NH}-\text{CH}_2-\text{CH}_2-$), 3.28 (br, $-\text{NH}-\text{CH}_2-\text{CH}_2-$), 2.5-1.5 (br, Backbone CH_2)

^{19}F NMR indicated no presence of fluorine left in sample

Raman (cm^{-1}): 1600 (Aromatic C-C) and 2159 (Alkyne)

Synthesis of p(hydroxyethylacrylamide-co-hostasol methacrylate) pentafluorophenol

The reaction and product are kept shield from light using aluminium foil at all times. HEAA (0.5 g, 4.34 mmol, 25 eq), 2% hostasol methacrylate (39.7 mg, 86 μ mol, 0.5 eq), plus varied amounts of DMPPFP (1 eq) and 4,4'-Azobis(4-cyanovaleric acid) (AVCA) as the initiator (0.5 eq) were placed into a glass vial with 8.0 mL of a 1:1 mix of toluene and methanol. 200 μ l of mesitylene as an internal NMR standard was added. A sample for NMR is taken and dissolved in deuterated chloroform. The glass vial was then sealed and degassed using N_2 for 30 minutes. Following this the reaction mixture is heated to 70 °C for 180 minutes at which time the reaction is quenched by exposure to air followed by cooling in liquid N_2 . An NMR sample of the crude mix is made up in deuterated methanol and the mixture is precipitated into diethyl ether from methanol three times to give an orange solid. Average 92% conversion.

^1H NMR (MeOD) 400MHz, ppm: 8.17-8.09 (br Hostasol aromatics) 5.52 (br, C_5H_{10} 3.68 (br, $\text{NH-CH}_2\text{-CH}_2\text{-}$), 2.5-1.5 (br, Backbone CH_2) 0.94 (br, Me)

^{19}F NMR (MeOD) 376MHz, ppm: -150.35 (1F,br s), -151.44 (1F, br s), -156.97 (1F, br s), -162.11 (1F, br s)

p(hydroxyethylacrylamide-co-hostasol methacrylate) dibenzocyclooctyne

p(hydroxyethylacrylamide-co-hostasol methacrylate) pentafluorophenol (1 eq), DBCO (10 mg, 36.2 μM , 1.05 eq) and triethylamine (TEA) (2e qs) are dissolved in 2 mL of deuterated methanol. The reaction mixture is then heated to 50 °C for 16 hours. The solution is then concentrated to approximately 0.5 mL and submitted for ^{19}F NMR. Following this the mixture is diluted to 20 mL of distilled H_2O and dialysed using dialysis tubing with an appropriate molecular weight cut off. The sample was then freeze-dried to afford the final product as a white powder, yield ~69%

^1H NMR (MeOD) 400MHz, ppm: 8.17-8.09 (br Hostasol aromatics) 7.5-7.0 (br, Benzyl) 5.52 (br, C_5H_{10} 3.68 (br, $\text{NH-CH}_2\text{-CH}_2\text{-}$), 4.42 (br, cyclooctyne ring CH_2), 2.5-1.5 (br, Backbone CH_2) 0.94 (br, Me)

^{19}F NMR indicated no presence of fluorine left in sample

Synthesis of Azide coated glass slides

Glass microscope slides were first cleaned using a 'Piranha' solution consisting of a 3:1 (v/v) mix of 98% H_2SO_4 and 30% H_2O_2 . [Note that Piranha solution is extremely hazardous and should always be freshly prepared in small quantities and handled using heavy nitrile gloves. Do not wipe up spillages with cloth or tissue as this will result in a fire. Piranha solution should always be disposed of with care using first manganese dioxide to destroy the peroxide and then sodium bicarbonate to neutralise the solution.] Piranha solution was prepared by

slow dropwise addition of H₂O₂ to H₂SO₄ [Note in this step the water component is being added to the acid component, the opposite of usual guidelines for preparing acidic solutions]. The glass slides were cleaned for 20 minutes, during the cleaning procedure the solution was kept on ice. Following this slides were rinsed with DI water and dried under N₂. Immediately afterwards the slides were immersed in 5mL of toluene solution containing 100 μL of (3-Glycidyloxypropyl)trimethoxysilane for 2 hours at room temperature. Subsequently the slides were washed with toluene and DI water and dried with N₂. The epoxy glass slides were then immersed into a bath containing a DMSO solution of NaN₃ (0.1177g, 4 eq) and NH₄Cl (0.0968g, 4 eq) wrapped in tin foil and held at 80 °C for 8 hours. The slides were then rinsed with DMSO, Ethanol, DI water and dried with N₂. Measured water contact angle: 53.4 ±0.6 °

Labelling of azido-glass slides using poly hydroxyethylacrylamide-co-hostasol methacrylate

1 μL of polymer at 0.01, 0.001 and 0.0001 mg.mL⁻¹ in DI water, were pipetted onto the azide slide and left for 2 hours. After which time the slide was washed exhaustively with DI water for 15 minutes and then imaged using a agilent microarray scanner, Red and Green Channels, using two lasers; a SHG-YAG laser (532 nm) and a helium-neon laser (633 nm).

4.6. References

- 1 R. B. Parker and J. J. Kohler, *ACS Chem. Biol.*, 2010, **5**, 35–46.
- 2 G. A. Rabinovich and M. A. Toscano, *Nat. Rev. Immunol.*, 2009, **9**, 338–52.
- 3 P. M. Rudd, *Science (80-.)*, 2001, **291**, 2370–2376.
- 4 J. D. Marth and P. K. Grewal, *Nat. Rev. Immunol.*, 2008, **8**, 874–87.
- 5 L. A. Lasky, *Annu. Rev. Biochem.*, 1995, **64**, 113–140.
- 6 D. H. Dube and C. R. Bertozzi, *Nat. Rev. Drug Discov.*, 2005, **4**, 477–488.
- 7 M. D. Mager, V. LaPointe and M. M. Stevens, *Nat. Chem.*, 2011, **3**, 582–589.
- 8 Z. Aguilar, R. W. Akita, R. S. Finn, B. L. Ramos, M. D. Pegram, F. F. Kabbinavar, R. J. Pietras, P. Pisacane, M. X. Sliwkowski and D. J. Slamon, *Oncogene*, 1999, **18**, 6050–6062.
- 9 M. M. Fuster and J. D. Esko, *Nat. Rev. Cancer*, 2005, **5**, 526–42.
- 10 R. S. Haltiwanger and J. B. Lowe, *Annu. Rev. Biochem.*, 2004, **73**, 491–537.
- 11 S.-K. Cha, B. Ortega, H. Kurosu, K. P. Rosenblatt, M. Kuro-O and C.-L. Huang, *Proc. Natl. Acad. Sci. U. S. A.*, 2008, **105**, 9805–10.
- 12 K. Ohtsubo, S. Takamatsu, M. T. Minowa, A. Yoshida, M. Takeuchi and J. D. Marth, *Cell*, 2005, **123**, 1307–21.
- 13 E. A. Partridge, C. Le Roy, G. M. Di Guglielmo, J. Pawling, P. Cheung, M. Granovsky, I. R. Nabi, J. L. Wrana and J. W. Dennis, *Science*, 2004, **306**, 120–4.
- 14 Y.-C. Liu, H.-Y. Yen, C.-Y. Chen, C.-H. Chen, P.-F. Cheng, Y.-H. Juan, C.-H. Chen,

- K.-H. Khoo, C.-J. Yu, P.-C. Yang, T.-L. Hsu and C.-H. Wong, *Proc. Natl. Acad. Sci. U. S. A.*, 2011, **108**, 11332–7.
- 15 H. Xiao, E. C. Woods, P. Vukojicic and C. R. Bertozzi, *Proc. Natl. Acad. Sci. U. S. A.*, 2016, **113**, 10304–9.
- 16 C. Büll, M. A. Stoel, M. H. den Brok and G. J. Adema, *Cancer Res.*
- 17 A. Bernardi, J. Jiménez-Barbero, A. Casnati, C. De Castro, T. Darbre, F. Fieschi, J. Finne, H. Funken, K.-E. Jaeger, M. Lahmann, T. K. Lindhorst, M. Marradi, P. Messner, A. Molinaro, P. V Murphy, C. Nativi, S. Oscarson, S. Penadés, F. Peri, R. J. Pieters, O. Renaudet, J.-L. Reymond, B. Richichi, J. Rojo, F. Sansone, C. Schäffer, W. B. Turnbull, T. Velasco-Torrijos, S. Vidal, S. Vincent, T. Wennekes, H. Zuilhof and A. Imberty, *Chem. Soc. Rev.*, 2013, **42**, 4709–27.
- 18 I. Ofek, D. L. Hasty and N. Sharon, *FEMS Immunol. Med. Microbiol.*, 2003, **38**, 181–191.
- 19 M. Matsusaki, K. Kadowaki, Y. Nakahara and M. Akashi, *Angew. Chemie Int. Ed.*, 2007, **46**, 4689–4692.
- 20 V. Berry and R. F. Saraf, *Angew. Chemie Int. Ed.*, 2005, **44**, 6668–6673.
- 21 A. I. Zamaleeva, I. R. Sharipova, R. V. Shamagsumova, A. N. Ivanov, G. A. Evtugyn, D. G. Ishmuchametova, R. F. Fakhrullin and G. M. Greenway, *Anal. Methods*, 2011, **3**, 509.
- 22 J. García-Alonso, R. F. Fakhrullin, V. N. Paunov, Z. Shen, J. D. Hardege, N. Pamme, S. J. Haswell and G. M. Greenway, *Anal. Bioanal. Chem.*, 2011, **400**, 1009–1013.
- 23 K. W. Dehnert, B. J. Beahm, T. T. Huynh, J. M. Baskin, S. T. Laughlin, W. Wang, P.

- Wu, S. L. Amacher and C. R. Bertozzi, *ACS Chem. Biol.*, 2011, **6**, 547–552.
- 24 S. T. Laughlin and C. R. Bertozzi, *Nat. Protoc.*, 2007, **2**, 2930–2944.
- 25 H. C. Hang, C. Yu, D. L. Kato and C. R. Bertozzi, *Proc. Natl. Acad. Sci. U. S. A.*, 2003, **100**, 14846–51.
- 26 S. Goon, B. Schilling, M. V Tullius, B. W. Gibson and C. R. Bertozzi, *Proc. Natl. Acad. Sci. U. S. A.*, 2003, **100**, 3089–94.
- 27 K. J. Yarema, S. Goon and C. R. Bertozzi, *Nat. Biotechnol.*, 2001, **19**, 553–558.
- 28 G. A. Lemieux and C. R. Bertozzi, *Chem. Biol.*, 2001, **8**, 265–75.
- 29 H. Hang and, C. R. Bertozzi, *JACS*, 2001, **123**, 1242-1243
- 30 K. J. Yarema, L. K. Mahal, R. E. Bruehl, E. C. Rodriguez and C. R. Bertozzi, *J. Biol. Chem.*, 1998, **273**, 31168–79.
- 31 J. Thorner, S. D. Emr, J. N. Abelson, C. L. Jacobs, K. J. Yarema, L. K. Mahal, D. A. Nauman, N. W. Charters and C. R. Bertozzi, *Methods in Enzymology*, 2000, **327**, 260-275.
- 32 T.-L. Hsu, S. R. Hanson, K. Kishikawa, S.-K. Wang, M. Sawa and C.-H. Wong, *Proc. Natl. Acad. Sci. U. S. A.*, 2007, **104**, 2614–9.
- 33 N. J. Sullivan, M. Peterson, Z. -y. Yang, W. -p. Kong, H. Duckers, E. Nabel and G. J. Nabel, *J. Virol.*, 2005, **79**, 547–553.
- 34 Z. Yang, H. J. Duckers, N. J. Sullivan, A. Sanchez, E. G. Nabel and G. J. Nabel, *Nat. Med.*, 2000, **6**, 886.
- 35 M. V. Croce, M. T. Isla-Larrain, S. O. Demichelis, A. Segal-Eiras, J. R. Gori and M.

- R. Price, *Breast Cancer Res. Treat.*, 2003, **81**, 195–207.
- 36 F.-G. Hanisch and S. Muller, *Glycobiology*, 2000, **10**, 439–449.
- 37 S. Schedin-Weiss, B. Winblad and L. O. Tjernberg, *FEBS J.*, 2014, **281**, 46–62.
- 38 L. A. Robertson, K. L. Moya and K. C. Breen, *J. Alzheimers. Dis.*, 2004, **6**, 489–95.
- 39 H. C. Hang, C. Yu, D. L. Kato and C. R. Bertozzi, *Proc. Natl. Acad. Sci. U. S. A.*, 2003, **100**, 14846–51.
- 40 J. M. Baskin, K. W. Dehnert, S. T. Laughlin, S. L. Amacher and C. R. Bertozzi, *Proc. Natl. Acad. Sci. U. S. A.*, 2010, **107**, 10360–5.
- 41 K. W. Dehnert, B. J. Beahm, T. T. Huynh, J. M. Baskin, S. T. Laughlin, W. Wang, P. Wu, S. L. Amacher and C. R. Bertozzi, *ACS Chem. Biol.*, 2011, **6**, 547–52.
- 42 S. T. Laughlin, J. M. Baskin, S. L. Amacher and C. R. Bertozzi, *Science*, 2008, **320**, 664–7.
- 43 K. W. Dehnert, J. M. Baskin, S. T. Laughlin, B. J. Beahm, N. N. Naidu, S. L. Amacher and C. R. Bertozzi, *Chembiochem*, 2012, **13**, 353–7.
- 44 E. Saxon, *Science*, 2000, **287**, 2007–2010.
- 45 N. J. Agard, J. A. Prescher and C. R. Bertozzi, *J. Am. Chem. Soc.*, 2004, **126**, 15046–7.
- 46 S. T. Laughlin, N. J. Agard, J. M. Baskin, I. S. Carrico, P. V. Chang, A. S. Ganguli, M. J. Hangauer, A. Lo, J. A. Prescher and C. R. Bertozzi, *Methods Enzymol.*, 2006, **415**, 230–250.
- 47 J. M. Baskin, J. A. Prescher, S. T. Laughlin, N. J. Agard, P. V. Chang, I. A. Miller, A. Lo, J. A. Codelli and C. R. Bertozzi, *Proc. Natl. Acad. Sci. U. S. A.*, 2007, **104**, 16793–

- 7.
- 48 M. D. Best, *Biochemistry*, 2009, **48**, 6571–84.
- 49 J. A. Codelli, J. M. Baskin, N. J. Agard and C. R. Bertozzi, *J. Am. Chem. Soc.*, 2008, **130**, 11486–93.
- 50 G. de Almeida, E. M. Sletten, H. Nakamura, K. K. Palaniappan and C. R. Bertozzi, *Angew. Chem. Int. Ed. Engl.*, 2012, **51**, 2443–7.
- 51 C. G. Gordon, J. L. Mackey, J. C. Jewett, E. M. Sletten, K. N. Houk and C. R. Bertozzi, *J. Am. Chem. Soc.*, 2012, **134**, 9199–208.
- 52 J. C. Jewett, E. M. Sletten and C. R. Bertozzi, *J. Am. Chem. Soc.*, 2010, **132**, 3688–90.
- 53 X. Ning, J. Guo, M. A. Wolfert and G.-J. Boons, *Angew. Chemie*, 2008, **120**, 2285–2287.
- 54 K. Sivakumar, F. Xie, B. M. Cash, S. Long, H. N. Barnhill and Q. Wang, *Org. Lett.*, 2004, **6**, 4603–6.
- 55 E. M. Sletten and C. R. Bertozzi, *Org. Lett.*, 2008, **10**, 3097–9.
- 56 J. Xu, T. M. Filion, F. Prifti and J. Song, *Chem. Asian J.*, 2011, **6**, 2730–7.
- 57 S. T. Laughlin and C. R. Bertozzi, *Nat. Protoc.*, 2007, **2**, 2930–44.
- 58 K. Yarema and C. Bertozzi, *Genome Biol.*, 2001, **2**, 1-10.
- 59 E. M. Sletten and C. R. Bertozzi, *Angew. Chem. Int. Ed. Engl.*, 2009, **48**, 6974–98.
- 60 M. A. Breidenbach, J. E. G. Gallagher, D. S. King, B. P. Smart, P. Wu and C. R. Bertozzi, *Proc. Natl. Acad. Sci. U. S. A.*, 2010, **107**, 3988–93.

- 61 S. J. Luchansky, K. J. Yarema, S. Takahashi and C. R. Bertozzi, *J. Biol. Chem.*, 2003, **278**, 8035–8042.
- 62 S. J. Luchansky, H. C. Hang, E. Saxon, J. R. Grunwell, C. Yu, D. H. Dube and C. R. Bertozzi, *Methods Enzymol.*, 2003, **362**, 249–272.
- 63 J. Du, M. A. Meledeo, Z. Wang, H. S. Khanna, V. D. P. Paruchuri and K. J. Yarema, *Glycobiology*, 2009, **19**, 1382–401.
- 64 M. L. Huang, R. A. A. Smith, G. W. Trieger and K. Godula, *J. Am. Chem. Soc.*, 2014, **136**, 10565–8.
- 65 B. Belardi, G. P. O’Donoghue, A. W. Smith, J. T. Groves and C. R. Bertozzi, *JACS*, 2012, **134**, 9549-9552.
- 66 J. J. Lundquist and E. J. Toone, *Chem. Rev.*, 2002, **102**, 555–578.
- 67 D. Fürniss, T. Mack, F. Hahn, S. B. L. Vollrath, K. Koroniak, U. Schepers and S. Bräse, *Beilstein J. Org. Chem.*, 2013, **9**, 56–63.
- 68 R. Whitfield, A. Anastasaki, V. Nikolaou, G. R. Jones, N. G. Engelis, E. H. Discekici, C. Fleischmann, J. Willenbacher, C. J. Hawker and D. M. Haddleton, *J. Am. Chem. Soc.*, 2017, **139**, 1003–1010.
- 69 G. R. Jones, Z. Li, A. Anastasaki, D. J. Lloyd, P. Wilson, Q. Zhang and D. M. Haddleton, *Macromolecules*, 2016, **49**, 483–489.
- 70 W. Tang. and K. Matyjaszewski, *Macromolecules* , 2006, **39**, 4953-4959
- 71 W. Tang, Y. Kwak, W. Braunecker, N. V. Tsarevsky, M. L. Coote and K. Matyjaszewski, *JACS*, 2008, **130**, 10702-10713.

- 72 V. Corbière, V. Dirix, S. Norrenberg, M. Cappello, M. Remmelink and F. Mascart, *Respir. Res.*, 2011, **12**, 15.
- 73 D. Neumann, O. Kohlbacher, H.-P. Lenhof and C.-M. Lehr, *Eur. J. Biochem.*, 2002, **269**, 1518–24.
- 74 N. E. Zachara, K. Vosseller and G. W. Hart, *Curr. Protoc. Mol. Biol.*, 2011, **Chapter 17**, Unit 17.6.
- 75 J. Nicolas, E. Khoshdel, D. M. Haddleton, C. Peinado, S. Kelly, E. Fitzpatrick, S. D. Carrington, D. Brayden and D. M. Haddleton, *Chem. Commun.*, 2007, **553**, 1722.
- 76 A. J. Limer, A. K. Rullay, V. S. Miguel, C. Peinado, S. Keely, E. Fitzpatrick, S. D. Carrington, D. Brayden and D. M. Haddleton, *React. Funct. Polym.*, 2006, **66**, 51–64.
- 77 T. J. Collins, *Biotechniques*, 2007, **43**, 25–30.

Chapter Five

Conclusions

5.1 Conclusions

Glycans interactions with multivalent receptors and proteins are vitally important controllers of information in biological systems. Developing new methods to probe these fundamental interactions is vitally important. In this work we have highlighted the importance of subtleties involved in probing glycan-protein interactions. In **chapter two**, we have shown that increasing glyco-conjugate density does not necessarily correlate with increased affinity, or increased inhibition, and that conversely, a lack of inhibitory activity does not correlate to no interaction. Careful assay design is vital if the purpose is to investigate the interactions taking place over identifying potential inhibitory compounds. The inclusion of nominally non-binding mannose to multivalent heterogeneous polymers resulted in a decrease in avidity but an increase in the inhibition of RCA₁₂₀ compared to the isovalent homogeneous polymers. The relationship between mannose density, inhibition, and, avidity was non-linear and was ascribed to an increased association rate, while the rate of dissociation stayed constant. Meanwhile no inhibition of CTxB was observed, but BLI analysis was used to demonstrate that the heterogeneous polymers do have ~10 μ M avidity towards CTxB. This highlights that, in line with other reports, that the structure of the polymer scaffold and its ability to match the geometry of the receptors can have a greater impact on the binding than the isomerism of the sugar units.

In **chapter three** we have shown the development of a high-through put gold nanoparticle based, label free, screening system for the analysis of protein-carbohydrate interactions. The lower limit on the concentration of gold required for detection of binding was established and it was shown that multivalent binding effects can effectively be used to out compete monosaccharide interactions and reduce the need for time consuming purification steps that result in a loss of nanoparticle concentration. This helps move this process towards a large scale system appropriate for use in industry to screen huge libraries of heterogeneous environments. Several ‘lead’ heterogeneous sugar combinations of mannose and galactose were identified for studying the interactions of DBA, RCA₁₂₀ and SBA lectins. Further to this it was shown that increasing the flexibility of the linker between the sugar and the particles resulted in a loss of binding towards all five lectins. This again highlights that for multivalent receptor binding, offering a rigid scaffold with the correct orientation over a flexible linker can have a dramatic impact on the binding. This highlights the need to consider both the scaffold and ligand when attempting to rationally design inhibitors and biosensors. The use of high through-put libraries as developed here may lead to the discovery of unexpected scaffolds and/ or heterogeneous ligand combinations that would be difficult to predict otherwise.

Finally in **chapter four**, we have shown that the polymeric modification of the cell glycocalyx is possible via metabolic engineering of *O*-linked glycans and sialic acid biosynthesis. It was shown that polymeric modification of A549 cells did not inhibit cell surface accessibility and opens the door to ‘hybrid’ cells with augmented, abiotic cell functionality for probing the cell and its environment. This circumvents the issues encountered when attempting cell-surface initiated polymerisations.

Overall this work has highlighted and explored the challenges associated with glycan and multivalent receptor interactions that must be met, in order to successfully overcome some of

the most pressing issues in healthcare science; including the diagnosis and treatment of diseases such as cancer, and the mounting antibiotic resistance crisis.

Appendix One

Chapter Two Supplementary Information

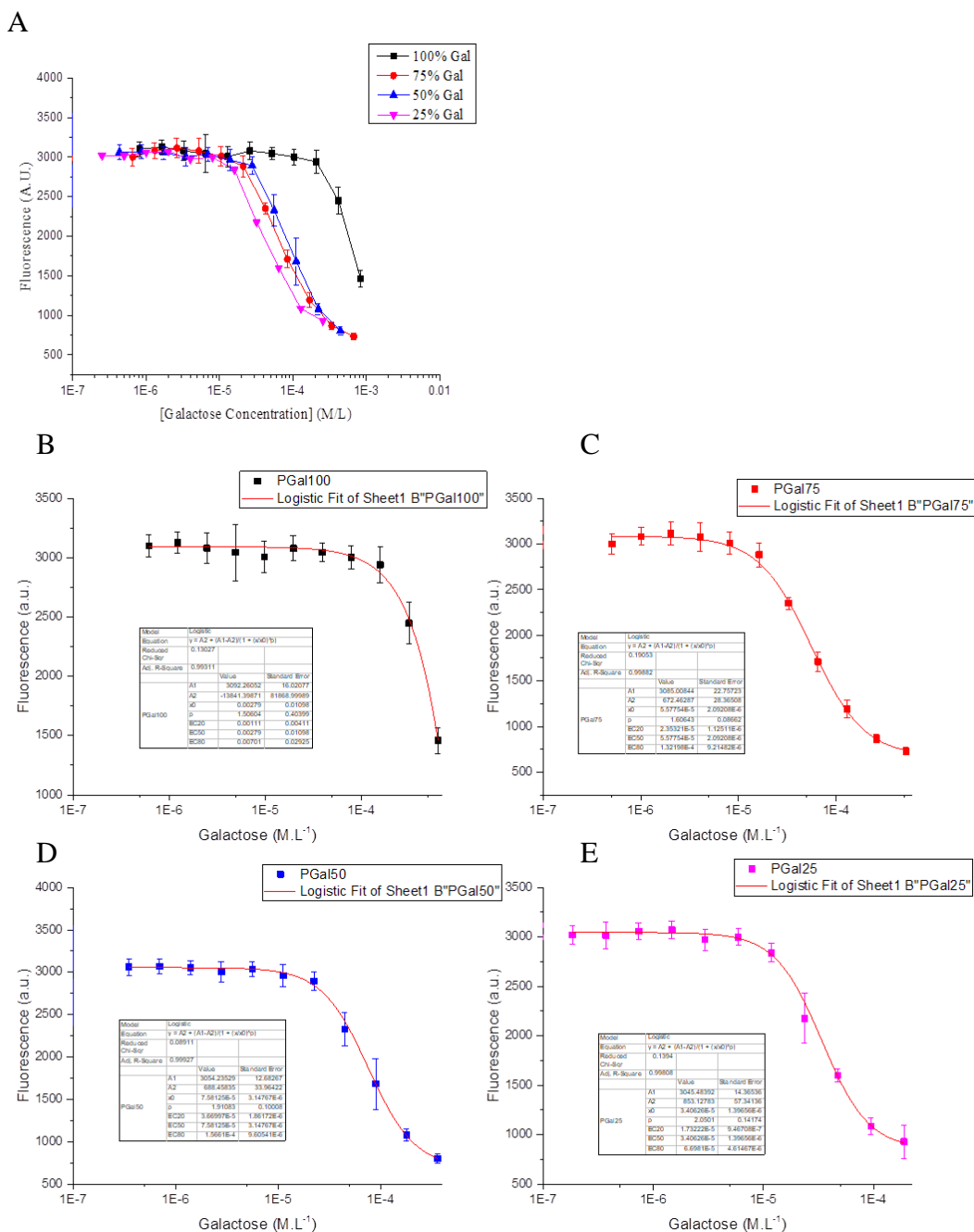


Figure S1. RCA120 inhibitory data by total galactose concentration. A) Comparison of all inhibitory curves. C-E, fitted curves.

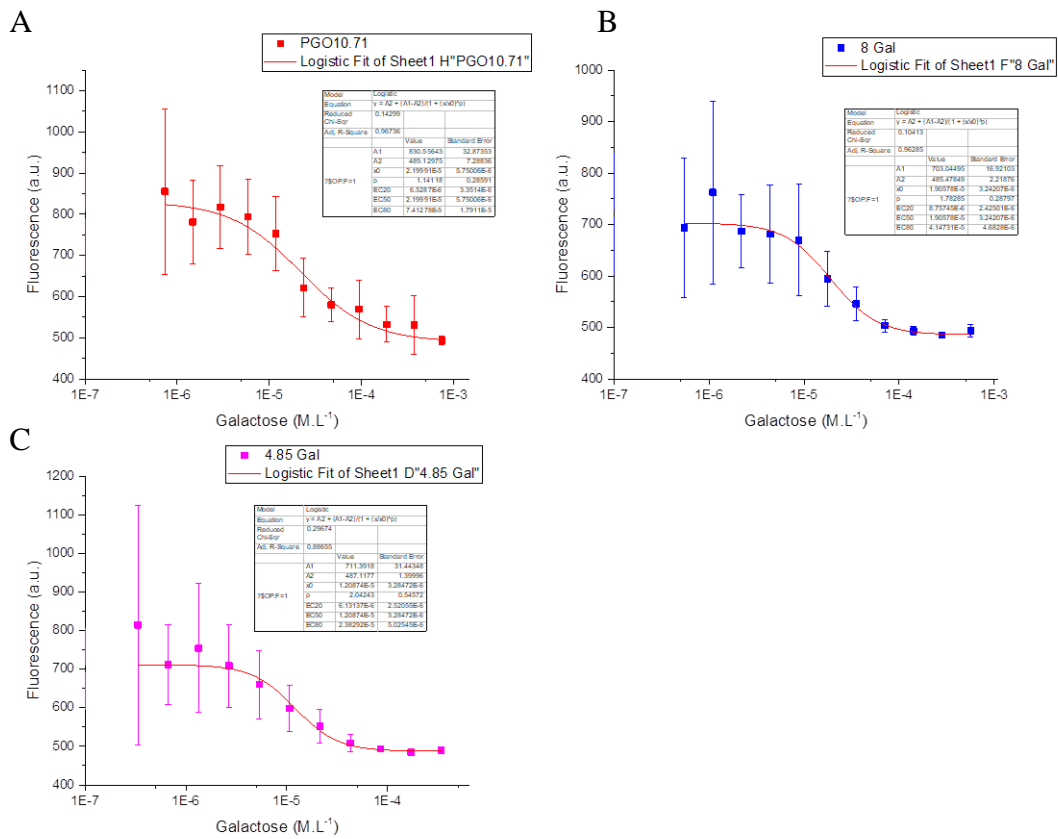


Figure S2: RCA, Homogeneous polymers in Galactose Concentration.

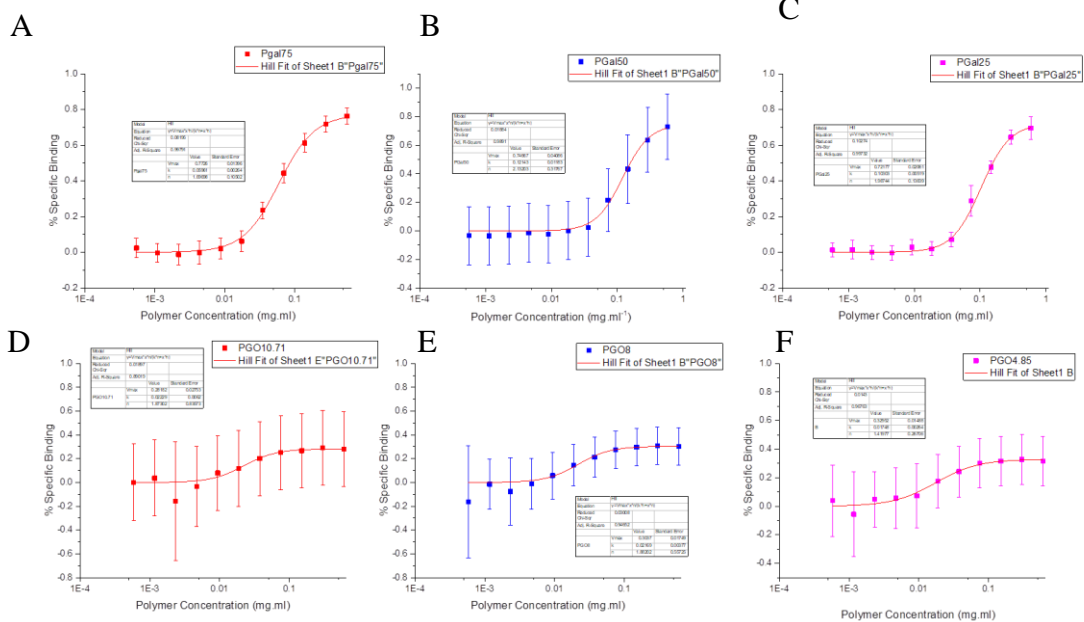


Figure S3: Percentage specific binding (i.e. percent inhibition) vs concentration for both heterogeneous and homogenous libraries.

Glycopolymer-Lectin Interactions using Bilayer Interferometry

To enable off rates to be calculated the dissociation phase was fitted independently. The fits are shown below.

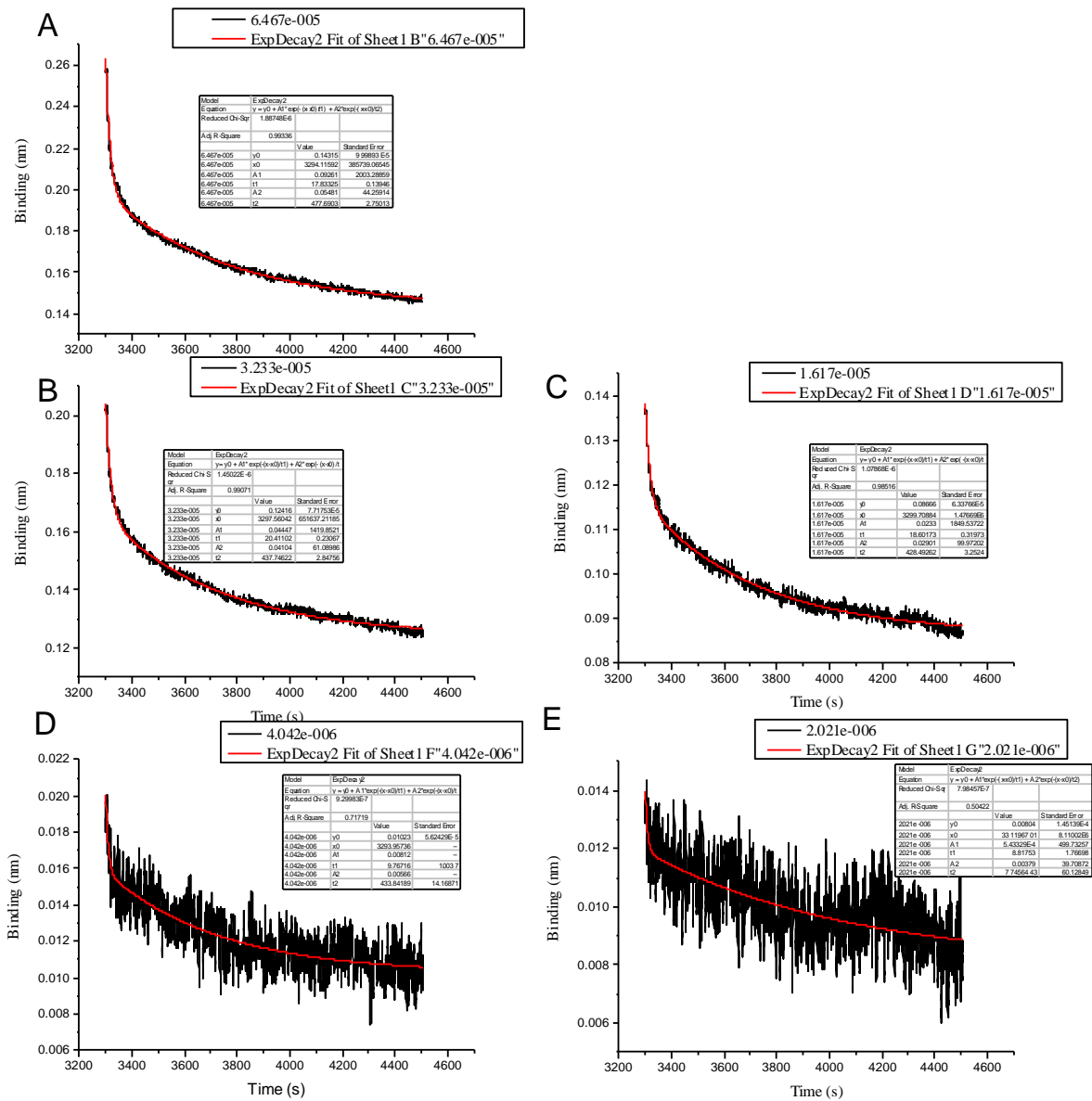


Figure S6. RCA120 with PGal25. Concentrations shown in legend, as [Polymer].

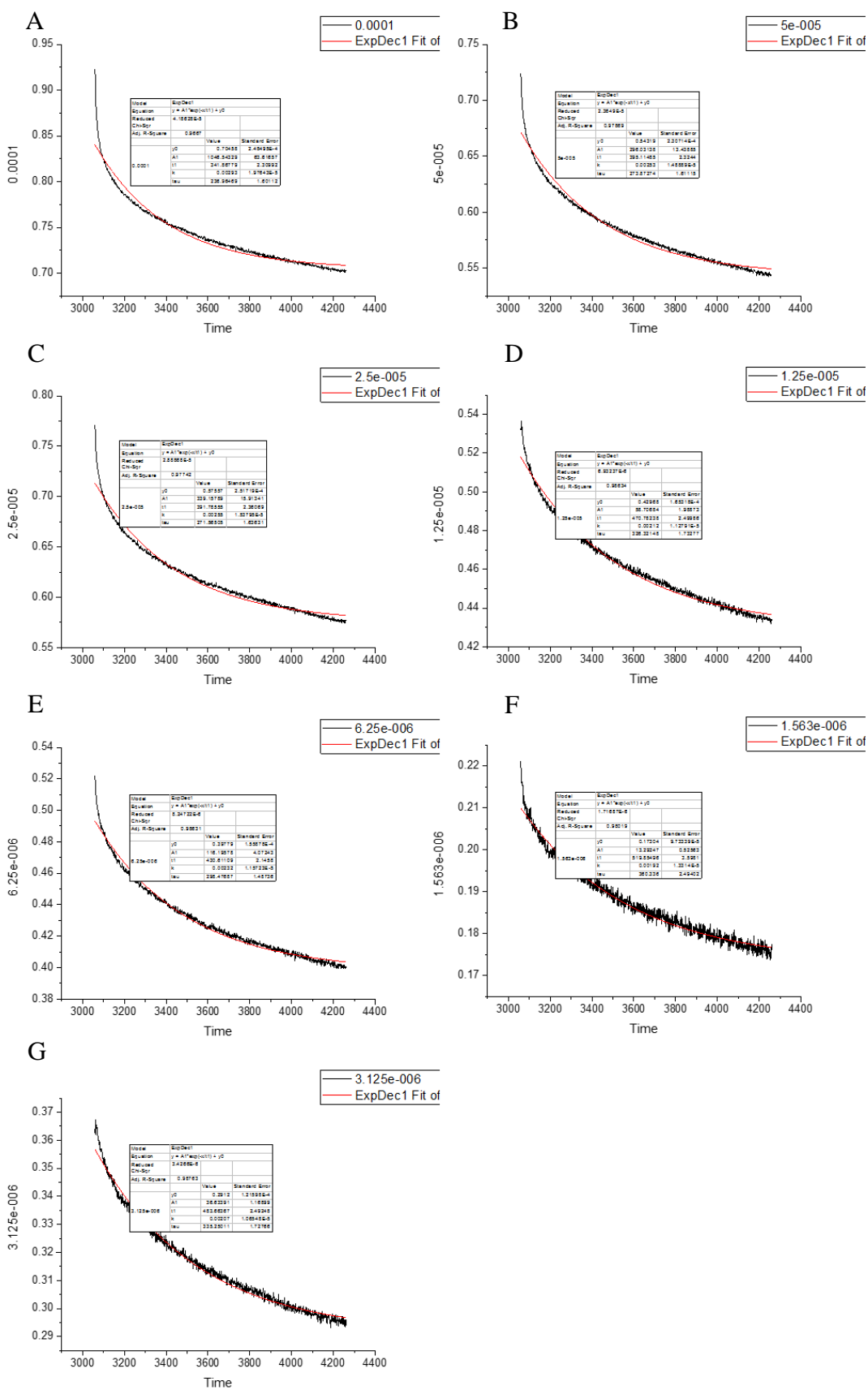


Figure S RCA120 with PGO25. Concentrations shown in legend, as [Polymer].

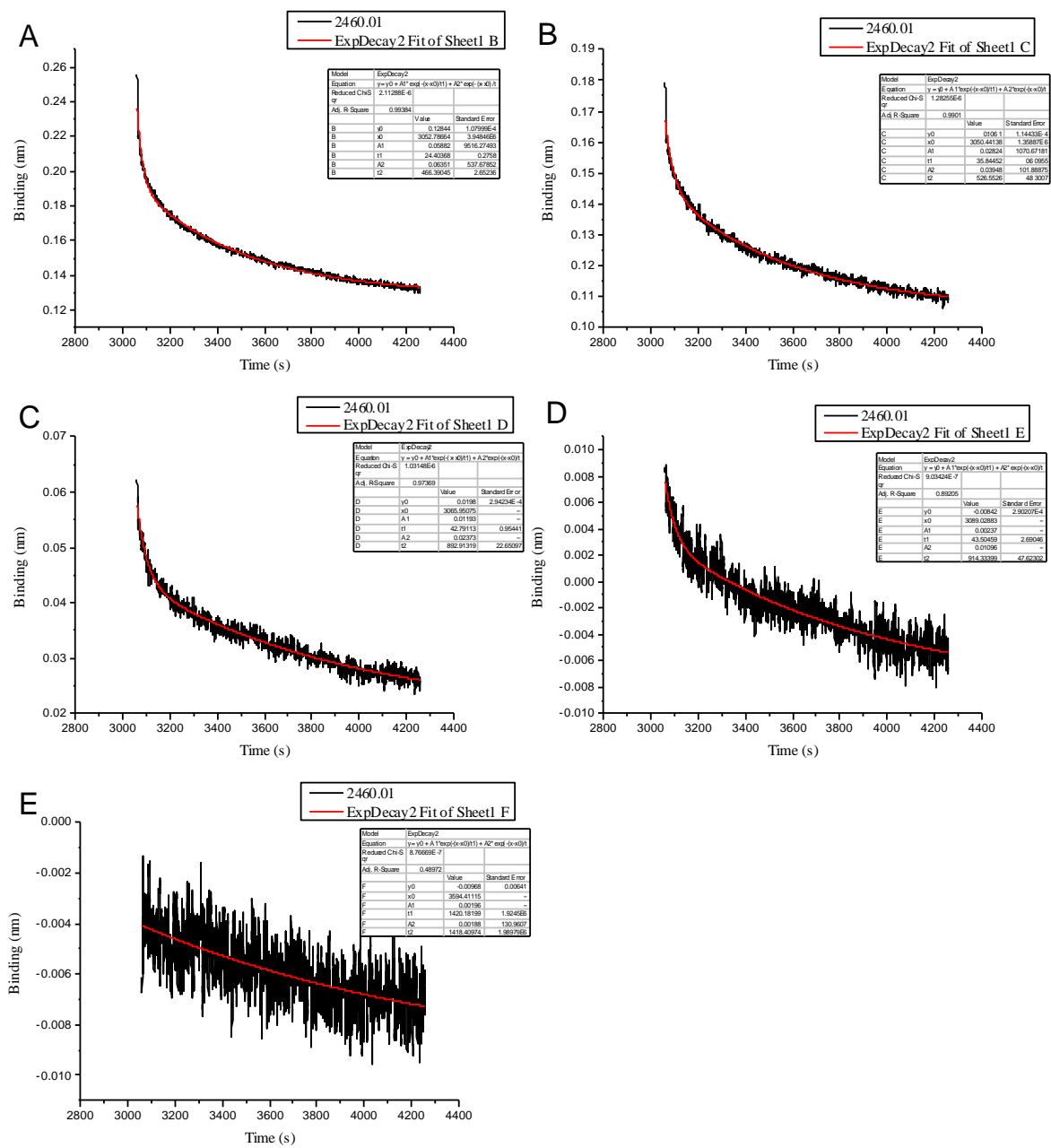


Figure S7. RCA120 with PGal50. Concentrations shown in legend, as [Polymer].

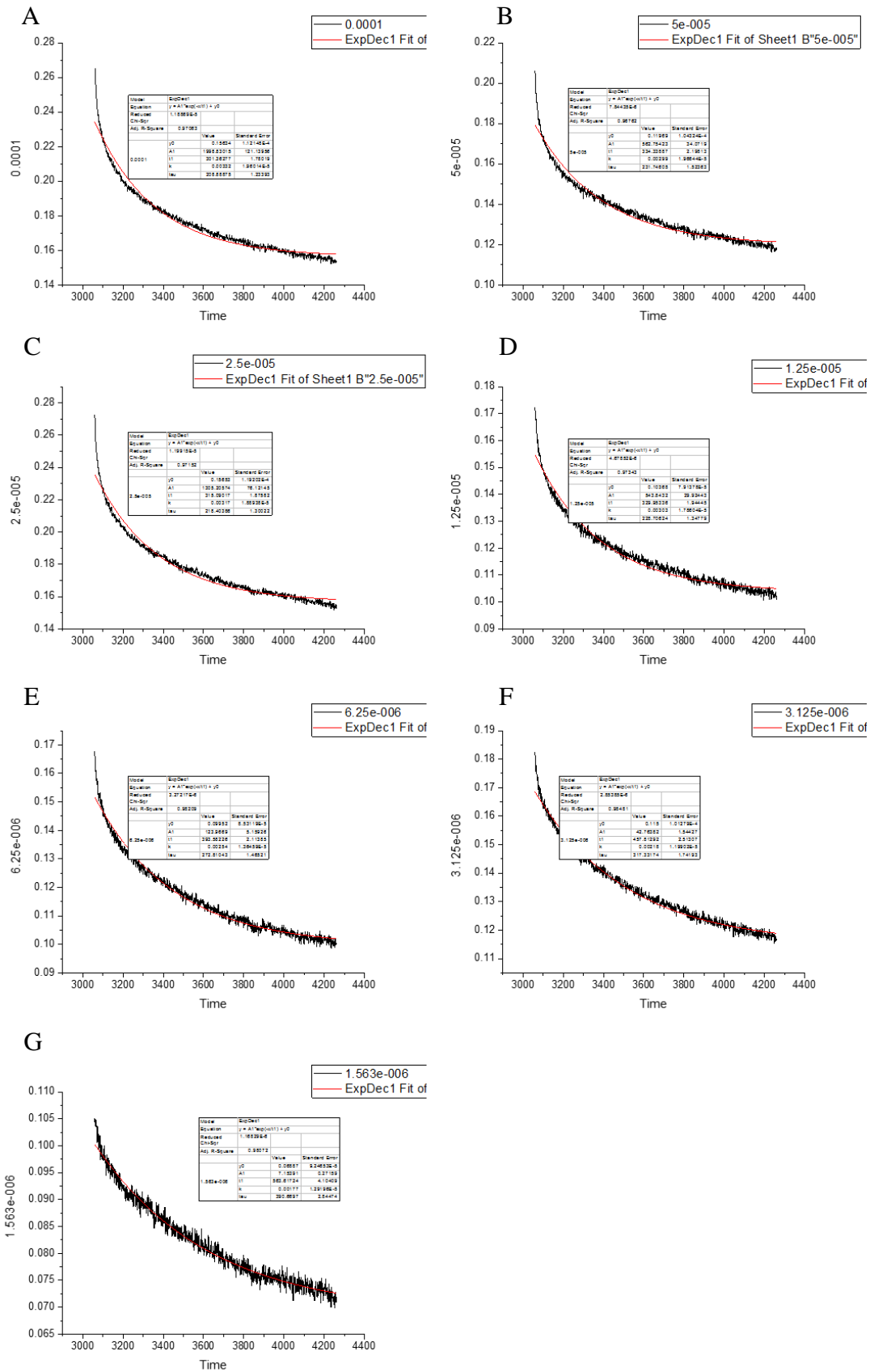


Figure RCA120 with PGO50. Concentrations shown in legend, as [Polymer].

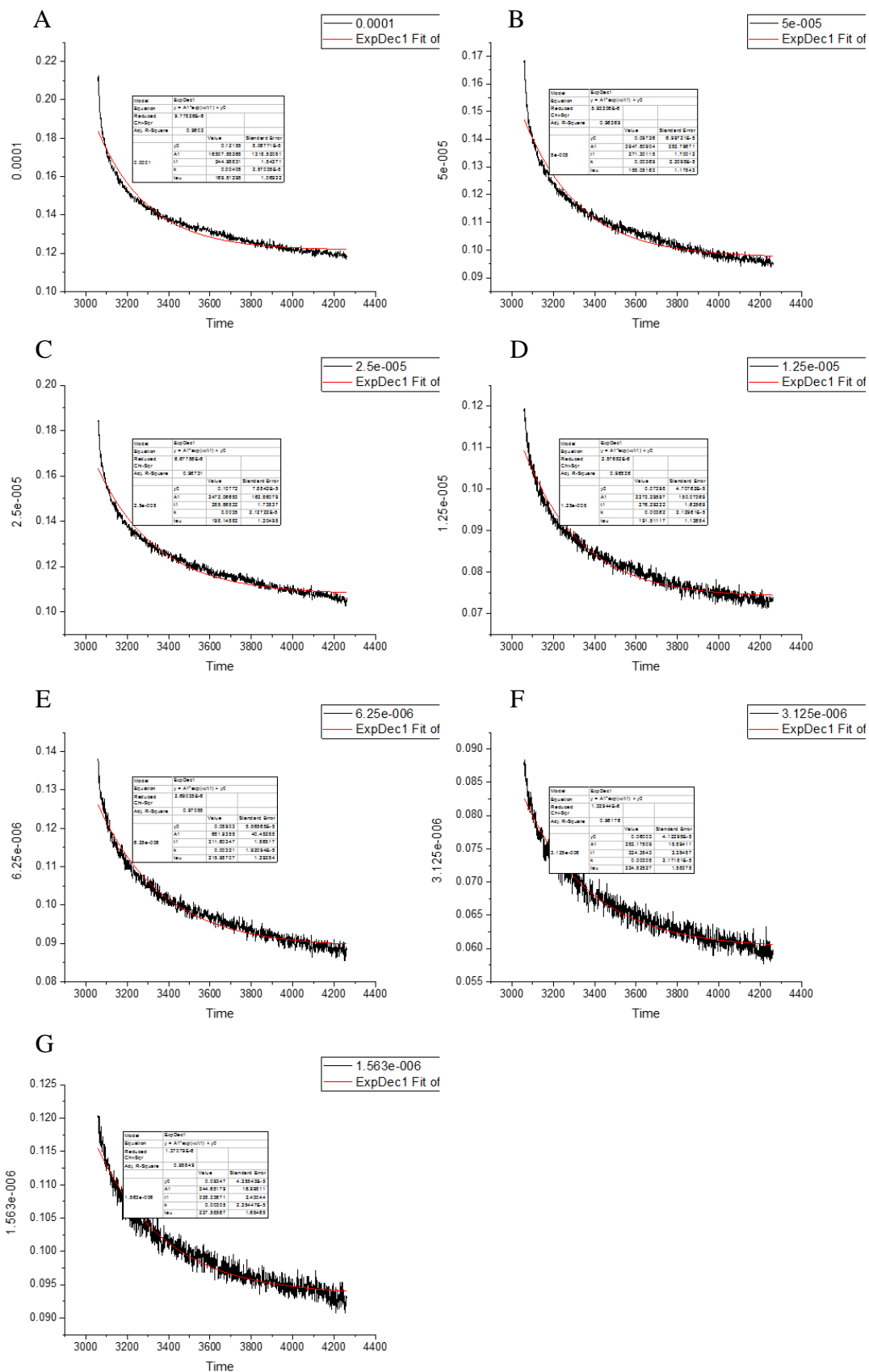


Figure RCA120 with PGO75. Concentrations shown in legend, as [Polymer].

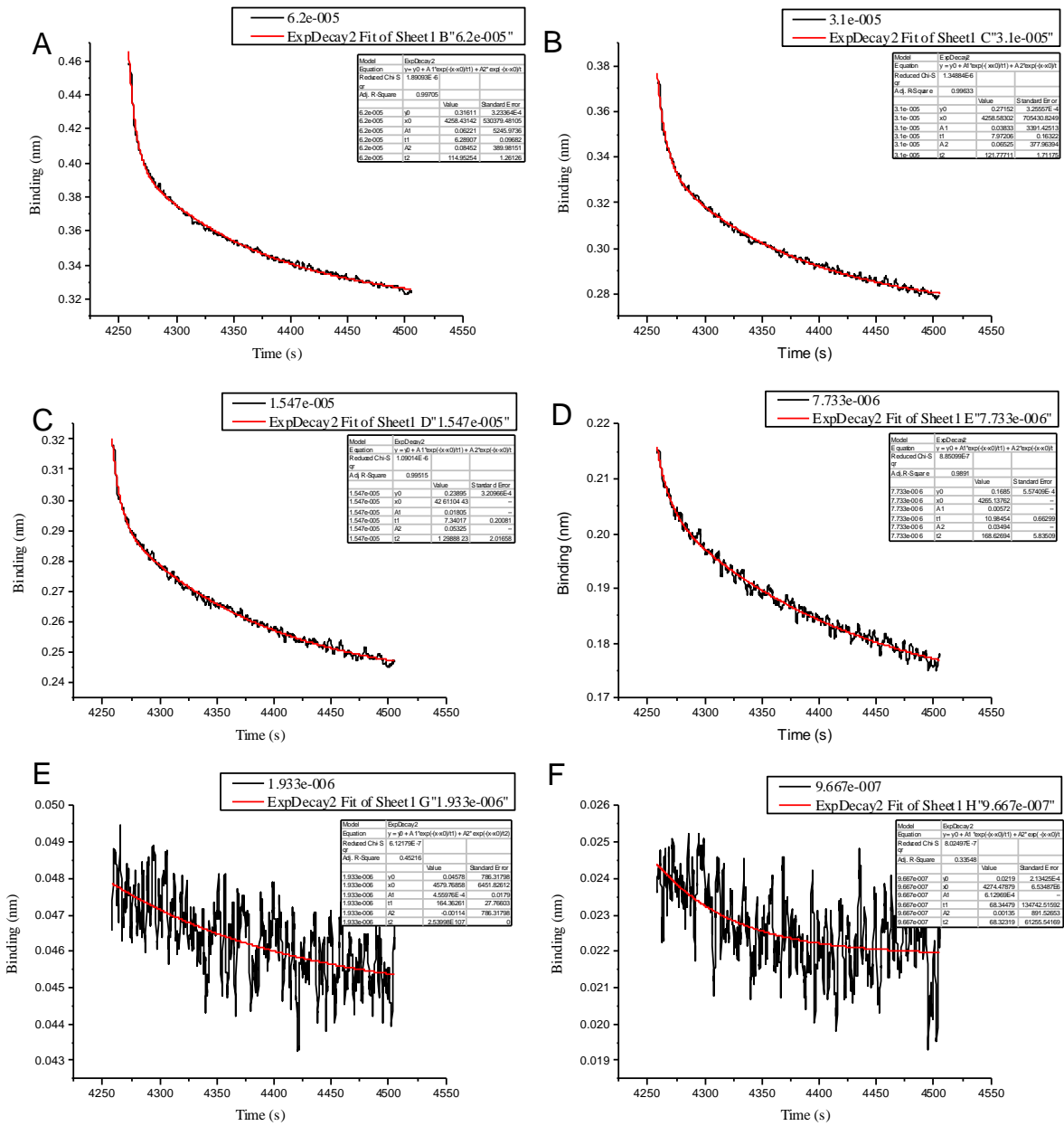


Figure S8. RCA120 with PGal75. Concentrations shown in legend, as [Polymer].

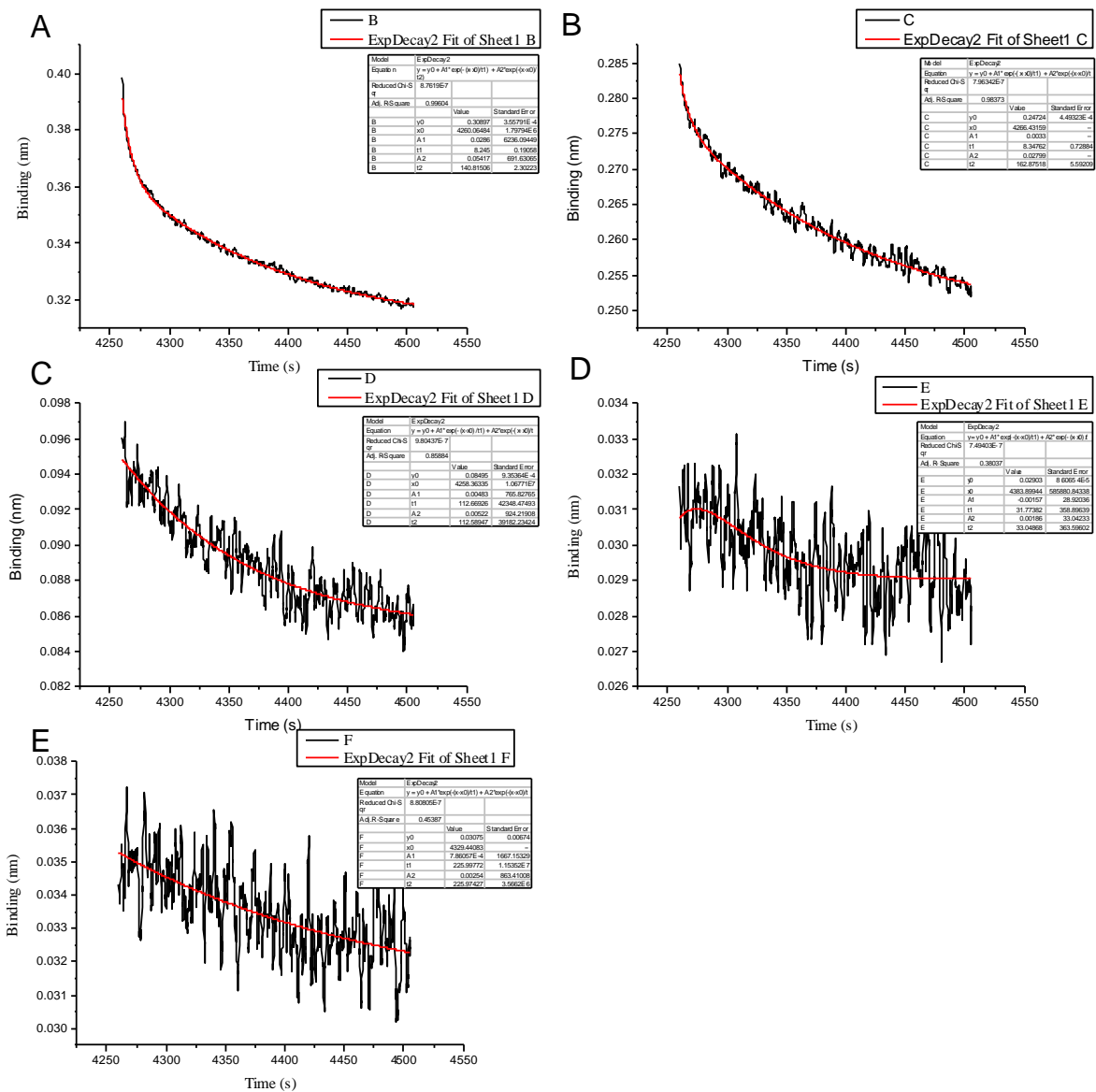


Figure S9. RCA120 with PGal100. Concentrations shown in legend, as [Polymer].

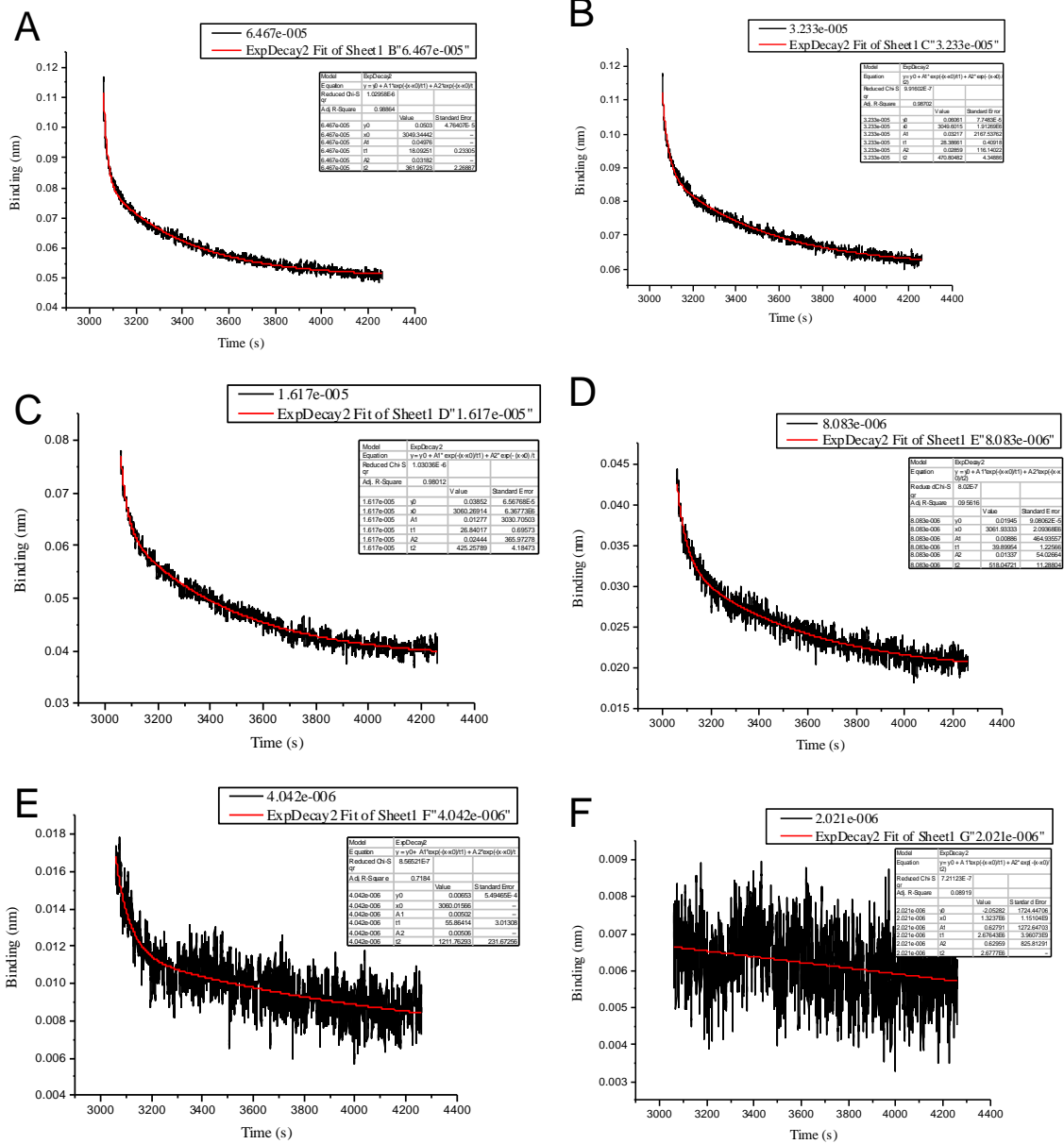


Figure S10. CTXB with PGal25 Concentrations shown in legend, as [Polymer].

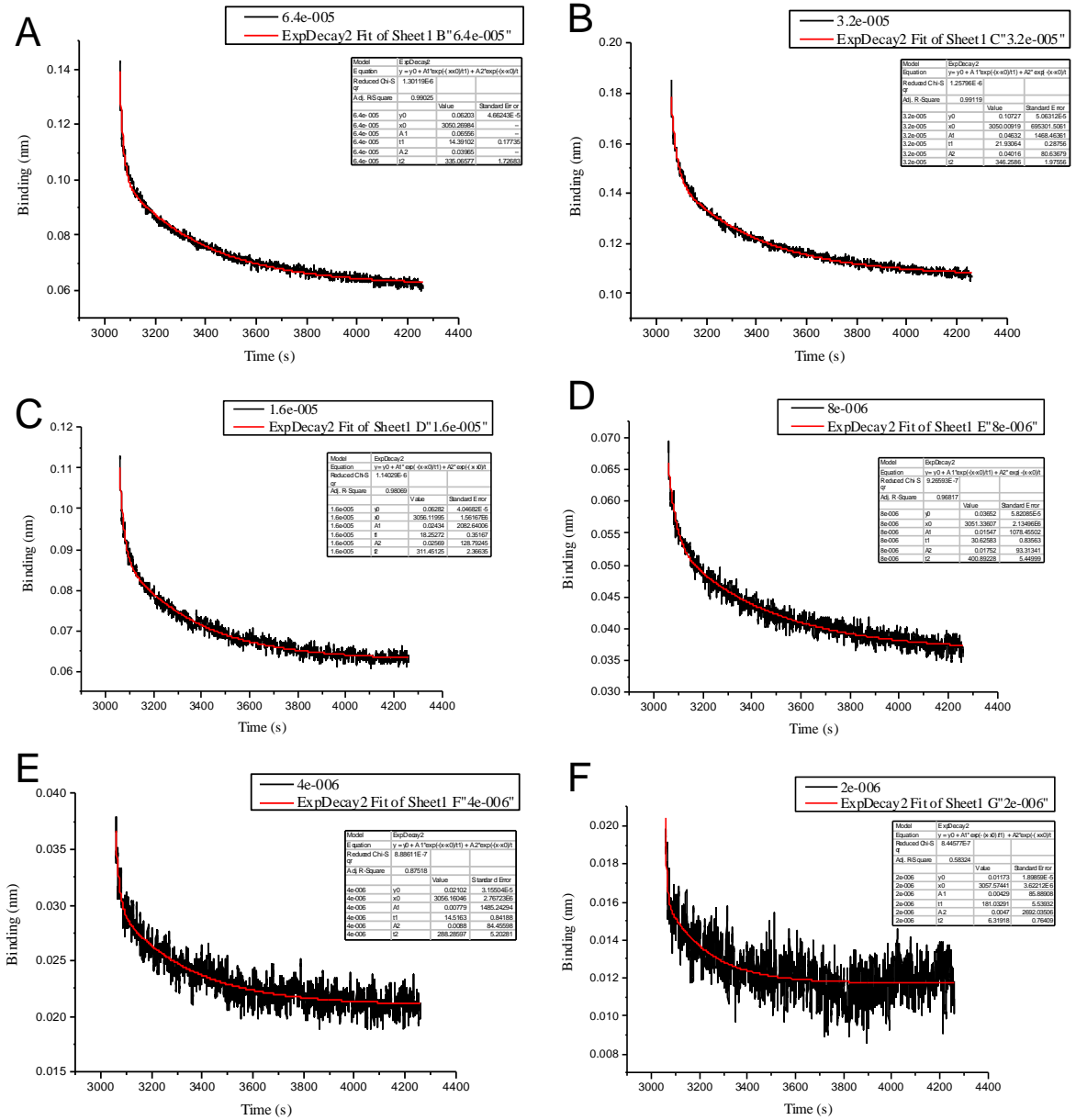


Figure S11. CTXB with PGal50 Concentrations shown in legend, as [Polymer].

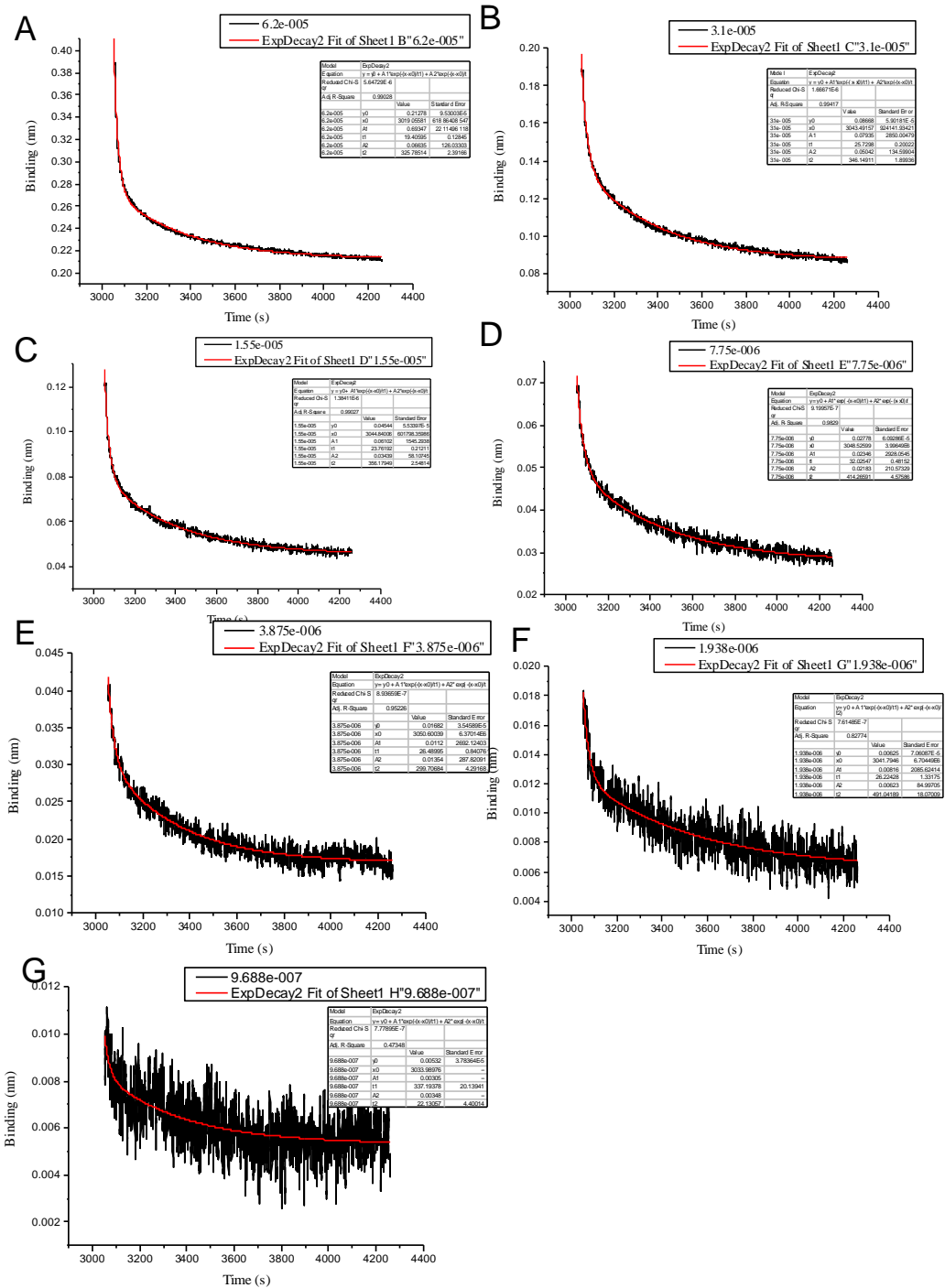


Figure S12. CTXB with PGal75 Concentrations shown in legend, as [Polymer].

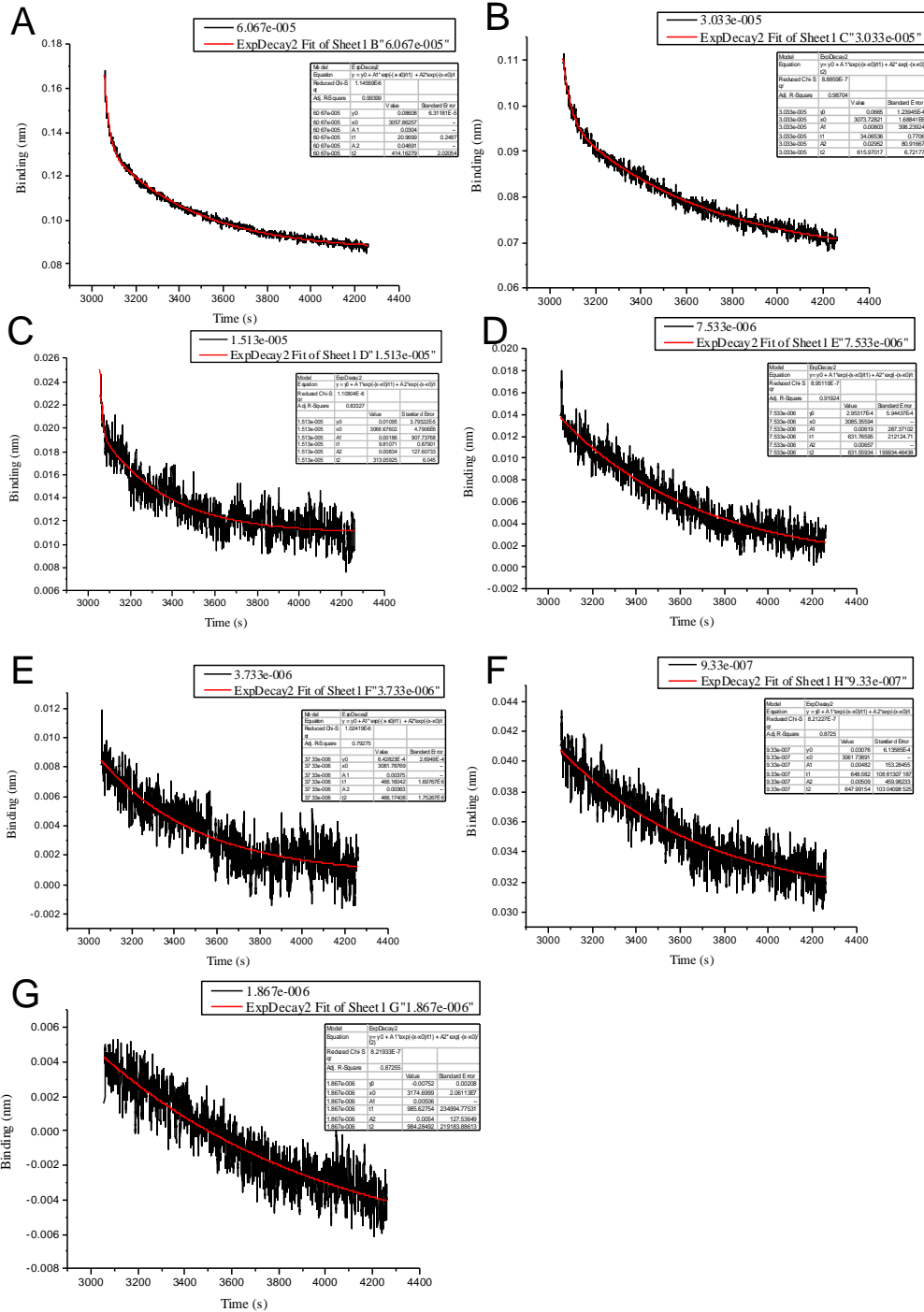


Figure S13. CTXB with PGal100 Concentrations shown in legend, as [Polymer].

Kd Estimation by Steady state

To provide an additional measure of affinity, KD was approximated by the steady state treatment. In short, the final BLI signal intensity (after dissociation phase had plateaued) verse both polymer and galactose concentration. Fits of this are shown below.

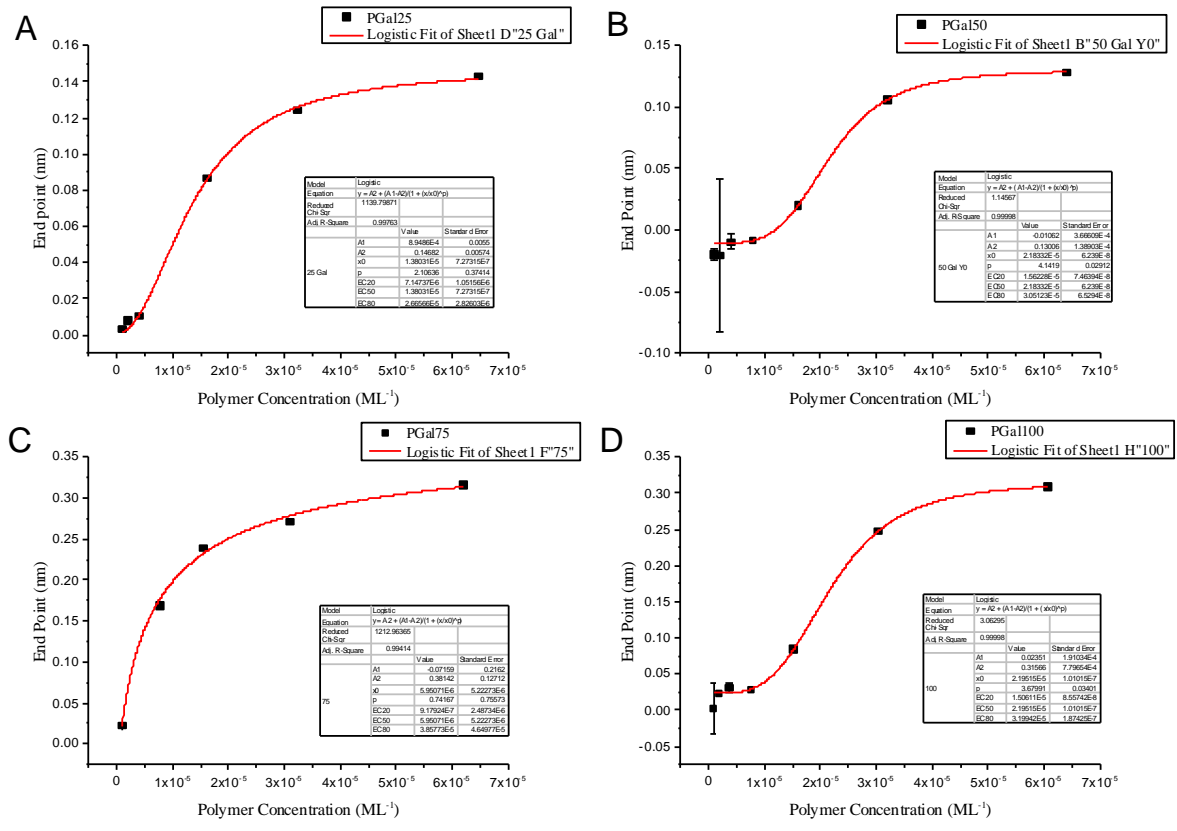


Figure S14. KD by steady state of RCA glycopolymers, by polymer concentration

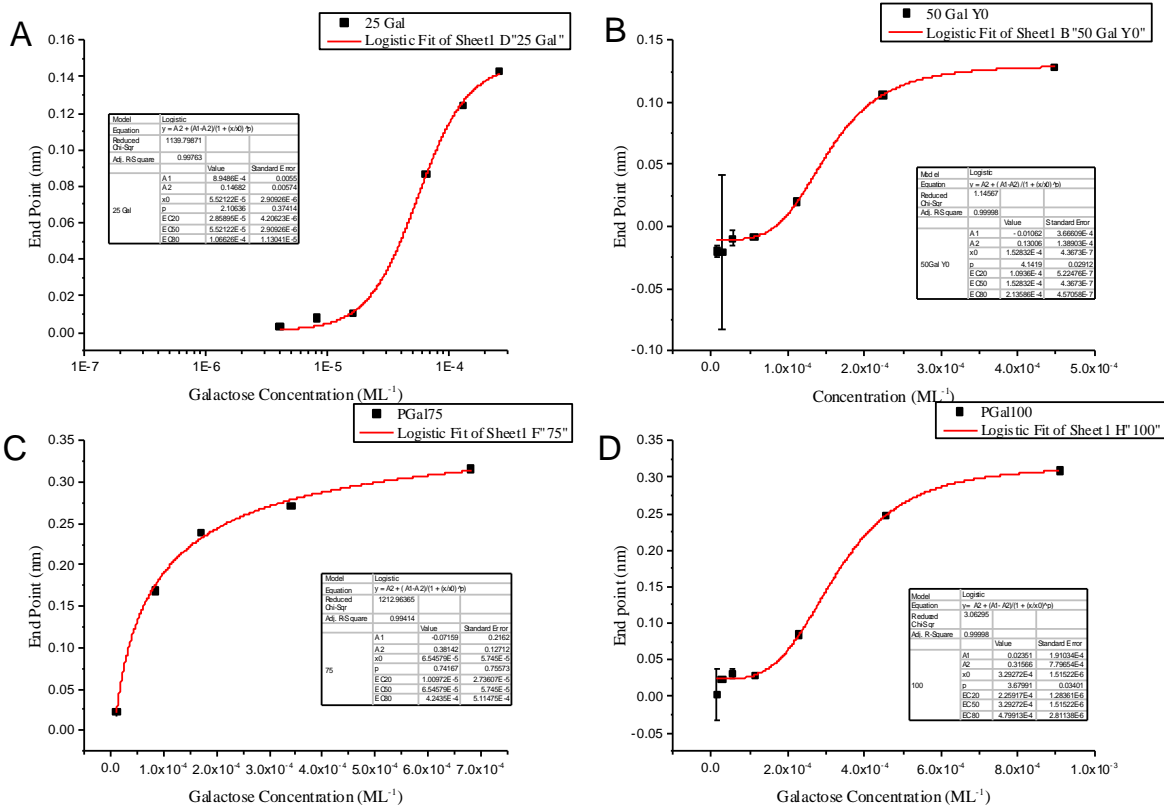


Figure S15. KD by steady state of RCA glycopolymers, by galactose concentration

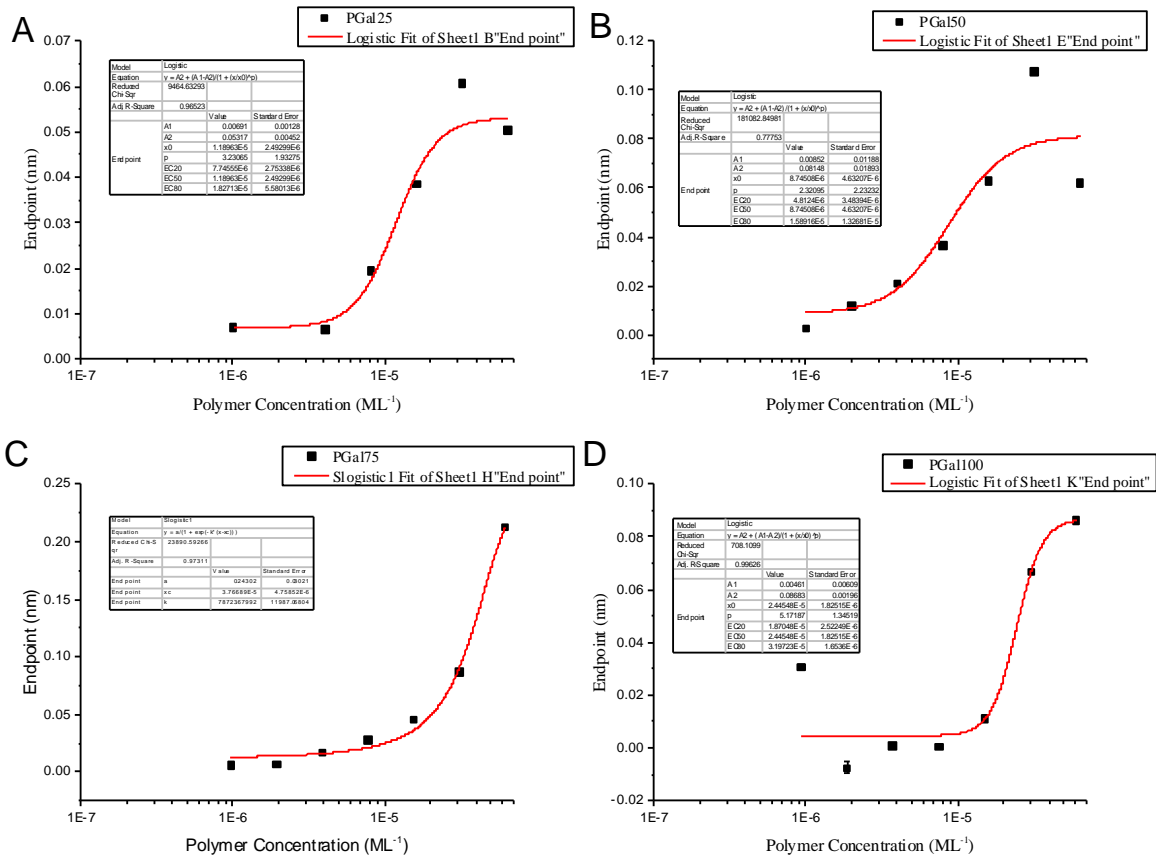


Figure S16. KD by steady state of CTXB with glycopolymers, by polymer concentration

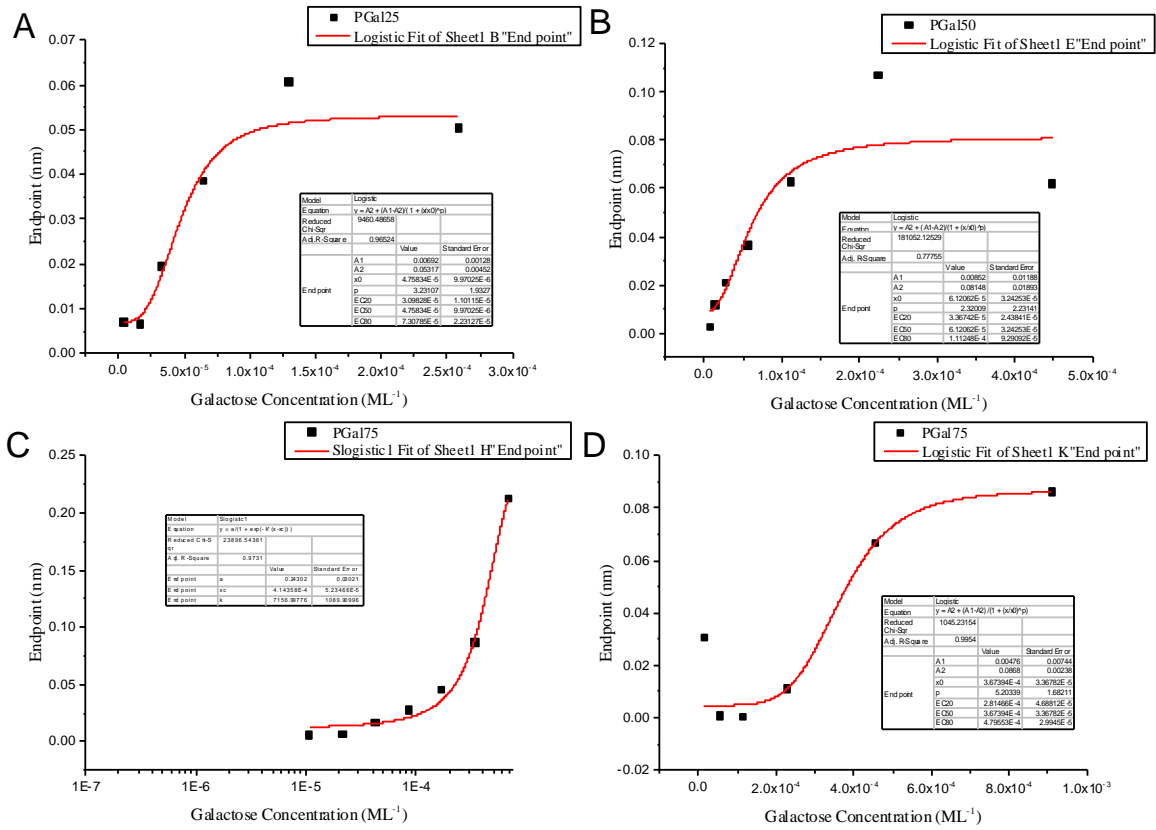


Figure S17. KD by steady state of CTXB with glycopolymers, by galactose concentration

Appendix Two

Table S2.1: Consortium for functional glycomics nomenclature


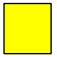
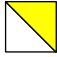

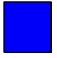
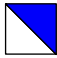

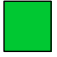




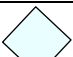
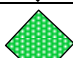


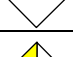

Sugar	Hexose	<i>N</i> -Acetylhexosamine	Hexosamine
Galactose			
Glucose			
Mannose			
Fucose			
Xylose			

Table S2.2: Acidic Sugars

Acidic Sugars	Symbol
NeuAc	
NeuGc	
KDN	
GlcA	
IdoA	
GalA	
ManA	

Appendix Three: Collaborative Papers

Polymer
Chemistry



PAPER

View Article Online
View Journal | View Issue



Cite this: *Polym. Chem.*, 2017, **8**, 4576

Poly(acryloyl hydrazide), a versatile scaffold for the preparation of functional polymers: synthesis and post-polymerisation modification†

Daniel N. Crisan,^a Oliver Creese,^a Ranadeb Ball,^a Jose Luis Brioso,^a Ben Martyn,^b Javier Montenegro^{b,c} and Francisco Fernandez-Trillo^{a*}

Here we present the synthesis and post-polymerisation modification of poly(acryloyl hydrazide), a versatile scaffold for the preparation of functional polymers: poly(acryloyl hydrazide) was prepared from commercially available starting materials in a three step synthesis on a large scale, in good yields and high purity. Our synthetic approach included the synthesis of a Boc-protected acryloyl hydrazide, the preparation of polymers via RAFT polymerisation and the deprotection of the corresponding Boc-protected poly(acryloyl hydrazide). Post-polymerisation modification of poly(acryloyl hydrazide) was then demonstrated using a range of conditions for both hydrophilic and hydrophobic aldehydes. These experiments demonstrate the potential of poly(acryloyl hydrazide) as a scaffold in the synthesis of functional polymers, in particular those applications where *in situ* screening of the activity of the functionalised polymers may be required (e.g. biological applications).

Received 30th March 2017,
Accepted 2nd July 2017

DOI: 10.1039/c7py00535k

rsc.li/polymers

Introduction

There is an increasing interest in developing polymers for biomedical applications and we now increasingly see polymers that play an "active" role in biology and reproduce or interact with biological functions. Representative examples include glycopolymers that mimic and interfere with glycan recognition,^{1–4} polymers for gene delivery that mimic some of the characteristics of viral vectors,^{5–9} or therapeutic polymers such as antimicrobial polymers.^{10–13} One common requirement when developing polymers for these applications is the need to synthesise libraries of polymers that incorporate highly functional monomers based on for instance carbohydrates, amine or cationic moieties. However, and despite the availability of a large toolbox for the synthesis of polymers,^{14–17} there are still many functional groups which are incompatible with existing polymerisation techniques. A common approach to solve this incompatibility is to employ post-polymerisation

modification,^{18–20} where polymer "scaffolds" are made with reactive moieties that are inert to the polymerisation conditions, but can then be modified post-polymerisation to give other functional groups. The success of this strategy relies on the nearly quantitative conversion of this initial reactive moiety to give functionalised polymers. Not surprisingly, these post-polymerisation protocols have often relied on highly efficient and orthogonal chemistries, *i.e.* click chemistries.^{21–26}

Despite the progress in this area, one potential limitation of these post-polymerisation strategies is the low aqueous solubility and stability of some of these reactive polymer scaffolds. Thus, additional steps must be employed following post-polymerisation modification and prior to biological evaluation, including the removal of protecting groups. Moreover, the current paradigm assumes that candidate polymers need to be isolated/purified prior to biological evaluation. However, this is inefficient, time-consuming and expensive, since efforts are invested in isolating candidate polymers that do not show any biological activity. The introduction of automation to polymer synthesis has the potential to facilitate some of these steps,²⁷ but it can result in even larger libraries of functional polymers, with the subsequent increase in cost associated to purification and isolation.

To address some of these limitations, we have recently reported the application of poly(acryloyl hydrazide) as a reactive polymer scaffold for the *in situ* preparation of polymeric gene vectors for the delivery of siRNA.²⁷ Polymers carrying hydrazides as reactive moieties are ideal to develop a post-poly-

^aSchool of Chemistry, University of Birmingham B15 2TT, UK
E-mail: f.fernandez-trillo@bham.ac.uk

^bSchool of Chemistry, University of Warwick CV47AL, UK

^cDepartamento de Química Orgánica y Centro Singular de Investigación en Química Biomédica e Materiais Moleculares (CIQUS), Universidade de Santiago de Compostela E-15782, Spain. E-mail: javier.montenegro@usc.es

† Electronic supplementary information (ESI) available: Additional NMR and UV-Vis spectra, additional tables and proposed mechanism for impurities. See DOI: 10.1039/c7py00535k



Appendix Four: Intended Publications

Invited review:

Synthesising glycomaterials with specificity as well as affinity.

Journal of materials chemistry B.

S. J. Richards, B. Martyn, L. Otten. M. I. Gibson

Collaboration:

A Robust and Convenient Method for Determining Dispersity by ^1H NMR Spectroscopy

E.G.B. Eden, T.R. Congdon, B.T. Martyn, M. Barrow, T. Ratvijitvech, M.E. Briggs, M.I. Gibson, A.I. Cooper, and D.J. Adams.

The work presented in **Chapter two** has been submitted to *Angewandte Chemie*

The work presented in **Chapter three** and **Chapter four** are to be written as publications.

Appendix Five

Copyright Permissions

NATURE PUBLISHING GROUP LICENSE TERMS AND CONDITIONS

Sep 29, 2017

This Agreement between Mr. Benjamin Martyn ("You") and Nature Publishing Group ("Nature Publishing Group") consists of your license details and the terms and conditions provided by Nature Publishing Group and Copyright Clearance Center.

License Number	4198150149383
License date	Sep 29, 2017
Licensed Content Publisher	Nature Publishing Group
Licensed Content Publication	Nature Chemistry
Licensed Content Title	Exploring and exploiting chemistry at the cell surface
Licensed Content Author	Morgan D. Mager, Vanessa LaPointe, Molly M. Stevens
Licensed Content Date	Jul 22, 2011
Licensed Content Volume	3
Licensed Content Issue	8
Type of Use	reuse in a dissertation / thesis
Requestor type	academic/educational
Format	print and electronic
Portion	figures/tables/illustrations
Number of figures/tables/illustrations	1
High-res required	no
Figures	Figure 1: Representation of a cell surface.
Author of this NPG article	no
Your reference number	
Title of your thesis / dissertation	Materials for Advanced Medicinal Applications
Expected completion date	Sep 2017
Estimated size (number of pages)	230
Requestor Location	Mr. Benjamin Martyn Chemistry Department University of Warwick

	Coventry, West Midlands CV4 7AL United Kingdom Attn: Mr. Benjamin Martyn
Billing Type	Invoice
Billing Address	Mr. Benjamin Martyn Chemistry Department University of Warwick
	Coventry, United Kingdom CV4 7AL Attn: Mr. Benjamin Martyn
Total	0.00 GBP
Terms and Conditions	

Terms and Conditions for Permissions

Nature Publishing Group hereby grants you a non-exclusive license to reproduce this material for this purpose, and for no other use, subject to the conditions below:

1. NPG warrants that it has, to the best of its knowledge, the rights to license reuse of this material. However, you should ensure that the material you are requesting is original to Nature Publishing Group and does not carry the copyright of another entity (as credited in the published version). If the credit line on any part of the material you have requested indicates that it was reprinted or adapted by NPG with permission from another source, then you should also seek permission from that source to reuse the material.
2. Permission granted free of charge for material in print is also usually granted for any electronic version of that work, provided that the material is incidental to the work as a whole and that the electronic version is essentially equivalent to, or substitutes for, the print version. Where print permission has been granted for a fee, separate permission must be obtained for any additional, electronic re-use (unless, as in the case of a full paper, this has already been accounted for during your initial request in the calculation of a print run). NB: In all cases, web-based use of full-text articles must be authorized separately through the 'Use on a Web Site' option when requesting permission.
3. Permission granted for a first edition does not apply to second and subsequent editions and for editions in other languages (except for signatories to the STM Permissions Guidelines, or where the first edition permission was granted for free).
4. Nature Publishing Group's permission must be acknowledged next to the figure, table or abstract in print. In electronic form, this acknowledgement must be visible at the same time as the figure/table/abstract, and must be hyperlinked to the journal's homepage.
5. The credit line should read:
Reprinted by permission from Macmillan Publishers Ltd: [JOURNAL NAME] (reference citation), copyright (year of publication)
For AOP papers, the credit line should read:
Reprinted by permission from Macmillan Publishers Ltd: [JOURNAL NAME], advance online publication, day month year (doi: 10.1038/sj.[JOURNAL ACRONYM].XXXXX)

Note: For republication from the *British Journal of Cancer*, the following credit lines apply.

Reprinted by permission from Macmillan Publishers Ltd on behalf of Cancer Research UK: [JOURNAL NAME] (reference citation), copyright (year of publication) For AOP papers, the credit line should read:

Reprinted by permission from Macmillan Publishers Ltd on behalf of Cancer Research UK: [JOURNAL NAME], advance online publication, day month year (doi:

10.1038/sj.[JOURNAL ACRONYM].XXXXX)

6. Adaptations of single figures do not require NPG approval. However, the adaptation should be credited as follows:

Adapted by permission from Macmillan Publishers Ltd: [JOURNAL NAME] (reference citation), copyright (year of publication)

Note: For adaptation from the *British Journal of Cancer*, the following credit line applies.

Adapted by permission from Macmillan Publishers Ltd on behalf of Cancer Research UK: [JOURNAL NAME] (reference citation), copyright (year of publication)

7. Translations of 401 words up to a whole article require NPG approval. Please visit <http://www.macmillanmedicalcommunications.com> for more information. Translations of up to a 400 words do not require NPG approval. The translation should be credited as follows:

Translated by permission from Macmillan Publishers Ltd: [JOURNAL NAME] (reference citation), copyright (year of publication).

Note: For translation from the *British Journal of Cancer*, the following credit line applies.

Translated by permission from Macmillan Publishers Ltd on behalf of Cancer Research UK: [JOURNAL NAME] (reference citation), copyright (year of publication)

We are certain that all parties will benefit from this agreement and wish you the best in the use of this material. Thank you.

Special Terms:

v1.1

Questions? customercare@copyright.com or +1-855-239-3415 (toll free in the US) or +1-978-646-2777.



**JOHN WILEY AND SONS LICENSE
TERMS AND CONDITIONS**

Sep 29, 2017

This Agreement between Mr. Benjamin Martyn ("You") and John Wiley and Sons ("John Wiley and Sons") consists of your license details and the terms and conditions provided by John Wiley and Sons and Copyright Clearance Center.

License Number	4192541242443
License date	Sep 19, 2017
Licensed Content Publisher	John Wiley and Sons
Licensed Content Publication	Angewandte Chemie International Edition
Licensed Content Title	Synthetic Multivalent Ligands as Probes of Signal Transduction
Licensed Content Author	Laura L. Kiessling,Jason E. Gestwicki,Laura E. Strong
Licensed Content Date	Mar 24, 2006
Licensed Content Pages	21
Type of use	Dissertation/Thesis
Requestor type	University/Academic
Format	Print and electronic
Portion	Figure/table
Number of figures/tables	1
Original Wiley figure/table number(s)	Figure 5
Will you be translating?	No
Title of your thesis / dissertation	Materials for Advanced Medicinal Applications
Expected completion date	Sep 2017
Expected size (number of pages)	230
Requestor Location	Mr. Benjamin Martyn Chemistry Department University of Warwick Coventry, West Midlands CV4 7AL United Kingdom Attn: Mr. Benjamin Martyn
Publisher Tax ID	EU826007151
Billing Type	Invoice
Billing Address	Mr. Benjamin Martyn Chemistry Department University of Warwick Coventry, United Kingdom CV4 7AL Attn: Mr. Benjamin Martyn
Total	0.00 GBP

TERMS AND CONDITIONS

This copyrighted material is owned by or exclusively licensed to John Wiley & Sons, Inc. or one of its group companies (each a "Wiley Company") or handled on behalf of a society with which a Wiley Company has exclusive publishing rights in relation to a particular work (collectively "WILEY"). By clicking "accept" in connection with completing this licensing transaction, you agree that the following terms and conditions apply to this transaction (along with the billing and payment terms and conditions established by the Copyright Clearance Center Inc., ("CCC's Billing and Payment terms and conditions"), at the time that you opened your RightsLink account (these are available at any time at <http://myaccount.copyright.com>).

Terms and Conditions

- The materials you have requested permission to reproduce or reuse (the "Wiley Materials") are protected by copyright.
- You are hereby granted a personal, non-exclusive, non-sub licensable (on a stand-alone basis), non-transferable, worldwide, limited license to reproduce the Wiley Materials for the purpose specified in the licensing process. This license, **and any CONTENT (PDF or image file) purchased as part of your order**, is for a one-time use only and limited to any maximum distribution number specified in the license. The first instance of republication or reuse granted by this license must be completed within two years of the date of the grant of this license (although copies prepared before the end date may be distributed thereafter). The Wiley Materials shall not be used in any other manner or for any other purpose, beyond what is granted in the license. Permission is granted subject to an appropriate acknowledgement given to the author, title of the material/book/journal and the publisher. You shall also duplicate the copyright notice that appears in the Wiley publication in your use of the Wiley Material. Permission is also granted on the understanding that nowhere in the text is a previously published source acknowledged for all or part of this Wiley Material. Any third party content is expressly excluded from this permission.
- With respect to the Wiley Materials, all rights are reserved. Except as expressly granted by the terms of the license, no part of the Wiley Materials may be copied, modified, adapted (except for minor reformatting required by the new Publication), translated, reproduced, transferred or distributed, in any form or by any means, and no derivative works may be made based on the Wiley Materials without the prior permission of the respective copyright owner. **For STM Signatory Publishers clearing permission under the terms of the [STM Permissions Guidelines](#) only, the terms of the license are extended to include subsequent editions and for editions in other languages, provided such editions are for the work as a whole in situ and does not involve the separate exploitation of the permitted figures or extracts,** You may not alter, remove or suppress in any manner any copyright, trademark or other notices displayed by the Wiley Materials. You may not license, rent, sell, loan, lease, pledge, offer as security, transfer or assign the Wiley Materials on a stand-alone basis, or any of the rights granted to you hereunder to any other person.

- The Wiley Materials and all of the intellectual property rights therein shall at all times remain the exclusive property of John Wiley & Sons Inc, the Wiley Companies, or their respective licensors, and your interest therein is only that of having possession of and the right to reproduce the Wiley Materials pursuant to Section 2 herein during the continuance of this Agreement. You agree that you own no right, title or interest in or to the Wiley Materials or any of the intellectual property rights therein. You shall have no rights hereunder other than the license as provided for above in Section 2. No right, license or interest to any trademark, trade name, service mark or other branding ("Marks") of WILEY or its licensors is granted hereunder, and you agree that you shall not assert any such right, license or interest with respect thereto
- NEITHER WILEY NOR ITS LICENSORS MAKES ANY WARRANTY OR REPRESENTATION OF ANY KIND TO YOU OR ANY THIRD PARTY, EXPRESS, IMPLIED OR STATUTORY, WITH RESPECT TO THE MATERIALS OR THE ACCURACY OF ANY INFORMATION CONTAINED IN THE MATERIALS, INCLUDING, WITHOUT LIMITATION, ANY IMPLIED WARRANTY OF MERCHANTABILITY, ACCURACY, SATISFACTORY QUALITY, FITNESS FOR A PARTICULAR PURPOSE, USABILITY, INTEGRATION OR NON-INFRINGEMENT AND ALL SUCH WARRANTIES ARE HEREBY EXCLUDED BY WILEY AND ITS LICENSORS AND WAIVED BY YOU.
- WILEY shall have the right to terminate this Agreement immediately upon breach of this Agreement by you.
- You shall indemnify, defend and hold harmless WILEY, its Licensors and their respective directors, officers, agents and employees, from and against any actual or threatened claims, demands, causes of action or proceedings arising from any breach of this Agreement by you.
- IN NO EVENT SHALL WILEY OR ITS LICENSORS BE LIABLE TO YOU OR ANY OTHER PARTY OR ANY OTHER PERSON OR ENTITY FOR ANY SPECIAL, CONSEQUENTIAL, INCIDENTAL, INDIRECT, EXEMPLARY OR PUNITIVE DAMAGES, HOWEVER CAUSED, ARISING OUT OF OR IN CONNECTION WITH THE DOWNLOADING, PROVISIONING, VIEWING OR USE OF THE MATERIALS REGARDLESS OF THE FORM OF ACTION, WHETHER FOR BREACH OF CONTRACT, BREACH OF WARRANTY, TORT, NEGLIGENCE, INFRINGEMENT OR OTHERWISE (INCLUDING, WITHOUT LIMITATION, DAMAGES BASED ON LOSS OF PROFITS, DATA, FILES, USE, BUSINESS OPPORTUNITY OR CLAIMS OF THIRD PARTIES), AND WHETHER OR NOT THE PARTY HAS BEEN ADVISED OF THE POSSIBILITY OF SUCH DAMAGES. THIS LIMITATION SHALL APPLY NOTWITHSTANDING ANY FAILURE OF ESSENTIAL PURPOSE OF ANY LIMITED REMEDY PROVIDED HEREIN.
- Should any provision of this Agreement be held by a court of competent jurisdiction to be illegal, invalid, or unenforceable, that provision shall be deemed amended to achieve as nearly as possible the same economic effect as the original provision, and the legality, validity and enforceability of the remaining provisions

of this Agreement shall not be affected or impaired thereby.

- The failure of either party to enforce any term or condition of this Agreement shall not constitute a waiver of either party's right to enforce each and every term and condition of this Agreement. No breach under this agreement shall be deemed waived or excused by either party unless such waiver or consent is in writing signed by the party granting such waiver or consent. The waiver by or consent of a party to a breach of any provision of this Agreement shall not operate or be construed as a waiver of or consent to any other or subsequent breach by such other party.
- This Agreement may not be assigned (including by operation of law or otherwise) by you without WILEY's prior written consent.
- Any fee required for this permission shall be non-refundable after thirty (30) days from receipt by the CCC.
- These terms and conditions together with CCC's Billing and Payment terms and conditions (which are incorporated herein) form the entire agreement between you and WILEY concerning this licensing transaction and (in the absence of fraud) supersedes all prior agreements and representations of the parties, oral or written. This Agreement may not be amended except in writing signed by both parties. This Agreement shall be binding upon and inure to the benefit of the parties' successors, legal representatives, and authorized assigns.
- In the event of any conflict between your obligations established by these terms and conditions and those established by CCC's Billing and Payment terms and conditions, these terms and conditions shall prevail.
- WILEY expressly reserves all rights not specifically granted in the combination of (i) the license details provided by you and accepted in the course of this licensing transaction, (ii) these terms and conditions and (iii) CCC's Billing and Payment terms and conditions.
- This Agreement will be void if the Type of Use, Format, Circulation, or Requestor Type was misrepresented during the licensing process.
- This Agreement shall be governed by and construed in accordance with the laws of the State of New York, USA, without regards to such state's conflict of law rules. Any legal action, suit or proceeding arising out of or relating to these Terms and Conditions or the breach thereof shall be instituted in a court of competent jurisdiction in New York County in the State of New York in the United States of America and each party hereby consents and submits to the personal jurisdiction of such court, waives any objection to venue in such court and consents to service of process by registered or certified mail, return receipt requested, at the last known address of such party.

WILEY OPEN ACCESS TERMS AND CONDITIONS

Wiley Publishes Open Access Articles in fully Open Access Journals and in Subscription journals offering Online Open. Although most of the fully Open Access journals publish open access articles under the terms of the Creative Commons Attribution (CC BY)

License only, the subscription journals and a few of the Open Access Journals offer a choice of Creative Commons Licenses. The license type is clearly identified on the article.

The Creative Commons Attribution License

The [Creative Commons Attribution License \(CC-BY\)](#) allows users to copy, distribute and transmit an article, adapt the article and make commercial use of the article. The CC-BY license permits commercial and non-

Creative Commons Attribution Non-Commercial License

The [Creative Commons Attribution Non-Commercial \(CC-BY-NC\)License](#) permits use, distribution and reproduction in any medium, provided the original work is properly cited and is not used for commercial purposes.(see below)

Creative Commons Attribution-Non-Commercial-NoDerivs License

The [Creative Commons Attribution Non-Commercial-NoDerivs License](#) (CC-BY-NC-ND) permits use, distribution and reproduction in any medium, provided the original work is properly cited, is not used for commercial purposes and no modifications or adaptations are made. (see below)

Use by commercial "for-profit" organizations

Use of Wiley Open Access articles for commercial, promotional, or marketing purposes requires further explicit permission from Wiley and will be subject to a fee.

Further details can be found on Wiley Online

Library <http://olabout.wiley.com/WileyCDA/Section/id-410895.html>

Other Terms and Conditions:

v1.10 Last updated September 2015

Questions? customercare@copyright.com or +1-855-239-3415 (toll free in the US) or +1-978-646-2777.



Introduction, Figure 1 was originally authored by Lucienne Otten, University of Warwick, for her thesis, copyright 2015. Permission granted for both print and electronic use.

Poly(acryloyl hydrazide), a versatile scaffold for the preparation of functional polymers: synthesis and post-polymerisation modification

D. N. Crisan, O. Creese, R. Ball, J. L. Brioso, B. Martyn, J. Montenegro and F. Fernandez-Trillo, *Polym. Chem.*, 2017, **8**, 4576–4584.

- Published by The Royal Society of Chemistry.

A Robust and Convenient Method for Determining Dispersity by ^1H NMR Spectroscopy

E.G.B. Eden, T.R. Congdon, B.T. Martyn, M. Barrow, T. Ratvijitvech, M.E. Briggs, M.I. Gibson, A.I. Cooper, and D.J. Adams. *Submitted*.